REDUCED ORDER MODELLING OF BONE RESORPTION AND FORMATION

By Adam Moroz

A thesis in a partial fulfilment of the requirements for the degree of

DOCTOR OF PHYLOSOPHY

Submitted to

De Montfort University

September 2011

ACKNOWLEDGMENTS

The author would like to express his gratitude to his advisor, Prof David Ian Wimpenny, for his guidance and support during this project. He has been an inspiring and attentive mentor throughout authors stay at De Montfort University. The author also would like to thank Dr. Geoff Smith without whose involvement this project would not have been possible.

ABSTRACT

The bone remodelling process, performed by the Bone Multicellular Unit (BMU) is a key multi-hierarchically regulated process, which provides and supports various functionality of bone tissue. It is also plays a critical role in bone disorders, as well as bone tissue healing following damage. Improved modelling of bone turnover processes could play a significant role in helping to understand the underlying cause of bone disorders and thus develop more effective treatment methods. Moreover, despite extensive research in the field of bone tissue engineering, bonescaffold development is still very empirical. The development of improved methods of modelling the bone remodelling process should help to develop new implant designs which encourage rapid osteointegration.

There are a number of limitations with respect to previous research in the field of mathematical modelling of the bone remodelling process, including the absence of an osteocyte loop of regulation. It is within this context that this research presented in this thesis utilises a range of modelling methods to develop a framework for bone remodelling which can be used to improve treatment methods for bone disorders. The study concentrated on dynamic and steady state variables that in perspective can be used as constraints for optimisation problem considering bone remodelling or tissue remodelling with the help of the grafts/scaffolds.

The cellular and combined allosteric-regulation approaches to modelling of bone turnover, based on the osteocyte loop of regulation, have been studied. Both approaches have been studied different within wide range of rate parameters. The approach to the model validation has been considered, including a statistical approach and parameter reduction approach. From a validation perspective the cellular class of modes is preferable since it has fewer parameters to validate. The optimal control framework for regulation of remodelling has been studied. Future work in to improve the models and their application to bone scaffold design applications have been considered. The study illustrates the complexity of formalisation of the metabolic processes and the relations between hierarchical subsystems in hard tissue where a relatively small number of cells are active.

Different types/modes of behaviour have been found in the study: relaxational, periodical and chaotic modes. All of these types of behaviour can be found, in bone tissue. However, a chaotic or periodic modes are ones of the hardest to verify although a number of periodical phenomena have been observed empirically in bone and skeletal development. Implementation of the allosteric loop into cellular model damps other types of behaviour/modes. In this sense it improves the robustness, predictability and control of the system.

The developed models represent a first step in a hierarchical model of bone tissue (system versus local effects). The limited autonomy of any organ or tissue implies differentiation on a regulatory level as well as physiological functions and metabolic differences. Implementation into the cellular phenomenological model of allosteric-like loop of regulation has been performed. The results show that the robustness of regulation can be inherited from the phenomenological model.

An attempt to correlate the main bone disorders with different modes of behaviour has been undertaken using Paget's disorder in bone, osteoporosis and some more general skeleton disorders which lead to periodical changes in bone mass, reported by some authors. However, additional studies are needed to make this hypothesis significant.

The study has revealed a few interesting techniques. When studying a multidimensional phenomenon, as a bone tissue is, the visualisation and data reduction is important for analysis and interpretation of results. In the study two novel technical methods have been proposed. The first is the graphical matrix method to visualise/project the multidimensional phase space of variables into diagonal matrix of regular combination of two-dimensional graphs. This significantly simplifies the analysis and, in principle, makes it possible to visualise the phase space higher than three-dimensional. The second important technical development is the application of the Monte-Carlo method in combination with the regression method to study the character and stability of the equilibrium points of a dynamic system. The advantage of this method is that it enables the most influential parameters that affect the character and stability of the equilibrium point to be identified from a large number of the rate parameters/constants of the dynamic system. This makes the interpretation of parameters and conceptual verification of the model much easier.

TABLE OF CONTENTS

LIST OF ABBREVIATIONS

2D	Two dimension
3D	Three dimension
ALP	Total alkaline phosphatase
ATP	Adenosine triphosphate
AVHs	anterior vertebral body heights
BM	Bone marrow
BMD	Bone mineral density
BMP	Bone morphogenic protein
BMPR	Bone morphogenic protein receptor
BMU	Basic multicellular unit
CA	Cellular automata
CAD	Computer aided design
CATE	Computer aided tissue engineering
CCA	Canonical correlation analysis
CANCORR	Canonical correlation subroutine in SAS
Cbfa1	Transcription factor (Runx2/Cbfa1) for osteoblast differentiation
CNS	Central nervous system
CSF	Colony stimulating factor
ECM	Extracellular matrix
ER(α,β)	Estrogen receptor
EGF	Epidermal growth factor
FE	Finite element (method)
FEA	Finite element analysis
FGF	Fibroblast growth factor
FGFR	Fibroblast growth factor receptor

GF	Growth factor
GM-CSF	Granulocyte macrophage colony stimulating factor
GR	Glucocorticoid receptor
HA	Hydroxyapatite
Hb	Hemoglobin
HGF	Hepatocyte growth factor
hPHT	Human parathyroid hormone
IL	Interleukin
IGF	Insulin-like growth factor
IGFBP	IGF binding protein
K_d	Dissociation constant
K_M	Michaelis constant
KNF	Koshland-Nemethy-Filmer model
LIF	Leukemia inhibitory factor
LBMD	Lumbar bone mineral density
M-CSF	Macrophage-colony stimulating factor
mRNA	Messenger ribonucleic acid
MWC	Monod-Wyman-Changeux model
NAD	Nicotinamide adenine dinucleotide
NF	Necrosis factor
NF-kB	Nuclear factor kappa-light-chain-enhancer of activated B cells
Obl	Osteoblast
OC	Optimal control
Ocl	Osteoclast
Oct	Osteocyte
ODE	Ordinary differential equation
ODE	Ordinary differential equation

OHPr/Cr	Hydroxyproline/creatinine
OPG	Osteoprotegerin
PDGF	Platelet-derived growth factor
PG	Prostaglandins
PTH	Parathyroid hormone
RANK-L	Receptor activator of NF-kappaB ligand
RANK	Receptor activator of NF-kappaB
RNA	Ribonucleic acid
SAS	Statistical analysis system ®
sEGF	Salivary epidermal growth factor
TGF	Transforming growth factor
THA	Total hip arthroplasty
TNF	Tumor necrosis factor
TNFR	Tumor necrosis factor receptor
VEGF	Vascular endothelial growth factor
V_{max}	Maximal velocity of enzyme reaction
YSM	Years since menopause

1 Introduction

1.1 Background

The mathematical modelling of many biological processes is a powerful tool not in just verification of the understanding of these processes on systemic regulative and qualitative level, but also a generationg understanding and new biological engineering approaches for treatment/correction in metabolic networks and tissues. However, before any discussions of modelling, it needs to understand thorouphly the biological process involved in these processes, in particular of the remodelling process in bone tissue, which is of particular interest in this study.

Bone, together with cartilage, forms the skeleton, which is the hard structural system that supports body locomotion and protects internal organs. Damage to the human skeleton can create significant problems leading to pain, reduced mobility, morbidity and may even give rise to life threatening medical conditions. The complex nature of bone has only been recognised relatively recently. Loveridge (1999) remarked that bone is “more than a stick”, it is a metabolic active tissue which is under a steady process of development and renewal called remodelling. An improved knowledge of the mechanisms at work during the remodelling of bone could play an important role of improving the health of patients, particularly in an aging population

Bone comprises of two types of tissue**;** cortical and trabecular bone. Cortical bone is very compact and provides 75% of the weight of the human skeleton, whereas trabecular bone has an open porous structure of lattice-shaped spicules. Trabecular bone tissue provides three quarters of the bone surface that is involved in bone remodelling. It is highly metabolically active and therefore sensitive to metabolic disorders.

Bone consists of both organic and inorganic material. The main organic component of bone tissue is osteoid which contains collagen and non-collagen proteins. Collagen is the most significant part of structural osteoid and comprises about 95% of its volume. The inorganic

part of bone tissue contains hydroxyapatite (HA), a microcrystalline mineral which is initially deposited in layers as calcium phosphate and is later transformed into apatite crystals. Many other ions and minerals (carbonates, magnesium, potassium, calcium, fluorine etc) are present in the inorganic part of bone tissue and have an important metabolic role and influence the mechanical properties of the bone. The mineral components of bone are stored in both the cortical and trabecular bone.

Micro-damage or aging of bone tissue causes the release of molecular messengers and the bone multicellular unit (BMU) is activated; this is known as the damage signalling phase. Histologically, the shape of lining cells becomes cubic-like (originally flat). There are indications that osteocytes are also involved at the start of the remodelling process (Martin, 2000).

In response, the osteocytes signal the osteoclasts, then the recruitment phase commences. The osteoblast precursors start to synthesise messengers which interacts with the surface of osteoclasts precursors. As a result these differentiate into mature multinucleous osteoclasts, which develop the "ruffled border" and start to resorb bone tissue. During the resorption phase mature osteoclasts resorb bone within the resorption cavity. At every separate bone remodelling site resorption lasts about two weeks. At the end of this process the remaining osteoclasts die by means of apoptosis. In the osteoblast recruitment phase osteoblasts differentiate from bone marrow stromal cells. During the osteoid formation phase active osteoblasts fill the absorbed cavity forming the non-mineralised new tissue (osteoid). One can see a complex coordination and hierarchy between different osteo cells involved in bone remodelling.

This project concentrates on the two quite distant levels of biological organisation: one phenomenological, cellular level and molecular level, phenenologically formulated through the non-linear Michaelis-Menten transfer function. However, generally speaking, all biological systems are characterized by more complicated multilevel non-linear interconnections and multilevel interpenetrating feedbacks resulting in very complex system

regulation. Due to these links between different biological levels of organization (e.g. cellular, molecular) new functionalities emerge as important life properties from this multileveled complexity. They can be characterized by complex organization, optimal adaptation, self-replication and co-evolution. In general, biological systems are far from equilibrium due to multiple control loops maintaining the biological system homeostasis.

It could be noted that the complex hierarchical structure and control in biological systems have been developed during a long period of evolution. Many regulatory processes have a dynamic and cyclic nature manifesting different characteristic time scales. Just phenomenological behaviour and control in such a multileveled biological system can be considered in the framework of a dynamical system approach. Additionally, from an energetical (linked to the thermodynamic perspective), biological systems are too far from equilibrium state, therefore only a dynamic approach can be used to investigate their complex behaviour. Many attempts to describe the informational processes in bio-systems on the basis of entropy-informational principals have failed - possibly because bio-systems are really multileveled, autonomic, dissipative and intelligent systems. In this project the phenomenological method for deriving a nonlinear dynamical model is be adopted, which is used in a study of regulatory processes in the BMU. The experience available in the design and analysis of dynamic systems is exploited in this process.

1.2 Aims and objectives

The overall aim of the project was to develop the model of bone tissue resorption and formation that can explain the relaxation times of bone tissue restoring and therefore can be useful in further studies on bone graft remodelling.

To achieve this in the project it was aimed:

- To revise the existing mathematical models of remodelling.
- To revise molecular mechanisms (Michaelis-Menten, Hill) involved in BMU regulation and develop an approach to incorporate non-linear control.

- To develop a regulation model of BMU activities, based on the Optimal Control approach.

1.3 Structure of the thesis

The thesis is divided into 7 chapters, the structure and content of thesis is shown in Table 1.1.

Chapter number	Title	Description
2	Literature review	The complexity if the regulation of bone remodelling is presented with particular attention to the existing mathematical models of bone remodelling.
3	Objectives and methodology	In this chapter the aims and objectives of the study are presented. The methodology of model development is then described and approach is justified.
4	Cellular model	The approach to develop cell-level phenomenological mathematical model is presented. Different ranges of the rate constants employed are studied.
5	Allosteric approach to bone turnover model	The approach to implement the allosteric mechanism to a cell-level model is described and numerical experiment results are presented.
6	Optimal control approach to the regulation of bone remodelling	Dynamic optimal control approach to the control of bone remodelling is presented.
7	Conclusions and Further Work	The conclusions, recommendations and further work arising from results of Chapters 4-6 are presented.

Table 1.1 Overview of the thesis

2 Bone tissue resorption and formation

2.1 Bone tissue remodelling

Bone is a tissue with a unique mechanism of regeneration (commonly referred to as remodelling or turnover). It is one of the simplest examples of tissue regenerating processes in animals and so the study of it could help to form a foundation for understanding more sophisticated metabolic and cellular cycles in the body. However, it should be said that the bone remodelling process and skeletal growth are quite different processes.

2.2 Basic multicellular unit (BMU)

The BMU can be regarded as a team of cells, which are active in bone remodelling. The BMU is the active element of bone tissue, which over a period of time results in the local resorption and rebuilding of the bone tissue. This is referred to as remodelling. It is probably one of the simplest tissues due to the limited variety (only two types) of active cells which participate in bone regeneration. The generally accepted concept of the Basic Multicellular Unit (BMU) is that it is comprised of two cell types; osteoclasts and osteoblasts (Compston, 2002). In addition to these "active" cells BMU also contains the active mesenchymal cells and capillary loops. The size of a BMU is 0.05-0.1 mm^3 and an adult organism, under normal physiological conditions, 10^5-10^6 BMU function simultaneously.

2.2.1 Osteoclasts

Osteoclasts are multinucleous large bone tissue cells that are specialised microphages (Blair et al., 2008). Their main function is tissue resorption. Osteoclasts are only present in a small lacunes (cavities) on the surface of bone during the bone demineralisation/resorption phase. Osteoclasts are formed by the union of several mononucleosis originators of the monocytes family which originate from stem cells in the bone marrow. Osteoclasts work together with osteoblasts to resorb and remodel the bone in a controlled process of reconstruction. Bone remodelling is finely balanced process, which provides bone with the

properties of stiffness and elasticity. For a variety of reasons it is possible for resorption of the bone to become predominant and this can lead to many types of bone disorders.

The multistage process of osteoclast differentiation and maturation is triggering by integrin and is then controlled by many chemical signals, including receptor activator for nuclear factor κ B ligand (RANKL), macrophage colony-stimulating factor (M-CSF), and Osteoprotegerin (OPG), Blair et al. (2007). Stem cells and osteoblasts secrete RANKL and M-CSF. This process can be activated by Parathyroid hormone (PTH) and inhibited by OPG. RANKL and M-CSF interacts with the correspondent receptor on the membrane of precursor cells (a common precursor for both osteoclasts and monocytes-monofags) and triggers cell differentiation in favour of osteoclasts. This process can be inhibited by OPG.

Differentiated osteoclasts accumulate on the bone surface to form a cytoskeleton which enables a resorption cavity (microspace between the osteoclasts and bone tissue) to develop. This process involves a protein, integrin avb3. The osteoclast layer within the cavity forms folds and as a result the resorption surface is significantly enlarged. The media inside of the resorption cavity is acidic due to the addition of protons. The intercellular pH of osteoclasts is sustained by HCO^{3-}/Cl^{-} interchange across the antiresorptive membrane. The HCO^{3-} ions move from the cell in extracellular space and ions Cl^{-} comes from extracellular space into the osteoclast cytoplasm. Cl^{-} ions are secreted by means of ionic canals within the folded osteoclast membrane. As a result of this processes the pH of the resorptive cavity drops to about 4.5. This acidic environment creates conditions for resorption of the mineral part of the bone. Degradation of the organic component of bone occurs due to the presence of cathepsin A, an enzyme that is synthesising and secreting in the resorption cavity by osteoclasts.

2.2.2 Osteoblasts

Osteoblasts are mononuclear cells which play a principal role in the process of bone remodelling by the formation of new bone following tissue resorption by osteoclast activity.

Osteoblasts are located on internal and external bone surfaces in close proximity to intensive bone formation (2-8% of the total bone surface). Together with osteoclasts, they form the so-called Basic Multicellular Units (BMU). Active osteoblasts are cubic or cylindrical shaped cells having minute processes (typically 5nm wide and about few dosens nm long). The main function of osteoblasts is the creation of the organic extracellular bone matrix, synthesis of extracellular bone material and participation in osteoid creation and its subsequent mineralization.

Osteoblasts originate from mesenchymal cells. The following stages of osteoblasts development are indicated: proto-osteoblast proliferation, maturation and differentiation. Osteoprogenitors (flat, plane cells) secrete growth transforming factors (transforming growth factor- β, TGF- β, TGF-beta). These factors trigger osteoblasts proliferation. Proliferation is accelerated by the osteoblastic protein osteopontin (Hashimoto et al. 2003). Proliferating osteoblasts synthesise the main protein component of the extracellular matrix (collagen type I) and also proteins which stimulate cell proliferation (histons, c-fos-protooncogen, c-myc-protooncogen).

Maturating osteoblasts adopt a cubic shape and secrete alkaline phosphotase, a protein that participates in osteoid mineralisation. At the mineralization phase osteoblasts produce osteocalcin which is the second main protein of bone tissue.

The main part (~3 quarters) of osteoblasts (Jilka et al., 1998) die by programmed (preordained) apoptosis. The remaining cells transform into two other types of cells in bone tissue; lining cells which form the mono-layer of cells that line the external and internal bone surfaces and osteocytes which are the bone cells that form the 3D lattice in the bone tissue. Lining cells are also called as mesenchymal bone cells or osteogenic cells.

Differentiation and osteoblasts activity is controlled by a number of hormonal and chemical signals of an autocrine (endogenous) and paracrine (exogenous) nature (Yamaguchi et al., 2000). In order to recognise and respond to these signals osteoblasts have the number of receptors on their membrane. The binding of these signal ligands to the receptors activate

the transmission of the signals which finally reach the cell nuclei. The osteoblasts nuclei consequently develop further regulatory signals for controlling the metabolic processes. Such hormonal signal messengers are, for example, estrogens and parathyroid hormone. Others local factors (for example growth factors, necrosis factors etc.) also activity participate in the regulation of osteoblasts activity. By coordination with the other cells, through many levels of regulation, osteoblasts provide the basic function of bone remodelling.

2.2.3 Osteocytes

The primary function of osteocytes is to trigger a molecular indicator when bone tissue is damaged, through for instance injury (Burr and Martin, 1993; Vatsa et al., 2007). The branch like structure of osteocytes creates a functional syncytium (network) inside the bone tissue (see Colopy et al. 2004; You et al., 2004). Depending on the condition of the bone tissue locally (at rest or remodelling) the syncytium also includes a large number of lining cells. The precise mechanism of osteocyte operation is a subject of intense debate but it is clear that they provide a signal for osteoclast activity to resorb of the damaged areas of bone, followed by subsequent tissue rebuilding by osteoblasts to generate healthy remodelled bone.

2.2.4 Lining cells

Lining cells are osteoblastic cells that transform into a layer of cells on the surface of the bone. A lining cell is an inactive post-proliferated cell that covers the surfaces of the bone tissue which are not undergoing resorption or formation. Lining cells are results of the transformation of osteoblasts to form “flat” cells that cover about 70-80% of total bone surface in adult skeleton. These cells form a “hematocellular” barrier on the bone.

Observations indicate that these cells can be reactivated into active osteoblastic cells when required, through signalling from the osteocytes. It is suggested that these cells participate in bone remodelling by synthesis and emission of cytokines and other intermediates, which perform the signalling control and activate osteoclasts. Lining cells

cooperate with osteocytes, which the syncytium produce, and perform control signals, which are proportional to the mechanical loading. It has been shown that osteocytes can send inhibition signal to osteoblasts to decrease the rate of bone formation.

2.2.5 Bone remodelling regulation from a phenomenological cellular perspective

Regulation of bone tissue remodelling depends on local factors like cytokines (paracrine and autocrine), growth factors, mechanical loading, nitric oxide and intercellular communication (Troen, 2003). BMU endocrine regulation takes place as a result of hormones and insulin, secreted by system of glands, and acting upon receptors on cellular membranes of osteocells. BMU function is remodelling of bone tissue by highly coordinated activity of osteoclasts and osteoblasts. This cellular construction activity takes place over a relatively long time period. The entire cycle of resorption and bone rebuilding may take several months to complete.

2.2.5.1 Osteoclasts

The large multi-nucleus cells, osteoclasts, are characterised by high levels of activity of tartrate-resistant alkaline phosphotase. In mature bone tissue about 0.1-1% of the surface area is populated by lacunes. 90-95% of these lacunes contain osteoclasts, engaged in active resorption; the remainder of the lacunes are empty. The area where the osteoclasts contact the bone tissue gives two regions, which are differentiated morphologically; a ruffled border and a much lighter edge. Under the action of enzymes and hydrogen ions secreted by osteoclasts the bone matrix is dissolved and disintegrates.

2.2.5.2 Osteoblasts

Active osteoblasts form osteoid plates, along newly formed bone tissue, by forming collagen fibres and proteoglicans (major component of the animal extracellular matrix) which the osteoblasts synthesise. In the formation zone there are about 300-400 osteoblasts. In a

period of 8 to 9 days they form a layer of osteoid (non-mineralised matrix) about 12µm deep. After about 12 days of osteoid maturation the mineralization phase starts. Around 10% of osteoblasts transforms into osteocytes and are integrated into the mineralised matrix. The remainder of the osteoblasts become inactive state and are left on the surface of the newly formed bone, forming the hematocellular barrier of flat lining cells. The active life of osteoblasts is approximately 2 to 3 weeks.

2.2.5.3 Osteocytes

Osteocytes are localised in lacunes in the mineralised matrix of the bone. Every cell is in contact (in communication) with neighbouring cells by means of a number of processes in the bone canals (canaliculus). Osteocytes in normal conditions provide inter-tissue transport of resources, minerals and products of metabolism and participate in coordination/control of the activity of all osteocells. Cell-cell communications between all three types of osteocells (osteoclasts, osteoblasts, osteocytes) plays an important role in the control of bone turnover. Well-known that the gap junctions, transmembrane channels are important mechanisms of this communication (Simon and Goodenough et al., 1998; Civitelli, 2008).

Recently several authors have highlighted the importance of the level of osteocyte regulation, for example, the role of osteocyte apoptosis as a part of the mechanotransduction control mechanism (Noble, 2003; Taylor et al., 2003; Bonewald, 2004).

2.2.5.4 Histological/Cellular scheme of remodelling

Micro-damage or aging of bone tissue causes the release of molecular messengers and BMU is activated (damage signalling phase). Histologically, the shape of lining cells becomes cubic-like (originally flat). There are indications that osteocytes are also involved at the start of the remodelling process (Martin, 2000).

In response to the osteocyte signals the osteoclast recruitment phase commences. The osteoblast precursors start to synthesise messengers which interacts with the surface of

osteoclasts precursors. As a result these differentiate into mature multinucleous osteoclasts which develop the "ruffled border" and start to resorb bone tissue.

During the resorption phase mature osteoclasts resorb bone within the resorption cavity. At every separate bone remodelling site resorption lasts about two weeks. At the end of this process the remaining osteoclasts die by means of apoptosis.

In the osteoblast recruitment phase osteoblasts differentiate from bone marrow stromal cells. During the osteoid formation phase active osteoblasts fill the absorbed cavity forming the non-mineralised new tissue (osteoid). When the osteoid reaches a depth of about 6-12μm the mineralisation phase commences and the osteoblasts transform into new bone tissue, see a general scheme in Fig.2.2.1.

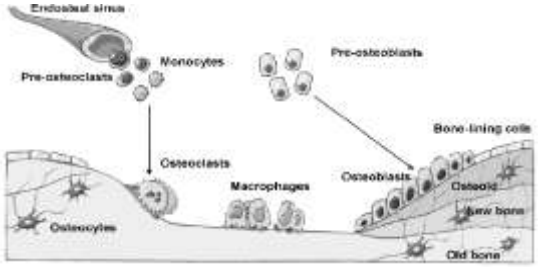

Fig.2.2.1. Diagrammatical overview of the bone remodelling process.

The remodelling process can be summarised by the following characteristics: life span of BMU – 6 to 9 months; bone volume replaced/formed by one BMU around 0.2 to 0.3 mm^3; life span of osteoclasts is about 12 to 15 days; life span of osteoblasts is around 10 weeks; the average interval between two episodes of remodelling in the same area of bone is typically 2 to 4 years; the average rate of bone tissue remodelling is approximately 10% per year (cortical bone ~ 5% a year, trabecular bone ~ 25% a year). These characteristics are very useful when considering/developing a model of bone remodelling.

It is recognised that the bone remodelling is a "coupled process" (see, for example, Hill P.A., Orth, 1998; Martin and Sims, 2005) when the bone resorption and bone formation is highly coordinated by some "coupling factors" involving paracrine, autocrine signals and cell-to-cell contacts. This process is highly organised, comprises the coordination of different

osteocells' types and local molecular agents. In this way osteoclasts regulate the recruitment and functionality of osteoblasts.

2.3 Regulatory factors of bone remodelling

2.3.1 Local growth factors

Growth factors (GF) and differentiation factors are polypeptides that exert multiple effects on target cells, including mitosis, gene expression, cell shape, polarisation and secretion (Govinden and Bhoola, 2003). These effects consequently depend on other factors of target cells such as cell-cell interaction, cell-matrix interaction and stage of maturation (differentiation). The growth factors that affect bone and bone cells are described in great detail in the literature, for example Heymann et al., 1998; Conover and Rosen 2002; Hurley et al., 2002; Rosen 2002. Particular attention is paid to growth factors which have shown similar effects in both in vitro and in vivo.

2.3.1.1 Insulin-like growth factors

IGF-1 and IGF-2 are one-chain polypeptides that have 70 and 67 amino acids respectively. The homology (similarity) of these two hormones is about 62% and they have about 50% identical amino acids to insulin (Denley et al., 2005). However, they have different antigens and are regulated in a different way. Each of these hormones has its own specific receptors (primarily IGF-IR) and binding proteins (IGFBPs), Martel-Pelletier et al., 1998; Rosen, 2000; Zofkova, 2003.

In vitro, osteoblasts produce these insulin-like growth factors and IGFBP-1-6 (Thomas *et al.*, 1999; Massicotte, 2006). The osteoblasts differentiation is stimulated by IGF-1. IGF-1 also endorses collagen production. This insulin-like growth factors protects bone matrix degradation (Tirapegui, 1999; Rosen, 2000; McQueeney et al., 2001; Smink et al., 2002; Zofkova, 2003; Oh and Chun, 2003; Meinel et al., 2003).

A decrease in circulating IGF-1 level in mice leads to a decline in longitudinal growth (Yakar et al., 2002). IGF-1 has a mild mitogenic effect on osteoblastic cells in a culture and stimulates the collagen type-1 production. Some research indicates that IGF-I stimulates replication by preosteoblasts, and new bone formation by osteoblasts (McCarthy and Centrella, 2001; Rosen, 2003). The production of IGF-1 in the liver and others organs is regulated by estrogens (McCarty, 2003).

All above indicates that IGF-1 is involved in osteogenesis and homeostasis of bone tissue; experiments conducted in-vivo in humans and some mammal's supports in-vitro data that IGF increases the level of bone turnover. However additional research is needed to complete its local micro-physiological role in bone remodelling.

2.3.1.2 TGFs (tumour growth factors)

TGFs are polypeptides containing about 400 amino acids. It is one of the main types of growth factors in the bone matrix, Mundy et al., 1995. In the cell culture the TGF-β effects are sometimes are called "multifunctional" because of the number of cellular and intercellular responses that it causes, including up-regulation of other growth factors (Massague, 1998; Lebman and Edmiston, 1999; Blobe et al., 2000; Massague and Wotton, 2000; Wu and Kumar, 2000). TGF-β is a potent growth inhibitor for a vast variety of cells. In the majority of cells types it inhibits proliferation, however, in some osteocells it up-regulates the mitosis (Yue and Mulder, 2001). In many cells, including osteoblasts, TGF-β increases collagen synthesis and the development of the intracellular matrix (Jaunberzins et al., 2000). It has been shown to have a positive influence on the synthesis of extracellular matrix in vitro (Wluka et al., 2001). TGF-β has a spectrum of effects, between them it is modulation of osteoclasts maturation, (Lari et al., 2007). In differentiated cells TGF-β blocks the phenotypical maturation, TGF-β1 inhibits osteoclasts differentiation (Lari et al., 2007).

Taking into account the different effects that TGF-β produces on bone tissue, is suggested that this growth factor plays a significant role in bone turnover and remodelling.

2.3.1.3 Bone morphogenic proteins

Bone morphogenic proteins (BMPs), with the exception of BMP1 are members of the TGF-β "superfamily" (30-40% homology), (Xiao, 2007). BMP1 is different, however, as this is a metalloprotease that metabolises procollagen I, II, and III. BMPs have been exploited (extracted and purified) due to their ability to induce ectopic osteogenesis after implantation into skin or into muscle. BMP is known as a dimeric polypeptide molecule, containing two chains. The chains have a 40-50% similarity of primary structure to that of TGF- β, Vaibhav et al., 2007. (Chen et al., 2004). Like TGF-β, these proteins are expressed during the development of bone tissue. BMP-2, BMP-4, and BMP-7 are considered to play an important roles in the bone remodelling control (Hogan, 1996; Wozney and Rosen, 1998; Sakou et al., 1999; Schmit et al., 1999; Reddi, 2001). In vitro spectrum of BMPs -2, -3, -4 and -7 up-regulates the exhibition of osteoblastic properties in osteocell derivatives Ji et al., 2000. As opposed to TGF-β, BMPs are rarely expressed and recently a number of studies have been undertaken to understand their physiological role in bone remodelling (Chen et al., 2004; Xiao, 2007). The differentiation of osteoblasts is strongly influenced by BMP from mesenchymal stem cells. BMP-2 is known as key mediator of osteoblast differentiation. In some animal models (Bax et al., 1999; Hekman et al., 1999; Southwood et al., 2004) and clinical trials (Johnson and Urist, 1998; Bulstra et al., 1999) it has been indicated that BMPs enhance fracture healing. BMP-4 promotes the osteogenic phenotype in vitro (Cho et al., 2003) and is expressed by differentiated osteocells at the site of fracture healing (Nakase et al., 1994; Cho et al., 2002). Localised delivery of growth factors is important method for bone healing following fractures (Luginbuehl et al., 2004). Though BMPs belong to the TGF-β superfamily, the effects of TGF-β are often the opposite to BMPs.

Control of the BMP signalling pathway is carried out by a complex array of receptors (BMPR) with inherent serine/threonine kinase activity (Yamashita et al., 1996; Miyazono, 1999; Harrison et al., 2004; Cao and Chen, 2005; Simeoni and Gurdon, 2007). BMPs affinity to receptors is significantly amplified when both receptors (type I and II) are located in close

proximity to one another. In the process of signal transduction the type I receptor initiates phosphorylation of specific intracellular proteins called Smads (Kloen et al., 2003).

2.3.1.4 Fibroblast growth factors

Fibroblast growth factors (FGFs) encompass at least twenty three known homological polypeptides (Ornitz, 2000) that contain 150-250 residuals which bind to and activate four transmembrane tyrosine kinase receptors FGFRs 1–4). FGFs have molecular weight between 2O–35 kDa. At different stages of development these peptides are expressed in number of tissues.

FGFs initiate the proliferation and differentiation of epithelial and mesenchymal cells (Nimmagadda, 2007). Some fibroblast growth factors initiate angiogenesis (Gerwins et al., 2000; Rennel et al., 2003). FGFs also stimulate wound healing and tissue repair.

In earlier research it has been revealed that FGFs have an important regulatory function in bone formation (Mayahara et al., 1993; Nakamura et al., 1995). More recent studies also indicate the involvement of FGFs in bone formation; formation of mesoderm (Okazaki et al., 1999; Montero et al., 2OOO; Kruithof et al., 2006), its expression in bone tissue at development, ossification (Delezoide et al., 1998), angiogenesis (new blood vessel growth from existing vessels), production of endothelial cells, macrophages and osteocells (Gerwins et al., 2000; Rennel et al., 2003).

Lazarus and coauthors have studied the expression of all known FGFs and FGFRs in the postnatal growth plateand conclude that FGF signaling is vital for endochondral bone formation, Lazarus et al., 2007. Other insight into the fibroblast growth factors one can find in reviews of Delrieu, 2000; Wang and McKeehan, 2003; Nugent and Iozzo, 2000. However, to understand the role of FGFs in bone remodelling and bone healing additional research is still needed.

There are several other growth factors that affect osteoblasts proliferation in-vitro, for example epidermal growth factor (EGF), (Chien et al., 2000; Herbst, 2004; Dreux et al.,

2006). Some hypotheses suggest that EGF indirectly effects sphingolipid singnaling and biosynthesis in osteoblasts, that play a role in intracellular calcium mobilization (Carpio et al., 2000). EGF affects both osteoclastic bone resorption and osteoblastic bone formation (Ibbotson et al., 1986). Recently, a number of other factors which have been studied less intensively have been found to play a role in bone remodelling, for example heparin–binding, EGF and salivary epidermal growth factor sEGF (Yucel-Lindberg and Brunius, 2006).

Osteocells also produce colony stimulation factors (CSFs), also referred to as hematopoietic growth factors, which regulate bone marrow production of cells of hematopoietic lines. CSF-1 (monocyte/macrophage CSF) plays a role in osteoblasts/osteoclasts interactions during the process of osteoclasts differentiation (Hershey and Fisher 2004). Multipotential colony-stimulating factor or IL-3 can also play role in osteoclasts genesis and interactions between bone tissue and bone marrow.

To conclude, many growth factors affect osteoblastic cell lineage in-vitro and some stimulate bone formation in vivo (FGF, CSF). Some of the factors are consecutively involved in fracture healing (trombocyte growth factor, FGF, TGF), Maniscalco et al., 2004. None of them is unique to bone tissue. A selective factor that can encourage tissue formation at the remodelling process, in the same way as erythropoetin stimulates erythropoiesis, has not been identified as yet.

2.3.2 Mediatory factors

2.3.2.1 Cytokines

Cytokines (lymphokines) are a group of polypeptides that are produced by white blood cells (lymphocytes) and participate in cell interactions at inflammation and other immune system reactions. Bone remodelling has many common characteristics with the inflammation process, including osteoclasts' interactions with microphages and osteoblasts' with fibroblasts. The production and response of lymphokines is similar to those for cytokines (e.g. interleukins). It is accepted that cytokines do not have any specialised cellular, tissue or

organ source and are produced by all cells. They have autocrine, paracrine and even systemic levels of cell communication. It has been shown that cytokines produced by one cell can induce or inhibit cytokines production in other cell. This suggests that these cytokines can consequently stimulate or inhibit synthesis of other cytokines. As a result, a complex network of possible interactions between cytokines and cells emerges, which appears as a cascade of interdependent reactions that produces substantial amount of different substances that have synergists and antagonists (Whitfield et al., 2002; Wozney, 2002).

Two well known interleukins IL-1α and IL-1β have a molecular weight of around 17.5 kD and share about 25% homology. They have similar activity; however have different effects in different systems. Interleukin IL-1 is synthesised by macrophages, however, that was found that IL-1 can be secreted by OBls (Manolagas, 1995). IL-1α and IL-1β are shown to be participated in the process of tissue resorption related to inflammation in rheumatoid arthritis. This bone loss is a major unresolved problem of rheumatoid arthritis (Nakamura and Jimi, 2006).

In a number of studies have shown that bone particles stimulate secretion of IL-1α and IL-1β from peripheral mononucleic blood cells and monocytes, extracted from patients with extrogen deficiency, also produce high level of these interleukins. This indicates that IL-1α and IL-1β can be involved in the development of postmenopausal osteoporosis (Silver et al., 1996; Teitelbaum, 2004).

1L-1, -6, and -11 directly increase the rate of osteoclast formation, development and activity (Manolagas, 1995; Troen, 2003). Earlier reports imply that IL-4 can be involved in development of a mineral content in osteoblastic-like cells in human (Ueno et al., 1992).

Interleukin IL-6 has a molecular weight 26 kDa (184 amino acids). It is secreted by macrophages, fibroblasts, as well as osteoblasts as a response to IL-1 and others factors (Johnson et al., 2000). In relation to bone tissue that was established the osteoblasts produce interleukin-6 to encourage osteoclast development. In addition IL-6 is known as an anti-apoptotic agent for osteoblastic cell types (Jilka et al., 1998). Studies suggest that IL-6, as

well as IL-1, are responsible intermediators for an increase in bone resorption. Earlier studies indicate PH-dependent hard tissue resorption is partly modulated by interleukin-6, through its production by osteoblasts (Lowik et al., 1989), as well as through estrogens deficiency (Kassem et al., 1996; Koka et al., 1998). However, some reports suggest that IL-6 is not an important factor for mediation of bone loss through estrogen deficiency (Zhang et al., 2004).

Palmqvist and coauthors studied human and the human soluble interleukin-6 regarding the effects on bone resorption. They did not find any effects, when these interleukins examined separately (Palmqvist et al., 2002). All above indicates that IL-6 is fairly strongly involved into bone resorption, however these data need to be more revised/verified in further experiments. Interleukin-6 binds to its receptor; receptor is linked to another glico-proteins which transmit the signal (Mariette, 2004).

Also there are reports that microgravity-induced alterations in the bone resorption process can be intermediated through a molecular mechanisms involved the interleukin-6 and prostaglandin E_2 interplay in osteoclast maturation and bone tissue resorption (Kumei et al., 1996).

Interleukin-8 is producing by macrophages, osteoblasts and stromal cells in bone marrow (Rougier et al., 1998) and has a number of similarities to FGF. It has a chemotaxic effect on endothelian cells and on some cells induces angiogenesis (Koch et al., 1992; Hu et al., 1993). There are reports that IL-8 inhibits bone resorption by osteoclasts in rats (Fuller et al., 1995) but stimulate osteoclasts to resorb bone in nude mice and could be considered as a possible target for medication to avoid tissue metastases (Singh et al., 2006).

The effect of other cytokines, which can be involved in bone remodelling have been less exhaustively studied, Li et al., 2006. IL-11 stimulates the proliferation of primitive stem cells (Schendel and Turner 1998; Heyman and Rousselle, 2000). There are reports that IL-18 inhibits osteoclast formation in vitro (Horwood et al., 1998).

2.3.2.2 Tumour necrosis factor

The action of TNF on bone and bone cells (Feng, 2005*)* is similar to that of IL-1. Like IL-1 the TNF-α production by peripheral mononuclear cells is higher in the blood of women with osteoporosis (Mundy, 1993; Mundy et al., 1995). TNF-α is recognized as a potent stimulator of bone resorption via signalling through TNFR1. TNF-α is produced by osteoblastic cells and can potently activate osteoclasts in bone marrow (Fuller et al., 2002).

2.3.2.3 LIFs

LIFs - leukemia inhibitory factors is a class cytokines, namely interleukin-6 and is one other factor in the activation of bone formation. LIF has molecular weight about 20 kDa (172 amino acids residuals) and is produced by a number of cells and affects several cell types. Its main role is to maintain embryonic stem cells in an undifferentiated state, for example, in mice, (Nichols et al., 1990). LIF affects osteoblastic cells by the receptors expressed in rat calvaria cell culture (Liu et al., 2002). As for many other cytokines, their actual role in bone tissue morphology and pathology is not well established.

2.3.2.4 Wnts

Wnts are soluble glycoproteins (family about 20) with a molecular mass of 39–46-kDa, which are postranslationally modified. They are rich in cysteine amino acid residuals and are modified by lipids to obtain the activity. There are known few signalling pathways, the so-called canonical pathway is the most studied. It sometimes is called as Wnt/beta-catenin pathway. Wnts trigger a series of intracellular molecular processes leading to osteoblast maturation, Bonewald and Johnson, 2008. Dysfunction in the Wnts signalling pathways leads to number of diseases, including high bone mass disorder, which is congenital in nature (Boyden et al., 2OO2; Little et al., 2OO2, Westendorf et al., 2OO4, Shi et al., 2OO7). The expression of osteoblast markers, collagen type I and osteocalcin seems are not affected by Wnts (Rawadi et al., 2003). In several skeletal mass disorders, gene mutation is responsible for Wnt production and causes severe changes in bone density, Westendorf et al., 2004. Wnts-dependent pathway is the major way of regulation of osteoblastogenesis. In the

same time there are number of molecular factors which interact with this pathway effecting control of bone remodelling process. Sclerostin, one of the key regulatory factors expressed by osteocytes, is antagonistic to bone formation by inhibiting so-called canonical Wnts' signalling pathway. Sclerostin production by Oct is inhibited by mechanical stress; see Lin et al., 2009. Dickkopf-1 (Dkk-1) is an inhibitor of Wnt, it plays important role affecting the Wnts' signalling pathway, Li et al., 2006. It is a factor that restrains of Obls' and cementobalsts differentiation, Nemoto et al., 2009. DKK-1 inhibits the development of oestrogen deficiency on RANKL expression and Ocl differentiation, Wang et al., 2007. An intracellular protein β-catenin (~90kDa) is a molecular constituent involved in Wnts signalling. Recent studies indicate important role of combined Wnt/ catenin regulation in modulation bone homeostasis, see article Kramer et al., 2010 and its references. There are suggestions that β-catenin can take part indirectly in regulation of Octs, which are implicated in Ocl's control, Kneissel, 2011. Glycogen synthase kinase-3 (GSK-3) participates in phosphorylation of β-catenin and block Wnt's signalling pathway, Kapadia et al., 2005. In some cases of Wnt signalling, when the activity of GSK-3 is suppressed, beta-catenin is accumulating and it modulates target Wnts transcriptions, Wang et al., 2009.

2.3.3 Eicosanoids

Eicosanoids are polyunsaturated fat acids that are derivatives of arachidonic acid. There are four known families of eicosanoids - the prostaglandins, prostacyclins, the thromboxanes and the leukotrienes, from which prostaglandins play important function in control of bone turnover.

2.3.3.1 Prostaglandins

Prostaglandins (PGs) participate in the inflammatory process and affect the resorption and formation of bone tissue in vivo and osteocells in vitro. Early in vivo research indicates that PGs synthesis inhibitors, such as indometacin, decrease bone resorption by reducing

osteoclastic activity (Lerner, 1982). Prostaglandin PGE2 is a potent inducer of cortical and trabecular bone formation in humans and animals **(**Machwate et al., 2001). Recent studies report that PGE2 interacts with the IL-6 signalling pathways during osteoclastogenesis and appears as an effect on the OPG/RANKL/RANK system (Liu et al., 2006). In vitro, primary PGE2 is secreted by osteoblasts cell lineage and has an effect as on osteoblastic as well as osteoclastic cells.

Yoshida et al. (2002), reported that the prostaglandins receptor EP4 activation induces bone remodelling in vivo and that EP4-selective drugs may be beneficial in humans with osteoporosis. PGE and PGE2 are produced by osteoblastic cell lineage. The affect of PGE2 is mediated by subfamilies of G-protein-coupled plasma-membrane receptors, that increase of the activity of adenylate cyclase, which leads to the increase of intracellular cAMP and Ca^{2+} (Kobayashi et al., 2005). Some of these receptors are expressed as on osteoblasts) as well as on osteoclasts (Wang et al., 2005). It was also shown that PGE2 is similar to PTH in that it increases intracellular calcium in osteoblastic cells. The observed affects of PGE on osteocells in vitro and in vivo indicates that these local factors participate in bone tissue metabolism. It is possible that they have a role when tissue react to mechanical stimuli, fracture healing and within normal bone remodelling and the inflammatory process.

Finally, multiple observed PGE effects on osteocells in vitro and in vivo indicates about participation of these local factors in bone tissue metabolism. They, possibly also play a role in the response on mechanical load, fracture reparation and at normal bone remodelling and at inflammatory process also.

2.3.4 Local growth factors in scaffold surface modification

2.3.4.1 Role of local factors in BMU functioning

The complete spectrum of bioactive substances that are involved in bone remodelling and regeneration processes is not limited to local factors that are mentioned in above section.

However, the number of already accepted schemes of the remodelling process (like RANK/RANKL/OPG) probably creates the core of these regulation pathways.

2.3.2.2 Localised delivery

Meinel et al., studied the effects of an insulin like growth factor I delivery system on fracture healing. They found reduced inflammation in presence of IGF I when molecule was physically contained inside a microsphere made from poly(lactide-co-glycolide). The effects found of this medication was linked to significant, progressive, and dose-dependent bone tissue regeneration, Meinel et al., 2003.

2.3.4.3 Cell enhancement

Recently one can see significant growth in a number of studies on the cell enhancement implemented by mentioned above biological factors. These factors, in particular BMP, FGF, PDGF, IGFs have been studied in relation to application in bone tissue regeneration and repair, Canalis 1980; Bax et al., 1999; Fakhry et al., 2005. Some researchers have been studed the incorporation of growth factors to stimulate osteoblasts/osteoclasts into scaffold (Kanczler and Oreffo, 2008).

2.4 Systemic factors - hormones

Osteoclasts, osteoblasts and their precursors are regulated by a number of systemic factors, including hormones like parathyroid hormone, vitamin D, calcitonin, glucocorticoids, sex hormones (steroids, estrogens, androgens) that are heavily involved in calcium homeostasis.

2.4.1 Parathyroid hormone

Parathyroid hormone (PTH), the hormone of bone tissue resorption, is a polypeptide containing 84 amino acid residuals and is an important systemic regulator of skeletal growth

(Swarthout et al., 2OO2; Parfit, 2003; Qin et al., 2OO4; Shao et al., 2OO6). PTH acts by binding to the type 1 PTH receptor (Mannstadt et al., 1999). This receptor belongs to a class II G protein-coupled receptors. In vivo PTH increases the number and activity of osteoclasts, leading to a change in osteoblast shape and an emergence of "ruffled border" in osteoclasts (King et al., 1978; Feister et al., 2000). PTH stimulates calcium release from bone tissue and increase Ca^{+2} concentrations in blood in vivo (Poole and Reeve, 2005). That was shown that PTH stimulates osteoclasts formation in bone marrow culture (Okada et al., 2003). It seems that PTH affects osteoclasts in an indirect way since PTH receptors are located on osteoblasts but are not found on the surface of osteoclasts (Potts and Jappner, 1997; Hodsman et al., 1999). Recently Yamauchi and coauthors studied the expression of PTH receptors (PTH1R) using long-term cultures of foetal rat calvaria (RC) when Obl cells maturation (Yamauchi et al., 2006). They concluded that "PTH receptor expression changes during the osteoblastic lineage and that the highest number of receptors occurs at the differentiated stage prior to osteoblast maturation".

Parathyroid hormone effects resorption of bone not only by increase of osteoclasts activity but also affects others osteogenic cells that have parathyroid hormone receptors. Parathyroid hormone stimulates secretion of collagenase by lining cells. This enzyme dissolves the protective layer of the bone matrix ond prepares its surface for osteoclastic resorption. Few pathways of effects OBLs on OCLs resorbtion are discussed in the literature (Wu and Kumar, 2000). For first is that PTH can change overall form of osteoblastic layer, Rodan and Martin, 2006. Such a changes can be observed in lining cells at appearance of Ocl near to bone matrix (Dobnig and Turner 1996). Second, OBls synthesise neutral collagenase and PTH stimulates secretion of this enzyme. Collagenase dissolves protective matrix layer, which cover mineralised tissue and prepares bone surface for osteoclastic resorption. Third way- the OBl participation in resorption is linked to its possible involvement into OCl differentiation.

Parathyroid hormone effects also metabolic activity of osteoblastic cells at least in culture. Parathyroid hormone decreases mRNA and the protein levels of collagen type I (Feister et al., 2000), it modulates protein level or mRNA (Seto et al., l999) as well as the level of others osteoblastic markers. It was shown in vivo that in result of all these processes the bone formation decreases. PTH has strong effect on formation of sponge bone as in rats as well in humans when dosage is lower. Cell targets for anabolic PTH effect possibly differ from those that mediate PTH stimulation of bone resorption. As it is well known the majority of PHT effects on bone tissue are anabolic (Martin, 2004). Even some progress in study of mechanisms of the bone formation is done (Jones et al., 2006) the stimulation by PHT hormone is not yet fully understood.

Parathyroid hormone stimulates production of IGF in osteoblastic cells, however these effects cannot be repeated by administering exogenic IGF-1 (McCarthy et al., 1991).

It was reported that the pathway of PTH signal transmission/transduction includes adenylate cyclase activation/stimulation. It was also shown that PTH co-increases the level of intracellular calcium in osteoblastic cells, Dixon et al., 1995. Jilka et al., reported about a significant increase in population of Obl in bone tisue, its remodelling rate and bone mineral density under parathyroid hormone administration (Jilka et al., 1999).

Full set of conditions of PTH anabolic effect on bone are multiple, and still not clearly understood. Jilka, 2007. However, involvement in this RANKL/OPG regulatory pathway is necessary to PTH anabolic effect, Martin, 2004. Mechanisms, which give the PTH an anabolic effect to bone are not clear, some authors stress the important role of vascular system in this effect, Taylor et al., 2010.

2.4.2 Calcitonin

Hormone is a peptide containing about 30 amino acids. In bone tissue it targets osteoclasts. It is secreted by C-cells of the thyroid (parafollicular cells) as a response to increasing levels of calcium in the blood stream (opposing the effects of PTH). It maintains

calcium homeostasis and conserves calcium, obtained from food, within the skeleton (Zaidi et al., 2002; Elefteriou, 2008).

The use of calcitonin with therapeutic purposes increases BMD in elderly women (Body, 2002). Some authors reported positive effect of the calcitonin administration on BMD in the spine (Kaskani et al., 2005) and vertebral fractures (Ishida and Kawai, 2004).

At the cellular level calcitonin is a very powerful direct inhibitor of osteoclasts' activity and their formation (Chambers and Magnus, 1982; Takahashi et al., 1988; Quinn et al., 1999). In situ calcitonin causes the disappearance of osteoclasts' ruffled border after about half an hour after its administration (Wada et al., 1995, 1996; Ikegame et al., 2004). In vitro calcitonin causes the OCl crumple at concentration about 10^{-12} M and inhibition of cavity formation in bone by OCls (Wada et al., 1995, 1996). Rat OCls have large amount of calcitonin receptors, counted by hundred of thousands on one cell (Nicholson et al., 1986). Several osteoclast calcitonin receptors have subsequently been cloned and sequenced since described by Goldring et al., 1993. A number of isoforms of this receptor has been identified (Beaudreuil et al., 2004). The role of integrins in calcitonin receptor signalling in OCls functions has been suggested (Duong at al., 2002).

It is known that calcitonin stimulates cAMP accumulation in target cells and majority of calcitonin effects can be modelled with the help of cAMP or stimulating cAMP agents like prostaglandin E2 (Vignery and McCarthy 1996). Also it was shown, that in the calcitonin transmition process the calcium signalling is involved. Calcitonin inhibits osteoclasts formation from precursors in bone marrow and mRNA expression in isolated osteoclasts (Suzuki et al., 1996). There are indications that calcitonin can also affect osteoblastic cells.

2.4.3 Vitamin D

Vitamin D is usually known as a group of hormones and their metabolites having two main active forms D_2 (ergocalciferol) and D_3 (cholecalciferol), Jones, 2002. Its active forms play a critical role in Ca^{2+} homeostasis by regulating its absorption, bone tissue resorption,

osteocell differentiation and PTH secretion (Anderson et al., 2003; Kochupillai, 2008). Active metabolites of vitamin D increase Ca^{2+} assimilation. The moving of these ions through intestines cells is an active process. In bone formation osteoblasts use calcium phosphate for formation of new tissue. Osteocells have receptors to vitamin D and are responsible for the affect of this hormone in vitro, but the direct role of vitamin D on bone tissue in vivo is not fully understood (Kochupillai, 2008). It is suggested that vitamin D indirectly affects bone formation by protecting osteoblasts against apoptosis or causing the development of preosteoblastic cells into osteoblasts (Duque et al., 2004). Lack of vitamin D creates defects in bone mineralization (Omdahl et al., 2002). Vitamin D deficiency results in high levels of osteoblast apoptosis leading to a significant decrease in the population of Obl (Priestwood and Duque, 2003).

In vitro vitamin D has an expressed and steady effect on osteoblastic cells; it increases activity of alkaline phosphatase, concentration of Ca^{2+}, affected by fibroblast growth factors-2 and fibroblast growth factors-β in osteoblasts (Bosetti et al., 2007); vitamin D reduces mineralization, with additive inhibitory effects on viable cell number in vitro (Shi et al., 2007). Vitamin D3 increases osteocalcin secretion in vivo (Martinez et al., 2001) and other osteoblastic marker – osteopontin, Jono et al., 1998. Summarisingly, Atkins et al., 2007, suggested the control of autocrine and paracrine mechanisms over vitamin D3 metabolism influence on the osteoblast functions. Vitamin D and its derivatives as 1,25-dihydroxy vitamin D, are used in treatment of osteoporosis (Kelman and Lane 2005; Epstein 2006).

2.4.4 Steroid hormones

Estrogens, corticosteroids androgens, progesterone and similar hormones to vitamin D, thyroid hormone and retinoids, interact by means of structurally homologous nuclear receptors, that creates a subfamily of the steroid/thyroid receptor superfamily. Steroid hormones control bone remodelling in a number of ways. They can interact directly on the osteoclasts (Troen, 2003) and osteoblasts, as well as affecting the differentiation/proliferation

of cells. They can also regulate the expression of genes which target osteoblasts, for example alkaline phosphotase, osteopontin and osteocalcin. The regulation of the calcification of the matrix and cell migration by steroid hormones is also described in the literature.

2.4.4.1 Corticosteroids/Glucocorticoids

The action of glucocorticoids is species-specific. In humans glucocorticoids increase bone-resorption and decrease bone formation, resulting in bone mass losses. A surplus of glucocorticoids, under prolonged steroidal therapy or Cushing syndrome, a fall in BMD and to osteopenia that in turn leads to osteoporosis in 30-50% of cases. In rats glucocorticoids increase the differentiation of osteoblasts and their precursors, enhancing the ability of these cells to create the mineralised matrix. Some of these effects are accomplished indirectly via BMP-6. IGFs and their binding proteins (IGFBPs) are very important for bone development and can participate in the regulation of glucocorticoids in osteoblasts. Glucocorticoids influence the synthesis of collagen and result in osteoblast-specific lowering of osteocell adhesion of collagen type I and fibronectine. Glucocorticoids decrease bone resorption in rats by inducing apoptosis of osteoclasts. In mice glucocorticoids stimulate bone resorption and osteoclast formation but depress osteoblast activity by inhibiting proliferation and differentiation of osteoblast precursors.

2.4.4.2 Mineralocorticoids

Mineralocorticoids (group of steroid hormones produced by the adrenal cortex) and their receptors are found in osteoblasts. Receptors have been found in the chondrocytes of growing ribs and long bones. These receptors can bind these types of glucocorticoids.

2.4.4.3 Sex steroids, estrogens

Estrogens are highly important for bone tissue development and maturation and maintaining the skeleton in a steady state. The link between estrogen deficiency and bone

disorders such as osteoporosis was first proposed by Albright (Albright et al., 1940). However their direct action on bone tissue is still under discussion. There are strong indications that estrogens influence the osteoblasts and osteoclasts (Troen, 2003; D'Amelio et al., 2008). Number of studies indicates that estrogens can slow down bone losses in patients with osteoporosis.

Estrogens regulate bone remodelling by modulation cytokines production and growth factors in bone marrow and osteocells. Osteogenic induction of osteoclast differentiation is promoted by osteoblasts and depends on the presence of the IL-6 receptors on osteoblast membranes. It seems that the protective effect of estrogens is linked to the apoptosis regulation of osteocells. It induces apoptosis of isolated osteoclasts.

It is known that the estrogens receptors ERα and ERβ are two different proteins coded by two different genes from two different chromosomes (Sharma and Thakur, 2006). The expression of isoforms, it seems, differentially controls in the OBl's differentiation. These two proteins are found in grows plates (laminae) in rats, mice and humans.

The acceleration of a decrease in BMD can be linked to the change in concentration of oestrogen and Ocls' function (Marie, 1999).

2.4.4.4 Androgens

Androgens are male hormones, belong to C_{19} steroids, which control functioning of the male genital system. Receptors for these steroids are found in all three types of bone cells (Mizuno et al. 1994; Notelovitz, 2002). The androgens protect the bone tissue content by effecting the interleukin-6 thynthesis (Manolagas, 1995). It is known that androgens stimulate the proliferation and differentiation of osteoblasts and their precursors increase the activity of androgen receptors (AR). Observed low level of androgen in males can cause the development of activity of Ocls and decrease in BMD (Huber et al., 2001). The androgens receptors are found as in osteoblasts as in osteoclast-like cells (Van der Schueren and Bouillon, 1995). In humans these receptors are found in the developing bones in chondrocytes

as well as osteoblasts and to a lesser extent in osteocytes and mononucleous cells in the bone marrow. It is also known that androgens can be transformed into extrogens by aromatase, an enzyme from the cytochrome 450 superfamily (Miki et al., 2007).

2.5 Extracellular matrix

It thought that the interaction of osteocells with the extracellular matrix can be an significant factor in of bone tissue. Matrix molecules that lie under cells-precursors can transmit important local signals for the cells that migrate into this local area. It is suggested that in the process of bone remodelling the surface that needs to be remodelled may contain molecular instructions for osteoclast precursors that migrate into this area. Moreover, the area after osteoclast resorption, where tissue formation starts, may also contain specific molecules that instruct osteoblasts. For example, osteoclasts as well as osteoblasts synthesise and secrete osteopontin, ligands for integrins, (Denhardt and Noda, 1998; Giachelli and Steitz, 2000) that can act as receptor linkage for transmission of information signals from the extracellular matrix into the cells.

Osteoclast adhesion is predominantly made available by integrins (Nakamura et al., 1999). Integrins are the large superfamily of receptors, that are linked to the cell surfaces, that contains α-(120-180kDa) and β-(90-110kDa) subunits. Integrins are vital for the cell sensing capacities of mechanical alterations and intracellular stress transmation to the call environment. There are about eighteen α- and eight β- units that can bind in different combinations (Sheppard, 2000; Hynes, 2002; Luo et al., 2007; Wipff and Hinz 2008). In Ocls higher is the level of αvβ3 integreens (the αvβ3 integrin is the most important in case of OCls adhesion, Nakamura et al., 1999), which are receptors for vitronectin, as well as bounded osteopontin, bone sealoprotein and fibronectin, that has lower affinity. Rat and human Obls express the receptor binding collagen and receptor binding fibronectin (Wipff and Hinz, 2008). Human Obls also express range of chains providing receptor spectrum, needed for interaction of collagen and lamipin (α_2 β_1) or collagen, fibronectin and laminin ($\alpha_3\beta_1$). The rat

Obls contain also β_5- and lower level of α_v chains. $\alpha_v\beta_5$- chains also play role of receptor of vitonectin (Wipff and Hinz, 2008). However the role of extracellular matrix in regulation of BMU activity is quite poor studied. (Gronthos et al., 2001; Mao and Schwarzbauer, 2005).

2.6 Bone multicellular unit regulation

2.6.1 The local and systems factors in BMU regulation

In the BMU activation phase factors, including PTH, PGE, TNF, IL-1, IL-6, NO, 1,25-dihydroxy form of vitamin D up-regulate the process. As a result of micro-cracks there is a release of cytokines and other factors which initiate BMU activity. System factor such as estrogens down regulate the activation phase.

Osteoclasts recruitment is up-regulated by RANKL and down regulated by OPG and granulocyte M-CSF. In this stage osteoblasts precursors start to synthesise RANKL which interacts with RANK on the surface of osteoclasts precursors. As a result these differentiate into mature multinucleus osteoclasts which develop the "ruffled border" and start to resorb bone tissue.

The resorption phase is up-regulated by integrins and some interleukins and down-regulated by estrogens, calcitonin, interferon, TGFs (Watkins and Seifert, 2000). During this phase mature osteoclasts resorb bone. Osteoclast activity is stimulated by cytokines: interleukins-1, TNFα, RANKL, interleukin-6, interleukins-11, M-CSF, GM-CSF.

In the osteoblasts recruitment phase osteoblasts differentiate from bone marrow stromal cells. Transcription factor Runx2(Cbfa1) is necessary for their differentiation (Stein et al., 1996). Wnts, BMPs, PTH, TGF-β also play an important role by up-regulating this process. There are indications that osteoblast differentiation is down regulated by leptin (Magretic et al., 2002).

During the osteoid formation phase active osteoblasts fill the absorbed cavity forming the osteoid. They synthesise growth factors, osteopontin and osteocalcin. TGFβ, BMPs up-regulate osteoid formation this process whilst glucocorticoids down regulate it.

When the osteoid layer reaches about 6µm the osteoblasts commence mineralisation. The mineralisation phase is up-regulated by calcium and phosphates and down-regulated by pyrophosphates.

2.6.2 RANKL/RANK/OPG in regulation of bone remodelling

RANKL (the receptor activator of NF-KappaB Ligand) is a TNF family member. This local factor is also known as OPGL, ODF, TRANCE. It binds to RANK receptors on the hematopoietic osteoclasts precursor surface and stimulates its differentiation. It also prompts the inactive osteoclasts to become active and undertake bone resorption. RANKL inhibits apoptosis of osteoclasts (Fuller et al., 1998; Lacey et al., 1998; Burrgess et al., 1999).

When injected, RANKL induces hypercalcemia, wich leads to observed bone loss, with more maturated OCls and increased tissue resorption surface and without an observed change in OCl number (Lacey et al., 1998). Loss of RANKL expression induces osteopetroses.

RANK is a member of family of receptors known as tumour necrosis factor (known also as ODAR). It is expressed on the surface of hematopoietic osteoclasts precursor cells. It is a receptor for RANKL on osteoblastic cells. Over expression of soluble RANK mimics osteopetrosis.

OPG (known as OCIF, TR-1, FDCR-1) is also an element of family of receptors known as TNFR superfamily. The soluble decoy macromolecule OPG is a receptor for RANKL and it is produced by osteoblastic cells. OPG inhibits RANKL binding to RANK, blocking osteoclasts formation and consequently increasing bone mass (Simonet et al., 1997). OPG protects bone tissue by down-regulating osteoclastogenesis and promoting osteoclast apoptosis (Romas et al., 2002). Its over expression induces osteopetrosis, and its loss of expression induces osteoporosis.

OPG and RANKL are principal regulators of bone tissue resorption (Kostenuik, 2005), the balance between RANKL and OPG production is central to the regulation of

resorptive activity of osteoclasts. RANK, RANKL, OPG being the integrating molecular intermediates of many others bone remodelling mediators. It is known that oestrogen modulates RANKL and OPG and it is a major pathway for action of this mediator. RANK, RANKL, OPG play the key role in formation, differentiation and activity of Osteoclasts.

2.7 Some bone pathologies related to the bone tissue remodelling disorders

Considered above short overview of data on bone tissue physiology illustrates that bone is a dynamical tissue with a large number of different regulatory mechanisms. Bone is also an important participant/player of mineral exchange. The lasting for all life processes of active formation and remodelling of bone tissue is an integral characteristic of metabolic activity of this tissue. These processes from one hand side are the important mechanisms of mineral homeostasis, and from other hand side they provide structural-and-mechanical adaptation to changing conditions. Also very important are situations when these functioning conditions cannot be fully provided by the bone tissue because of some metabolic disorders or even some damages to tissue – fractures. Then the balance between the physiological-and-metabolic issues and structural-and-mechanical becomes even more important.

2.7.1 Osteoporosis

Osteoporosis usually is known as the overal losses of bone tissue that lead the through substantial weakneses of mechanical properties. At the age of about thirty of life the peak of bone mass is achieved. Later it is a steady loss in BMD. This loss can be linked to an increase in the activity of osteoclastic cells, see for example, Priestwood et al., 2003. Moreover, usually further acceleration in decline of bone tissue density is detected after age of ~70. This reduction is usually related to the fuctioning of osteoblasts. Based on histomorphometric analysis osteoporosis usually can be defined as loss of bone larger than about 1/10 of (Kanis et al., 1994).

Some suggestions are that the cytokine's dependent osteoclastogenesis activation is the basis of osteoporosis development. Overal bone tissue loss is caused by this activation (Komeda and Takeuchi, 2003). The observed disbalance in the RANKL/RANK/OPG regulatory pathway plays important role in this kind of disorder, Jilka, 2003. T-lymphocytes activation leads to hyperexpression of RANKL in different cells, including Ocls and to decrease of OPG production. It is known that RANKL belongs to the superfamily of tumour necrosis factors (TNF) and is a powerful mediator of bone resorption. At the RANKL interaction with its receptor RANK, it stimulates differentiation and activity of osteoclasts as well as production of cytokines IL-6 and IL-11 and T-lymphocytes proliferation. OPG is known as decoy soluble receptor of RANKL, inhibits osteoclastogenesis, competitively inhibiting RANKL-RANK binding. In this way, the increase of the RANKL-OPG binding ratio leads to osteoclasts' activation and increase of bone tissue resorption, (Brosch et al., 2003; Kostenuik, 2005).

The coupling of the processes of bone resorption and remodelling and morphological disturbances of bone tissue indicate that under osteoporosis it has a role of systemic disorder when the slowdown of one mechanism (remodelling) leads to reduction/slowdown of another mechanism (resorption), Marie, 2006. That leads to transition of all bone remodelling system onto another lower level, when remodelling potential (in terms of our model) is considerably reduced.

The majority of the medical treatments for bone (biphospahnates, harmones) are directed at decreasing the tissue resorption; however recent developments in hormone replacement therapy, which is in clinical use for few decades, are based on anabolic approaches (e.g. PHP). These two approaches reflect the two different stages of bone homeostasis – resorption and remodelling. Nevertheless, to find a real increase in the mineral density may take several years. PTH administration significantly reduces the number of skeletal fractures in patients with postmenopausal osteoporosis; it significantly increases the

BMD in patients (Neer et al., 2001). However, there is no data indicating complete cure for osteoporosis, just treatments that arrest or slow its progress.

2.7.2 Paget's disease

Another disorder, which is directly related to the disturbance and the lack of sinchronisation in the bone remodelling, is the Paget's disease of bone, Paget, 1877; Tiegs, 1997; Bender, 2003. Paget's disease is usually known as a chronic bone disorder that develops in elderly people. In review of 889 patients from 27 to 100 years Davie and coworkers found that the median was 63 years for males and 67 years for females, Davie et al., 1999. It is well-known that Paget's disease is linked to the skull, spine (vertebral column), pelvis and long bones. Affected bones become thinner, their structure is disordered; on a tissue roentgenogram sclerotic changes (plaques) can be found. The disease has no symptoms, though it is sometimes accompanied by pain and bone deformation and higher susceptibility/tendency to fracture. From 889 patients 107 fractures were linked to Paget's disease, however the most common problem was worsening pain, the diagnosis of osteosarcoma was only made in two patients (Davie et al., 1999). The bone deformation accompanied is in a line with another medical term "osteitis deformans". In summary, the cause of Paget's disease is still not fully understood.

It is known that Juvenile Paget's disease can be trated as quite uncommon disorder characterising by both increased bone resorption and formation (Bakwin and Eiger, 1956). This state characterised by grataer tissue remodelling rate that weekens the bone and leads to fractures and development of skeletal abnormality. It can be linked to some mutations in the gene which encodes OPG leading to the increased hard tissue remodelling in patients (Janssens et al., 2005). Because of this some researchers suggested that this disease could be named as OPG deficiency.

2.7.3 Remodelling in damaged bone tissue

When bone is damaged, resorbable bone implants and bio-scaffolds offer many distinct advantages over conventional metallic devices: artefact free postoperative radiographic evaluation, closer matching of mechanical properties to bone, rapid osteointegration and elimination of the long-term problems associated with metallic implants (stress shielding, loosening, potentially harmful by-product and rejection). New methods of scaffold production, including the use of layer manufacturing (Braddock et al., 2001; Yan et al., 2003; Vozzi et al., 2002, 2003) provide the opportunity to precisely control the architecture of scaffolds and this opens up the possibility to produce optimised scaffolds. However, despite some promising results (Taboas et al., 2003; Yan et al., 2003; Koegler et al., 2004; Jansen et al., 2004), the full potential of this approach is limited by a number of factors. Biological parameters (like bone resorption and formation constants) are important optimisation variables in the design of scaffolds.

The complex bone remodelling process occur in native bone. The same mechanisms also come into play when a scaffold is implanted and is subsequently resorbed and replaced by bone. The bone remodelling parameters are important variables to be considered in the scaffold design alongside factors such as mechanical performance, for example. From the point of view of computer-aided tissue engineering (CATE) it would be ideal if the individual biochemical, physiological and pharmaco-kinetical parameters could be incorporated directly into the design system and the final output would be the scaffold macro-parameters (for example, porosity and topology). An intermediate stage in such an approach could be application of bone remodelling parameters within the finite element algorithm, which is already used in scaffold design (Ruimerman et al., 2005). The bone remodelling parameters have a dynamic origin and it should be possible for them to be derived directly from a mathematical model of the bone remodelling cycle. In normal healthy bone resorption and formation rates are in a dynamic balance with new bone being formed as old damaged bone is resorbed – this entire process is controlled by loops of regulation based on chemical and

mechanical stimuli. A misbalance in the scaffold resorption and bone formation rates can result in the over-formation of new bone (osteopetrosis) or when resorption exceeds the formation of new bone this can lead to bone loss (for example, osteoporosis). In the case of bioresorbable scaffolds a similar balance between resorption and formation must be reached to ensure that the mechanical integrity of the implant is maintained without undermining biological efficacy. The development of a mathematical model which represents the remodelling process (including the loops of regulation) would provide an important tool for understanding how this balance is maintained and moreover provide the critical parameters for modelling/designing optimised bone scaffolds.

However, at present a rather fragmented understanding of the bone remodelling process exists and limited research has been undertaken to investigate the behaviour modes of BMU dynamic models. Analysis of these modes could provide the key to determining how certain the loops of regulation maintain the balance between resorption and formation of a tissue, and bone tissue particularly.

The current biochemical and histo-chemical understanding of bone remodeling processes is based on certain assumptions. These include the Basic Multicellular Unit (Compston, 2002), in which the emerging activity is controlled by a number of feedback loops. These include genetic, physiological and immune, which function at the tissue, cellular and molecular levels. On the last level, the participation of many molecular messengers is very difficult to investigate *in vivo*. Even the general animal semantic model of such processes is not yet completed and is still in the state of re-verification and continual refinement. An explanation for this could be the experimental difficulties in the measurement of very tiny molecular messengers, with short life-spans. Moreover, the messengers are difficult to separate from the receptors (even dead) due to considerable binding constants. In addition, the difficulties of conducting biochemical experiments *in vivo* are magnified when working within the hard tissue environment. This obstacle forces researchers to develop

cellular level models that incorporate some participation of molecular messengers involved in the regulation loop.

The mathematical modelling of bone turnover could help researchers to verify the general vision of bone remodelling regulation and provide an important insight into problems related to the kinetics of the processes. The rates of competitive processes that occur during bone remodeling are of particular interest because anomalies in these rates can result in certain bone disorders, for example Paget's disease.

The dynamic systems approach, based on modelling with ordinary differential equations (ODE's) is still the most commonly used technique for modelling bio-medical phenomena. Technically these methods are highly developed, as is their use in modelling of biomedical processes. The advantage of applications of these methods is the possibility of deriving a clear interpretation based on a conceptually verified history. For example, some publications (Komarova et al., 2003; Lamaire et al., 2004) on the application of ODE's to bone modelling describe a model based on the analysis of the autocrine and paracrine properties of osteoclast-osteoblast interactions (which are involved directly in bone remodeling as the basic cell of the BMU).

2.8 Mathematical models of bone remodelling

2.8.1 Early models of bone remodelling

About 120 years ago the anatomist Julius Wolff (1892, 1986) from Germany derived a formal link between bone tissue structure and applied to bone loads. This was represented later by Roux (1895) as a concept of functional adaptation. However, the first mathematical approach applied to bone tissue function was undertaken by Pauwels (Pauwels, 1965). He developed a mathematical framework for the Roux theory. Pauwels suggested that there is an optimal level of mechanical signal that results in a balance of bone tissue resorption and creation. Finally, a mathematical model was developed by Kummer (1972) based on ordinary differential equations (ODE's), where the rate change in bone mass is proportional to cubic

function of strain σ. The value of empirical proportionality constant can define different modes of behaviour from damped/undamped oscillations to an asymptotic convergence node.

The use of Finite Element (FE) methods to describe bone properties started in the early 1980's. The FE method was applied to bone remodelling in early work by Huiskes et al. (1985; 1987; 1989) when the strain adaptive remodelling theory was formulated and implemented. This was based on experimental studies of the mechanical parameters of trabecular hard tissue employing the combined remodelling theory and the FE method. Authors applied this approach to the development of prostheses and the shape optimisation of hip prosthesis design. Further investigations were also undertaken by Weinans and co-workers in 1992 and 1994 and van Rietbergen et al., 1993.

In subsequent years many other authors studied how the density, morphology of bone tissue, overall bone structure are related to the local mechanical loading (Carter, 1987 and Carter et al., 1987; 1996; Hart and Davy, 1989; Baeupre et al., 1990, Chow et al., 1998). Femoral cancellous bone architecture has been studied by Carter and coworkers (1989) with respect to associations to the loading history. They found explanations for morphology changes in the femur taking into account the multiple directions of the joint loading. Jacobs and co-workers (Jacobs et al., 1995) studied the stability of numerical algorithm describing bone tissue turnover at modelling and discuss the preferences a node-based finite element approach. Carter et al. (1996) studied the role of mechanical factors in bone growth. This work demonstrated that geometry and density alterations in adult bone can be related to physical activity. These alterations can be simulated by bringing into play the same rule used during development. Fischer et al. (1996) have studied the influence of implants on the sensitivity of bone adaptation simulations to the alterations in loads. The authors found that different mechanical loads can produce similar BMD (bone mineral density) distributions. In the following decade (1990's) the activity in mathematical modelling in the field of bone remodelling, bone physiology and bone tissue mechanical property analysis significantly increased.

2.8.2 Last decades

In recent decades numerous mathematical approaches and models of bone remodelling have been developed. However, much of this work focuses on only part of remodelling process (Davidson et al., 2004; Ruimerman et al., 2005). Other researchers have employed the so-called "BMU density" or "Activation frequency" but do not attempt to probe into the internal mechanisms at play within the BMU (Langton et al., 1998 or Tayyar et al., 1999, recently).

This simplified "black box" approach has enabled important progress to be made in the modelling of the overall mechanism of the remodelling process, without a need to fully understand the internal processes occurring within the BMU.

In developing their strain-adaptation remodelling concept, Mullender and Huiskes (1997) further examined whether the sensors of the mechanical property of cancellous bone tissue can be modelled by the Oct's network or the population of cells that cover the bone. Response to the mechanical stress has been studied by these authors with respect to this postulation about sensorical properties of the osteocytes and lining cells network as the controlling cancellous bone remodelling in response for mechanical stress. However, they summarised about inssufficency of experimental data in support for their suggestions.

A 3-dimensional simulation model of trabecular bone turnover was developed by Tayyar et al. (1999) to mimic changesin actual structure and cellular remodelling events that occur in trabecular bone. The authors highlighted the important role of perforation, which accounts for around 40% of overall bone loss.

An interesting stochastic approach to bone remodelling simulation was developed by Langton and co-workers (Langton et al., 1998, 2000). This was based on a finite element simulation to predict the connection of the relative stiffness with density of the tissue. The authors showed the link of mechanical integrity to the damage level. In their later work the authors, (Langton et al., 2000) investigated the effects of anabolic treatments of cancellous

bone disorder after menopause. They studied the increase in tissue in tissue as a result of treatment applied at different levels. A stochastic approach has been applied to a simplified case. They found indications which allows them to put forward an idea of an intervention on early stages to stop the weakening of structure of hard tissue.

2.8.3 Research in the last decade (finite element based models)

The last decade has been characterised by quite intensive research into several diverse approaches. 2-dimensional simulation of trabecular surface remodelling was performed by Tsubota et al. (2001) for proximal femur in humans. The adaptation of trabecular tissue at local level in connection to the functional changes at the cancellous tissue has been studied by Tsubota and coworkers in this investigation. The results of this work clearly shows the link between these two levels of tissue organisation. Trabecular level seems to be linked to the function cancellous tissue as a result of applied mechanical load.

In work by Doblare and Garcia (2001) an interesting FE framework for bone remodelling was developed. The authors have studied the total hip replacement. The research has been focused on the remodelling processin bone tissue before and after surgery and led to the development of a mathematical model for anisotropic bone remodelling (Doblare and Garcia, 2001). The developed model was also employed to study the remodelling process in the undamaged tissue of femur. The results of the simulation obtained from the model showed close correlation with the experimental data. The authors found the indications of correlation of the bone tissue structural properties, including local mechanical properties and mechanical loads main directions. Some observations, including the mechanical stress, were mathematically explained in the framework of this model. A concept of remodelling tensor, analogous to the standard damage tensor was proposed by Doblare and Garcıa (2002). This tensor provides the total characteristics of the bone microstructure and its stiffness. The model can predict the anisotropy distribution in the proximal femur with reasonable accuracy. In later work Doblare et al. (2005) discussed the use of a previously developed frameworks, the

natural element method, in biomechanics. The authors provide some examples demonstrating the performance of the method. In addition the authors studied the influence of inter fragmentary movement on callus growth using a computational simulation of fracture healing (Garsia-Aznar et al., 2007). They investigated whether it is possible to forecast some geometrical properties of callus on the basis of investigation the mechanical effects ot stem cells. The authors concluded that the local pattern of mechanical imputs is able to predict properties of fracture of the callus tissue.

Fernandes et al. (2002) studied the bone remodelling around cementless stems using computational modelling. They found that bone in-growth does not occur over the full coated surfaces. They found that regions where separation or high relative displacement occurs prevent attachment by bone in-growth. This prediction by the model is in good agreement with clinical bone in-growth observations.

The special behaviour of adaptive bone remodelling has also been investigated by Garcıa et al. (2002). These mathematical approaches have been implemented in FE code to determine the bone behaviour after implantation of an artificial fixation or prosthesis. The results demonstrate the benefits of computational simulation to predict the effectiveness (short and long-term) of possible orthopaedics treatments.

The experimental and theoretical evidence of whether residual stress can initiate damage in porous bone cements has been studied by Lennon et al. (2002). A physical model was built which allowed the damage in the cement layer on the femoral side of total hip replacement to be visualised. On this basis a mathematical framework for prediction of residual stress due to shrinkage was developed. The framework uses the thermal history of the material for predicted when stress-locking occurs and estimates the resulting thermal stress. Using FE analysis the authors, have calculated the residual stress distribution in cement layers and compared this prediction to the measured stress in a physical model.

Pothuaud and coworkers (Pothuaud et al., 2005) have investigated mathematical modelling employing the autologous osteogenic cells in new tissue formation. In this study a

new tissue remodelling and repartition with new material process has been studied numerically using numerical model. The model was based on population with autologous osteogenic cells. Samples were subsequently implanted into rabbits and made functional by enhancing with some a cyclopeptides, for 2 and 4 weeks after implantation. The authors conclude that the proposed approach can be useful when study the tissue formation inside bone scaffolds with macroporosity.

Nowlan and Prendergast (2005) investigated the appearance of an optimal mechanoregulation reaction in a population of individuals through a genetic approach. The population of individuals were created using several genetic assumptions. The results of simulations implied the existence of convergence in considered tissue growth numerical models. Nevertheless, authors suggested about a set of individual control schemes for spectrum of mechano regulatory processes that survive after number of generations. The computational model developed by Nowlan and Prendergast argues with some literature schemes of natural selection role in evolution of the skeletal constitution in direction to functional optimality. The authors proposed that the evolutionary development of skeletal regulation might be directed to non-optimal skeletal phenotypes, Nowlan and Prendergast, 2005.

The simulations of the ligament reconstraction in the in anterior cruciate have been performed by Pena and coworkers, Pena et al. (2005). They have been employing 3D FE medelling of the effect of graft stiffness and graft tensioning. Authors found important function of graft initial stiffness and tensioning in anterior cruciate ligament reconstruction as an interesting mechano-physiological effect related to the post reconstruction period.

A computer simulation of surface remodelling of trabecular bone has been carried out by Tsubota and Adachi (2005). They investigated the spatial and temporal regulation of the cancellous bone organisation. This type of regulation occurs in bone cellular activities as a reaction on mechanical input. Authors found that the simulation results indicate the temporal and spatial changes that the trabecular tissue goes through. These changes depend on the

mechanical load applied. The results obtained clearly imply a control of the spatial and temporal organisation of the trabecular tissue could be linked to the sensitivity of the osteocells to mechanical load.

The existing bone turnover theory based on strain-adaptive approach has been analysed in work of Turner et al. (2005). The authors revised approach and developed a model which was combined with the anatomic 3D FE models. On the framework of approach authors forecast the changes in periprosthetic apparent density. The numerical experiment was conducted for several femoral parts with altered structures. Developed model predicted the changes in tissue and showed close correlation with clinical densitometry measurements. The authrs concluded that the developed approach employing mechanical imputs can successfully explain the majority of adaptive tissue remodelling results suggest that a large proportion of adaptive bone remodelling transformations. It is suggested that developed methods might be applied to the implant design modifications, and custom-fit implant selection, to the pre-clinical tests of customised implants.

A formal approach has been developed by Ruimerman and coauthors in a 3-dimensional finite element model (Ruimerman et al., 2005). The core idea of the approach is that the osteoclastic cells can initiate activity of osteoblastic cells. Then tissue formation can be considered as bone formation as an outcome of the increase of the strain in hard tissue. The role of microcracks and disuse (paucity of loading) was in promoting osteoclast resorption was also studied. Simulations using the model provide a reasonably adequate explanation of the development of the morphological detail of trabecular bone during growth and the results compare favourably to experimental measurements in (porcine) trabecular bone in development.

Bitsakos and co-workers employed a strain adaptive remodelling approach for simulation of bone densitometry measurements (Bitsakos et al., 2005). The authors developed the framework of this model in respect of changes to the periprosthetic compensative reaction of hard tissue to various loads of musclular loading arrangements. The authors created two FE

models of the same bone to allow simulation of changes in BMD (bone mineral density) around prosthesis over time to be performed. It was summarised that the general character of the changes in the considered hard tissue is in a good concent with experimental data. The overall outcome of investigation support suggestions that loading pattern in the simulated agorithm employing finite element technique could provide the broader understanding of the bone turnover process.

It is also possible to use the FE method for numerical simulation of the process of bone spur (osteophytes) formation when used in combination with quantitative bone remodelling theory. He and Xinghua (2006) extended their previous research which focused on prediction of the external bone shape after remodelling (Xinghua et al., 2002; 2005) to the simulation of pathological change of bone, for example osteophytes on the edge of a bone structure. These results can be useful for better understanding of the connection between morphological abnormities of bone tissue and the mechanical environment.

Grover et al. (2007) described a biomechanical mathematical model of rabbit ankle. This model predicts a criticality in biomechanical investigation of skeleton in vivo. Their conclusions are in a good agreement with the experimentally measured parameters in vivo. This work extends beyond previous models by providing quantitative forecasting of the value of mechanical loads in studied animals.

2.8.4 Modelling of BMU activity from a biochemical perspective

The after surgeric tissue changes in bone tissue at total hip arthroplasty (THA) operation have been studied in relation to preoperative tissue mass properties in the framework of the strain-adaptive remodelling approach by Kerner, Huiskes and colleagues (Kerner et al., 1999). The combination of FE analysis and bone turnover theory was employed in the model to simulate the adaptive bone remodelling after THA. In this study authors found the inverse correlation of the value of predicted bone losses with the primary BMD.

A number of researchers have explored the use of an adaptive bone remodelling approach to understand the mechanisms occurring within the BMU. Mathematical formulations using the adaptive bone remodelling approach have been implemented in FE code to predict the bone behaviour when an artificial fixation is used or prosthesis implanted (Garcia et al., 2002). This work also included a brief review of the main bone remodelling models.

An interesting formal framework was suggested by Lemaire and colleagues proposed for explanation of coupling between osteoclasts and osteoblasts (Lemaire et al., 2004). The authors proposed that this model could also be used for explanation few hard tissue disorders such as vitamin D deficiency, oestrogen deficiency, glucocorticoid surplus in tissue. The framework disscuss possible advantages of multi-therapies when at the same time anabolic therapies are used in combination with therapies preventing the resorption of the tissue.

A novel formal model has been proposed by Martin and Buckland-Wright (2004). Their work offers identification of main reasons which influence the tissue resorption. Also the detailed and comprehensive robustness study of model has been undertaken. The Michealis-Menten kinetics has been used to explain the activity levels at different stages of tissue remodelling. The important factors for lovering the tissue resorption has been categorised using developed model. Based on this work the authors also propose some effective “bottle neck” places to develop the therapies to decrease the velocity of hard tissue remodelling.

Matsuura et al. (2003) formulated a formal approach that models the bone remodelling phenomena. The model involves an interface equation which determines the surface of the bone. The associated discrete model is formulated and its stable solvability is verified. The results of numerical simulations were compared with bone data from around a dental implant, supported by newly formed spongy bone, show qualitative agreement.

2.8.5 Recent years 2007-2009 in FE

Ruffoni and coworkers developed a mathematical model of the remodelling and mineralization process. This has been used to show that the BMD distribution can be considered as a criterion of the mineralization process. They demonstrated that the histogram shape of the BMD distribution for trabecular bone can directly reflect the mineralization kinetics (Ruffoni et al., 2007). The authors found indications that the turnover rate of the bone remodelling process influences the peak position and the shape of the BMD distribution.

The study of quantative evaluation of BMD and the distribution of mechnical parameters of elasticity in a human mandible has been conducted by Reina et al. (2007) using their FE model of bone remodelling with the purpose to predict mechanical properties of the tissue behaviour. The tissue density distribution was numerically estimated together with the anisotropical directions in varios locations of mandible. The calculated data was in good agreement while validated in the set of clinical trials with at a good significance level.

Recently a number of very interesting models of bone remodelling were developed. The mechanical load effect on the hard tissue turnover was the main objective of work of Li and co-workers (Li et al., 2007). Their results suggest that bone resorption at the neck of a dental implant takes place due to overload of the grinding surface of the bicuspid and molar teeth but that eventually resorption stopped before reaching the coarse threads.

The local factors in bone and synchronized effects of mechanical force during tissue remodelling have been considered in a mathematical model described by Maldonado et al. (2008). The results obtained in numerical study of external inputs (nitric oxide or prostaglandin) and simultaneous mechanical load were in good qualitative agreement with the tissue adaptative reaction.

Garcıa-Aznar et al., (2007) recently presented a mathematical model for forecasting bone development and its specialisation with respect to mechanical inputs. They investigated the way the characteristic features of calluses (size and shape) are dependent on mechanical stimuli. Among these predictions they found that callus size correlates with interfragmentary

increase. The authors conclude that the geometry of fractures in the tissue can be described and predicted by the model. The known experimental findings support the results of model simulations. Finally, it is suggested in the article that geometry of mechanical stimuli determines the geometry and volume of fracture calluses.

Using nonlinear partial differential equations a model that describes the spatial and temporal development of the population densities of osteocell types, the extracellular matrix types and growth factors was developed by Geris et al., 2000. The study in particular highlights the role of angiogenic growth factors in spatial restructuring of the vascular network in the process of bone healing. The authors stressed in addition that the realistic description of cells migration is an important factor, as well as proper understanding and formalisation of the local and temporal distributions of the cells in tissue. Findings of the authors described in their work could be one of important tools in consideration the role of the healing system in hard tissue. The results of the paper might find their application in development bone tissue healing trials. (Geris et al., 2008).

2.8.6 Models related to the physiology of remodelling

In one of the first physiological models developed, Fyhrie and Kimura (1999) analysed the role of the transport mechanisms (metabolite diffusion and active transport) in the functionin and homeostasis of trabecular tissue. Authors proposed the suggested that the transport mechanisms for trabecular survival are due to the collection of mechanisms. In the framework of the model, the connection between tissue volume and its surface has been illustrated employing the diffusion kind of the transport of metabolites in blood flow. Another important finding was that during periods of mechanical disuse, the bone volume fraction declines exponentially. A correspondent mathematical model shows that the mechanical stress can change the trabecular tissue volume by the change of the transport of substances between the tissue parts. Technically, the study at microscopic level of blood flow has been unalysed using modification Darcy–Navier–Stokes equation.

Interesting study on the level of relationship between bone tissue damage and the remodelling process has been conducted by Martin (2002). The controversial concept on the hard tissue remodelling initiation in the nearness of microdamage has been proposed. The author considered the indications that remodelling BMUs can migrate about few millimetres from the place of the BMU recruitment. A system of corresponding phenomenological equations has been derived. The author conclude that the simulations support the BMU migration concept by indication proper density of resorbed tissue in nearness of a microdamage. The author stressed the lack of the experimental basis that can be relevant to the simulation results.

An interesting biological adaptive control model treating adaptation as multi levelled phenomenon which includes mechanical and biological levels has been proposed by Davidson et al. (2004). The model tekes into account the external mechanical factors with relation to the mechanobiological role of the hard tissue. The rules of Newtonian mechanics are believed to be applied to the resulting system. In the result, the linear adaptation characteristics equation is obtained for the the main response in the derived model. The exponential and oscillatory trajectories are found as the main modes of behaviour in the model. These concrete type of solution depends on the environmental input.

An interesting mathematical model of bone remodelling mediated by parathyroid hormone was proposed by Rattanakul et al. (2003), where the authors simulated the response of tissue remodelling to estrogen and PTH therapy. The authors particularly concentrated their interest on the temporal effect of PTH hormone and any effect of oestrogen substitution therapy on bone tissue turnover. The proposed model has shown a limit cycle that transfers into chaotic behaviour.

The microdamage and trabecular bone volume was the scope of Nyman et al. (2004) study with respect to the results of the bisphosphonate level. The authors have been performed a theoretical study employing the Frost idea of a mechanostat (Frost, 1964; 2001). The postmenopausal trabecular bone taken as a continuum space has been used to apply

strain-adaptive concept of the bone tissue remodelling (Frost, 1964; 2001). Several important practical implications of the results of this work were proposed. The authors conclude in practical terms that certain bisphosphonates have to be deliberately created to make available the proper level of minimal restraint in bone formation accompanied by and a highest decrease in the bone multicellular unit resorption.

The bone marrow is an important media of cells, substrates and oxygen that entirely supports bone remodelling. An interesting transport model for oxygen/oxygen-carbon dioxide in human bone marrow was developed by Kumar et al. (2004, 2008). From the numerical simulation of these relatively complex models the authors came to the conclusion obout criticality of effects in oxigen transport in human bone marrow tissue. Particularly interesting was the conclusion about importance of Haldane effect than the Bohr effect. The form of pH regulation curve and the extravascular oxygen concentration were at the nececary levels for cellular proliferation and growth.

2.8.7 Statistical models

A few notable statistical models have been developed over the last decade. A number of authors applied powerful statistical techniques to the available data regarding different disorders, particularly for bone disorders in aged women. Vestergaard et al. (2001) compared methods of predicted BMD from clinical and biochemical variables. Three statistical methods: multiple regression, logistic regression, and discriminant analysis have been applied to the data for 2000 women of perimenopausal age. The authors found that concentrations of serum osteocalcin, serum bone specific alkaline phosphatase to be reproducible risk factors for low BMD.

The BMU performance in the tissue in menopausal bone has been studied in the framework of a theoretical approach by Hernandez et al., (2003). They conducted a numerical experiment describing the BMU performance using the clinical histomorphometric data. One of the objective of their study was to find the relationship in alteration of BMU

performance with mineral density of menopausal bone. The authors found that the alteration in tissue remodelling in postmenopausal bone can be related to an observed in clinical situations decrease in BMD. Two main factors; ovearal alteration in tissue remodelling the transitory alteration in time of menopause can be linked to bone mineral density loss found in clinical practice. Finally, in the work it is concluded that the consideration of alteration the basic multicellular unit performance can be used to improve the strategies in postmenopausal osteoporosis treatment.

Taylor and co-workers described a model that predict the stress fractures distribution in the bones of athletes, soldiers and other individuals during periods of intensive exercise (Taylor et al., 2004). As with previous work conducted by the authors in 2001 (Taylor and Kuiper, 2001) they used the Weibull probabilistic distribution, to calculate the probability of failure as a function of time under cyclic loading. The model correctly predicted that 17% of the individuals studied would succumb to stress fractures.

An interesting statistical model for skeletal recovery of the loss of bone BMD in NASA astronauts during spaceflight has been developed using the dataset throughout the more than 40 years of space travel (Sibonga et al., 2007). The authors described the skeletal recover of astronauts after their return to Earth – they found that BMD recover exhibited an exponential character.

With respect to the possible clinical application of MRI, Helgason et al. (2008) reviewed the formal linkage of mechanical properties of bone tissue and it's the tissue density. The study was performed used the data available from public sources. The correctly normalised data from the trials conducted in comparable way has been used to develop the elasticity–density functional dependence. The authors have proposed the method relevant to the verification of the accuracy of the elasticity–density relationships in various experimental situations.

2.8.8 Extended remodelling models - fracture healing

Normal and abnormal healing is also an important issue that requires an understanding of bone remodelling process. A rising amount of works is devoted to developing mathematical modelling approaches to fracture healing.

A mathematical framework for model fracture healing was developed by Bailon-Plaza and Van Der Meulen in a series of works. In the one of their first studies the authors have investigated the affects of some factors of growth on fracture healing. They developed a 2D mathematical model of the tissue healing for relatively small sizes/stability of a fracture gap. Modelling of mesenchymal cell migration has been used to simulate the inflammatory and tissue regeneration stages of healing. The authors found evidence that the velocity of the osteoblasts production of osteogenic GF and the duration of the initial release of GFs at the time of injury are the most important parameters for entire ossification and successful healing. The influence of various levels and timing has been investigated in their second study (Bailon-Plaza and Van Der Meulen, 2003) where coauthors examined the action of mechanical stimulus on the healing of fractures. The authors successfully explained the advantages and disadvantages (positive and negative effects) of different loading intensity. The delay of mechanical doad indicated some negative effects according to their results.

An attempt to develop a model of diaphyseal healing has been undertaken by Shefelbine et al. (2005). Authors used FEA and the fuzzy logic in combination. The consequent tissue turnover stages in the fracture gap has been simulated by created algorithm. The authors concluded about trabecular tissue structure as dependent on mechanical load applied. Finally they suggest the usfullness of a particular model, which describes the hard tissue differentiation.

2.8.9 Optimal control methods in the modelling of bone tissue remodelling

Recently dynamic optimal control (DOC) methods have been applied to a number of biochemical (Rico-Ramirez et al., 2003), biotechnology (Smets et al., 2004) and biomedical

problems, including the optimisation of cancer radiotherapy (Ledzewicz and Schattler, 2007). DOC methods can create the basis for optimal regulation of many biochemical processes, including the regulation of bone remodelling/scaffold remodelling. Optimal control methods may be useful when seeking to optimise (minimise energetical losses, etc) a bone remodelling process.

Recent examples of OC models dealing with bone remodelling described in the literature include, Harrigan and coworkers in their early work from 1996 (Harrigan et al., 1996). They described an optimal structures approach to the remodelling of bone adjacent to intramedullary stems. Using FE models and structural optimization they have extended the work of Huiskes (Huiskes et al., 1987) to cover internal tissue remodelling around intramedullary implants. Employing numerically stable remodelling algorithms based on optimization, the authors developed an analytical relationship that predicts when bone will remain around an intramedullary implant demonstrating a direct application of the optimisation methods to the remodelling theory.

Further, Ledzewicz and Schättler (2007), develop a mathematical model, considering the treatment of bone marrow for cancer using chemotherapy as an optimal control problem. Using the Pontryagin maximum principle they have shown that optimal controls show a classical bang–bang like form.

2.8.10 Review of selected BMU models

Many BMU models are interesting from both the technical and biological perspectives. However, some are of particular interest as they achieve a combination of both the mathematical and biological perspectives of the problem. Presented below are some of these key models.

2.8.10.1 Paracrine/Autocrine control model

In a series of works Komarova and co-workers developed a phenomenological cellular model of bone remodelling based on the ODE technique (Komarova et al., 2003; Komarova, 2005). In this model the authors proposed that the BMU plays a crucial role in remodelling and proposed a simplified scheme of OBl-OCl interactions, Fig.2.8.1.

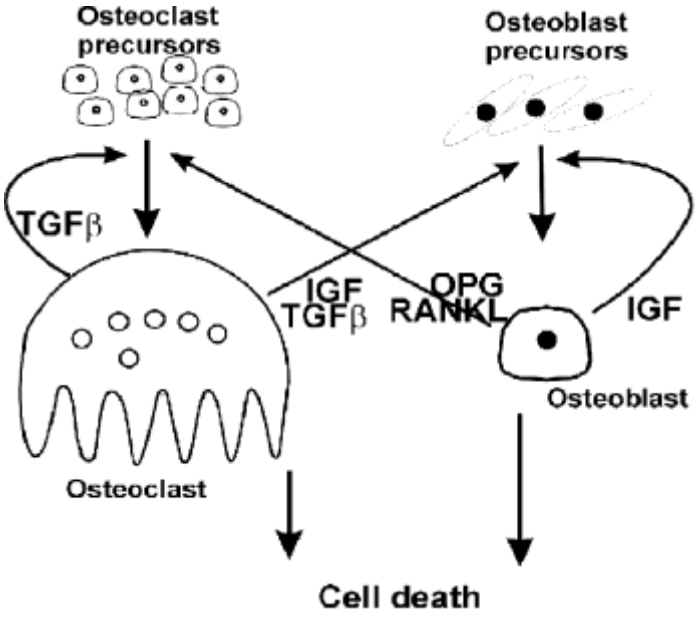

Fig.2.8.1 Scheme of osteoclast-osteoblast interactions adapted from the Komarova model (Komarova et al., 2003). According to Komarova et al., 2003, vertical arrows designate the cellular pathway of reqruitment and death/apoptosis of Obls and Ocls. Fine arrows schematically illustrate the autocrine and paracrine controls. For detailed description see the original paper.

Finally, on the base of this scheme the Komarova and coauthors formulated a mathematical model

$$\frac{dx_1}{dt} = \alpha_1 x_1^{g11} x_2^{g21} - \beta_1 x_1,$$
$$\frac{dx_2}{dt} = \alpha_2 x_1^{g12} x_2^{g22} - \beta_2 x_2,$$
$$\frac{dz}{dt} = -k_1 y_1 + k_2 y_2,$$
$$y_i = \begin{cases} x_i - \bar{x}_i, if\,(x_i > \bar{x}_i) \\ 0, if\,(x_i \le \bar{x}_i) \end{cases}$$

where "x_1 and x_2 are the number of osteoclasts and osteoblasts correspondingly; α_i and β_i are activities of cell production and removal; g_{ij} is the net effectiveness of osteoblast- or

osteoclast-derived autocrine or paracrine factors; z is total bone mass, k_i is normalized activity of bone resorption and formation, y_i are the numbers of cells actively resorbing or forming bone, and $\bar{x}_i$ are the numbers of cells at steady state", Komarova et al., 2003.

The authors explore the parametric space g_{ij} and investigate the stability of the system analytically. They studied the effect of altering parameters on dynamical behaviour and establish an influence of the parameter values leading to stable oscillations in state variables. The oscillation period depends on the rate parameters that can be linked to autocrine/paracrine regulation.

This model allowed the authors to analyse the OBl-OCl dynamic behaviour. Within the model framework, unstable behaviour may account for the pathological bone remodelling found in Paget's disease. The authors conclude about the type of behaviour which in their opinion is linked to the parameter that represents the autocrine regulation of osteoclasts.

However, the authors admitted that the model has several limitations, one of which is that the only types of cell included are osteoblasts and osteoclasts. From a number of studies it follows that OCts also play an important role in tissue remodelling, producing the molecular signals to initiate the process.

2.8.10.2 The Osteoblasts/Oosteoclasts differentiation model

Rattanakul et al. (2003) developed a model for the differentiation of osteoblasts and osteoclasts in bone, based on the effect of PTH control. The model behaviour has a limit cycle and a chaotic pattern for a range of parameter values in accordance with some clinical observations. Core model:

$$\frac{dP}{dt} = \frac{c_1}{k_1 + C} - d_1 P$$

$$\frac{dC}{dt} = \frac{(c_2 + c_3 P)BC}{k_2 + P^2} - d_2 C$$

$$\frac{dB}{dt} = c_4 P - \frac{c_5 PB}{k_3 + P} - d_3 B$$

where $P(t)$ denotes the level of PTH above the basal level, $C(t)$ - the number of active osteoclast cells, $B(t)$ - the number of active osteoblast cells; $c1$ and $k1$ being positive constants, d_1 the removal rate constant; $c4$ is the specific rate at which PTH stimulates reproduction of active osteoblasts; $c2$, $c3$, and $k2$ are positive constants; $d1$, $d2$, and $d3$ are rate constants. The authors demonstrated that several types of nonlinear dynamic behaviours can be deduced from the model, which closely simulates available clinical data. The model is exhibits limit cycle behaviour, which can evolve into chaotic dynamics.

2.8.10.3 Model incorporating RANK-RANKL-OPG pathway

Compared to the Komarova model, the scheme mechanism (Fig.2.8.2) proposed by Lemaire et al. (2004) is considered more detailed in the sense of the role of PTH in bone remodelling control. This model is the first which incorporates the RANK-RANKL-OPG pathway which, as mentioned previously, is widely accepted as being essential for the regulation of osteoclast formation.

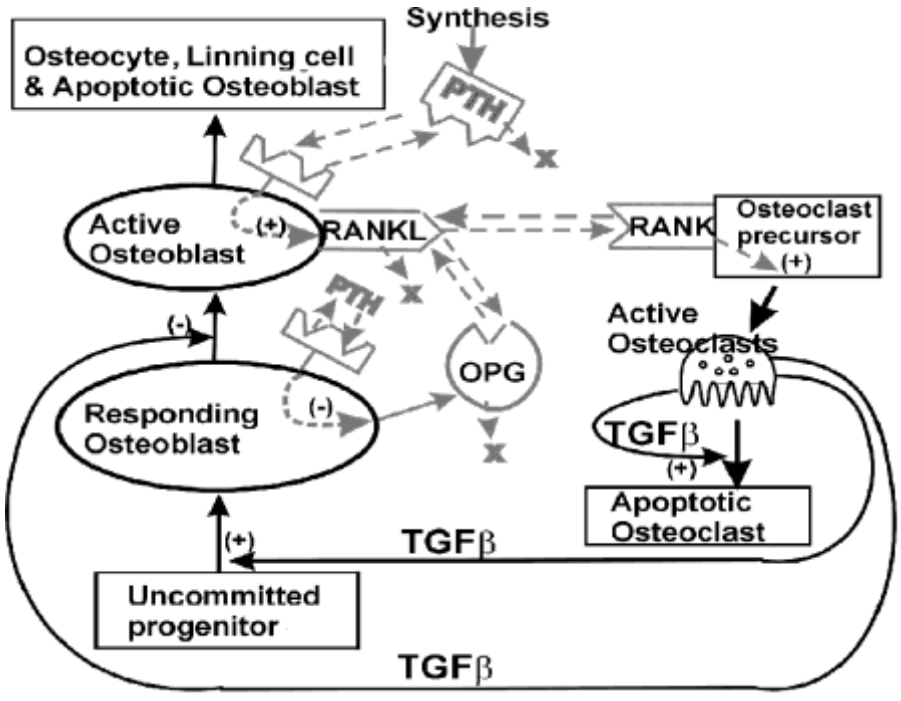

Fig. 2.8.2 Schematic diagram of osteoclast-osteoblast interactions from Lemaire et al., model (Figure adapted from Lemaire et al., 2004). The ovals represent osteobast cells. The solid arrows represent streams of material., eg. TGFβ. For detailed description see the original paper.

The system equations are

$$\frac{dR}{dt} = D_R \pi_C - \frac{D_B}{\pi_C} R$$
$$\frac{dB}{dt} = \frac{D_B}{\pi_C} R - k_B B$$
$$\frac{dC}{dt} = D_C \pi_L - D_A \pi_C C$$

where R is the concentration of responding osteoblasts, B is the concentration of active osteoblasts, C is the concentration of the active osteoclasts and

$$D_B = f_0 d_B, \pi_C = \frac{C + f_0 C^S}{C + C^S}, \pi_L = \frac{K \bullet L}{K}$$

and π_L is the complex function of the number of parameters (Lemaire et al., 2004).

Lemaire et al. (2004) formulated a model of the interactions between osteoblast and osteoclast functions within the limits of the known bone remodelling molecular-and-cellular framework. The ODE model formulates the assumption that the relative proportions of immature and mature osteoblasts can control the degree of osteoclast activity. The main suggestion is that the regulation of the osteoblasts by the osteoclasts depends on their stage of differentiation. Within the framework of this model, the authors found number of therapies. The model also predicts that increasing in the preosteoblast pool size can be an important factor for bone formation therapies. The authors proposed a scheme for the cellular control of bone remodelling based upon the RANK/RANKL/OPG core cytokine system to examine osteoclast functions. Based on their model the authors have considered some different therapeutic interventions against major bone diseases - oestrogen deficiency, 1,25(OH)2D3 deficiency, senescence, glucocorticoid excess and their recommended therapies. They suggested that the absence of any therapy is particularly efficient against oestrogen deficiency or 1,25(OH)2D3 deficiency. The authors suggest that almost all effective therapies are correlated to “an increase in a given parameter which is related to an essential ingredient of therapeutic bone regrowth”.

2.8.10.4 Biological adaptive control model

A mechanical analogue of multi-factorial bone density adaptation has been developed by Davidson et al. (2004).

The model equation is

$$m\ddot{x} = \sum_{i=1}^{n} (F_{Ai}(x) + F_{Di}(\dot{x}) + F_{Ei}(t))$$

where, $\boldsymbol{x}$ = current value of bone density (response of the system); $\boldsymbol{x}$ = desired value of bone density of cellular trait number "i" (positions arbitrarily chosen); $\boldsymbol{k_i}$ = stiffness of cellular trait number $\boldsymbol{i}$; $\boldsymbol{c}$ = damping of the system; $\boldsymbol{m}$ = inertia of the system; $\boldsymbol{F_E(t)}$ = external forces dependent on time

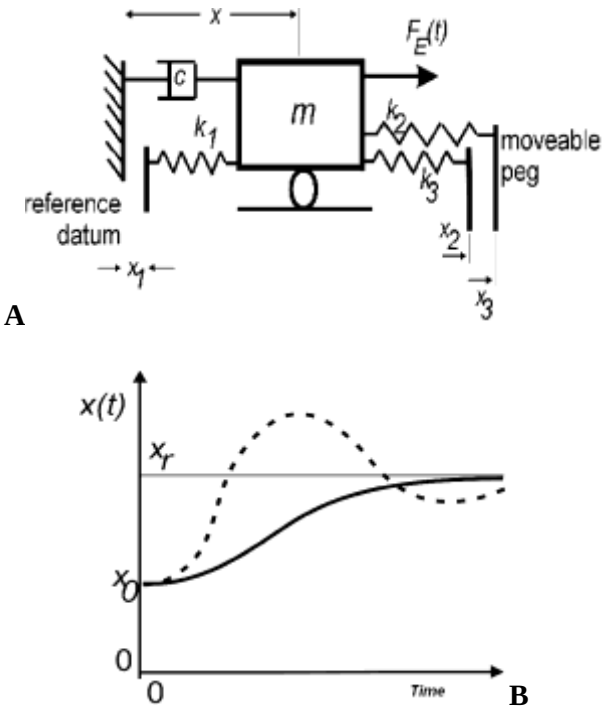

Fig.2.8.3 A, the components of the linear harmonic oscillator model, adapted from Davidson et al. (2004). B, model solutions. For detailed description see the original paper.

The solutions indicate over-(solid line) and under-damped (dashed line) kinetics in the process of bone density changes, Davidson et al. (2004).

2.8.10.5 A bioregulatory model

An interesting bioregulatory model, implementing major characteristical features of bone regeneration angiogenesis and cell migration, has been developed by Geris et al., (2008). Schematically the model is presented in Fig.2.8.4.

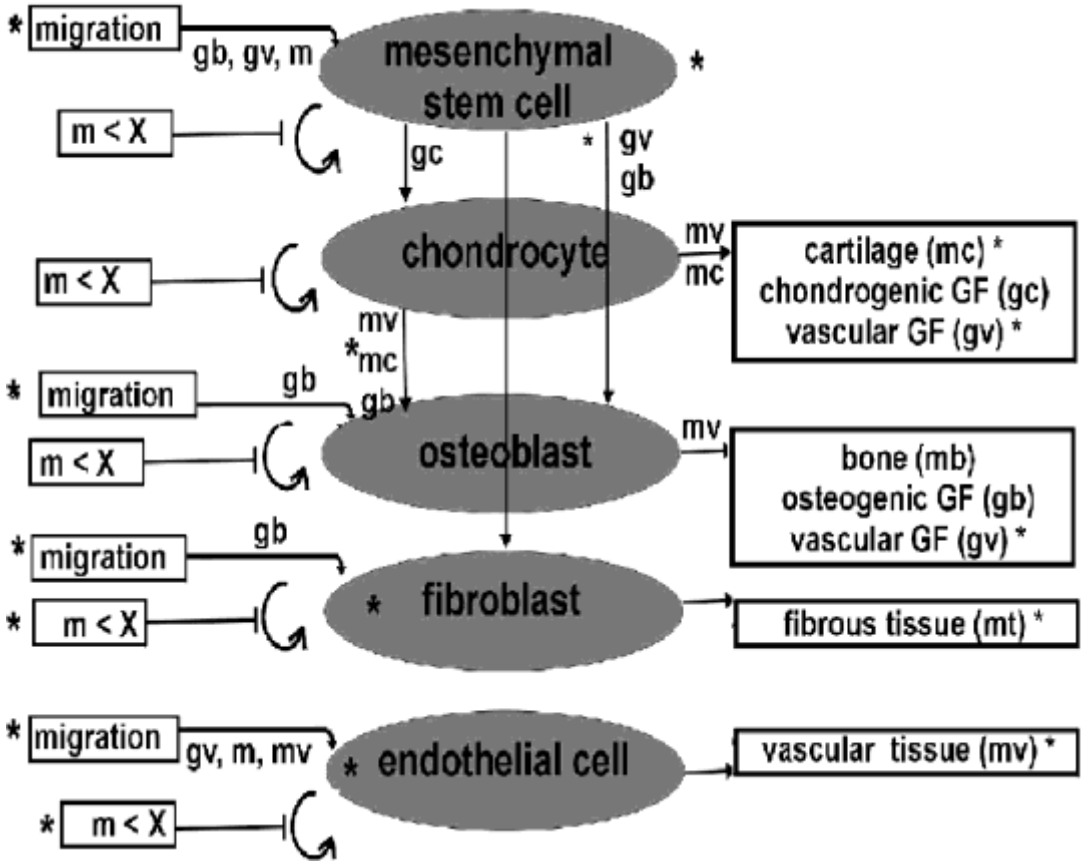

Fig.2.8.4 A schematic overview of the mathematical model. Model variables (detailed explanation of model development can be found in Geris et al., 2008): cm - mesenchymal stem cells, cc- chondrocytes, cb - osteoblasts, mb - bone extracellular matrix and a gb - generic osteogenic growth factor, gc - chondrogenic growth factor, cv - the density of endothelial cells, mv - vascular matrix and gv- generic angiogenic growth; cf - concentration of fibroblasts variable, mf - fibrous tissue, mc - cartilage density. For detailed description see the original paper.

The taxis–diffusion–reaction type (Geris et al., 2008) model is a partial differential equation system which deals with parameters designated in Fig.2.8.4. It describes complex processes in bone during the fracture healing as well as the response to biochemical imputs.

$$\frac{\partial c_m}{\partial t} = \nabla[D_m \nabla c_m - C_{mCT} c_m \nabla(g_b + g_v) - C_{mHT} c_m \nabla m]$$
$$+ A_m c_m [1 - \alpha_m c_m] - F_1 c_m - F_2 c_m - F_4 c_m,$$
$$\frac{\partial c_f}{\partial t} = \nabla[D_f \nabla c_f - C_f c_f \nabla g_b] + A_f c_f [1 - \alpha_f c_f] + F_4 c_m - F_3 d_f c_f,$$
$$\frac{\partial c_c}{\partial t} = A_c c_c [1 - \alpha_c c_c] + F_2 c_m - F_3 c_c,$$
$$\frac{\partial c_f}{\partial t} = \nabla[D_f \nabla c_f - C_f c_f \nabla g_b] + A_f c_f [1 - \alpha_f c_f] - F_4 c_m - F_3 d_f c_f,$$
$$\frac{\partial c_b}{\partial t} = \nabla[C_b c_b \nabla g_b] + A_b c_b [1 - \alpha_b c_b] + F_1 c_m + F_3 c_c - d_b c_b,$$
$$\frac{\partial c_v}{\partial t} = \nabla[D_v \nabla c_v - C_{vCT} c_v \nabla g_v - C_{vHT} c_v \nabla m_v] + A_v c_v [1 - \alpha_v c_v] - d_v c_v,$$
$$\frac{\partial m_f}{\partial t} = P_{fs}(1 - k_f m_f) c_f - Q_f m_f m_c c_b,$$
$$\frac{\partial m_c}{\partial t} = P_{cs}(1 - k_c m_c) c_c - Q_c m_c c_b,$$
$$\frac{\partial m_b}{\partial t} = P_{bs}(1 - k_b m_b) c_b,$$
$$\frac{\partial m_v}{\partial t} = P_{vs}(1 - k_v m_v) c_v,$$
$$\frac{\partial g_c}{\partial t} = \nabla[D_{gc} \nabla g_c] + E_{gc} c_c - d_{gc} g_c,$$
$$\frac{\partial g_b}{\partial t} = \nabla[D_{gb} \nabla g_b] + E_{gb} c_b - d_{gb} g_b,$$
$$\frac{\partial g_v}{\partial t} = \nabla[D_{gv} \nabla g_v] + E_{gvb} c_b + E_{gvc} c_c - g_v(d_{gv} + d_{gvc} g_v).$$

For detailed description see the original paper, Geris et al., 2008. The model predicts results similar to experimental observations in a number of compromised fracture healing cases.

2.8.11 Conclusions

As one can see there is a number of mathematical and statistical methods and approaches for the modelling of mechanical and biological properties of bone tissue have been developed. However, even though there has been considerable success in bone tissue modelling many limitations still remain. One of the most important is that there is no one, global, consistent single framework that can create a micro-physiological phenomenological model of bone remodelling and of BMU functioning.

This probably follows from the fact that any tissue, including bone tissue, has a number of levels of regulation that are made up of a system level of control (body level of organisation, physiological level) and a local tissue level. The balances of these levels are highly important for proper tissue functioning and supporting other organs in their physiological function. The study of the hierarchical co-interaction of the integrative phenomenological cellular level of bone remodelling organisation versus molecular loops of local control and the implementation of this into a formal framework is an important issue in finding a balanced mathematical model.

The models described above go some way to illustrate the complexity of the bone remodelling mechanism. However, the simplifications intrinsic in the modelling process may allow us to clarify the process further by ranking the levels of regulation (according to the hierarchy of regulation) and in addition allow insights into the basic modes of the microphysiological behaviour of the bone turnover process (at the tissue level). Such models also give us an overview of the remodelling process and its part in the overall physiologically balanced homeostasis and even highlight a specific topic or mechanism.

Alongside the difficulties of modelling the bone remodelling process many FE models treat the BMU as a 'black-box' having some phenomenological properties. Biochemico-physiological models of BMU are over simplified and are therefore limited in scope, dealing with only selected regulation loops.

In particular all models to date have failed to contain osteocite activity. We can see that the implementation of new regulation loops (e.g. osteocytes) creates a more complete picture of regulation but increases the number of qualitative modes increasing the descriptive complexity.

The sheer number of local and systemic control factors found at a local level, as discussed in section three, mean that although it may be possible to model local conditions fairly precisely, the global regulative pattern is still too complex to fully comprehend.

3 Methodology

3.1 Aims and objectives

The literature review was undertaken with respect to the mechanisms of bone resorption and formation, its control and existing mathematical models of bone remodelling. The results of the literature review were presented in Chapter 2 and some of the key findings are listed below:

- Previously developed models demonstrate a limited and unclear interpretation of autocrine and paracrine regulation. Moreover, there is also an unclear interpretation of information from the population biokinetics approaches.
- The role of osteocytes in terms of regulative feedback has largely been overlooked and there has only been a limited approach to consider the allosteric regulation.
- Previous work has demonstrated the difficulties in analysing the effects of the rate parameters on the stability of the equilibrium points.
- The dynamic systems and population biokinetics approach are not well enough understood in modelling of bone remodelling.
- The approach employed for the control/optimal regulation of BMU and bone remodelling is insufficiently clear.

The relaxational modes are quite well studied and understood in bone remodelling. However, other types of behavioural modes, like cyclic or chaotic, are less well understood but could be as important in explanation of disorders in bone remodelling, like Paget's disease or osteoporosis. Therefore one of the main objectives of this study was the investigation of the role of modes of behaviour in bone remodelling, using mathematical modelling.

Regeneration of tissue is one of the most important issues when tissue is damaged. There are different approaches to support this regeneration, for example structural support by providing a tissue scaffold is an important method which is directly linked to tissue engineering. Optimisation of scaffold properties, so called scaffold variables, is a task that can be derived from studying bone tissue remodelling properties. The model can be developed to provide a dynamic constraint for optimisation of remodelling and a useful tool in developing resorbable implants/scaffolds.

Any tissue, including bone tissue has a number of levels of regulations that can be divided as system level of control (body level of organisation, physiological level) and local tissue level. The balance of this level is highly important for proper tissue functioning and supporting other organs by its physiological function. Studying of hierarchical co-interaction of integrative phenomenological cellular level of bone remodelling organisation versus molecular loops of local control and implementation of this into formal model was one of the tasks of the present study.

Because of multivariable character of data that can be obtained from experiments, and multivariable character of studying tissue and processes and description, the approach to data reduction and visualisation was an important technical issue that was included in this study also.

The overall aim of this project is to develop a model of bone remodelling (BMU) containing the osteoclast's level of regulation and study approaches to formulate the control of bone remodelling within this model in an optimal way.

Specific objectives are:

- To revise the existing mathematical models of bone remodelling to provide a more complete picture of cellular interactions of the Basic Multicellular Unit (BMU) with the network of osteocytes in bone tissue. Formulate the mathematical model to incorporate the osteocyte level of regulation.
- To revise important allosteric mechanisms involved in BMU regulation and develop approaches to incorporate formally these mechanisms within the framework of existing models.
- Study the steady solutions of this model, which have a physiological sense. Analyse the behaviour of the models developed across a wide range of biologically relevant constants in order to assess the validity of the models.
- Formulate an optimal control approach to regulate the BMU model behaviour regarding certain criteria.

3.2 Population kinetic methodology and model formulation

The population kinetics approach methods are based on few assumptions.

The first assumption is that there is a positive feedback characteristic for any biological species from viruses to humans. This positive feedback reflects the basic, principal property of any bio-system – autocatalysis, self-replication, self-multiplication. In the population dynamics ODE models, this is formally introduced as a first order term with a positive coefficient. In a classical one-dimensional Malthus model (1798) it is formalised as the velocity of self-reproduction of a biological population (population density) is proportional to the value of existing population

$$\frac{dn}{dt} = an \tag{3.1}$$

where n is population size (population density), a is a positive coefficient. The first order of the term is sometimes linked to assumption of an unlimited resource of substrate/energy, which is in-line with the chemical kinetics models of autocatalysis.

The second assumption is that when the substrate and energy resource is limited, it can be treated as a tightening of competition for this resource. It can be implemented formally as a negative second order-term in the differential equation. In fact it is reflecting a situation when a biospecies comes close to total consumption of a substrate-energetical resource of its existance. Then, a combination of these two terms in the one dimensional case gives the well known Verhulst-Pearl equation (Verhulst, 1838)

$$\frac{dn}{dt} = an - bn^2 \tag{3.2}$$

where a, b are positive coefficients. In this study we applied similar ideology.

When this approach/ideology is extended to the interaction of two or more biospecies, the ODE kinetic systems becomes;

$$\frac{dn_1}{dt} = a_1 n_1 - b_1 n_1 n_2, \frac{dn_2}{dt} = a_2 n_1 n_2 - b_2 n_2^2 \tag{3.3}$$

where n_1 , n_2 are population densities of two different species, a_1, a_2, b_1, b_2 are positive coefficients. The second term in the first equation and first term in the second equation describe the so-called predator-pray, or producer-consumer relations, when the biomass produced at the first level, biomass of a producer (n_1) is consumed by the species of the second level (n_2).

For three levels of consumption/regulation, the dynamic system can be written as

$$\begin{aligned} \frac{dn_1}{dt} &= a_1 n_1 - b_1 n_1 n_2 \\ \frac{dn_2}{dt} &= a_2 n_1 n_2 - b_2 n_2 n_3 \\ \frac{dn_3}{dt} &= a_3 n_2 n_3 - b_3 n_3^2 \end{aligned} \tag{3.4}$$

The methodology, based on these three main assumptions with different variations, is implemented into different models within models of biological/population kinetics based on ODE.

Such a relation as discussed in the models above, from the regulatory perspective can be treated as a positive or negative feedback in the regulation of population (population density) of the species. In a tissue, this feedback, is not represented by a predator-pray mechanisms but by the apoptosis or death of the cells expressed by the second terms in the equations with b coefficients. In fact similar ideology was employed in other mathematical models of bone remodelling (Komarova et al., 2003, Putra et al., 2010). In this study similar methodology, based on combination ODE methods in modelling and population dynamics ideology has also been implemented.

3.3 Optimal control methodology employed

The optimal control methodology was implemented based on the fundamental work of Pontryagin et al., 1962, Gelfand and Fomin 1963.

In a general case the optimal control problem accordingly to Pontryagin maximum principle, Pontryagin et al., 1962, can be written as

$$J = \int_{t_0}^{\tau} l(x_1,...x_i...x_N, u_1,...u_j,...u_M)dt \to \min, i = 1...N,\ j = 1..M \qquad (3.5a)$$

subject to dynamical constrains

$$\frac{dx_i}{dt} = f_i(x_1,...x_i...x_N, u_1,...u_i,...u_M), i = 1...N,\ j = 1..M \qquad (3.5b)$$

and $x_i(\tau_0) = x_{i0}$ and end-point condition $x_i(\tau)$ is free,

where $x_1,...x_i...x_N$ are the state variables, $u_1,...u_i,...u_M$ are the control variables, $f_i(x_1,...x_i...x_N, u_1,...u_i,...u_M)$ is a function, J is objective functional, $l = l(x_1,...x_i...x_N, u_1,...u_i,...u_M)$ is the "running cost" of the optimal control that is referred as instantaneous costs/losses for optimal control. Then accordingly to the Pontryagin maximum principle, a Hamiltonian function can be constructed as

$$H = \sum_{i=1}^{N} p_i f_i(x,u) - l(x,u) \qquad (3.6)$$

where p_i are the Lagrange multipliers or costate variables.

Then the canonical equations are

$$\frac{dx_i}{dt} = \frac{\partial H}{\partial p_i} = f_i(x,u) \quad \text{(state variable system)}$$

$$\frac{dp_i}{dt} = -\frac{\partial H}{\partial x_i} \quad \text{(adjoint/costate variable system)} \qquad (3.7)$$

$$\frac{\partial H}{\partial u_j} = 0 \quad \text{(necessary conditions for optimality),}$$

and transversality condition: $p_i(\tau)=0$ (since time τ is free, so no terminal condition is specified, the constant $p_i(\tau)$ could be assumed equal to zero). Also, since the Hamiltonian function (3.6) is not dependent on time explicitly, the first integral of this problem is *H=Const*.

The alternative approach to this optimal control problem is directly based on variational calculus, see, for example, Gelfand and Fomin, 1963, because the control could be chosen as formally unlimited: it could formally vary from *0* to ∞. The objective functional could remain

as (3.5a) subject to constraints (3.5b) and boundary conditions $x_i(\tau_0) = x_{i0}$ and free end-point condition. Then the Lagrange method can be applied

$$L = l(x,u) + \sum_{i=1}^{N} p_i \left(\dot{x}_i - f_i(x,u) \right) \tag{3.8}$$

and the Euler-Lagrange equations will be

$$\begin{aligned} &\frac{\partial L}{\partial x_i} = \frac{dp_i}{dt}, \frac{\partial L}{\partial u_j} = 0 \\ &\frac{\partial L}{\partial p_i} = \dot{x}_i - f_i(x,u) = 0 \end{aligned} . \tag{3.9}$$

Although the technique of variational approach looks different from the maximum principle formulation, they lead to the same results. The system (3.9) in fact coincides with (3.7) reflecting the point that the maximum principle is the non-classical method for solving the variational problem in the case of open-loop control. In the case the Lagrange function (3.8) is not explicitly dependent on time so an another form of the first integral of the problem could be found in (Gelfand and Fomin, 1963):

$$H(x, \frac{dx}{dt}) = \sum_{i=1}^{N} \frac{\partial L}{\partial \frac{dx_i}{dt}} - L = Const \tag{3.10}$$

which could significantly simplify the process of finding analytical solution and play important role on the stage of interpretation. On the basis of this general approach two different enzyme control models were investigated. In the OC developments of the project, the OC applications to biokinetics in works of (Van Impe and Bastin, 1995; Rahman, and Palanski, 1996; Van Riel et al., 2000; Giuseppin and van Riel, 2000; Cacik et al., 2001; Sengupta and Modak, 2001; Keesman and Stigter, 2002; Srinivasan et al., 2003; Smets, et al. 2002, 2004; Visser et al, 2004; Gadkar et al., 2006); Mohseni et al., 2009; Yüzgeç et al., 2009; Liang et al., 2008; Itik et al., 2009; Chávez et al., 2009; Eren-Oruklu et al., 2009; Acikgoz and Diwekar, 2010) have been used.

3.4 Rubustness, character of equilibrium of the equilibrium points. Numerical methods

The robustness of equilibrium points were studied by calculation of the Jacobian matrix, and analysis its eigenvalues. For some models, the points of equilibrium were found analytically, the elements of Jacobian matrix were found analytically as well. Then the eigenvalues were calculated numerically used standard procedure in Matlab and the scatterplots were produced and analysed. For the optimal control models, the numerical calculation of points of equilibrium were performed using the FSOLVE procedure in Matlab. For numerical methods to solve the formulated dynamic systems the Matlab and Mathcad software were used. The statistical calculations were performed using the SAS software version 9.1.

Numerical integration of the differential equation systems was done by a fourth-order the Dormand-Prince pair Runge-Kutta based *ode45* Matlab® algorithm (v7, the MathWorks Inc, 1998). Recalculations were performed using MathCad® Runge-Kutta subroutine *rkfixed,* MathCad 2000 Professional, MathSoft Inc., 1999.

5.5 Statistical methods. Canonical correlation analysis

Principal component analysis (PCA) is employed when the reduction of the dimensionality of a vector is needed. In this case the principal components are the orthogonal system of the linear combinations of measured variables. Application of PCA finds the first principal component as a linear combination along which the total dispersion obtains maximum. The second principal component is calculating in the way that the total dispersion obtains maximum subject to the orthogonality to the first principal component. As the result, the principal components are chosen as the linear combinations of original variables to maximise the total dispersion. Canonical correlation analysis (CCA) is an analogical method to PCA for analysis the relationship between two linear combinations of variables (Hotelling, 1935; 1936). Comparably to the multiple regression analysis, when a set of linear combination of

variables (independent variables) is analysed in respect to a single variable (dependent variable), CCA is a generalisation of multiple correlation/regression. Canonical weights show the unique impacts of every variable while the factor loads are the simple summary correlations.

CCA is a powerful method to study the structure of two sets of variables. For example, this method could be used in study of the correlation between two sets of concentrations of amino acids in blood. One of the sets can be the neurotransmitter amino acids and another set can be the amino acids characteristic to the transport in the blood.

3.6 Statement of novelties

The literature review conduction let to state the novelties expected in this project:

- Modification/development of the existing mathematical model (Komarova et al., 2003) of bone remodelling in sense of more completed cellular interactions of basic multicellular unit with osteocytes, the cells incorporated into bone tissue.
- Development of an approach to phenomenological formulation of the molecular mechanisms regulation the BMU activity and approach to incorporate these mechanisms into the expected model.
- Formulation of the criteria related to the energetical/metabolic optimisation losses for the development a regulation model of BMU activities.

It was expected that the results would increase the understanding of bone remodelling from the perspective of the rates of bone tissue formation and resorption.

4 Cellular approach to bone remodelling model

4.1 The osteocyte loop control introduction into the BMU model

This study investigates a possible dynamic systems option based on known modelling approaches**,** but with a reduced number of parameters and employing a rather general assumption of the relationship between bone cells and bone material mass. The prototype of such an approach is implemented in works Komarova and coauthors (2003, 2004).

Although the model developed by Komarova et al. (2003) predicts different modes of dynamic behaviour of the BMU in bone remodeling control, a number of limitations to this model were identified by the authors of this model. Among these limitations is a need for improvement to the autocrine regulation loop, whilst at the same time the paracrine regulation loops employ quite a wide range of parameters (e.g. power ~ -0.5) rather beyond the biologically relevant range. Additionally, many publications indicate the importance of the level of osteocyte regulation, for example, the role of osteocyte apoptosis as a part of the mechanotransduction control mechanism (Noble, 2003; Taylor et al., 2003; Bonewald, 2004), and role of stress (Nakamura, 2003).

For this reason the role of osteocyte's apoptosis in the bone remodelling regulation loop and the requirement to redevelop the model in such a way that the autocrine and paracrine control would be more biologically relevant from a generalised point of view were critical aspects to the development of the model. The regulation loops that control the activity of the BMU were refined and attempted to introduce the cybernetic point of view that the control should be minimised from both the (catabolic) energetic point and metabolic point of view. For example, a reason for this could be the limitation of the transport into the bone of the energetic substrates such as, for example, ATP and oxygen, as well other substrates. The changes from basic bone turnover rate could destabilise the metabolic optimality not only on the local (bone) level but could also create a supply problem for the body. The whole number of molecular messengers of the bone remodelling process should not exceed a particular limiting level to

avoid overloading the metabolic process of remodelling, both at the local tissue level and the body level.

Additionally, it is believed that in order to produce a robust bone remodeling process the regulation needs robustness at a number of regulation levels, and indeed cellular levels. The molecular biochemical regulation loops at the tissue level are only organised by cell interactions via common compartments (body or tissue media) such as marrow-media, lacunocanalicular microcirculatory system of periosteocytic fluid in the case of bone. The active interaction units are the osteocells. Phenomenological cellular models must reflect the tissue infrastructure of regulation and function in the whole body and, from the other side the very robust biochemical pathways. To answer what is the primary controlling factor is akin to answering what is the first, the chicken or the egg. In the case of a multicellular organism and tissue, an evolutionary process is taking place. Probably, from the evolutionary point of view, the cellular level is even more important, because the multicellular body evolved from cellular colonies with initially poor communication. Taking into account this point, this section attempts to develop and analyse the possibility of a cellular model and robustness at this level.

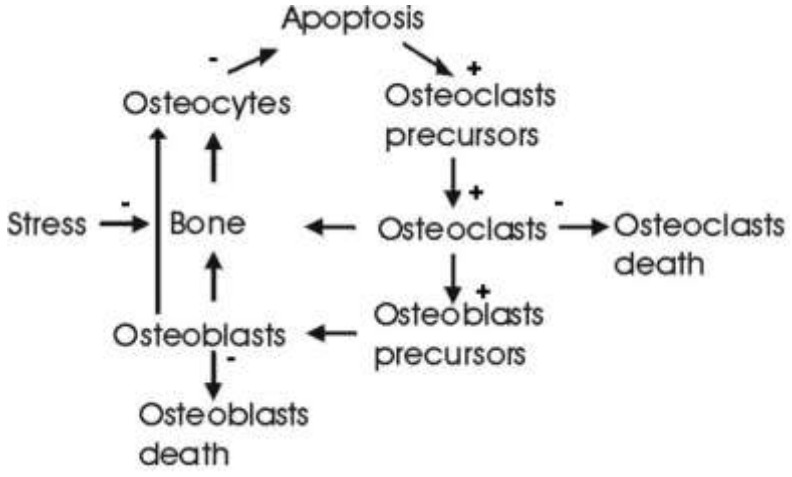

Fig. 4.1 Schematic representation of interaction between the cells in BMU. Arrows represent the control loops of regulation in BMU on the cellular level.

The resulting cell-level control scheme based on the introduction of the osteocytes control loop could be presented as in Fig.4.1, where osteocytes' apoptosis initiates the osteoclasts maturation from the osteoclasts' precursors.

A dynamical model, which generalises the Komarova model (Komarova et al., 2003) and Putra model (Putra et al., 2010) and includes osteocyte's level of regulation could be written as

$$\begin{aligned}\dot{x}_1 &= f^{+}_{OCl}(x_1, x_2, x_3) - f^{-}_{OCl}(x_1, x_2)\\ \dot{x}_2 &= f^{+}_{OBl}(x_1, x_2) - f^{-}_{OBl}(x_2, x_3, x_4)\\ \dot{x}_3 &= f^{+}_{OCt}(x_2, x_4) - f^{-}_{OCt}(s, x_3)\\ \dot{x}_4 &= f^{+}_{B}(x_2) - f^{-}_{B}(x_1)\end{aligned} \tag{4.1}$$

where x_1 is the population density of osteoclasts (Ocls), x_2 is the population density of osteoblasts (Obl), x_3 is the population density of osteocytes (Octs), x_4 is the bone mass of a volume unit (BM). In Komarova et al., 2003, the changes in bone mass was presented "as relative change from initial value (100%)". In this study the parameter x_4 follows Komarova et al., 2003 definition in the changes in bone mass, however initial value was taken as 1.0. The quantity *s* is the level of mechanical stress. Functions

$$f^{+}_{OCl}(x_1, x_2, x_3),\ f^{+}_{OBl}(x_1, x_2),\ f^{+}_{OCt}(x_2, x_4),\ f^{+}_{B}(x_2) \tag{4.2}$$

describe the paracrine and autocrine positive feedback loops of regulation,

$$f^{-}_{Ocl}(x_1, x_2),\ f^{-}_{Obl}(x_2, x_3, x_4),\ f^{-}_{Oct}(s, x_3),\ f^{-}_{B}(x_1) \tag{4.3}$$

describe negative regulation feedbacks. This model appears as certain generalisation of models by Komarova et al. (2003), Lemaire et al. (2004) and Putra et al. (2010). The dependence in these feedback functions is undertaken with the purpose of reducing the number of parameters based on the following assumptions: $f^{+}_{OCl}(x_1, x_2, x_3)$ - osteoclasts regeneration has autocrine properties and is initiated by osteocyte's apoptosis, following Noble (2003), Taylor et al. (2003), Bonewald (2004); osteoclasts degradation function, $f^{-}_{OCl}(x_1, x_2)$ - depends on regulation by osteoblasts and osteocytes; $f^{+}_{OBl}(x_1, x_2)$ - osteoblast activation positive feedback loop related to the bone material density, $f^{-}_{OBl}(x_2, x_3, x_4)$ - osteoblast's transformation to osteocytes, lining cells and their apoptosis; $f^{+}_{OCt}(x_2, x_4)$ - osteocytes differentiation from osteoblasts depends on the bone material generated, $f^{-}_{OCt}(s, x_3)$ - osteocytes apoptosis is dependent on the stress attitude and

the bone density; and, finally, $f_B^+(x_2)$ - the bone mass formation is dependent on the osteoblasts density and the bone resorption function $f_B^-(x_1)$ depends on osteocytes level.

In fact, the Komarova model implicitly contains the predator-pray elements. In case when the power coefficients are integer (1,2) the model would similar to the second-order predator pray model.

4.2 Model simplification: BMU regulation by Ocls-Octs interactions

4.2.1 Model formulation

The system (4.1) can be further simplified when the particular functions (4.2-4.3) are chosen. Based on the model developed by Komarova et al. (2003) and Putra et al. (2010), it can be suggested particular dependence of f_i^+ and f_i^-, which gives the following system

$$\begin{aligned} \dot{x}_1 &= a_1 x_1 - b_{12} x_1 x_3 - b_{01} x_1 x_2 \\ \dot{x}_2 &= a_{01} x_1 x_2 - b_2 x_2 x_4 - b_{23} x_2^2 \\ \dot{x}_3 &= a_3 x_4 - s x_3 \\ \dot{x}_4 &= -k_1 x_1 + k_2 x_2 \end{aligned} \tag{4.4}$$

where b_{12}, a_{01}, a_{21}, a_3 are the autocrine and paracrine constants formalising the positive regulation loops, b_{12}, b_{01}, b_2, b_{23} are the removal constants and negative regulation loop constants, and k_1, k_2 are constants of direct bone resorption by osteoclasts and formation by osteoblasts, s – the attitude of the mechanical stress.

In the first equation of the model, which describes the osteoclasts kinetics, the first term formalises the positive feedback, e.g. autocrine regulation of osteoclasts, the second term describes negative paracrine feedback by osteocytes and the third term describes degradative regulation on osteoclasts by osteoblastic cells (when the role of osteoclasts is considered and the bone formation starts). An explanation of the negativity of the second term in this equation follows. The main suggestion of this model is that the osteoclasts are regulated/initiated by Osteocytes. In this case it is logical to suggest that the term describing this regulation is

proportional to the population density (amount) of osteoclasts, x_1 and the difference $(x_3 - x_3^{St})$, where x_3^{St} is stationary concentration of osteocytes. When damage to the bone happens, then $x_3 < x_3^{St}$ and the $(x_3 - x_3^{St})$ is negative and the product of x_1 and the bracket $x_1(x_3 - x_3^{St})$ should be a positive to create positive feedback, so, since $x_3 > 0$ this term should have a negative coefficient $-b_{12}$, then $-b_{12}x_1(x_3 - x_3^{St})$ will create a positive feedback relatively to an decrease of osteocytes from normal state when bone is not damaged. It also can be rewritten as $-b_{12}x_1(x_3 - x_3^{St}) = b_{12}x_1x_3^{St} - b_{12}x_1x_3 = a_1x_1 - b_{12}x_1x_3$, where $a_1 = b_{12}x_3^{St}$. This in fact is an explanation of first and second terms in the differential equation for osteoclasts.

In the second equation, the first term describes positive feedback in osteoclasts-osteoblasts regulation, the second term formalises the decrease of the osteoblasts due to their change into osteocytes and the last quadratic term describes their apoptosis/death. The third equation describes the changes in the population density of osteocytes. The first term in the right part suggests that the surplus rate of osteocytes is proportional to the bone mass when the bone mass formed. The removal/apoptosis of osteocytes is proportional to the microgravitation/mechanical stress or "metabolic fatigue" of the bone tissue with the rate constant s. Increased mechanical stress (microgravity) will increase the apoptosis of osteocytes. The last equation is adopted from Komarova model (Komarova et al, 2003). Taking into account considerations by Komarova et al., 2003, in this study the same range of the rate constant was adopted, extended for a decimal order in the widest case.

The concrete link of molecular factors, (GFs, cytokines, hormones) to the reta parameters of the model is difficult to suggest. The cellular models, described in literature (Komarova et al. (2003), Lemaire et al. (2004) and Putra et al. (2010) have also problems with this. That can be explained by microscopic character of action of factors and macroscopic, phenomenological character of rate parameters included in population models.

4.2.2 Equilibrium points

To find the equilibrium points of the system (4.4) one needs to make the right parts of the system equal to zero, then a system of algebraic equations is obtained:

$$\begin{aligned} &a_1 x_1 - b_{12} x_1 x_3 - b_{01} x_1 x_2 = 0 \\ &a_{01} x_1 x_2 - b_2 x_2 x_4 \ - b_{23} x_2^2 = 0 \\ &a_3 x_4 - s x_3 = 0 \\ &- k_1 x_1 + k_2 x_2 = 0 \end{aligned} \tag{4.5}$$

Then starting from the last equation one can find $x_2 = k_1 x_2 / x_1$. Substituting this into the others equations of (4.5) one can find the nontrivial solution. Designating $Z = a_{01} k_2 a_3 b_{12} + b_2 s k_1 b_{01} - b_{23} k_1 a_3 b_{12}$ one can write

$$x_1 = \frac{a_1 b_2 k_2 s}{Z}, x_2 = \frac{a_1 b_2 k_1 s}{Z}, x_3 = \frac{a_1 a_3 (a_{01} k_2 - b_{23} k_1)}{Z}, x_4 = \frac{s a_1 (a_{01} k_2 - b_{23} k_1)}{Z} \tag{4.6}$$

and the trivial solution:

$$x_1 = 0, x_2 = 0, x_3 = x^*, x_4 = {sx^*}/{a}, \tag{4.7}$$

where x* can have any value; $x^* \in [0, \infty]$. The latter means that all the axes x_3 and x_4 are the solution when $x_1 = x_2 = 0$. Designating right parts of (4.4) as F_i one can find the Jacobian matrix:

$$\begin{aligned} &\frac{\partial F_1}{\partial x_1} = -b_{12} x_3 + a_1 - b_{01} x_2, \frac{\partial F_1}{\partial x_2} = -b_{01} x_1, \frac{\partial F_1}{\partial x_3} = b_{12} x_1, \frac{\partial F_1}{\partial x_4} = 0; \\ &\frac{\partial F_2}{\partial x_1} = a_{01} x_2, \frac{\partial F_2}{\partial x_2} = a_{01} x_1 + b_2 x_4 - 2 b_{23} x_2, \frac{\partial F_2}{\partial x_3} = 0, \frac{\partial F_2}{\partial x_4} = -b_2 x_2; \\ &\frac{\partial F_3}{\partial x_1} = 0, \frac{\partial F_3}{\partial x_2} = 0, \frac{\partial F_3}{\partial x_3} = -s, \frac{\partial F_3}{\partial x_4} = a_3; \\ &\frac{\partial F_4}{\partial x_1} = -k_1, \frac{\partial F_4}{\partial x_2} = k_2, \frac{\partial F_4}{\partial x_3} = 0, \frac{\partial F_4}{\partial x_4} = 0; \end{aligned} \tag{4.8}$$

Employing (4.8) it is possible to study the character of equilibrium for the trivial (4.7) and nontrivial (4.6) points. Let us note that the quantity z plays very significant role in determination the equilibrium.

4.3 The character of stability in a wide range of the rate constants

As one can see from previous section, the system (4.5) has two solutions the point of equilibrium which give two points of equilibrium; one is the trivial point (4.7), and the second is the non-trivial point (4.6), axis x_4 which formalises the total bone mass. The nontrivial point is of particular interest for this study because it gives the non-zero values for population densities of osteocells in bone tissue. The range of parameters that cover the possible physiological values of the system has been studied numerically by the Monte-Carlo method by generating random combinations of rate parameters, uniformly and exponentially distributed in certain range. The consideration of the rate constants has been made on the basis of the Komarova model (Komarova et al., 2003). The upper and lover estimates were extended to the following range: a_1, 200.0- 30000. day^{-1} ; b_{12}, 0.002-0.05 $cell^{-1}day^{-1}$; b_{01}, 1.0-40.0 $cell^{-1}day^{-1}$; a_{01}, 1.50-300.0 $cell^{-1}day^{-1}$; b_2, 50.0-1000.0 $cell^{-1}day^{-1}$; b_{23}, 0.001-0.09 $cell^{-1}day^{-1}$; a_3, 1000-66000 day^{-1}; s, 0.001-2.0 $cell^{-1}day^{-1}$; k_1, 0.01-1.0 day^{-1}; k_2, 0.00003-0.003 day^{-1}. The range of the rate parameters has been chosen to satisfy the population densities of osteocells in one cubic millimetre. According to some authors the population concentration of osteoclasts in one cubic millimetre is about 20; of osteoblasts in one cubic millimetre is about 10^3; osteoclasts in one cubic millimetre is about 20; the population concentration of osteocytes in one cubic millimetre is about 10^4. As in was mentioned above, the parameter $x_4$characterising the bone mass (which in figures is designated as BM) was chosen following the Komarova et al works, 2003; 2005 as relative bone mass of one cubic millimetre, which was chosen as equal to unit in the steady state.

The values of the nontrivial steady state are shown graphically in Fig.4.2. One can see the scatter plot of non-trivial equilibrium points in the projection from 4-dimensional space of Ocl, Obl, Oct and BM (total bone mass of a volume unit). A more detailed scatter-plot of the population densities (variables Ocl, Obl, Oct and total bone mass of a unit) against each other is shown in Fig.4.3. One can see the scatter of Ocl density in the range of 5 to 50, Obl from several hundreds to several thousands, Osteocytes from hundreds to thousands. The bone mass variable was employed as the relative, which in steady state equals to 1.

Since the relationship between the location of the main stability point and the rate constants, indicated in (4.6) is quite complicated, in order to study the influence of these constants on the position and the character of equilibrium, the Monte Carlo method (Metropolis and Ulam, 1949) and further regression analysis (Pearson, 1901) was applied to establish the link. The application of Monte Carlo method in combination with regression analysis is shown in Tables 4.1-4.7 and the results are summarized in Tables 4.8-4.11.

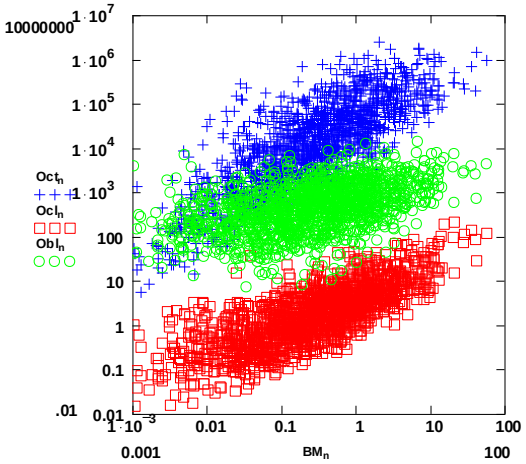

Fig. 4.2 Scatterplot of calculated positions of equilibrium of osteocells (OCl, osteoclasts; OB, osteoblasts; OCt, osteocytes) against the total bone mass (BM) for the system (4.4). Calculations were performed using the following set of parameters: a_1, 200.0- 30000. day^{-1} ; b_{12}, 0.002-0.05 $cell^{-1}day^{-1}$; b_{01}, 1.0-40.0 $cell^{-1}day^{-1}$; a_{01}, 1.50-300.0 $cell^{-1}day^{-1}$; b_2, 50.0 -1000.0 $cell^{-1}day^{-1}$; b_{23}, 0.001-0.09 $cell^{-1}day^{-1}$; a_3, 1000-66000 day^{-1}; s, 0.001-2.0 $cell^{-1}day^{-1}$; k_1, 0.01-1.0 day^{-1}; k_2, 0.00003-0.003 day^{-1}.

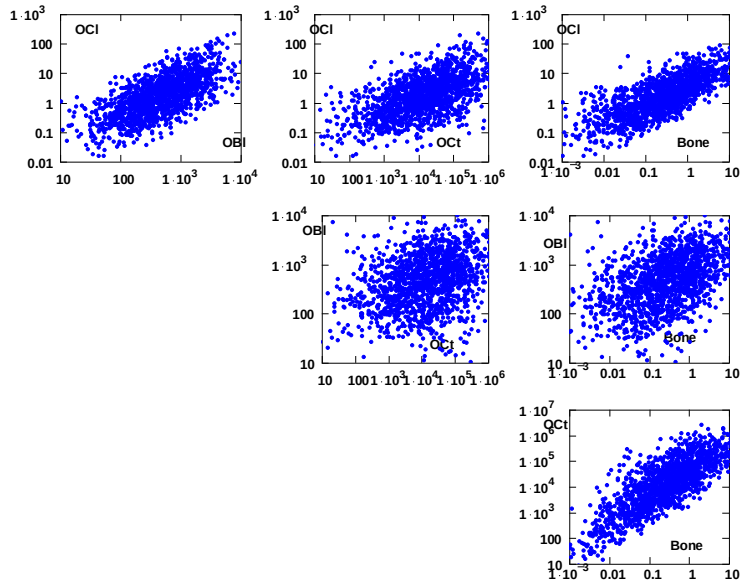

Fig.4.3 Detailed graphical matrix showing a scatter plot of population densities of Ocl,Obl,Oct,bone in 4D space of these quantities. Exponential distribution of the rate parameters for the system (4.4). Calculations were performed using the set of parameters, Fig.4.2.

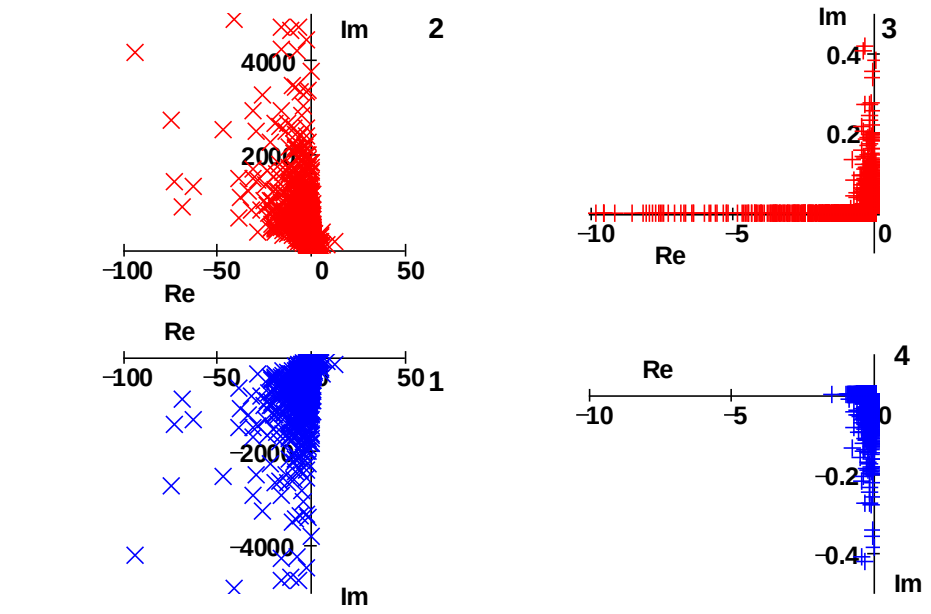

Fig. 4.4 Scatter plot of the eigenvalues (4.8) for the system (4.4). Calculations were performed using the set of parameters, Fig.4.2.

One can see from Fig.4.2-4.3, that the values of the state variables are scattered in several decimal orders, so the logarithm of these values has been used in calculations.

ln(Ocl)	BETA	St. Err. of BETA	B	St. Err. of B	t(2951)	p-level
Intercept			0.2670	0.0562	4.7493	0.0000
a1	1.0478	0.0165	0.0005	0.0000	63.6954	0.0000
b12	-0.0548	0.0068	-17.5487	2.1738	-8.0730	0.0000
b01	-0.6599	0.0174	-0.2688	0.0071	-37.9813	0.0000
a01	-0.2248	0.0181	-0.0105	0.0008	-12.4430	0.0000
b2	0.1352	0.0195	0.0022	0.0003	6.9531	0.0000
a3	-0.0636	0.0068	0.0000	0.0000	-9.3522	0.0000
s	0.2028	0.0157	1.5680	0.1218	12.8788	0.0000
k1	-0.7857	0.0166	-13.9157	0.2935	-47.4150	0.0000
k2	0.8896	0.0174	4416.50	86.4404	51.0930	0.0000
a1^2	-0.5598	0.0164	0.0000	0.0000	-34.1445	0.0000
b01^2	0.3364	0.0173	0.0073	0.0004	19.4088	0.0000
a01^2	0.1243	0.0179	0.0000	0.0000	6.9357	0.0000
b2^2	-0.0713	0.0195	0.0000	0.0000	-3.6662	0.0003
s^2	-0.1322	0.0157	-1.2238	0.1456	-8.4053	0.0000
k1^2	0.4147	0.0164	18.2681	0.7243	25.2227	0.0000
k2^2	-0.5117	0.0173	-1841851.4	62441.18	-29.4974	0.0000

Table 4.1 Quadratic regression analysis: the logarithm of the population density of the osteoclast as a function of the rate constants. The range of the constants as in Fig.4.2.

Ln(Obl)	BETA	St. Err. of BETA	B	St. Err. of B	t(2950)	p-level
Intercept			5.996	0.051	118.494	0.000
a1	1.304	0.018	0.000	0.000	72.333	0.000
b12	-0.070	0.007	-17.914	1.899	-9.435	0.000
b01	-0.838	0.019	-0.272	0.006	-43.988	0.000
a01	-0.255	0.020	-0.010	0.001	-12.853	0.000
b2	0.157	0.021	0.002	0.000	7.352	0.000
a3	-0.134	0.017	0.000	0.000	-7.956	0.000
s	0.253	0.017	1.557	0.106	14.641	0.000
k1	0.254	0.018	3.590	0.256	14.003	0.000
k2	-0.180	0.019	-713.331	75.514	-9.446	0.000
a1^2	-0.699	0.018	0.000	0.000	-38.900	0.000
b01^2	0.436	0.019	0.008	0.000	22.942	0.000
a01^2	0.134	0.020	0.000	0.000	6.801	0.000
b2^2	-0.078	0.021	0.000	0.000	-3.680	0.000
a3^2	0.064	0.017	0.000	0.000	3.796	0.000
s^2	-0.166	0.017	-1.222	0.127	-9.612	0.000
k1^2	-0.154	0.018	-5.403	0.633	-8.541	0.000
k2^2	0.071	0.019	203957.451	54545.224	3.739	0.000

Table 4.2 Quadratic regression analysis: the logarithm of population densities of osteoblast as a function of the rate constants. The range of the constants as in Fig.4.2.

ln(Oct)	BETA	St. Err. of BETA	B	St. Err. of B	t(2949)	p-level
Intercept			9.185	0.092	100.365	0.000
a1	0.753	0.019	0.000	0.000	40.650	0.000
b12	-0.047	0.008	-20.992	3.387	-6.197	0.000
b01	-0.446	0.020	-0.252	0.011	-22.873	0.000
a01	0.744	0.020	0.048	0.001	36.671	0.000
b2	-0.329	0.022	-0.007	0.000	-15.049	0.000
b23	-0.067	0.008	-16.549	1.909	-8.667	0.000
a3	0.492	0.017	0.000	0.000	28.608	0.000
s	-0.785	0.018	-8.422	0.190	-44.382	0.000
k1	-0.625	0.019	-15.372	0.457	-33.602	0.000
k2	0.765	0.020	5271.252	135.282	38.965	0.000
a1^2	-0.395	0.018	0.000	0.000	-21.460	0.000
b01^2	0.233	0.019	0.007	0.001	11.986	0.000
a01^2	-0.422	0.020	0.000	0.000	-20.996	0.000
b2^2	0.147	0.022	0.000	0.000	6.738	0.000
a3^2	-0.244	0.017	0.000	0.000	-14.192	0.000
s^2	0.422	0.018	5.415	0.227	23.868	0.000
k1^2	0.287	0.018	17.522	1.129	15.523	0.000
k2^2	-0.444	0.020	-2218402.2	97533.478	-22.745	0.000

Table 4.3 Quadratic regression analysis: the logarithm of the osteocytes populational density as a function of the rate constants. The range of the constants as in Fig.4.2.

ln(BM)	BETA	St. Err. of BETA	B	St. Err. of B	t(2950)	p-level
Intercept			-1.9178	0.0794	-24.1524	0.0000
a1	0.8962	0.0199	0.0005	0.0000	44.9695	0.0000
b12	-0.0441	0.0082	-16.2801	3.0266	-5.3791	0.0000
b01	-0.5430	0.0210	-0.2549	0.0099	-25.8516	0.0000
a01	0.8800	0.0218	0.0475	0.0012	40.3077	0.0000
b2	-0.4125	0.0235	-0.0078	0.0004	-17.5491	0.0000
b23	-0.0839	0.0083	-17.2415	1.7061	-10.1060	0.0000
a3	-0.0544	0.0082	0.0000	0.0000	-6.6255	0.0000
s	0.1772	0.0190	1.5798	0.1695	9.3180	0.0000
k1	-0.7715	0.0200	-15.7488	0.4087	-38.5310	0.0000
k2	0.9305	0.0211	5324.9	120.8	44.0609	0.0000
a1^2	-0.4738	0.0198	0.0000	0.0000	-23.8979	0.0000
01^2	0.2715	0.0209	0.0068	0.0005	12.9660	0.0000
a01^2	-0.5024	0.0216	-0.0002	0.0000	-23.2073	0.0000
2^2	0.1926	0.0235	0.0000	0.0000	8.1938	0.0000
s^2	-0.1141	0.0190	-1.2169	0.2027	-6.0030	0.0000
k1^2	0.3683	0.0199	18.7006	1.0086	18.5419	0.0000
k2^2	-0.5406	0.0210	-2242797	87136.6	-25.7389	0.0000

Table. 4.4 Quadratic regression analysis: the logarithm of the BM as a function of the rate constants. The range of the rate constants as in Fig.4.2.

ln(Re1)	BETA	St. Err. of BETA	B	St. Err. of B	t(2952)	p-level
Intercept			-1.364	0.068	-19.948	0.000
a1	1.130	0.022	0.001	0.000	52.385	0.000
b12	-0.052	0.009	-18.313	3.109	-5.889	0.000
b01	-0.694	0.023	-0.309	0.010	-30.468	0.000
a01	-0.035	0.009	-0.002	0.000	-3.879	0.000
b23	0.950	0.019	185.101	3.755	49.290	0.000
a3	-0.054	0.009	0.000	0.000	-6.111	0.000
s	0.254	0.021	2.145	0.174	12.326	0.000
k1	0.077	0.022	1.489	0.416	3.575	0.000
k2	-0.160	0.023	-869.602	123.732	-7.028	0.000
a1^2	-0.616	0.021	0.000	0.000	-28.674	0.000
b01^2	0.337	0.023	0.008	0.001	14.834	0.000
b23^2	-0.482	0.019	-2199.329	87.449	-25.150	0.000
s^2	-0.186	0.021	-1.883	0.208	-9.047	0.000
k1^2	-0.074	0.021	-3.576	1.031	-3.470	0.001
k2^2	0.074	0.023	289096.048	89296.697	3.237	0.001

Table 4.5 Quadratic regression analysis: the logarithm of the real part of Re1 eigenvalue of matrix the non-trivial equilibrium point as a function of the rate constants. The range of the rate constants as in Fig.4.2.

Re4	BETA	St.Err. of BETA	B	St.Err. of B	t(2961)	p-level
Intercept			-0.0015	0.0020	-0.7216	0.4706
a01	0.0224	0.0035	0.0001	0.0000	6.4558	0.0000
b2	-0.0166	0.0035	0.0000	0.0000	-4.8031	0.0000
s	-0.9808	0.0034	-0.9465	0.0033	-284.2997	0.0000
k1	-0.0461	0.0084	-0.1020	0.0185	-5.5170	0.0000
k2	-0.0238	0.0035	-14.7722	2.1474	-6.8791	0.0000
k1^2	0.0317	0.0083	0.1745	0.0457	3.8150	0.0001

Table 4.6 Quadratic regression analysis: the real part of Re4 eigenvalue as a function of the rate constants. The range of the rate constants as in Fig.4.2.

ln(Im1)	BETA	St.Err. of BETA	B	St.Err. of B	t(2950)	p-level
Intercept			4.135	0.051	81.825	0.000
a1	1.441	0.020	0.000	0.000	72.019	0.000
b12	-0.077	0.008	-17.702	1.896	-9.335	0.000
b01	-0.355	0.021	-0.104	0.006	-16.810	0.000
a01	0.411	0.022	0.014	0.001	18.702	0.000
b2	0.198	0.024	0.002	0.000	8.371	0.000
a3	-0.148	0.019	0.000	0.000	-7.951	0.000
Ss	0.286	0.019	1.584	0.106	14.910	0.000
k1	-0.375	0.020	-4.767	0.256	-18.619	0.000
k2	0.496	0.021	1764.8	75.415	23.402	0.000
a1^2	-0.769	0.020	0.000	0.000	-38.551	0.000
b01^2	0.180	0.021	0.003	0.000	8.531	0.000
a01^2	-0.227	0.022	0.000	0.000	-10.432	0.000
b2^2	-0.107	0.024	0.000	0.000	-4.520	0.000
a3^2	0.070	0.019	0.000	0.000	3.739	0.000
s^2	-0.187	0.019	-1.241	0.127	-9.769	0.000
k1^2	0.183	0.020	5.765	0.632	9.125	0.000
k2^2	-0.298	0.021	-769127	54473.237	-14.119	0.000

Table 4.7 Quadratic regression analysis: the logarithm of the imaginary part of Im1 eigenvalue of matrix the non-trivial equilibrium point as a function of the rate constants. The range of the rate constants as in Fig.4.2.

Using the MC/regression method, the dependence of the relaxation constants to the equilibrium state can also be characterized. The results of the regression analysis are shown in Tables 4.2-4.7. The determination coefficient R-square for the osteocells' regression R^2 is in the range 0.77-0.87, which gives the confidence level between 0.13-0.23. The effect of the rate parameters can be characterized just as a tendency.

	ln(Ocl)	ln(Obl)	ln(Oct)	ln(BM)	ln(Re1)	ln(Re3)	Re4	ln(Im1)
R-square	0.870	0.84	0.830	0.800	0.770		0.960	0.800
a1	1.0478	1.304	0.753	0.8962	1.130			1.441
b12	-0.0548	-0.070	-0.047	-0.0441	-0.052			-0.077
b01	-0.6599	-0.838	-0.446	-0.5430	-0.694			-0.355
a01	-0.2248	-0.255	0.744	0.8800	-0.035	-1.285	0.022	0.411
b2	0.1352	0.157	-0.329	-0.4125		0.738	-0.016	0.198
b23			-0.067	-0.0839	0.950			
a3	-0.0636	-0.134	0.492	-0.0544	-0.054			-0.148
s	0.2028	0.253	-0.785	0.1772	0.254	0.106	-0.980	0.286
k1	-0.7857	0.254	-0.625	-0.7715	0.077	1.144	-0.046	-0.375
k2	0.8896	-0.180	0.765	0.9305	-0.160		-0.023	0.496
a1^2	-0.5598	-0.699	-0.395	-0.4738	-0.616			-0.769
b12^2								
b01^2	0.3364	0.436	0.233	0.2715	0.337			0.180
a01^2	0.1243	0.134	-0.422	-0.5024		0.738		-0.227
b2^2	-0.0713	-0.078	0.147	0.1926		-0.346		-0.107
b23^2					-0.482			
a3^2		0.064	-0.244					0.070
s^2	-0.1322	-0.166	0.422	-0.1141	-0.186	-0.074		-0.187
k1^2	0.4147	-0.154	0.287	0.3683	-0.074	-0.591	0.031	0.183
k2^2	-0.5117	0.071	-0.444	-0.5406	0.074			-0.298

Table 4.8 Summary table on the Monte-Carlo application.

	Mean	Minimum	Maximum	Range	Variance	Std.Dev.	St.Error
OCL	6.102881	0.01788	291.5624	291.5445	215.0817	14.66566	0.269197
OBL	986.3794	3.78394	18773.52	18769.74	1680265	1296.25	23.79342
OCT	96076.13	5.64747	2676867	2676861	4.85E+10	220306.7	4043.857
BM	1.09865	0.00101	56.45885	56.45784	12.19788	3.492546	0.064108

Table 4.9 The average population concentrations, maximum and minimum values and statistical deviations for the osteocells (cell/mm^3) for the model (4.5) and the relative bone mass, BM.

	Mean	Minimum	Maximum	Range	Std.Dev.	Error
RE1	-4.119	-125.912	-0.001	125.911	7.759	0.142
RE2	-4.119	-125.912	-0.001	125.911	7.759	0.142
RE3	-0.545	-14.365	-0.007	14.357	0.804	0.015
RE4	-0.203	-1.575	-0.001	1.574	0.187	0.003
IM1	566.545	3.358	8787.537	8784.179	757.616	13.906
IM2	-566.545	-8787.537	-3.358	8784.179	757.616	13.906
IM3	0.018	0.000	0.408	0.408	0.042	0.001
IM4	-0.018	-0.408	0.000	0.408	0.042	0.001

Table 4.10 Resulting statistics on the real and imaginary parts of the eigenvalues for the range of the rate constants as in Fig.4.2.

	Mean	Minimum	Maximum	Range
a1	3557.5	201.0	26532.3	26331.3
b12	0.007	0.002	0.044	0.042
b01	4.675	1.050	29.257	28.207
a01	38.364	1.542	234.659	233.117
b2	138.091	50.005	830.721	780.716
b23	0.010	0.001	0.093	0.092
a3	7676.2	1302.1	65052.6	63750.5
s	0.200	0.001	1.576	1.575
k1	0.093	0.010	0.646	0.636
k2	0.00035	0.00003	0.00231	0.00228

Table 4.11 The mean values of the rate constants, used in the study the wide range of the rate parameters.

Nevertheless, in the linear segment, Table 4.1 indicates that the a_1, s and k_2 rate constants have a significant positive effect of on the osteoclastic population density, whereas b_{01}, a_{01} and k_1 have a negative effect. In the quadratic region, the same coefficients have an opposite effect. Similar results are observed for the regression analysis of the population concentration of the all osteocells, Tables 4.2-4.7. Regression for the logarithm of Obl, Table 4.2, indicates that a_1, b_2, k1 and *s* have a positive influence on the Obl population density, while the b_{01}, k_2 have a negative impact. These constants have an opposite effect of in the quadratic sector. Table 4.3 indicates the positive effect of a_1, a_{01}, a_3 and k_1 on the Oct population density and their negative effect in quadratic sector. Table 4.4 shows that a_1, a_{01}, k_2 have positive effect on the logarithm of total bone mass and a negative effect in quadratic sector. The rate parameters a_1, b_{01}, b_{23} and s have a strong impact on the real part of the first eigenvalue Re1, Table 4.5, which is linked to the relaxation constant. The rate parameter *s* indicates a strong negative effect on the real part of fourths eigenvalues, Table 4.6. Table 4.7 indicates that the a_1, b_{01}, a_{01}, s and k_1 and k_2 have effects on the imaginary part of first eigenvalues.

The results of the Monte Carlo method application are summarised in Tables 4.8-4.11. One can see the different effects of the rate parameters on the rate constants and the real and imaginary part of the eigenvalues. The rate constant a_1 has a positive effect on the level of all state variables, osteocells and BM. Parameter b_{01} has a negative impact on the osteocells and BM. The effect of other rate constants varies. Table 4.9 shows the average population densities, maximum

and minimum values and statistical deviations for the osteocells (cell/mm^3) for the model (4.5) and the relative bone mass, BM. It indicates reasonable agreement with the experimental estimation of the osteocells concentration in the bone tissue, which can be considered as the validation of the model. Also some disagreement is seen in the relaxation time (Table 4.10, Re4=0.2, which gives the characteristic time about 10 days), and quite poor statistical significance (R-square less than 0.9, Table 4.8), can be related to the very wide range of the rate parameters employed (Table 4.11), so it was a need to short this range.

4.4 Middle range of the rate constants

As was mentioned in Section 4.2, the application of a wide range of rate constants, (even though this is quite a good in description of overall population densities and total bone mass, see Table 4.9), leads to poor statistical significance and gives a characteristic time lower than the relaxation time to the equilibrium/steady state. Taking this into account the range of rate constants was reduced to a_1, 1200-4300 day^{-1} ; b_{12}, 0.002-0.02 cell^{-1}day^{-1}; b_{01}, 1.5-3.5 cell^{-1}day^{-1}; a_{01}, 3.0-24.0 cell^{-1}day^{-1}; b_2, 50- 420 cell^{-1}day^{-1}; b_{23}, 0.005-0.007 cell^{-1}day^{-1}; a_3, 1300-20000 day^{-1}; s, 0.02-0.4 cell^{-1}day^{-1}; k_1, 0.01-0.04 day^{-1}; k_2, 0.0002-0.0006 day^{-1} and the uniform distribution of the rate constants within these intervals was applied.

Using the Monte Carlo method and regression analysis described in the Section 4.3, the dependence of the position of the equilibrium point (Fig. 4.5-4.7, and Tables 4.12-4.22) and the relaxation to this equilibrium point has been numerically characterized. However, even for a reduced range of the rate parameters, the linear regression of Ocl on the rate constants gives just R^2=0.75 in the evaluation of the rate constants effect on bone mass. After the logarithmisation of osteocells population densities and total bone mass, the linear regression significantly improves the statistical significance (R-squared for Ocl is 0.90, for Obl R^2=0.870, for Oct R^2=0.960 and BM, R^2=0.95), as well as it was seen for wide range of parameters. In Tables 4.12-4.18 the results of MC/quadratic regression methods are shown. One can see that a reduction of the range of

parameters improves the significance of the model. The different impact of the rate constants on the equilibrium of the osteocells can also be seen.

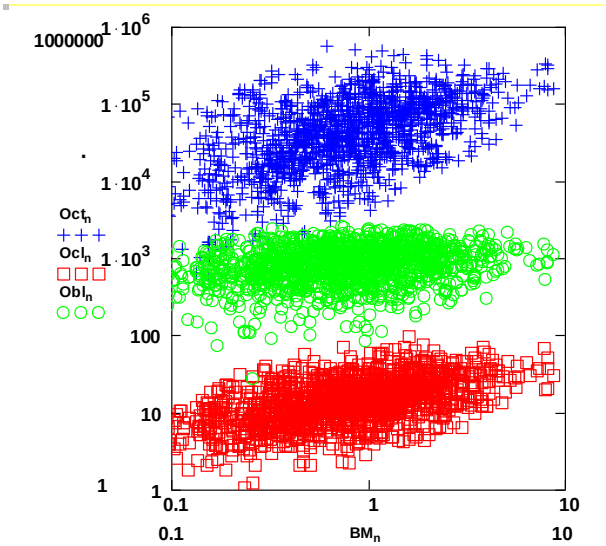

Fig. 4.5 Scatteplot of calculated positions of equilibrium of osteocells (Ocl, osteoclasts; Obl, osteoblasts; Oct, osteocytes) against the total bone mass (BM) for the system (4.4). Calculations were performed using the following set of parameters: a_1, 1200-4300 day^{-1} ; b_{12}, 0.002-0.02 $cell^{-1}day^{-1}$; b_{01}, 1.5-3.5 $cell^{-1}day^{-1}$; a_{01}, 3.0-24.0 $cell^{-1}day^{-1}$; b_2, 50- 420 $cell^{-1}day^{-1}$; b_{23}, 0.005-0.007 $cell^{-1}day^{-1}$; a_3, 1300-20000 day^{-1}; s, 0.02-0.4 $cell^{-1}day^{-1}$; k_1, 0.01-0.04 day^{-1}; k_2, 0.0002-0.0006 day^{-1}.

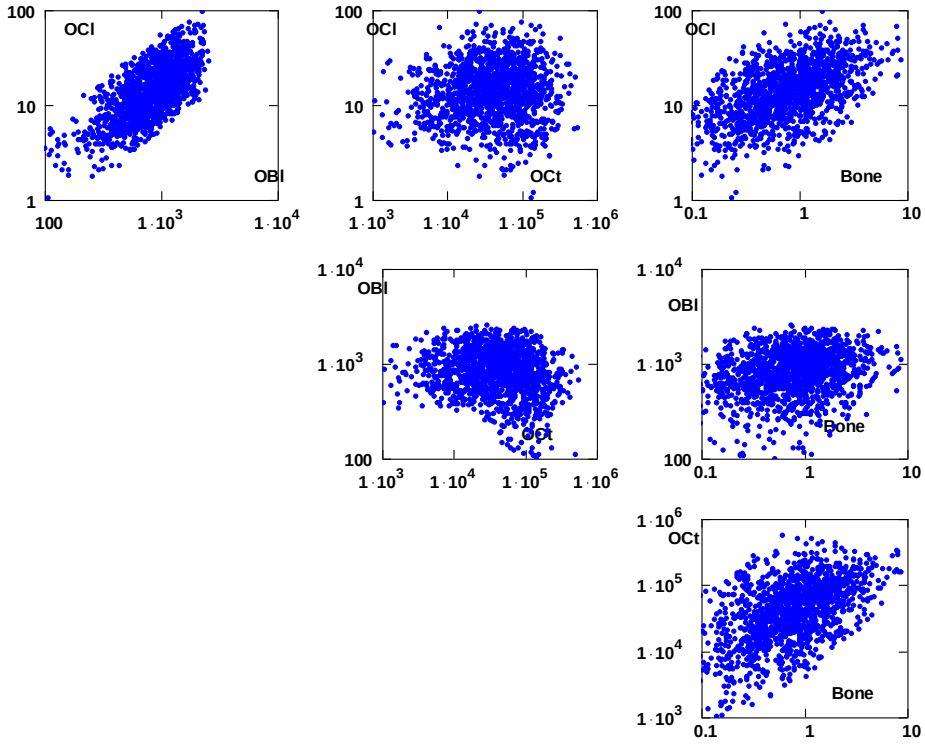

Fig. 4.6 Detailed graphical matrix illustrating scatterplot of populational densities of Ocl, Obl, Oct, total bone mass(Bone) in 4D space of these quantities. Calculations were performed using the set of parameters, Fig.4.5.

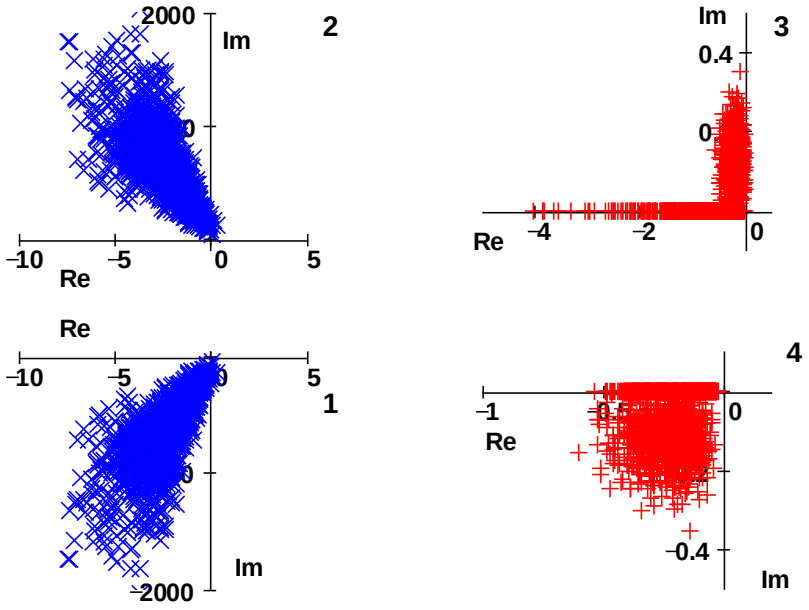

Fig. 4.7 Scattreplot of the eigenvalues (4.8) for the system (4.4). Calculations were performed using the set of parameters, Fig.4.2.

ln(BM)	BETA	St.Err. of BETA	B	St.Err. of B	t(9981)	p-level
Intercept			-1.248	0.062	-19.986	0.000
a1	0.818	0.017	0.001	0.000	49.303	0.000
b12	-0.175	0.012	-30.588	2.026	-15.100	0.000
b01	-0.426	0.024	-0.659	0.036	-18.101	0.000
a01	1.181	0.012	0.175	0.002	96.088	0.000
b2	-0.878	0.012	-0.007	0.000	-72.463	0.000
a3	-0.206	0.011	0.000	0.000	-18.776	0.000
s	0.601	0.011	4.926	0.086	57.000	0.000
k1	-0.621	0.016	-64.424	1.640	-39.293	0.000
k2	0.645	0.019	5004	145.917	34.298	0.000
a1^2	-0.436	0.017	0.000	0.000	-26.254	0.000
b12^2	0.044	0.012	346.411	90.417	3.831	0.000
b01^2	0.219	0.024	0.068	0.007	9.315	0.000
a01^2	-0.707	0.012	-0.004	0.000	-57.532	0.000
b2^2	0.440	0.012	0.000	0.000	36.328	0.000
b23^2	0.070	0.011	0.000	0.000	6.353	0.000
a3^2	-0.422	0.011	-8.021	0.200	-40.075	0.000
k1^2	0.287	0.016	589.297	32.426	18.174	0.000
K2^2	-0.371	0.019	-3573669	181331	-19.708	0.000

Table 4.12 Quadratic regression analysis: the logarithm of the BM as a function of the rate constants. The range of constants as in Fig.4.5. R^2=0.95.

ln(Ocl)	BETA	St.Err. of BETA	B	St.Err. of B	t(9981)	p-level
Intercept			1.804	0.060	30.191	0.000
a1	1.117	0.021	0.001	0.000	52.221	0.000
b12	-0.239	0.015	-30.938	1.938	-15.965	0.000
b01	-0.575	0.030	-0.660	0.035	-18.964	0.000
a01	-0.269	0.016	-0.030	0.002	-16.982	0.000
b2	0.572	0.016	0.004	0.000	36.588	0.000
a3	-0.273	0.014	0.000	0.000	-19.232	0.000
s	0.808	0.014	4.917	0.083	59.483	0.000
k1	-0.826	0.020	-63.580	1.568	-40.536	0.000
k2	0.803	0.024	4620.920	139.591	33.103	0.000
a1^2	-0.601	0.021	0.000	0.000	-28.117	0.000
b12^2	0.063	0.015	365.633	86.497	4.227	0.000
b01^2	0.297	0.030	0.068	0.007	9.796	0.000
a01^2	0.101	0.016	0.000	0.000	6.374	0.000
b2^2	-0.386	0.016	0.000	0.000	-24.697	0.000
b23^2	0.088	0.014	0.000	0.000	6.189	0.000
a3^2	-0.567	0.014	-7.990	0.191	-41.727	0.000
k1^2	0.397	0.020	604.454	31.020	19.486	0.000
k2^2	-0.453	0.024	-3237376	173470	-18.662	0.000

Table 4.13 Quadratic regression analysis: the logarithm of the population density of the osteoclast as a function of the rate constants. The range of the constants as in Fig.4.5. R^2=0.90.

Obl	BETA	St.Err. of BETA	B	St.Err. of B	t(9983)	p-level
Intercept			1350.985	38.976	34.662	0.000
a1	0.650	0.004	0.323	0.002	181.973	0.000
b12	-0.316	0.017	-27308.006	1486.295	-18.373	0.000
b01	-1.153	0.035	-883.135	26.701	-33.075	0.000
a01	-0.332	0.018	-24.297	1.335	-18.200	0.000
b2	0.538	0.018	2.241	0.075	29.955	0.000
a3	-0.332	0.016	-0.027	0.001	-20.344	0.000
s	0.709	0.016	2877.731	63.396	45.393	0.000
k1	0.323	0.023	16585.051	1202.949	13.787	0.000
k2	-0.114	0.004	-438798.973	13707.687	-32.011	0.000
b12^2	0.126	0.017	484661.875	66339.057	7.306	0.000
b01^2	0.755	0.035	115.255	5.319	21.669	0.000
a01^2	0.143	0.018	0.382	0.049	7.861	0.000
b2^2	-0.348	0.018	-0.003	0.000	-19.344	0.000
a3^2	0.131	0.016	0.000	0.000	8.051	0.000
s^2	-0.461	0.016	-4333.782	146.847	-29.512	0.000
k1^2	-0.187	0.023	-190104.046	23790.710	-7.991	0.000

Table 4.14 Quadratic regression analysis: the osteoblasts' population densities as a function of the rate constants. The range of constants as in Fig.4.5. R^2=0.87.

ln(Oct)	BETA	St.Err. of BETA	B	St.Err. of B	t(9981)	p-level
Intercept			9.628	0.065	147.082	0.000
a1	0.648	0.014	0.001	0.000	47.767	0.000
b12	-0.133	0.009	-29.775	2.123	-14.024	0.000
b01	-0.332	0.019	-0.659	0.038	-17.288	0.000
a01	0.928	0.010	0.176	0.002	92.364	0.000
b2	-0.681	0.010	-0.007	0.000	-68.773	0.000
a3	1.108	0.009	0.000	0.000	123.265	0.000
s	-0.892	0.009	-9.375	0.091	-103.508	0.000
k1	-0.475	0.013	-63.096	1.718	-36.717	0.000
k2	0.494	0.015	4915.7	152.9	32.142	0.000
a1^2	-0.347	0.014	0.000	0.000	-25.579	0.000
b12^2	0.031	0.009	310.310	94.768	3.274	0.001
b01^2	0.170	0.019	0.067	0.008	8.831	0.000
a01^2	-0.558	0.010	-0.004	0.000	-55.562	0.000
b2^2	0.339	0.010	0.000	0.000	34.265	0.000
a3^2	-0.680	0.009	0.000	0.000	-75.679	0.000
S^2	0.472	0.009	11.499	0.210	54.812	0.000
k1^2	0.214	0.013	563.192	33.986	16.571	0.000
k2^2	-0.280	0.015	-3456342	190056	-18.186	0.000

Table 4.15 Quadratic regression analysis: the logarithm of the osteocytes population densities as a function of the rate constants. The range of constants as in Fig.4.5. R^2=0.96.

Re1	BETA	St.Err. of BETA	B	St.Err. of B	t(9982)	p-level
Intercept			-0.882	0.142	-6.211	0.000
A1	-0.651	0.004	-0.001	0.000	-163.665	0.000
B12	0.322	0.019	83.659	4.980	16.798	0.000
B01	1.142	0.039	2.632	0.089	29.420	0.000
A01	-0.084	0.020	-0.019	0.004	-4.142	0.000
B2	-0.442	0.020	-0.006	0.000	-22.093	0.000
B23	-0.198	0.004	-460.22	9.229	-49.871	0.000
A3	0.348	0.018	0.000	0.000	19.172	0.000
S	-0.710	0.017	-8.673	0.212	-40.826	0.000
K1	-0.242	0.026	-37.283	4.031	-9.250	0.000
K2	0.114	0.004	1312.3	45.99	28.586	0.000
B12^2	-0.129	0.019	-1497.3	222.5	-6.736	0.000
B01^2	-0.743	0.039	-0.341	0.018	-19.131	0.000
A01^2	0.158	0.020	0.001	0.000	7.762	0.000
B2^2	0.350	0.020	0.000	0.000	17.489	0.000
A3^2	-0.147	0.018	0.000	0.000	-8.121	0.000
S^2	0.462	0.017	13.072	0.492	26.567	0.000
K1^2	0.180	0.026	550.93	79.73	6.912	0.000

Table 4.16 Quadratic regression analysis: the value of the real part of the first eigenvalue (Re1=Re2) of the of equilibrium point as a function of the rate constants. R^2=0.84. The range of the constants as in Fig.4.5.

Using the regression method, the dependence of the relaxation constants to the equilibrium state can also be numerically/quantitatively characterized. In Tables 4.12-4.18 the results of the regression analysis are shown. The determination coefficient R-square for this regression is in the range 0.86-0.96, which gives a confidence level of between 0.14-0.04. The effect of the rate parameters can be still characterized as a "tendency".

In the linear segment, Table 4.12 indicates that the a_1, a_{01}, s and k_1 rate constants have a significant positive effect on the total bone mass, whereas b_{01}, b_2 and k_1 have a negative effect. In the quadratic region, the same coefficients have an opposite effect. That was one of the reasons for the further reduction of the rate constant range to obtain a good linear regression that simplifies the interpretation. Similar results are observed for the regression results of the population concentration of the osteocells, Tables 4.13-4.15. Regression of the logarithm of Ocl, Table 4.13, indicates that of a_1, b_2, s and k_2 have a positive character of influence on Ocl population density, while the k_1 has an negative effect. These constants have an opposite effect in the quadratic sector. Table 4.14 indicates the positive effects of a_1, b_2, s and k_1 on Obl population density and their negative effect in quadratic sector. Table 4.15 shows that a_1, a_{01}, a_3, k_2 have a positive effect on the logarithm of population density of osteocytes and a negative effect in the quadratic sector.

The real (Re1-Re4) and imaginary (Im1-Im4) parts of the four eigenvalues of the Jacobian matrix (4.8) determine the character of stability of system (4.4) in the equilibrium (4.6). The regression analysis of the effect of the rate parameters on the logarithm of the real part Re1 of the first eigenvalue is shown in Table 4.16. The rate parameter a_1 has a negative impact on the real part of the first eigenvalue, Table 4.16, which is linked to the relaxation constant, as well as the rate parameters b_2 and s. Parameters b_{12}, b_{01} and a_3 indicate a positive effect. It is important to note that the parameter b_{12} plays a role describing the Ocl-Oct paracrine effect, while the rate constant b_{01} plays a role of decaying paracrine parameter for osteoclasts (the rate of their apoptosis invoked by the osteoblasts). The rate parameter k_1 gives a negative

impact on the Re1. The rate parameter k_2 produces a positive impact on the real part of the first eigenvalues, Re1.

There is little point in describing the dependence of state variables as a linear dependence on the rate parameters, as the dependence is essentially nonlinear, which in fact is also proved by the description in the framework of the quadratic regression (Tables 4.12-4.16).

Ln(Re3)	BETA	St.Err. of BETA	B	St.Err. of B	t(9987)	p-level
Intercept			-1.99	0.02	-72.82	0.00
b12	-0.021	0.003	-3.363	0.401	-8.381	0.000
b01	0.012	0.003	0.016	0.004	4.571	0.000
a01	-1.497	0.013	-0.200	0.002	-115.502	0.000
b2	1.027	0.013	0.008	0.000	80.352	0.000
s	0.188	0.011	1.391	0.082	16.889	0.000
k1	0.713	0.017	66.813	1.562	42.761	0.000
k2	-0.011	0.003	-78.697	17.803	-4.421	0.000
a01^2	0.904	0.013	0.004	0.000	69.752	0.000
b2^2	-0.466	0.013	0.000	0.000	-36.510	0.000
a3^2	-0.023	0.003	0.000	0.000	-9.184	0.000
s^2	-0.068	0.011	-1.170	0.191	-6.136	0.000
k1^2	-0.302	0.017	-560.668	30.901	-18.144	0.000

Table 4.17 Quadratic regression analysis: the logarithm of the real part of Re3 eigenvalue of the Jacobian matrix for the non-trivial equilibrium point as a function of the rate constants. R^2=0.95. The range of the constants as in Fig.4.5.

ln(Re4)	BETA	St.Err. of BETA	B	St.Err. of B	t(9986)	p-level
Intercept			-3.794	0.032	-117.695	0.000
b_{12}	0.188	0.020	20.182	2.167	9.313	0.000
b_{01}	-0.043	0.004	-0.041	0.004	-10.227	0.000
a_{01}	0.204	0.021	0.018	0.002	9.502	0.000
b_2	0.535	0.021	0.003	0.000	25.328	0.000
a_3	0.110	0.004	0.000	0.000	26.295	0.000
s	1.764	0.018	8.880	0.092	96.076	0.000
k_1	0.310	0.028	19.718	1.754	11.241	0.000
k_2	0.054	0.004	256.434	19.985	12.831	0.000
b12^2	-0.097	0.020	-462.960	96.727	-4.786	0.000
a01^2	-0.235	0.021	-0.001	0.000	-10.962	0.000
b2^2	-0.435	0.021	0.000	0.000	-20.613	0.000
s^2	-0.936	0.018	-10.919	0.214	-50.998	0.000
k1^2	-0.256	0.028	-322.482	34.691	-9.296	0.000

Table 4.18 Quadratic regression analysis: the logarithm of the real part of Re4 eigenvalue of matrix the non-trivial equilibrium point as a function of the rate constants. R^2=0.85. The range of the constants as in Fig.4.5.

The regression analysis results for the real part of the third eigenvalue Re3 are shown in Table 4.17. It can be seen, that the parameters b_2, and k_1 have a positive effect, while the rate parameters a_{01} and k_1^2 have the negative effect. A similar pattern of rate constant effects can be seen for the logarithm of the real part of the fourth eigenvalue, Re4. The rate parameters b_2, s and k_2 have a positive effect, while a_{01}^2, b_2^2, s^2 and k_2^2 show a negative one.

As it was already mentioned, the rate parameter b_{12} describes the negative feedback of the osteocytes on osteoclasts, and from the regression analysis, it follows that it will only have a moderate effect on the relaxation constants Re3 and Re4. It can be concluded that the increase of this parameter (strengthening of this feedback) decreases the time of system relaxation to steady state. It should be noted that the parameter *s* has the largest effect on Re4, which has the lowest level between all real parts of the eigenvalues, and because of this can be treated as the relaxation of the system to the steady state. The effect of this parameter on the steady state variables is also moderate.

Thus, for the relaxation parameter Re4, the rate parameters b_2, s and k_1 have the most significant effect (Table 4.18). As in the case for Re1-Re2, b_{12} plays a role describing the Ocl-Obl paracrine effect, while the rate constant b_{23} plays a role of decaying autocrine parameter for osteoblasts. The rate parameters k_1 and k_2 have a significant positive effect on the relaxational time.

Since the first two imaginary parts of the eigenvalues are equal and have an opposite sign, Im1=-Im2, and Im3=Im4=0, this equlibrium point can be classified as a stable focus. The analysis of the eigenvectors indicates that the fourth eigenvector is loaded by the osteocytes' population concentration and BM, which indicate that the slowest relaxation occurs in the linear combination of Oct and BM, which can be treated as the bone tissue.

It is easy to see from Table 4.11 that the slowest relaxation constant, Re4, related to the relaxation time of whole system, is about a month with a quite large standard deviation. However, the regression of the imaginary part gives R-square<0.9, which means that the results are not statistically significant.

	Mean	Minimum	Maximum	Range	Std.Dev.	Error
OCL	16	0	111	111	11	0
OBL	897	15	2690	2675	445	4
OCT	23361	306	1130000	1129694	71221	712
BM	1	0	15	15	1	0

Table 4.19 The average population concentrations, maximum and minimum values and statistical deviations for the osteocells' (cell/mm^3) for the model (4.5) and the relative bone mass, BM for the middle range of the rate parameters.

	Mean	Minimum	Maximum	Range	Std.Dev.
RE1	-2.40	-8.46	1.01	9.47	1.34
RE2	-2.40	-8.46	1.01	9.47	1.34
RE3	-0.56	-5.37	-0.03	5.34	0.55
RE4	-0.23	-0.61	-0.02	0.59	0.11
IM1	613.84	13.50	2830.00	2816.50	312.06
IM2	-613.84	-2830.00	-13.50	2816.50	312.06
IM3	0.06	0.00	0.35	0.35	0.07
IM4	-0.06	-0.35	0.00	0.35	0.07

Table 4.20 Resulting statistics on the real and imaginary parts of the eigenvalues for the middle range of the rate constants.

	Mean	Minimum	Maximum	Range
a1	2759.5	1200.0	4300.0	3100.0
b12	0.011	0.002	0.020	0.018
b01	2.494	1.500	3.500	2.000
a01	13.4	3.0	24.0	21.0
b2	235.8	50.0	420.0	370.0
b23	0.006	0.005	0.007	0.002
a3	10675.9	1300.0	20000.0	18700.0
s	0.210	0.020	0.400	0.380
k1	0.025	0.010	0.040	0.030
k2	0.000	0.000	0.001	0.000

Table 4.21 The statistics of the rate constants, employed for the middle range used.

	ln(Ocl)	Obl	ln(Oct)	ln(BM)	Re1	ln(Re3)	Ln(Re4)	ln(Im1)
R-square	0.900	0.870	0.960	0.950	0.840	0.950	0.820	0.850
a1	1.117	0.650	0.648	0.818	-0.651			1.359
b12	-0.239	-0.316	-0.133	-0.175	0.322	-0.021	0.188	-0.289
b01	-0.575	-1.153	-0.332	-0.426	1.142	0.012	-0.043	-0.256
a01	-0.269	-0.332	0.928	1.181	-0.084	-1.497	0.204	0.731
b2	0.572	0.538	-0.681	-0.878	-0.442	1.027	0.535	0.704
b23					-0.198			
a3	-0.273	-0.332	1.108	-0.206	0.348		0.110	-0.337
s	0.808	0.709	-0.892	0.601	-0.710	0.188	1.764	0.988
k1	-0.826	0.323	-0.475	-0.621	-0.242	0.713	0.310	-0.285
k2	0.803	-0.114	0.494	0.645	0.114	-0.011	0.054	0.400
a1^2	-0.601		-0.347	-0.436				-0.729
b12^2	0.063	0.126	0.031	0.044	-0.129		-0.097	0.075
b01^2	0.297	0.755	0.170	0.219	-0.743			0.136
a01^2	0.101	0.143	-0.558	-0.707	0.158	0.904	-0.235	-0.466
b2^2	-0.386	-0.348	0.339	0.440	0.350	-0.466	-0.435	-0.476
b23^2								
a3^2	0.088	0.131	-0.680	0.070	-0.147	-0.023		0.110
s^2	-0.567	-0.461	0.472	-0.422	0.462	-0.068	-0.936	-0.694
k1^2	0.397	-0.187	0.214	0.287	0.180	-0.302	-0.256	0.101
k2^2	-0.453		-0.280	-0.371				-0.251

Table.4.22 Summary table for meddle range set of the rate parameters.

Summarisingly, the effect of the rate constants in medium range, Table 4.22 shows the same pattern as in the wide range with an improved confidence. However, this is still in quadratic regression, and to study a linear effect of the rate constants needs a further reduction in the range of the rate constants. It also needs to note that the ranges of some rate parameters have been phenomologically chosen to reproduce the expected behaviour in the vicinity of the non-trivial steady-state.

4.5 The reduced (short) range of the rate constants

The wide and middle ranges of the rate parameters applied to the simulation, lead to quite a low confidence of the regression model. The R-square value for wide range parameters was about 0.75, R-square for middle range of the rate parameters was about 0.90. Therefore, the shorted range of the rate constants has been applied to illustrate ability of the method to obtain a good statistical significance. The range of constants in this case was: a_1, 3000-5000. day^{-1}; b_{12}, 0.002-0.004 $cell^{-1}day^{-1}$; b_{01}, 1.3-3.2 $cell^{-1}$ day^{-1}; a_{01}, 2.0-5.0 $cell^{-1}day^{-1}$; b_2, 40.0-65.0 $cell^{-1}day^{-1}$; b_{23}, 0.005-0.007 $cell^{-1}day^{-1}$; a_3, 1100-1700.0 day^{-1}; s, 0.02-0.04 $cell^{-1}day^{-1}$; k_1, 0.20-0.30 day^{-1}; k_2, 0.002-0.004 day^{-1}.

The scatterplot of the population concentrations of osteocells against the total bone mass is shown in Fig.4.8. The scatterplot of the osteocells againt each other and the total bone mass is illustrated in Fig.4.9. Finally, in Fig.4.10, the stability characteristics for the points calculated are presented. One can see that these scatterplots are quite a good much the scatterplots for the wide and medium case. Expected good statistical significance was found for the linear regression approach, that can be seen from Tables 4.23-4.30.

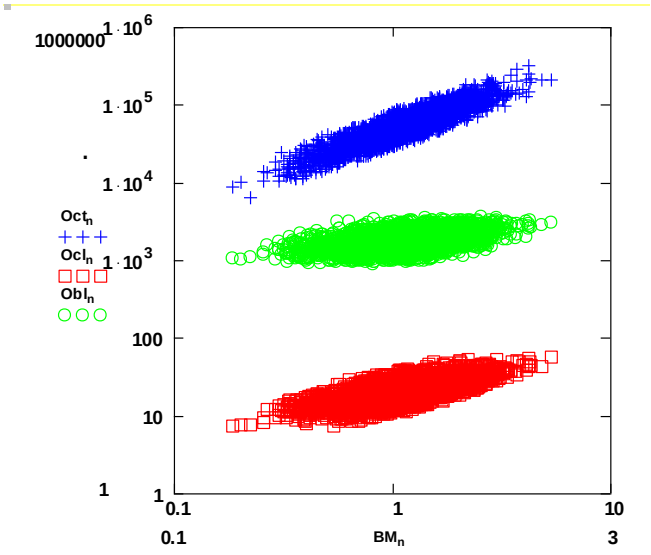

Fig. 4.8. Scatterplot for the system (4.4). Calculations were performed using the following set of parameters: a_1, 3000-5000. day^{-1}; b_{12}, 0.002-0.004 $cell^{-1}day^{-1}$; b_{01}, 1.3-3.2 $cell^{-1}$ day^{-1}; a_{01}, 2.0-5.0 $cell^{-1}day^{-1}$; b_2, 40.0-65.0 $cell^{-1}day^{-1}$; b_{23}, 0.005-0.007 $cell^{-1}day^{-1}$; a_3, 1100-1700.0 day^{-1}; s, 0.02-0.04 $cell^{-1}day^{-1}$; k_1, 0.20-0.30 day^{-1}; k_2, 0.002-0.004 day^{-1}.

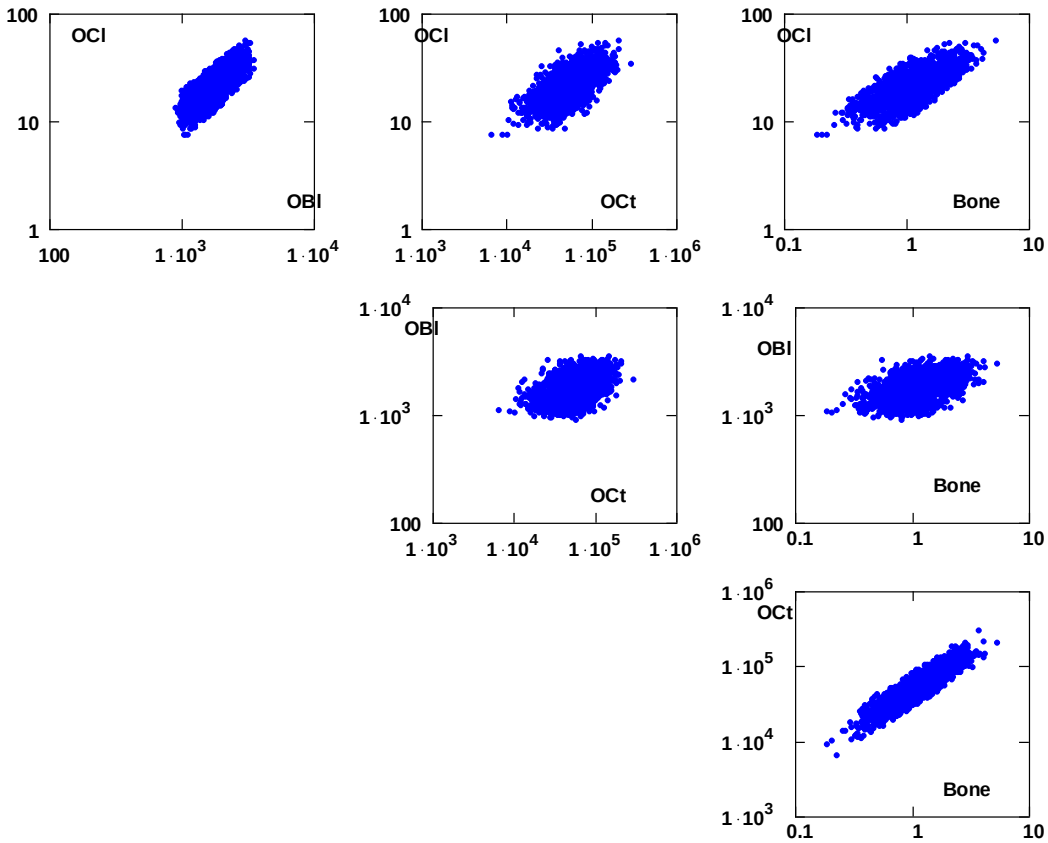

Fig.4.9 The graphical matrix illustrating a scatterplot of population densities of Ocl, Obl, Oct, BM (Bone) in 4D space of these quantities. The uniform distribution for the rate parameters of system (4.4). Calculations were performed using the set of parameters, Fig.4.8.

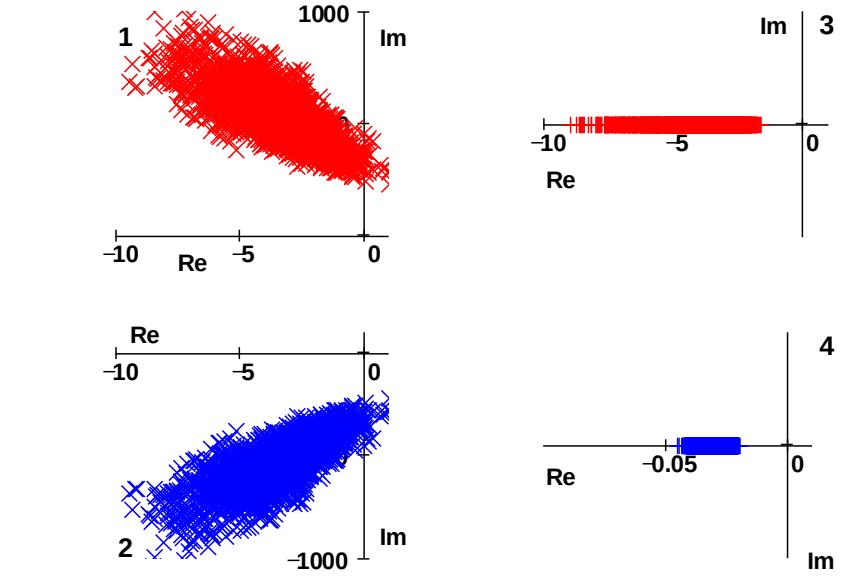

Fig. 4.10 Scattreplot of the eigenvalues (4.8) for the system (4.4). Calculations were performed using the set of parameters as in Fig.4.8.

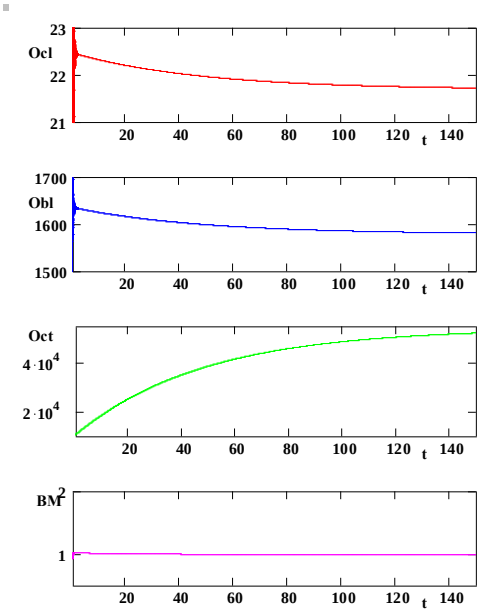

Fig. 4.11 Relaxation of the system to the steady state at following rate constants: a_1, 4590 day^{-1}; b_{12}, 0.00363 $cell^{-1}day^{-1}$; b_{01}, 2.79 $cell^{-1}\,day^{-1}$; a_{01}, 3.1 $cell^{-1}day^{-1}$; b_2, 57.9 $cell^{-1}day^{-1}$; b_{23}, 0.00647 $cell^{-1}day^{-1}$; a_3, 1100 day^{-1}; s, 0.021 $cell^{-1}day^{-1}$; k_1, 0.257 day^{-1}; k_2, 0.00353 day^{-1}. Re4=0.002, τ~50 days

ln(Ocl)	BETA	St.Err. of BETA	ln(Ocl)	BETA	St.Err. of BETA
a1	0.807	0.005	a1	0.403	0.001
b12	-0.024	0.000	b12	-0.024	0.001
b01	-1.329	0.003	b01	-0.668	0.001
a01	-0.037	0.000	a01	-0.036	0.001
b2	0.048	0.005	b2	0.018	0.001
b23			b23	-0.016	0.001
a3	0.080	0.004	a3	0.024	0.001
s	-0.572	0.006	s	-0.306	0.001
k1	1.055	0.004	k1	0.511	0.001
a1^2	-0.404	0.005			
b01^2	0.666	0.003			
b2^2	-0.031	0.005			
b23^2	0.002	0.000			
a3^2	-0.016	0.000			
s^2	-0.056	0.004			
k1^2	0.268	0.006			
k2^2	-0.545	0.004			

Table 4.23 The comparison of quadratic and linear regression for the osteoclasts population densities for the short range of the rate parameters as in Fig.4.8.

ln(Obl)	BETA	St.Err. of BETA	ln(Obl)	BETA	St.Err. of BETA
a1	1.022	0.006	a1	0.509409	0.00104
b12	-0.031	0.000	b12	-0.03155	0.00104
b01	-1.679	0.003	b01	-0.84344	0.001041
a01	-0.046	0.000	a01	-0.04582	0.00104
b2	0.060	0.006	b2	0.022908	0.00104
b23			b23	0.003715	0.001041
a3	-0.020	0.000	a3	-0.02034	0.00104
s	0.099	0.004	s	0.030956	0.00104
k1	0.060	0.007	k1	0.019374	0.00104
k2	-0.035	0.000	k2	-0.03528	0.001041
a1^2	-0.512	0.006			
b01^2	0.841	0.003			
b2^2	-0.038	0.006			
b23^2	0.002	0.000			
s^2	-0.068	0.004			
k1^2	-0.038	0.007			

Table 4.24 The comparison of quadratic and linear regression for the osteoblast population densities for the short range of the rate parameters as in Fig.4.8.

	BETA	St.Err. of BETA	ln(Oct)	BETA	St.Err. of BETA
a1	0.521	0.007	a1	0.263	0.001
b12	-0.016	0.000	b12	-0.016	0.001
b01	-0.872	0.004	b01	-0.438	0.001
a01	1.229	0.004	a01	0.531	0.001
b2	-0.469	0.008	b2	-0.238	0.001
b23	-0.032	0.000	b23	-0.033	0.001
a3	0.423	0.008	a3	0.216	0.001
s	-0.648	0.005	s	-0.337	0.001
k1	-0.398	0.009	k1	-0.241	0.001
k2	0.912	0.005	k2	0.404	0.001
a1^2	-0.257	0.007			
b01^2	0.438	0.004			
a01^2	-0.703	0.004			
b2^2	0.232	0.008			
a3^2	-0.206	0.008			
s^2	0.313	0.005			
k1^2	0.159	0.009			
k2^2	-0.509	0.005			

Table 4.25 The comparison of quadratic and linear regression for the osteocytes population densities for the short range of the rate parameters as in Fig.4.8.

n(BM)	BETA	St.Err. of BETA	ln(BM)	BETA	St.Err. of BETA
a1	0.570	0.008	a1	0.287	0.001
b12	-0.018	0.000	b12	-0.018	0.001
b01	-0.952	0.005	b01	-0.478	0.001
a01	1.342	0.005	a01	0.580	0.001
b2	-0.511	0.008	b2	-0.259	0.001
b23	-0.035	0.000	b23	-0.036	0.001
a3			a3	-0.012	0.001
s	0.069	0.006	s	0.017	0.001
k1	-0.434	0.010	k1	-0.263	0.001
k2	0.996	0.006	k2	0.442	0.001
a1^2	-0.282	0.008			
b01^2	0.478	0.005			
a01^2	-0.767	0.005			
b2^2	0.252	0.008			
a3^2	-0.012	0.000			
s^2	-0.052	0.006			
k1^2	0.173	0.010			
k2^2	-0.557	0.006			

Table 4.26 The comparison of quadratic and linear regression for total bone mass (BM) for the short range of the rate parameters as in Fig.4.8.

	BETA	St.Err. of BETA	Re1	BETA	St.Err. of BETA
a1	-0.437	0.002	a1	-0.434	0.002
b12	0.026	0.002	b12	0.027	0.002
b01	2.249	0.015	b01	0.744	0.002
a01	-0.863	0.015	a01	-0.250	0.002
b2	0.136	0.002	b2	0.136	0.002
b23	-0.297	0.002	b23	-0.298	0.002
a3	0.018	0.002	a3	0.020	0.002
s	-0.094	0.019	s	-0.027	0.002
k1	0.109	0.002	k1	0.113	0.002
k2	0.032	0.002	k2	0.032	0.002
b01^2	-1.514	0.015			
a01^2	0.617	0.015			
s^2	0.066	0.019			

Table 4.27 The comparison of quadratic and linear regression for real part of the first eigenvalues for the short range of the rate parameters as in Fig.4.8.

Re3	BETA	St.Err. of BETA	Re3	BETA	St.Err. of BETA
a01	2.481518	0.014681	a01	0.797	0.002
b2	-0.41725	0.001618	b2	-0.418	0.002
k1	-0.35266	0.001618	k1	-0.352	0.002
a01^2	-1.69487	0.014681			

Table 4.28 The comparison of quadratic and linear regression for real part of the third eigenvalues for the short range of the rate parameters as in Fig.4.8.

Re4	BETA	St.Err. of BETA	Re4	BETA	St.Err. of BETA
b12	-0.048	0.000	b12	-0.048	0.000
b01	0.200	0.004	b01	0.064	0.000
a01	-0.071	0.000	a01	-0.071	0.000
b2	0.093	0.008	b2	0.034	0.000
b23			b23	0.004	0.000
a3	-0.031	0.000	a3	-0.031	0.000
s	-0.991	0.000	s	-0.991	0.000
k1	0.099	0.009	k1	0.034	0.000
k2	-0.054	0.000	k2	-0.054	0.000
b01^2	-0.137	0.004			
b2^2	-0.059	0.008			
b23^2	0.004	0.000			
k1^2	-0.065	0.009			

Table 4.29 The comparison of quadratic and linear regression for real part of the fourth eigenvalues for the short range of the rate parameters as in Fig.4.8.

	BETA	St.Err. of BETA	ln(Im1)	BETA	St.Err. of BETA
a1	1.192	0.006	a1	0.597	0.001
b12	-0.036	0.000	b12	-0.037	0.001
b01	-0.912	0.004	b01	-0.471	0.001
a01	1.008	0.004	a01	0.470	0.001
b2	0.073	0.007	b2	0.026	0.001
b23			b23	-0.024	0.001
a3	0.117	0.005	a3	0.036	0.001
s	-0.386	0.008	s	-0.214	0.001
k1	0.759	0.005	k1	0.359	0.001
A1^2	-0.595	0.006			
B01^2	0.445	0.004			
A01^2	-0.542	0.004			
B2^2	-0.047	0.007			
B23^2	0.003	0.000			
A3^2	-0.024	0.000			
S^2	-0.080	0.005			
K1^2	0.174	0.008			
K2^2	-0.402	0.005			

Table 4.30 The comparison of quadratic and linear regression for the imaginary part of the first eigenvalues for the short range of the rate parameters as in Fig.4.8.

	Mean	Minimum	Maximum	Range	Std.Dev.
OCL	21.88258	6.38	64	57.62	8
OBL	1804.408	894	3600	2706	530
OCT	25431.74	5520	313000	307480	34489
BM	1.074085	0.156	5.28	5.124	0.65

Table 4.31 The average population densities, maximum and minimum values and statistical deviations for the osteocells (cell/mm^3) for the model (4.5) and the relative bone mass, BM, for the short range of the rate parameters as in Fig.4.8.

	Mean	Minimum	Maximum	Range	Std.Dev.	Ch.Time
RE1	-3.4	-10.7	1.74	12.44	1.77991	0.27
RE2	-3.4	-10.7	1.74	12.44	1.77991	0.27
RE3	-3.99	-9.23	-1.68	7.55	1.307088	0.25
RE4	-0.031	-0.0459	-0.0203	0.0256	0.005788	33.33
IM1	528.9	223	1060	837	128.8082	1.288082
IM2	-528.9	-1060	-223	837	128.8082	1.288082
IM3						
IM4						

Table 4.32 Resulting statistics on the real and imaginary parts of the eigenvalues for the short range of the rate parameters as in Fig.4.8.

	ln(Ocl)	ln(Obl)	ln(Oct)	ln(BM)	Re1	Re3	Re4	ln(Im1)
R-square	0.99	0.99	0.99	0.99	0.95	0.94	0.998	0.99
a1	0.403	0.509	0.263	0.287	-0.434			0.597
b12	-0.024	-0.032	-0.016	-0.018	0.027		-0.048	-0.037
b01	-0.668	-0.843	-0.438	-0.478	0.744		0.064	-0.471
a01	-0.036	-0.046	0.531	0.580	-0.250	0.797	-0.071	0.470
b2	0.018	0.023	-0.238	-0.259	0.136	-0.418	0.034	0.026
b23		0.004	-0.033	-0.036	-0.298		0.004	
a3	-0.016	-0.020	0.216	-0.012	0.020		-0.031	-0.024
s	0.024	0.031	-0.337	0.017	-0.027		-0.991	0.036
k1	-0.306	0.019	-0.241	-0.263	0.113	-0.352	0.034	-0.214
k2	0.511	-0.035	0.404	0.442	0.032		-0.054	0.359

Table 4.34 The summary table for linear regression for short range of the rate parameters as in Fig.4.8.

4.6 Discussion and possible extension of the model

In the introduction, it is stressed that the mathematical model developed by Komarova et al., (2003) predicts different modes of dynamic behaviour of the BMU, while demonstrating the critical role for osteoclast regulation in the control of bone remodelling. In their work, this role has been investigated in the framework of a dynamic system, where the osteocyte regulation at the cellular level was not formally considered. In fact, the osteocytes play a vital role in signalling mechanical damage (Compston, 2002, Taboas at al., 2003; Yan et al., 2003; Koegler et al., 2004; Jansen et al., 2004).

The introduction to the model of the osteocytes regulation loop obviously increases the dimensions of the dynamical system. However, one can see that the system, proposed in this

section, is still controlled with a minimal collection of cellular regulation loops and has just one non-trivial equilibrium point. The total number of regulation loops in the system that can be phenomenologically called paracrine is four. They can be classify as the term 1)modelling effect the Oct on Ocl, 2)formal modelling mutual regulative paracrine interaction of Ocl and Obl, and 3)the term effecting transformation of Obl into Oct when the new bone forms. In this sense, the number of terms (links) can be considered a minimal one.

From the technical perspective, the model presents quite good stability characteristics of the nontrivial point, which is also an advantage of this model. The stability point can be classified as a stable focus. This can be seen throughout, from Fig.4.4 and Fig.4.7 for the middle range of the rate parameters to the short range of parameters, Fig.4.10. For the short range of parameters from the 10,000 generated combination of the rate constants, the number of equilibrium points, different from stable focus, was less that 70. This illustrates the robustness of the system in sense of the stability of the solutions.

Finally, it can be seen that this minimal model gives a quite reasonable population densities of osteocells, Table 4.31, for a volume unit of 1 mm^3. The characteristic time of the relaxation is about 33 days, Table 4.32, which as well is can be considered physiologically as reasonable.

Again, since the relations between the state variables and the rate constants are quite complicated, the regression analysis in combination with the Monte-Carlo method is shown as being usable in studying the relations between osteocells, BM and characteristics of relaxation. The results show good statistical significance when applying this method, particularly for the short range of the rate constants, Table 4.34. However, the results from the short range constants and the wide range of constants show a very good consistency.

Indeed, over a range of the rate constants that have realistic biological cellular time scales for the bone model, regression method in combination with the Monte-Carlo method, can be used to predict the position of the system state variables in the multi dimensional phase

space, see Fig.4.2-4.3, Fig.4.5, Fig.4.7-4.9 and Tables 4.1-4.34 at different ranges of the rate parameters.

However, different state variables, population concentrations of Ocl, Obl, Oct and total bone mass (BM) indicate different R-square (R^2), which determines the quality of the statistical model. The linear regression of the relative bone mass BM in case of wide range of the rate parameters gives a poor R^2 value about 0.75, which in fact, only allows one to speak about a tendency. The logarithmisation of the state variables and reduction of the range of the rate constants gives R^2 about 0.90, see Table 4.34, which indicates a good significance level. The regression of logarithm of concentration of osteoclasts on the set of the rate parameters gives R^2=0.99 with a confidence level of 0.01. The linear regression of osteosites' population density and BM indicates R-square values: Obl, R^2=0.99 and Oct, R^2=0.99. For BM, the most influential parameters are a_1, b_{01}, a_{01} b_2 and k_1, k_2. The last parameters, k_1 and k_2 influence in an opposite way: k_2 has very strong positive effect, while k_1 has negative effect. Parameters a_{01} and b_{01} have the strongest effect on the population density of Ocl, Table 4.34. Parameters a_1 and b_{01} have similar but opposite effect on the Obl population density. The osteoclast's population is affected by the a_1, b_{01} and k_1, k_2 rate constants. Finally, performing linear regression that only includes the first order of the parameters, gives the R-square mainly as R^2=0.99, which gives the significant level about 0.01, Table 4.34.

About 15% of all points generated by the Monte-Carlo method in the wide rate parameters range shown in Fig.4.4, give a different stability type than the stable focus, which have a periodical character or are even chaotic. This type of processes also can be considered as likely taking place in the bone resorption-formation. Simplification of the model, as it was done in Moroz and Wimpenny, 2006, 2007 can describe periodical and chaotic character of behaviour.

Within the framework of this rather phenomenological level of modelling, the role of the diverse molecular factors in bone regulation, such as receptors and mediators, the state of the membrane, and hormonal or genetic system, are difficult to discuss exactly. The roles of these

or any other molecular messenger or substrate remain the subject of discussion in the biochemical literature, even for the generalised animal model, and so the development of a mathematical model, based on the molecular level of regulation in the bone, awaits more precise biochemical and biophysical data.

An interesting result obtained from the model described, is that by adjusting the rate control of particular model parameters, for example, by the mechanical stress/microgravity parameter *s* (Table. 4.34, Re4 column), it is possible to reduce the relaxation time to the steady state. This indicates that by increasing the mechanical stress (in a certain interval) in the framework of this model the recovering time rises.

The model described in this section has mainly the relaxational character of behaviour. The periodic modes of behaviour that take place in some region of the rate parameters, could be seem less real in such a dense tissue as bone is. On the other hand, they might be interesting from an energetical perspective. However, there is a lack of experimental evidence for such a sort of behaviour in hard tissue, apart from in the case of Paget's disease. The above result leads to the conclusion that a cyclic process, which is an optimal from the regulation point of view and should be taken into consideration.

Another crucial assumption is that the models have no spatial dimensions; they consider tissue as a homogeneous material with a quite fast diffusion of cells, substances and signals. Taking this into account methodologically, these models are rather more useful in describing the relaxation effects that are much easier to validate than in bone tissue.

One of disadvantages of this model is that the model describes the "multiplicative" osteoclasts'-osteoblasts' relations, that means it is rather limited to the ideology similar to "predator-pray" in population biomodelling. Because of this, it is interesting to introduce the nonlinear, non-multiplicative, Oct-Ocl relations into the model, which can be interpreted as the allosteric regulation modelling. The next section is devoted to studying such a simplest non-multiplicative Oct-Ocl relations in the framework of the Michaelis-Menten/Monod function.

5 Allosteric approach to bone remodelling model

5.1 On an allosteric model of bone remodelling

Paracrine and autocrine relations are very important parts of the cellular model of the bone remodelling cycle (Komarova et al, 2003). In order to study the possibility to change the focus by giving cell relationships based on the formal allosteric form, starting from classic Michaelis-Menten one-site molecular control and extending to the well known Hill pattern. All these forms of regulation have the potential to represent allosteric regulation and this could be very interesting when studying the RANKL/OPG balance regulation, for example, Lemaire et al., 2004.

Classical Michaelis-Menten kinetics (Michaelis and Menten, 1913) is one the most important working approximation of nonlinear regulation in many models in different fields of biochemistry, microbiology and biotechnology, for example, in pharmacological models (Kakuji and Akapi, 1994), chemostat models (Lenas and Pavlou, 1995), or batch-kinetics models (Tohyama et al., 2002; Srinivasan et al., 2003; Smets et al., 2004). A number of research publications discuss the Michaelis-Menten control approach applied to the enzyme network (Heinrich et al., 1985; Hofmeyr et al., 1993; Fell and Thomas, 1995; Elsner and Giersch, 1998; Ortega and Agenda, 1998; Yildirim, 2003). Recently, Michaelis-Menten kinetics has been used to describe the changing rates of cellular activity during bone resorption, Martin and Buckland-Wright, 2004. At the same time, there are models discussed with respect to modelling of the molecular feedback control in ligand-receptor regulation and in ligand transport regulation (Maalmi et al., 2001; Komarova et al., 2003; Rattanakul et al., 2003). In this study the Michaels-Menten control have been chosen, as a first-stage of the allosteric control extension of cellular model, section 2.2. Based on this result the model can be adapted to employ other well known molecular control mechanisms, like the Hill (Hill, 1962) mechanism or probably less relevant to the BMU control, the Adair (Adair, 1925),

Koshland-Nemethy-Filmer (Koshland et al., 1966), Monod-Wyman-Changeux (MWC), Monod et al., 1965) ones.

Effectively a study was undertaken to find prospective paracrine and autocrine parameters, following in some sense Komarova et al., 2003, but in the form of allosteric regulation terms. Such approach could probably produce the intermediate model from cellular to biochemical one.

5.2 Allosteric model development

It is well known that steoclastic and osteoblastic formation activities are well coordinated in framework of BMU and this coordination effectively balances calcium homeostasis with skeletal modeling and repair. Recently few BMU-related models are developed (Komarova et al., 2003; Lemaire et al., 2004), including based on predator-pray elements ideology (Putra et al, 2010). Models described by these authors predict many different modes of dynamic behaviour of the BMU in bone remodeling control. However there are some limitations.

5.2.1 Model development

These limitations have driven modification of the initial model, section 4. Firstly, osteocyte's apoptosis in the bone remodeling regulation loop has been considered, and secondly the autocrine and paracrine control has been enhanced to make it more biologically relevant. At third stage the autocrine and paracrine feedback function were chosen not in pure cellular form but more akin to the ligand-receptor response/binding function (Michaelis-Menten/Monod). Such function can be linked to the allosteric, competitive inhibition and other control degrees of freedom with a clear biochemical sense (rather than fractal values which are purely theoretical, Komarova et al., 2003). The regulation loops that control the activity of the BMU can be refined and attempted to introduce the cybernetic-like point of view, such that the control should be minimised from both the (catabolic) energetic point and

metabolic point of view. For example, a reason for this could be the limitation of the transport into the bone of the energetic substrates such as ATP and oxygen, as well others substrates. Changes from the physiologically normal bone resorption and formation rates could destabilise the metabolic optimality not only on the local (bone) level but could also create a supply problem for the body as a whole.

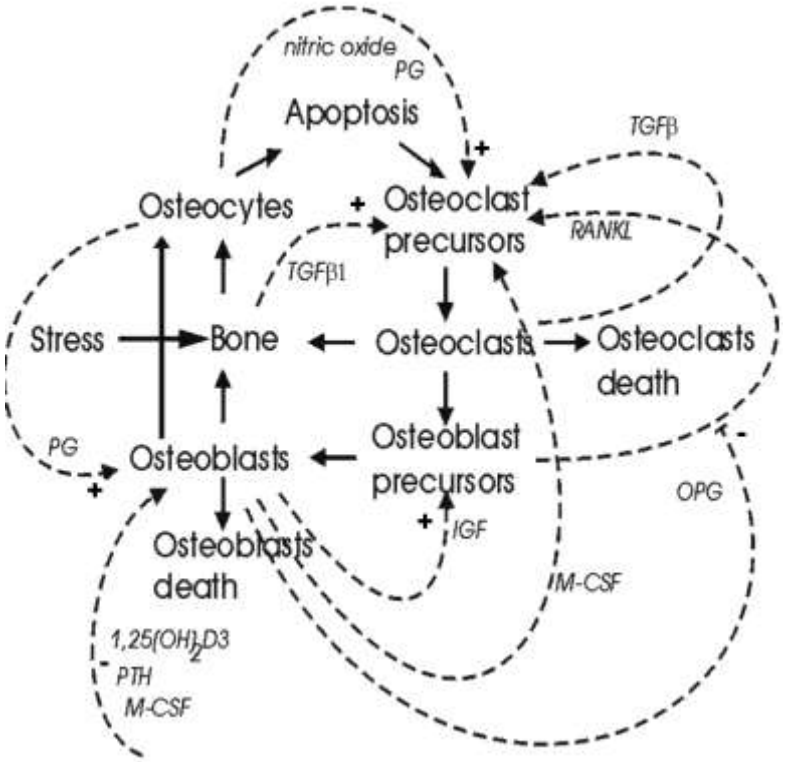

Fig. 5.1 Schematic representation of the cell interaction pattern in the extended BMU. Arrows represent the control loops of regulation in BMU on the cellular level. Dashed arrows represent molecular control pattern. PG, prostaglandin; TGFβ, TGFβ1, tumor growth factor; RANKL, receptor activator of nuclear factor κB ligand; OPG, osteoprotegerin; IGF, insulin-like growth factor; PTH, parathyroid hormone; 1,25$(OH)_2$ D3, vitamin D; M-CSF, macrophage-colony stimulating factor.

Additionally, the robustness is important at all levels of regulation. Therefore in order to produce a robust remodelling process the control should be tough at molecular level, indeed. Phenomenological cellular models can affect the tissue infrastructure of regulation and function in the whole body, as well as the very robust biochemical pathways. In the case of a multicellular organism and tissue, an evolutionary process is taking place. Probably, from the evolutionary point of view, the cellular level is even more important, because the

multicellular body evolved from cellular colonies with initially poor communication. Taking into account this point it has attempted to develop and analyse the possibility of a cellular model and robustness at this level.

The resulting cell-level control scheme based on the introduction of the osteocytes control loop could be presented as in Figure 5.1, where Oct apoptosis initiates the osteoclasts maturation from osteoclasts precursors (continues arrows). On the other hand, the terms paracrine and autocrine are just macroscopic formalisation of the action of microscopic local factors, resulting in a form of feedback control of the dynamic system model. The number of reported local factors is quite wide and shows the complexity of regulation at the micro-level.

It is widely accepted that OPG-RANK-RANKL pathway is the major pathway involved in bone remodelling, see for example, Hofbauer et al., 2000; Kong and Penninger, 2000; Theoleyre et al., 2004. The autocrine effect occurs due to pre-Ocl expression of RANK which is targeted by RANKL. It is interesting that RANKL can exist as a soluble protein about 31kDa so that Obl/stromal cells can induce Ocl formation in the absence of direct cell-to-cell contact, Horowitz, 2001. This forms another paracrine/autoctine degree of freedom in BMU regulation. Effectively, the RANK-RANKL balance is regulated by osteoprotegerin. The first incorporation of this pathway in a mathematical model was described by Lemair et al., 2004. However, as it follows from number of studies many others hormones, like PTH, growth factors, cytokines, vitamins and ions are involved in autocrine/paracrine regulation of BMU, e.g. in of bone resorption and formation. There are many indications that the number of factors (BMP-3, BMP-7, IGF I, IGF II, TGF-β3, FGF-2, VEGF) expressed by osteocytes are involved in outocrine/paracrine regulation of OBL and OCL, Table 1, Heino et al., 2004, reported on Oct factor that suits of the growth factor with stimulatory effect on Obl. There is a suggestion that Oct plays a fine-tuning role in bone remodelling. Bakker et al., 2001, who studied the possible role of nitric oxide in bone remodelling, suggests that Oct apoptosis attracts Ocl thereby activating remodelling. Westendorf et al., 2004, stressed the role of secreted 39-46 kDa cystein rich glycoproteins, Wnts and its role in signalling in Obl. Moseley

et al., 2003, discussed role of Interleukin-17 family (IL-17) cytokines, secreted by T-cells and their role cancer metastasis to bone and regulatory effects in Ocl precursor maturation. Additionally, bone cells also express a wide range of the neurotransmitter receptors as glutamate, γ-aminobutyric acid, purines and pyrimidines. The overall complexity of the regulation pattern of these local and homeostatic factors participating in differentiation, maturation and osteocells activity is illustrated in Table 5.1 and Fig.5.1, (dashed arrows).

Despite the fact that the effect of the majority of these factors is not direct and is mediated sometimes by a long sequence of other molecular intermediates/stages, the effective action could follow basic regulative forms, such as Michaelis-Menten one. For example, in the model incorporation of OPG-RANK-RANKL pathway, described by Lemaire et al., 2004, PTH involvement is essentially nonlinear and rather Michaelis-Menten in nature. Furthermore, Martin and Buckland-Wright, 2004, described an effective model based on the premise that the inhibitory effect on TGFb1 (TGFb1 – induced production of OPG by marrow osteoblasts stromal cells) reducing effectively RANKL accordingly to Michaelis-Menten kinetics, when the effective Michaelis-Menten constant for osteoclast's activity was introduced.

During development of the model an attempt was made to compromise between the level of microscopic interacting molecular factors and the macroscopic form of feedback function in the phenomenological model of regulation. Taking into account that in order to produce a robust bone remodelling process, the regulation needs robustness at all levels of control, and indeed at cellular and molecular levels. The final loop of regulation links together (in some way) the participating cells and their precursors, as well as the bone material and even integrates body homeostatic systems like ion balance or the immune system.

Local Factor/Receptor	Reference
Hormones:	
Parathyroid hormone (PTH)/PTHrP	Goltzman, 1999
1,25(OH)2 vitamin D3	Hofbauer et al., 1998
Glucocorticoid	Gao et al., 1998
Calcitonin	Komarova et al., 2003b
Growth Factors:	
Transforming GF β superfamily:	
BMP-3, BMP-7	Linkhart et al., 1996
TGF-β3	Thomadakis et al., 1999
Insulin-like GF	
IGF I, IGF II	Linkhart et al., 1996
PDGF	Zhang et al, 2002
Vascular endothelial GF (VEGF)	Wang et al., 1996; 1997
FGF (FGF-2)	Kawaguchi et al., 1994
Cytokines:	
IL-1, IL-6 IL-11,1317	Moseley et al., 2003
TNF α and β	Hofbauer et al., 1998, 1999; Nanes, 2003
Cyclosporine A	Chen et al., 2003
RANKL	Suda et al., 1999
Activin, Inhibin	Farnworth et al., 2001
WNTs	Westerndorf et al., 2004
Osteopontin	Denhardt and Noda, 1998
Low molecular weight factors	Laitala-Leinonen et al., 2006
Cystatin B	Sanjay et al., 2001
Calcium	Bakker et al., 2001; Fan et al., 2004
Nitric Oxide (NO)	Vatsa, 2007

Table 5.1 Some important local factors in Ocl, Obl and Oct activity regulation that could play paracrine and/or autocrine role. Adopted from Moroz and Wimpenny, 2007.

A dynamical model, that includes Michaelis-Menten type of feedback mechanisms into the cellular model can be rewritten as

$$\begin{aligned}
\dot{x}_1 &= x_1 f_{FB}(x_3, K_M) - f^{-}_{OBl}(x_2) x_1 \\
\dot{x}_2 &= x_2 f_{FB}(x_1) - f^{-}_{OBl}(x_2, x_4) \\
\dot{x}_3 &= f^{+}_{OCt}(x_4) - f^{-}_{OCl}(s, x_3) \\
\dot{x}_4 &= f^{+}_{B}(x_2) - f^{-}_{B}(x_1)
\end{aligned} \tag{5.1}$$

where x_1 is the populational concentration of osteoclasts, x_2 is the populational concentration of osteoblasts, x_3 is the populational concentration of osteocytes, x_4 is the total bone mass, *s* is the level of mechanical stress.

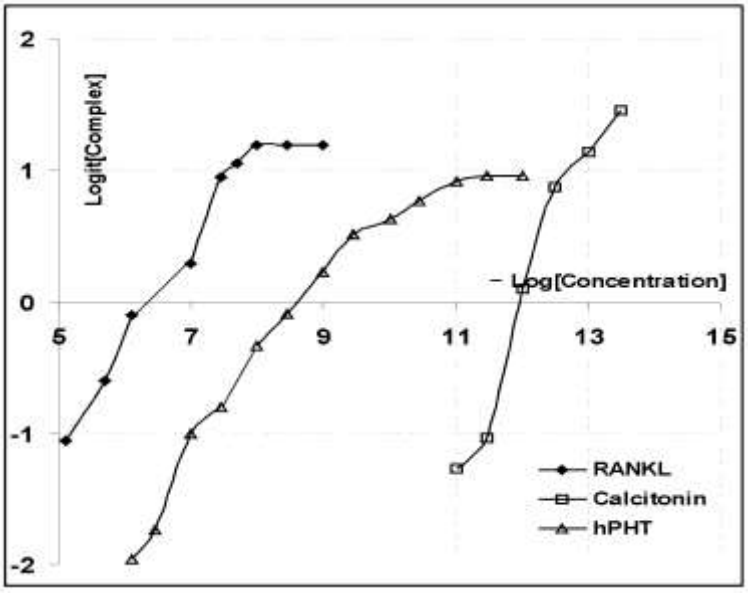

Fig. 5.2 The Hill (logit) plot of some important in bone regulation molecular ligands: data adopted from Hoare et al., 1999 for hPHT, from Beaudreuil et al., 2004 for calcitonin and for RANKL from Regmi et al., 2005.

Functions

$$f_{M-M}^{FB}(x_1, Km_1) = \frac{x_i}{Km_i + x_i},$$

$$f_{Hill}^{FB}(x_i, K_i) = \frac{x_i^2}{K_i^2 + x_i^2}, \qquad (5.2)$$

describe different types of non-linear feedback loops of regulation, Michaelis-Menten one-site molecular control (Michaelis and Menten, 1913) and other well known: Hill, Adair, Monod-Wyman-Changeux and Koshland-Nemethy-Filmer, and functions $f_{OBl}^{-}(x_4)$, $f_{OCt}^{-}(s, x_3)$, $f_B^{-}(x_1)$ describe negative regulation feedbacks due to apoptosis, death or transformation the cells. This study has been operating with population densities of cells. All constants were normalised (Michaelis-Menten, p50 concentration) to unity. All initial rate constants were chosen following Komarova et al., 2003. The feedback functions parameters were chosen that *p50* for all functions remained the same at concentration parameter equal to one, Fig. 5.2C.

Using a range of feedback control functions it is possible to model diverse molecular mechanisms of regulation. It is known that the molecular local factors act by a number of very specific molecular mechanisms, finally expressed in certain non-linearities in kinetic equations. Different allosteric ("other site") forms of factor-receptor regulation is a important molecular mechanism control of cell functions, and, particularly, cooperativity is the interesting degree of freedom in such a regulation, because it characterises the degree (sharp or gentle) with which the regulation reaches a threshold.

The highest cooperativity gives more robust regulation with a distinct threshold behaviour which is typical of many physiological parameters. For example this behaviour is seen in oxygen regulation when cooperativity of haemoglobin that posses 4 interacting binding sites, with cooperativity about 2.73 calculated accordingly to Hill, 1962. It can be suggested that it is more likely that the ideal cooperativity in the case of receptors exposed on osteocells, is limited to 2. This means that the number of binding centres on a receptor is also equal to 2. For example, TGF-b has two subunits, which bind to type II and type I receptors. Binding to the binding site on type II receptor causes the receptor to recruit by binding to second binding site on type I receptor, (Wingsfield et al., 1987; Thompson et al., 2004). After phosphorylation type I receptor it recruits and phosphorylates Smad2 or Smad3 in the long chain in targeting the TGF-B response element on DNA. In that way the entire process is cooperatively regulated. So Type I and type II TGF-β receptors are likely dimmers that could be associated with inhibitory factors and follow allosteric models of regulation having a cooperative character. TNF-α factor is a trimer (Wingsfield et al., 1987) and NF-kB regulatory receptor-activator protein it is likely that it has three binding sites exposed into extracellular medium. The existence of RANKL in a soluble form about 31kDa is interesting explanation that OBl/Stromal cells could induce OCl formation in the absence of direct cell-to-cell contact, Horowitz et al., 2001. This is another argument for considering molecular models of binding in BMU regulation.

Thus, it is very reasonable to choose the feedback functions that are capable of introducing the allosteric regulation. Additionally, the allosteric models have additional very

good interpretable control degrees of freedom, in contrast to fractal models, which are sometimes very difficult to interpret from the point of view of the molecular control.

Taking into account the importance of osteoclasts-osteocytes interaction, the dependence of f_i^+ and f_i^- can be proposed which yields the following system

$$\begin{aligned}
\dot{x}_1 &= \alpha_1 x_1 - \beta_{12} x_1 \frac{x_3}{K_{Oct} + x_3} - \beta_{01} x_1 x_2 \\
\dot{x}_2 &= \alpha_{01} x_1 x_2 - \beta_2 x_2 x_4 - \beta_{23} x_2^2 \\
\dot{x}_3 &= \alpha_3 x_4 - s x_3 \\
\dot{x}_4 &= -k_1 x_1 + k_2 x_2
\end{aligned} \tag{5.3}$$

where the designations are as for (2.1.4). In this model the Michaelis-Menten kinetics is only present in one term, due to insufficient experimental evidence to suggest that it should be present elsewhere.

5.2.2 Equilibrium state

To find the equilibrium points of system (2.2.1) one must set the right parts of the system to zero, then the system of algebraic equation is obtained:

$$\begin{aligned}
&\alpha_1 x_1 - \beta_{12} x_1 \frac{x_3}{K_{Oct} + x_3} - \beta_{01} x_1 x_2 = 0 \\
&\alpha_{01} x_1 x_2 - \beta_2 x_2 x_4 - \beta_{23} x_2^2 = 0 \\
&\alpha_3 x_4 - s x_3 = 0 \\
&-k_1 x_1 + k_2 x_2 = 0
\end{aligned} \tag{5.4}$$

Then starting from the last equation it can be seen that $x_2 = k_1 x_2 / x_1$. Substituting this into the equations of (2.1.5) one can find the nontrivial solution and can finally obtain the second order algebraic equation

$$A x_3^2 - B x_3 - C = 0 \tag{5.5}$$

where $$A = \frac{b_{01} k_1 b_2 s}{a_3 (a_{01} k_2 - b_{23} k_1)},$$

$$B = a_1 - AK_{Oct} - b_{12},$$

$$C = a_1 K_{Oct}.$$

Then one can obtain the roots of (5.2)

$$x_{3(a,b)} = \frac{1}{2A}\left(-B \pm \sqrt{B^2 + 4AC}\right) \tag{5.6}$$

when $(B^2 + 4AC) \geq 0$ the roots are real. Calculations of the equilibrium point when the sign "-" is in equation (5.6) yields the negative values for x_3 and other state variables.

Having calculated x_3 (5. 6) it is possible to find x_1, x_2 and x_4

$$\begin{aligned} x_2 &= \frac{k_1 \beta_2 s x_3}{a_3(\alpha_{01} k_2 - \beta_{23} k_1)} \\ x_4 &= \frac{s}{a_3} x_3 \\ x_1 &= \frac{k_2}{k_1} x_2 \end{aligned} \tag{5.7}$$

and the trivial solution:

$$x_1 = 0, x_2 = 0, x_3 = x^*, x_4 = sx^*/a \text{, where } x^* \in [0, \infty], \tag{5.8}$$

which indicates that the plane x_3, x_4 is the solution when $x_1=x_2=0$. Designating right parts of (2.2.1) as F_i one can find the Jacobi matrix:

$$\begin{aligned} &\frac{\partial F_1}{\partial x_1} = -\beta_{12} \frac{x_3}{K_{Oct} + x_3} + \alpha_1 x_1 - \beta_{01} x_2, \frac{\partial F_1}{\partial x_2} = -\beta_{01} x_1, \frac{\partial F_1}{\partial x_3} = -\beta_{12} \frac{K_{Oct} x_1}{(K_{Oct} + x_3)^2}, \frac{\partial F_1}{\partial x_4} = 0; \\ &\frac{\partial F_2}{\partial x_1} = \alpha_{01} x_2, \frac{\partial F_2}{\partial x_2} = \alpha_{01} x_1 - \beta_2 x_4 - 2\beta_{23} x_2, \frac{\partial F_2}{\partial x_3} = 0, \frac{\partial F_2}{\partial x_4} = -\beta_2 x_2; \\ &\frac{\partial F_3}{\partial x_1} = 0, \frac{\partial F_3}{\partial x_2} = 0, \frac{\partial F_3}{\partial x_3} = -s, \frac{\partial F_3}{\partial x_4} = \alpha_3; \\ &\frac{\partial F_4}{\partial x_1} = -k_1, \frac{\partial F_4}{\partial x_2} = k_2, \frac{\partial F_4}{\partial x_3} = 0, \frac{\partial F_4}{\partial x_4} = 0; \end{aligned} \tag{5.9}$$

Employing (2.2.5) it is possible to study the character of equilibrium in trivial (2.2.4) and nontrivial (2.2.3) points. Both these equilibrium points are interesting, however, to study the character of the trivial point, which in fact is the axis, further investigation is necessary.

5.3 Results of calculations in a wide range of constants

The behaviour of the mathematical model was evaluated using the Michaelis-Menten function in order to examine whether the model repeats the modes of the system, described in Section 2. In the majority of cases it produces the character of behaviour as in model (2.4) within a wide range of constants. The timescale for the model is linked to the unit of time in days, as in the model of Section 4. As mentioned in that section, the choice of initial constants was based on experimental histomorphometric data (Parfitt, 1994; Kato et al., 2001; Vashishth et al., 2002), which has also been estimated also by Komarova et al., 2003. One should note that even for the linear systems similar to above Eq.(5.2), the value of the rate constants is not directly related to the value of the formation or resorption rates that could be measured in experimental conditions. In this case it is expectedly difficult to validate the model constants, although, some general results like the character of local steady state remain topologically the same. The change of the rate parameters in Eq.(5.3) in wide range does not change the character of equilibrium, Figure 5.4 shows that it is quite robust.

Over the employed range of rate parameters, the trajectories have demonstrated a tendency to behave as a stable focus – in line with the findings for pure cellular model (4.4). One can possibly say that the stable focus prevails after the introduction of the Michaelis-Menten kinetics. The range of the rate parameters was slightly changed compared to the pure cellular model (4.4) and in addition they were also modified by introduction of the Michaelis-Menten control and other constants like K_{Oct}. Range of parameters used: K_{Oct}, 100-100000.0; a_1, 200.0- 30000. day^{-1} ; b_{12}, 0.002-0.05 $cell^{-1}day^{-1}$; b_{01}, 1.0-40.0 $cell^{-1}day^{-1}$; a_{01}, 1.50-300.0 $cell^{-1}day^{-1}$; b_2, 50.0 -1000.0 $cell^{-1}day^{-1}$; b_{23}, 0.001-0.09 $cell^{-1}day^{-1}$; a_3, 1000-66000 day^{-1}; s, 0.001-2.0 $cell^{-1}day^{-1}$; k_1, 0.01-1.0 day^{-1}; k_2, 0.00003-0.003 day^{-1}.

Direct application of the similar range of rate parameters as in Section 4 gives the results, illustrated in Fig. 5.3-5.5.

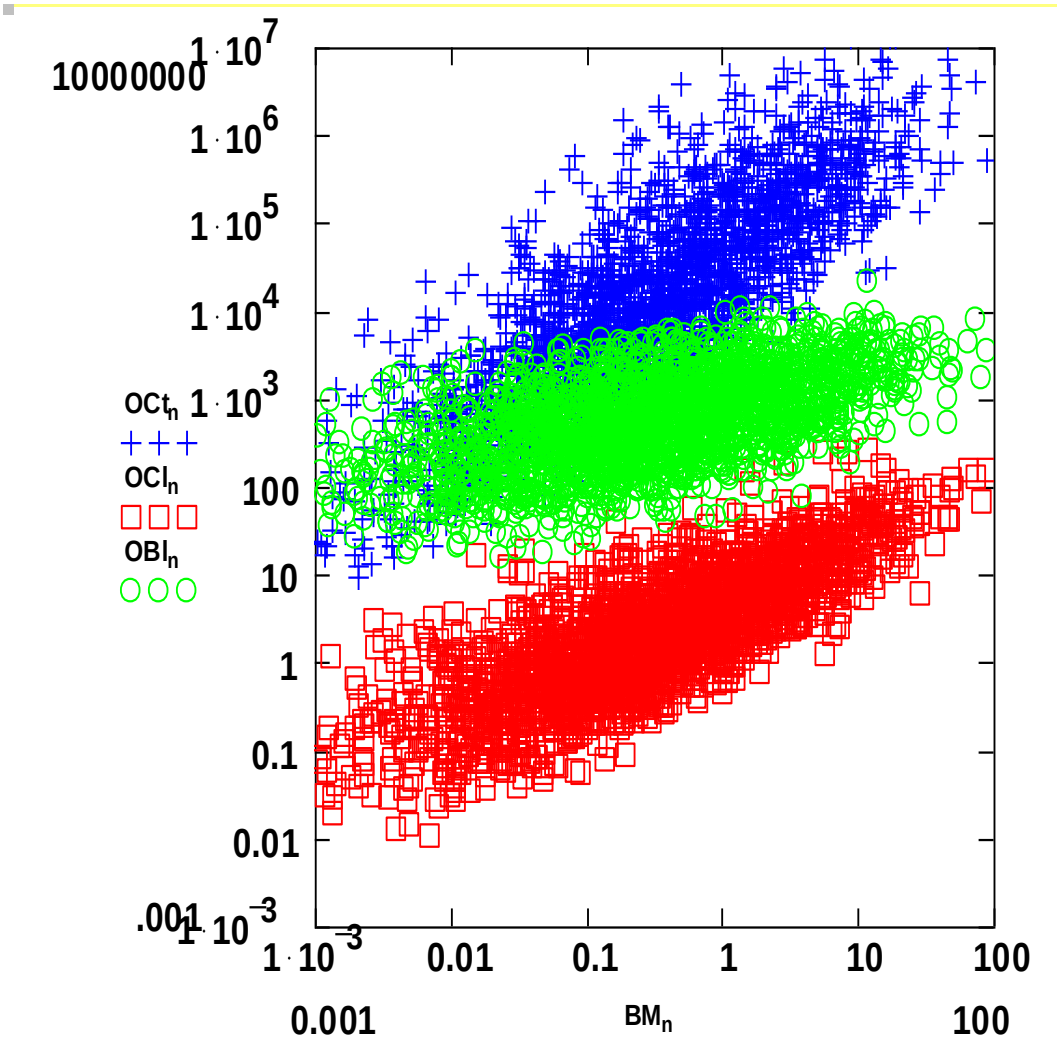

Fig.5.3 The scatterplot of numeric calculations for system (5.3) Calculations were performed using the range of parameters: K_{Oct}, 100-100000.0 cell mm^{-3}; a_1, 200.0- 30000. day^{-1}; b_{12}, 0.002-0.05 cell^{-1}day^{-1}; b_{01}, 1.0-40.0 cell^{-1}day^{-1}; a_{01}, 1.50-300.0 cell^{-1}day^{-1}; b_2, 50.0 -1000.0 cell^{-1}day^{-1}; b_{23}, 0.001-0.09 cell^{-1}day^{-1}; a_3, 1000-66000 day^{-1}; s, 0.001-2.0 cell^{-1}day^{-1}; k_1, 0.01-1.0 day^{-1}; k_2, 0.00003-0.0030 day^{-1}.

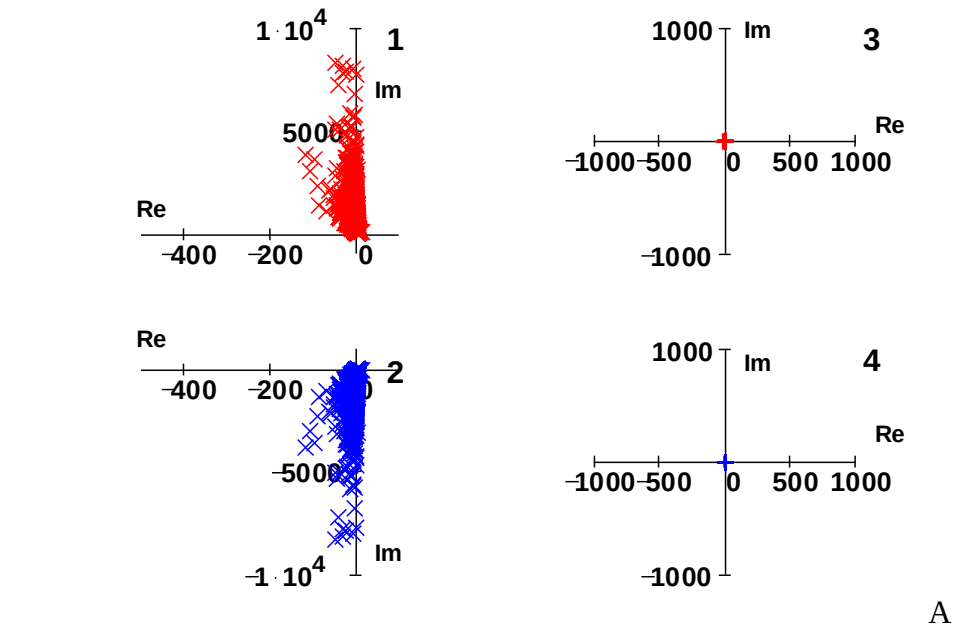

A

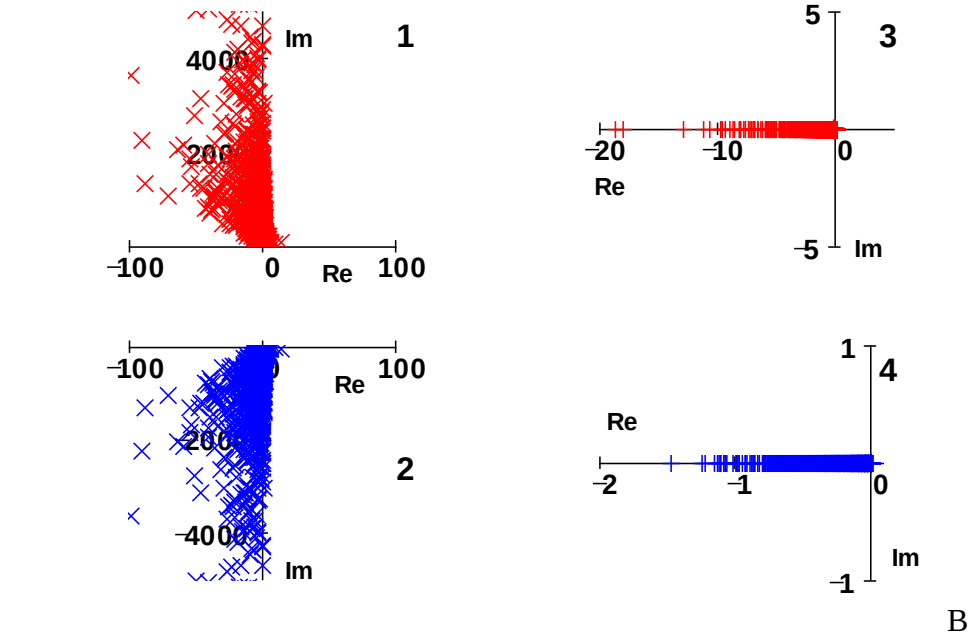

B

Fig. 5.4 Scatterplot of eigenvalues (5.9) at (5.6a) for system (5.3). A, large scale; B, small scale. Calculations were performed using the range of parameters as in Fig.5.3.

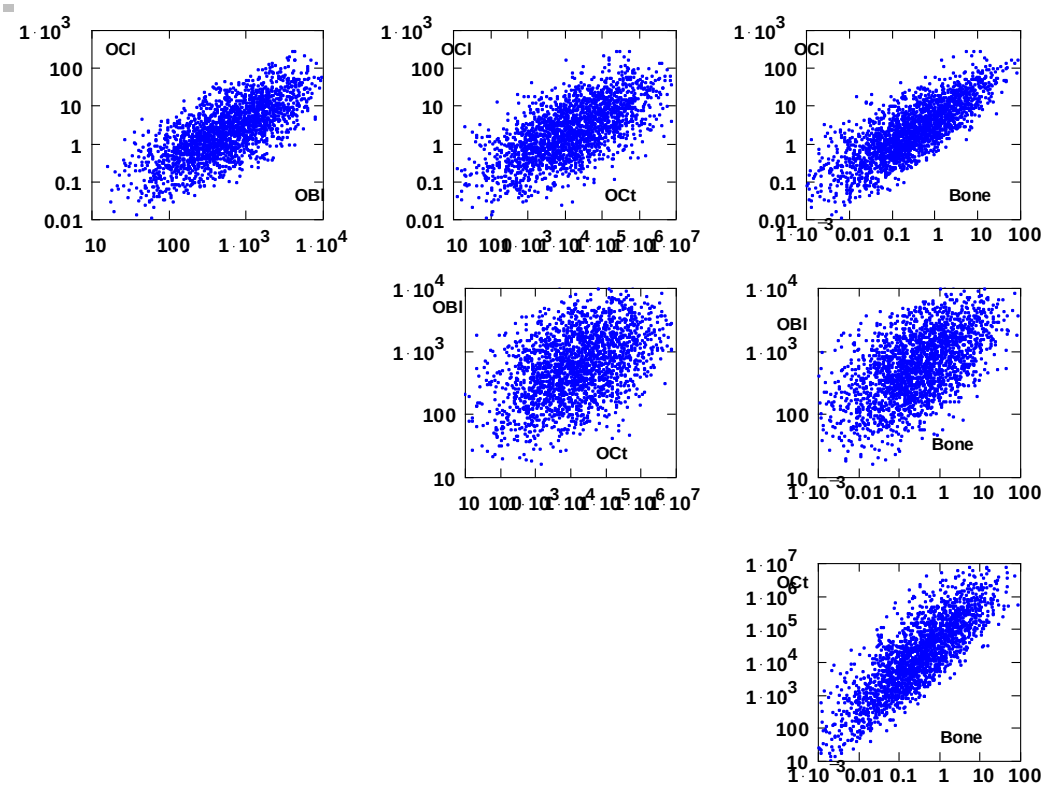

Fig.5.5 Detailed graphical matrix illustrating scatterplot of population densities of Ocl, Obl, Oct, bone in 4D space of these variables. The range of parameters as in Fig.5.3.

As seen in Figure 5.3, the population density of Ocl and Obl change in the range 0.01-100 and 10-10000 cells*mm^{-3} respectively. The Oct's population density varies from 10 to 10^7 and total bone mass varies from 0.001 to 100 cells*mm^{-3}. The graphical matrix diagram, Fig.5.5, indicates the individual scatterplots of all pairwise combinations of the state variables and illustrates wide range of rate constants. From Fig.5.4 can be seen that the main equilibrium point can be characterised as a stable focus. Indeed, from 3681 generated by Monte Carlo method combinations about 11% (410) were unstable having two conjugate eigenvalues with positive real part. Thus, from the point of view of stability the dynamical model is reliable, even when a wide range of rate constants was employed.

Application of regression methods to this dataset, where a wide range of rate constants was applied, returns poor determination coefficients for individual regressions. This can be explained by the fact that the relations in such a wide range can be significantly nonlinear so the reduction of the range of the rate constants was applied.

5.4 Model fitting in the middle range of the rate parameters

Reducing the range of rate constants to two decimal orders, K_{Oct}, 5000-500000 cell mm^{-3}; a_1,1200.0-4300.0 day^{-1}; b_{12},0.002-0.02 $cell^{-1}day^{-1}$; b_{01}, 1.5-3.5 $cell^{-1}day^{-1}$; a_{01},3.0-24.0 $cell^{-1}day^{-1}$; b_2, 50.0-420.0 $cell^{-1}day^{-1}$; b_{23}, 0.005-0.007 $cell^{-1}day^{-1}$; a_3, 1300-20000 day^{-1}; s, 0.02-0.4 day^{-1}; k_1, 0.01-0.040 day^{-1}; k_2, 0.0002-0.0006 day^{-1}, Fig.5.6, does not change the character of the stability of the equilibrium point, see Fig. 5.7, preserving the imaginary part for the first eigenvalue. The existence of an imaginary part indicates that for the points of equilibrium, the trajectories comprise the periodical character of movement with decaying amplitude. It also compacts the position of these points around the same region, Fig.5.8. However, the ranges of state variables' values of the generated data set can be considered as having an enhanced physiological regulatory meaning, Fig.5.7-5.8.

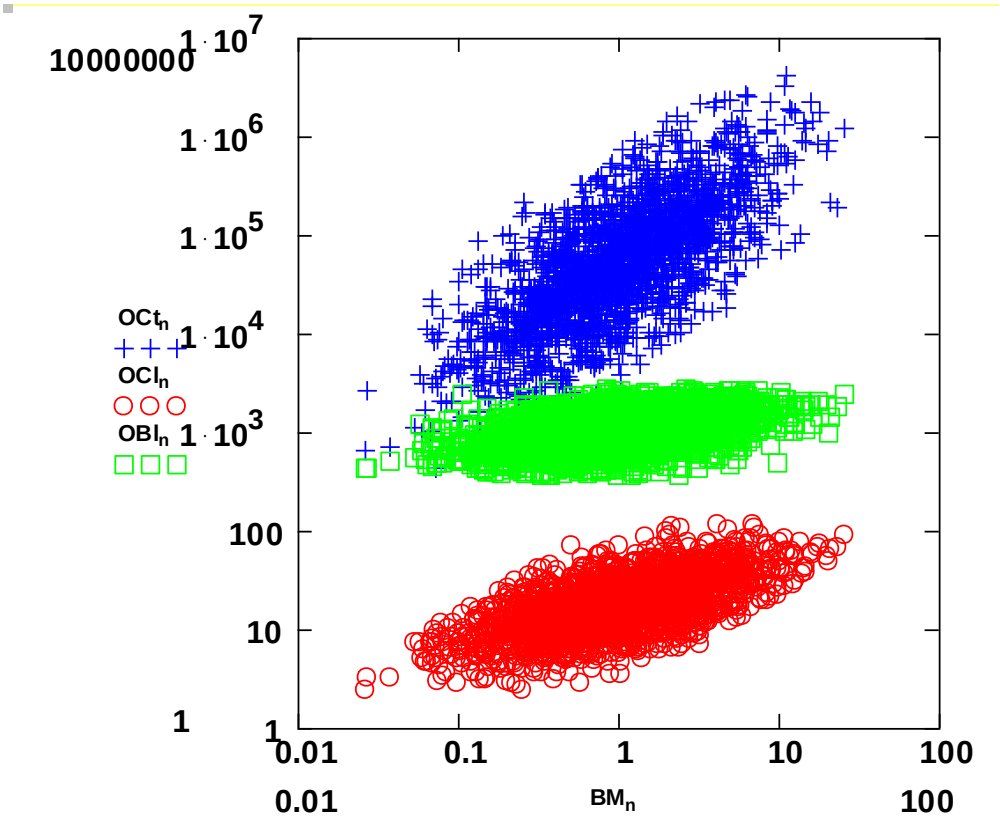

Fig.5.6 The scatterplot of osteocells against BM for system (5.3) with an extended range of rate parameters: K_{Oct}, 5000-500000 cell mm^{-3}; a_1, 1200.0-4300.0 day^{-1}; b_{12},0.002-0.02 $cell^{-1}day^{-1}$; b_{01}, 1.50-3.5 $cell^{-1}day^{-1}$; a_{01},3.0-24.0 $cell^{-1}day^{-1}$; b_2, 50.0-420.0 $cell^{-1}day^{-1}$; b_{23}, 0.005-0.007 $cell^{-1}day^{-1}$; a_3, 1300-20000 day^{-1}; s, 0.02-0.4 day^{-1}; k_1, 0.01- 0.04 day^{-1}; k_2, 0.0002-0.0006 day^{-1}.

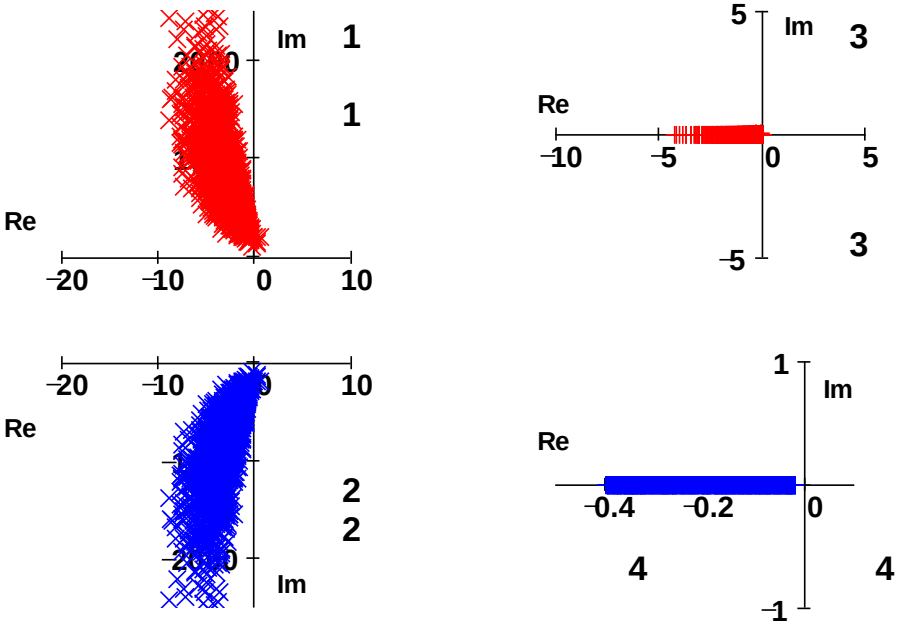

Fig. 5.7 The stability characteristics of the equilibrium point after extending the range of the rate constants. The range of parameters as in Fig.5.6.

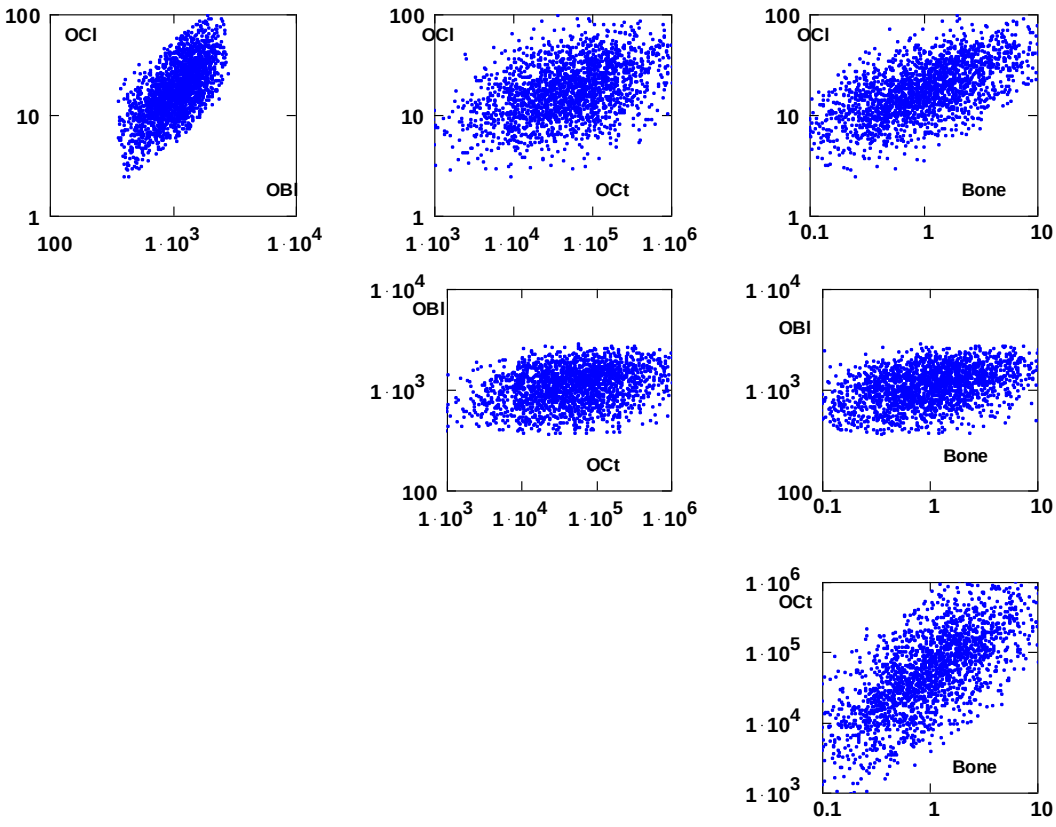

Fig.5.8 Detailed graphical matrix illustrating scatterplot of population densities of Ocl, Obl, Oct, BM in 4D space of these variables. The range of parameters as in Fig.5.6.

	ln(Ocl)	ln(Obl)	ln(Oct)	ln(BM)	Re1	Re3	ln(Re4)	Im1
R-square	0.98	0.98	0.92	0.95	0.93	0.70	0.90	0.90
a1	0.526	0.814	0.245	0.332	-0.745	0.018		0.624
b12								
b01	-0.366	-0.566	-0.165	-0.227	0.553			-0.229
a01			0.396	0.529	-0.107	0.585		0.472
b2			-0.377	-0.509	0.087	-0.467		
b23				-0.007	-0.220			
a3			0.448					
s		0.005	-0.481				0.944	
k1	-0.580		-0.280	-0.382	0.067	-0.366		-0.376
k2	0.462		0.221	0.302				0.290

Table 5.2 Summary table for MC/regression results for a set of the rate parameters from Fig.5.6.

From summary Table 5.2 one can see a good statistical significance for just the osteocells and total bone mass, however, the R-square for the relaxation parameters, in fact eigenvalues, is quite poor. Therefore the numerical experiment was again repeated for a shorter range of the rate parameters.

5.5 Short range of the rate parameters

The behaviour of the model has been studied in the short range of parameters aiming to improve the output of the regression analysis. Calculations were performed using the range of parameters: K_{Oct}, 100-100000; a_1, 3000.0-5000.0 day^{-1}; b_{12}, 0.002-0.004 $cell^{-1}day^{-1}$; b_{01}, 1.3-3.2 $cell^{-1}day^{-1}$; a_{01}, 2.0-5.0 $cell^{-1}day^{-1}$; b_2, 40.0-65.0 $cell^{-1}day^{-1}$; b_{23}, 0.005-0.007 $cell^{-1}day^{-1}$; a_3, 1100.0-1700.0 day^{-1}; s, 0.02 0.04 $cell^{-1}day^{-1}$; k_1, 0.2 0.30 day^{-1}; k, 0.002 0.004 day^{-1}. The results are shown in figures 5.9-5.11 and tables 5.2-5.11.

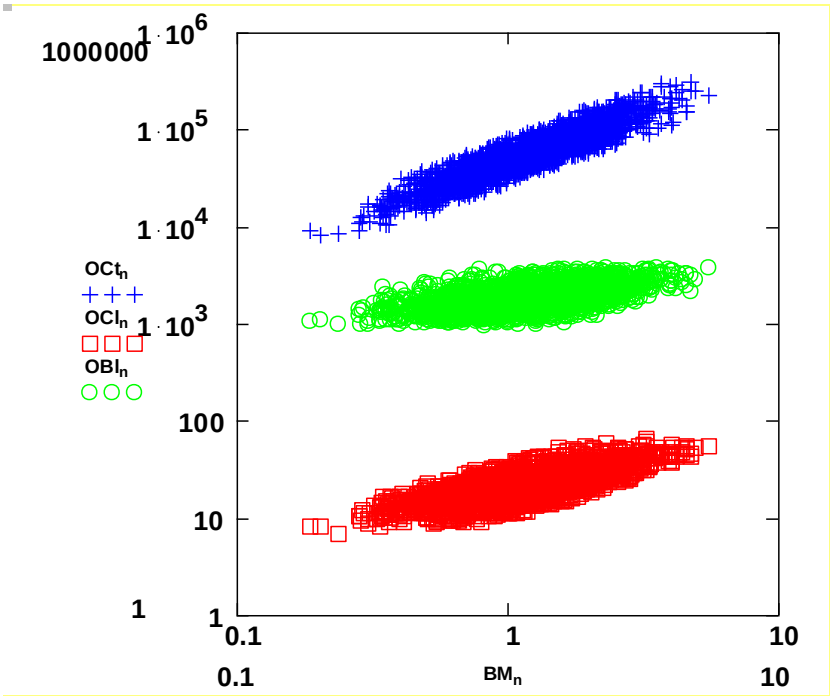

Fig. 5.9 The scatterplot of numeric calculations for system (5.3) Calculations performed using the range of parameters: K_{Oct}, 100.0-100000.0; a_1, 3000.0-5000.0 day^{-1}; b_{12}, 0.002-0.004 $cell^{-1}day^{-1}$; b_{01}, 1.3-3.2 $cell^{-1}day^{-1}$; a_{01}, 2.0-5.0 $cell^{-1}day^{-1}$; b_2, 40.0-65.0 $cell^{-1}day^{-1}$; b_{23}, 0.005-0.007 $cell^{-1}day^{-1}$; a_3, 1100.0-1700.0 day^{-1}; s, 0.02 0.04 $cell^{-1}day^{-1}$; k_1, 0.2 0.30 day^{-1}; k_2, 0.002 0.004 day^{-1}.

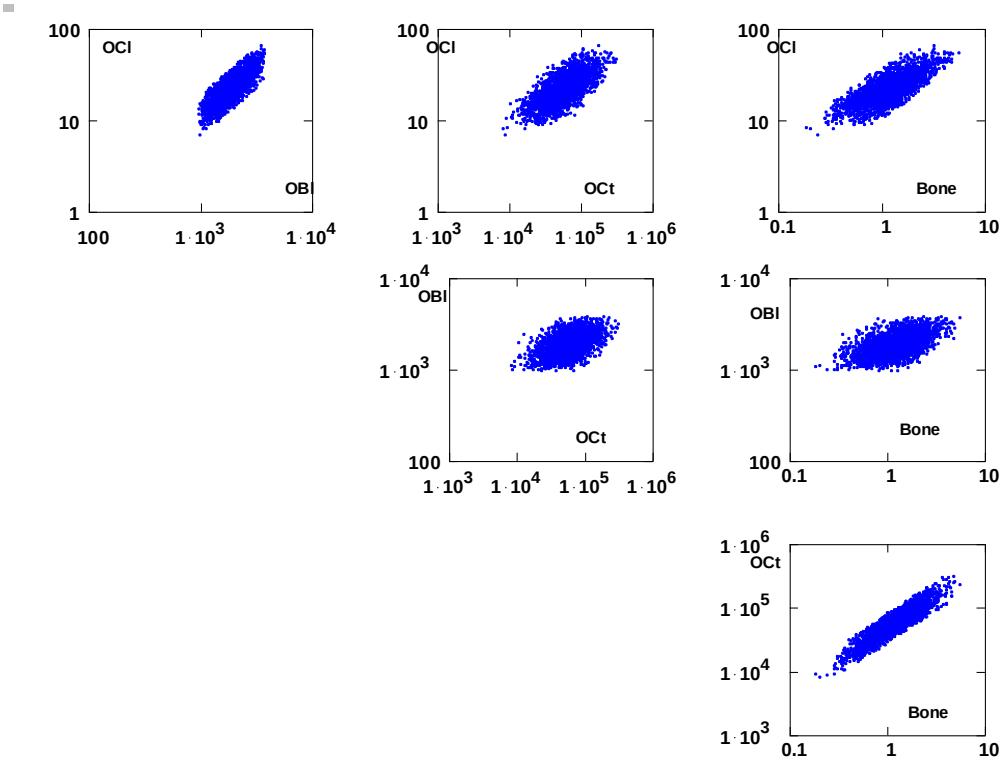

Fig.5.10 Detailed graphical matrix illustrating scatterplot of population densities of Ocl, Obl, Oct, BM in 4D space of these variables. The range of parameters as in Fig.5.9.

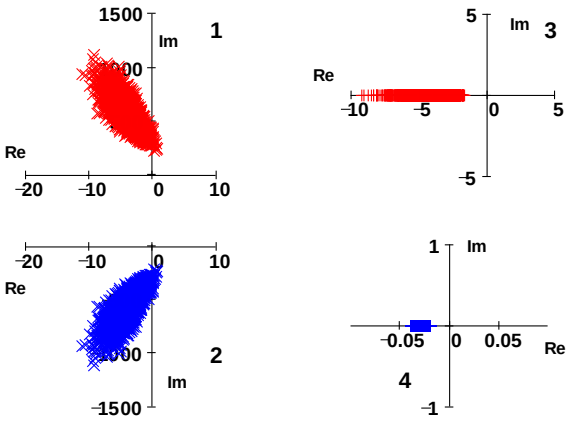

Fig.5.11 The scatterplot of real and imaginary parts of the four eigenvalues of system (5.4) in the range of parapeters indicated in Fig.5.9.

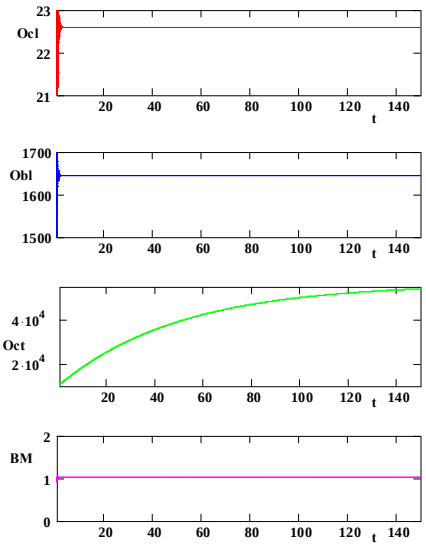

Fig.5.12 Relaxation of the system to the steady state at following rate constants: a_1, 4590 day^{-1}; b_{12}, 0.00363 $cell^{-1}day^{-1}$; b_{01}, 2.79 $cell^{-1}$ day^{-1}; a_{01}, 3.1 $cell^{-1}day^{-1}$; b_2, 57.9 $cell^{-1}day^{-1}$; b_{23}, 0.00647 $cell^{-1}day^{-1}$; a_3, 1100 day^{-1}; s, 0.021 $cell^{-1}day^{-1}$; k_1, 0.257 day^{-1}; k_2, 0.00353 day^{-1}, $K_{Oct}=8.4*10^4$. Re4=0.002, τ~50days

ln(Ocl)	BETA	St.Err.of BETA	B	St.Err.of B	t(9988)	p-level
Intercept			3.0649	0.0079	387.18	0.0000
KOct	-0.0007	0.0010	0.0000	0.0000	-0.74	0.0456
a1	0.3881	0.0010	0.0003	0.0000	401.58	0.0000
b12	0.0004	0.0010	0.2640	0.6320	0.41	0.6761
b01	-0.6740	0.0010	-0.4617	0.0007	-697.75	0.0000
a01	-0.0001	0.0010	0.0000	0.0004	-0.06	0.9466
b2	-0.0006	0.0010	0.0000	0.0001	-0.57	0.5674
b23	0.0010	0.0010	0.6423	0.6288	1.02	0.3070
a3	0.0007	0.0010	0.0000	0.0000	0.73	0.4609
s	0.0002	0.0010	0.0102	0.0622	0.16	0.8695
k1	-0.3045	0.0010	-4.0017	0.0127	-315.1	0.0000
k2	0.5221	0.0010	341.0841	0.6312	540.3	0.0000

Table.5.2 Linear regression analysis: the logarithm of population density of osteoclasts as a function of the rate constants. The range of the constants as in Fig.5.9. $R^2=0.99$.

ln(Obl)	BETA	St.Err. of BETA	B	St.Err. of B	t(9988)	p-level
Intercept			7.524	0.007	1117.821	0.000
KOct	-0.0012	0.0010	0.0000	0.0000	-1.1069	0.2684
a1	0.4955	0.0010	0.0003	0.0000	472.0264	0.0000
b12	0.0007	0.0010	0.3594	0.5374	0.6688	0.5036
b01	-0.8614	0.0010	-0.4618	0.0006	-820.8940	0.0000
a01	-0.0004	0.0010	-0.0001	0.0004	-0.3748	0.7078
b2	-0.0012	0.0010	0.0000	0.0000	-1.1346	0.2566
b23	0.0003	0.0010	0.1391	0.5346	0.2603	0.7947
a3	0.0006	0.0010	0.0000	0.0000	0.5670	0.5707
s	-0.0004	0.0010	-0.0192	0.0529	-0.3630	0.7166
k1	0.0018	0.0010	0.0188	0.0108	1.7394	0.0820
k2	0.0011	0.0010	0.5485	0.5367	1.0220	0.3068

Table.5.3 Linear regression: the logarithm of population density of osteoblasts as a function of the rate constants. The range of the constants as in Fig.5.9. R^2=0.99.

ln(Oct)	BETA	St.Err. of BETA	B	St.Err. of B	t(9988)	p-level
Intercept			10.9040	0.0143	763.9473	0.0000
Oct	0.0024	0.0011	0.0000	0.0000	2.1542	0.0312
a1	0.2536	0.0011	0.0003	0.0000	223.9967	0.0000
b12	-0.0017	0.0011	-1.6823	1.1396	-1.4762	0.0399
b01	-0.4388	0.0011	-0.4626	0.0012	-387.7189	0.0000
a01	0.5283	0.0011	0.3550	0.0008	466.4802	0.0000
b2	-0.2407	0.0011	-0.0192	0.0001	-212.6448	0.0000
b23	-0.0319	0.0011	-31.9348	1.1338	-28.1666	0.0000
a3	0.2179	0.0011	0.0007	0.0000	192.4627	0.0000
s	-0.3451	0.0011	-34.1780	0.1122	-304.6964	0.0000
k1	-0.2386	0.0011	-4.8238	0.0229	-210.7183	0.0000
k2	0.4054	0.0011	407.5504	1.1382	358.0760	0.0000

Table.5.4 Linear regression analysis: the logarithm of the osteocytes' population density as a function of the rate constants. The range of the constants as in Fig.5.9. R^2=0.99.

ln(BM)	BETA	St.Err. of BETA	B	St.Err. of B	t(9988)	p-level
Intercept			0.123	0.014	9.011	0.000
Oct	0.003	0.001	0.000	0.000	2.374	0.018
a1	0.276	0.001	0.000	0.000	234.248	0.000
b12	-0.001	0.001	-1.353	1.089	-1.243	0.214
b01	-0.478	0.001	-0.463	0.001	-405.716	0.000
a01	0.575	0.001	0.355	0.001	488.228	0.000
b2	-0.262	0.001	-0.019	0.000	-222.187	0.000
b23	-0.035	0.001	-31.912	1.083	-29.457	0.000
k1	-0.259	0.001	-4.818	0.022	-220.247	0.000
k2	0.442	0.001	407.6	1.088	374.871	0.000

Table.5.5 Linear regression analysis: the logarithm of the total bone mass (BM) as a function of the rate constants. The range of the constants as in Fig.5.9. R^2=0.99.

Re1	BETA	St.Err. of BETA	B	St.Err. of B	t(9988)	p-level
Intercept			-0.1442	0.1017	-1.4173	0.1564
KOct	0.0001	0.0024	0.0000	0.0000	0.0314	0.9749
a1	-0.4235	0.0024	-0.0014	0.0000	-175.84	0.0000
b12	-0.0030	0.0024	-10.267	8.1215	-1.2642	0.2062
b01	0.7558	0.0024	2.6695	0.0085	313.95	0.0000
a01	-0.2675	0.0024	-0.6024	0.0054	-111.06	0.0000
b2	0.1442	0.0024	0.0386	0.0006	59.886	0.0000
b23	-0.2834	0.0024	-951.09	8.0799	-117.78	0.0000
k1	0.1182	0.0024	8.0057	0.1631	49.073	0.0000

Table.5.6 Linear regression analysis: the real part of the first eigenvalues as a function of the rate constants. The range of the constants as in Fig.5.9. R^2=0.95.

Re3	BETA	St.Err. of BETA	B	St.Err. of B	t(9988)	p-level
Intercept			-0.1806	0.0686	-2.6343	0.0084
KOct	0.0084	0.0024	0.0000	0.0000	3.4512	0.0006
a1	-0.0016	0.0024	0.0000	0.0000	-0.6622	0.5079
b12	-0.0012	0.0024	-2.5942	5.4740	-0.4739	0.6356
b01	-0.0020	0.0024	-0.0047	0.0057	-0.8270	0.4082
a01	0.8011	0.0024	1.2058	0.0037	329.8478	0.0000
b2	-0.4244	0.0024	-0.0759	0.0004	-174.8040	0.0000
b23	0.0017	0.0024	3.7660	5.4460	0.6915	0.4893
k1	-0.3584	0.0024	-16.2324	0.1100	-147.6230	0.0000

Table 5.7 Linear regression analysis: the real part of the third eigenvalues as a function of the rate constants. The range of the rate constants as in Fig.5.9. R^2=0.95.

ln(Re4)	BETA	St.Err. of BETA	B	St.Err. of B	t(9988)	p-level
Intercept			-4.5545	0.0039	-1178.1	0.0000
KOct	0.0001	0.0009	0.0000	0.0000	0.0754	0.9399
a1	-0.0004	0.0009	0.0000	0.0000	-0.4943	0.6211
b12	0.0006	0.0009	0.2044	0.3086	0.6623	0.5078
b01	0.0002	0.0009	0.0001	0.0003	0.2556	0.7982
a01	-0.0004	0.0009	-0.0001	0.0002	-0.4446	0.6566
b2	0.0013	0.0009	0.0000	0.0000	1.5102	0.1310
b23	0.0003	0.0009	0.1174	0.3071	0.3822	0.7023
a3	-0.0001	0.0009	0.0000	0.0000	-0.0799	0.9363
s	0.9961	0.0009	34.1427	0.0304	1123.8	0.0000
k1	0.0010	0.0009	0.0068	0.0062	1.0953	0.2734
k2	-0.0002	0.0009	-0.0730	0.3083	-0.2369	0.8128

Table 5.8 Linear regression analysis: the real part of the logarithm of fourth eigenvalue as the function of the rate constants. The range of the constants as in Fig.5.9. R^2=0.99.

Im1	BETA	St.Err. of BETA	B	St.Err. of B	t(9988)	p-level
Intercept			0.8543	5.8152	0.1469	0.8832
KOct	-0.0003	0.0018	0.0000	0.0000	-0.1655	0.8686
a1	0.5467	0.0018	0.1394	0.0005	300.3238	0.0000
b12	-0.0010	0.0018	-265.6	464.3005	-0.5721	0.5673
b01	-0.4864	0.0018	-129.9	0.4861	-267.3223	0.0000
a01	0.4737	0.0018	80.67	0.3101	260.1905	0.0000
b2	-0.0010	0.0018	-0.0198	0.0368	-0.5375	0.5909
b23	0.0018	0.0018	452.2	461.9222	0.9791	0.3275
a3	0.0023	0.0018	0.0019	0.0015	1.2573	0.2087
s	0.0017	0.0018	41.48	45.7003	0.9078	0.3640
k1	-0.2174	0.0018	-1113.89	9.3266	-119.4317	0.0000
k2	0.3684	0.0018	93865.	463.7086	202.4233	0.0000

Table 5.9 Linear regression analysis: the imaginary part of the first eigenvalues as a function of the rate constants. The range of the constants as in Fig.5.9. R^2=0.99.

	Mean	Minimum	Maximum	Range	Std.Dev.	St.Error
OCL	23.2	6.78	68.1	61.32	8.98	0.090
OBL	1904.	958	3820	2862	578.0	5.781
OCT	25791	7860	311000	303140	39611	396.1
BM	1.15	0.184	5.77	5.586	0.728	0.007

Table 5.10 The average population concentrations, maximum and minimum values and statistical deviations for the osteocells for the model (5.3) and the total bone mass, BM.

	Mean	Minimum	Maximum	Range	Variance	Std.Dev.	Std.Error	R.Time
RE1	-3.7	-11.8	1.45	13.25	3.77	1.94	0.019	0.27
RE2	-3.7	-11.8	1.45	13.25	3.772	1.94	0.019	0.27
RE3	-4.0	-9.6	-1.70	7.90	1.685	1.298	0.013	0.25
RE4	-0.03	-0.04	-0.02	0.020	0.00003	0.00585	0.00006	33.3

Table 5.11. Resulting statistics of the real parts of the eigenvalues for the short range of rate parameters from Fig.5.9.

	ln(Ocl)	**ln(Obl)**	**ln(Oct)**	ln(BM)	Re1	Re3	ln(Re4)	Im1
R-square	0.99	0.99	0.99	0.99	0.95	0.95	0.99	0.99
KOct	-0.0007	-0.0012	0.0024	0.003	0.0001	0.0084	0.0001	0.001
a1	0.3881	0.4955	0.2536	0.276	-0.4235	-0.0016	-0.0004	0.555
b12					-0.0030	-0.0012	0.0006	-0.001
b01	-0.6740	-0.8614	-0.4388	-0.478	0.7558	-0.0020	0.0002	-0.483
a01			0.5283	0.575	-0.2675	0.8011	-0.0004	0.486
b2			-0.2407	-0.262	0.1442	-0.4244	0.0013	0.000
b23			-0.0319	-0.035	-0.2834	0.0017	0.0003	0.001
a3			0.2179			-0.0008	-0.0001	0.001
s			-0.3451			0.0004	0.9961	0.000
k1	-0.3045	0.0018	-0.2386	-0.259	0.1182	-0.3584	0.0010	-0.219
k2	0.5221		0.4054	0.442		0.0003	-0.0002	0.374

Table 5.12 Summary results of linear regression for the set of rate parameters from Fig.5.9.

Tables 5.2-5.11 indicate a significant improvement in the R-square of the linear regression. The final table shows that only Re1 and Re3 have the R-square values less than 0.99.

The results of numerical calculations for different feedback, shown above, indicate that the stable focus prevails irrespective of the Michaelis-Menten feedback function, Figure 5.11.

Thus the *s*-shaped Michaelis-Menten function, well-known in many regulatory networks, for example, in neural networks as the neuro-somatic threshold function (Demongeot et al., 2000) can be interesting for a cellular cooperative formation such as the BMU. Moreover, the employment of this nonlinear function in the BMU model can lead to stabilisation of equilibrium states which could explain some periodic relaxative modes. In comparison to fractal spaces, allosteric models have additional degree of freedom and very clear, interpretable values from the point of view of molecular control.

5.6 Discussion

In the introduction it was stressed that recently developed mathematical models of bone turnover (Komarova et al., 2003; Lemaire et al., 2004; Moroz et al., 2006) predict various modes of dynamic behaviour of the BMU. In this section the allosteric-like feedback control function has been investigated with respect to an extended dynamic system from Komarova et al, 2003, where 1) the osteocyte regulation at the cellular level is formally involved and 2) autocrine and paracrine regulations are chosen in an allosteric-like form. In fact, as mentioned, regarding the first development, osteocytes play a vital role in signalling mechanical damage (Compston, 2002; Skerry et al., 1989; Lanyon, 1996; Tomkinson et al., 1997; Noble et al., 1997; Burger and Klein-Nulend, 1999). Introduction this cellular regulation loop to the model has increased the dimension of the dynamic system. However, the designed system is still controlled with a small collection of cellular regulation loops. Such a form of model is also potentially

applicable to other types of allosteric regulation controls, for example to the Hill-like feedback function.

One of the major developments of this section is that the formulation and interpretation of paracrine and autocrine control is attempted in terms of allosteric regulation rather than a fractal form, when it is formulated as a regulator of the degree parameters. Concerning the Oct regulation loop, one can see from Eq. (5.2) and Figure 5.2 that it could be suggested that the feedback function which regulates Ocl response to OCt apoptosis is S-shaped (akin to many control feedback functions) and could have the Michelis-Menten or generally the Hill form. Such formulated models have an additional advantage - allosteric control degrees of freedom, clearly interpretable from the point of view of molecular control. In such a case the system could be described in terms of losses (metabolic losses), like in the problem of optimal control, when the bone remodelling is at the demand of minimising the substrate-energy losses for bone remodelling by balancing the metabolic cost of regulation against shortening the response time to mechanical/aging damage and physiological function of the skeleton. From the results of the numerical calculations (Section 5.3-5.5) it is possible to see the survival of a stable focus type of equilibrium (Fig. 5.4, 5.7, 5.11.) in the four dimensional phase space over different ranges of constants.

Obviously, within the framework of this quite phenomenological model, the role of the diverse molecular factors in bone regulation, such as receptors and mediators, the state of the membrane, and hormonal or genetic system, are difficult to include and discuss. The roles of these or any other molecular messenger or substrate remain the subject of broad discussion in biochemical literature (Section 1, literature review), even for a generalised animal model, and so the development of a mathematical model, based on the molecular level of regulation in the bone, awaits more precise biochemical and biophysical data.

The models above are just one subset of BMU models, within one combination of parameters, that could have other types of equilibrium (for example, the attracting limit cycle) in the range of parameters with biological meaning. Within the employed combination of

parameters, which result in a local minimum for the system, a stable focus steady state was found. This set is relevant to the combination for the pure cellular model, Section 2. This set/combination model has one decaying cyclic mode with large differences in frequencies.

The next stage of the development of this model is the derivation of an equation for scaffold material, which employs specific constants for sorption and resorption. It could be possible to model the integration of resorbable implant into the bone in such a way. The an equation could include the material parameters, scaffold design (porosity) parameters via fractality of the bone scaffold, surface modification parameters and cell enhancement parameters. Based on the above, one can suggest that in the framework of the generalised model (Eq.5.1) it is possible to find other steady states with a sound biological/biochemical interpretation. Moreover, the transformation bifurcation between these states could model the major mechanisms of the control of BMU and bone remodelling. The existence of such decaying periodical oscillations could be linked to a Paget's-disease-like physiological situation, when the overfeeding of the remodelling cycle occurs.

5.7 On the validation of the model

Validation of the bone remodelling models is a critical issue. The most important factor, preventing practical verification/validation of any model of bone tissue remodelling is that bone is a hard tissue and thus very difficult to experiment upon. The measurement of molecular parameters (concentrations, activities, binding constants etc.) is a timely process, so measured values can be significantly distorted from the in vivo values.

The models considered in this study account for the number of tiny regulatory processes, mentioned in the literature review section and are therefore predictably complicated. However, from the kinetic measurement perspective, the kinetic parameters usually measured are rather first-order kinetic constants while many constants in the model are second-order constants.

The models described in the Section 4 and 5.1-5.6, are the relaxation types of models, so they can be preferable from the validational perspective. These models have been studied numerically within the range of the rate constants having the same order as the Komarova et al. (2003) model. The mean relaxational time has the order of month.

Validation of allosteric constants incorporated into the model is even more difficult than in the case of the rate constants of the cellular model. The models considered (cellular, Section 4, and combined molecular-and-cellular models, Section 5) are very simplified, rather phenomenological models. In these circumstances the verification can be considered to be related to the main conclusions of the modes, like for example the character of behavioural modes. Considering the spectrum of behavioural modes some indications in recent literature can be found.

Some statistical studies, which have been performed on pre- and postmenopausal women, show the cyclic (periodical) behaviour of bone remodelling, Mazuoli et al., 2002; 2006. Authors even titled their paper from 2002 as "Cyclical behaviour of bone remodeling and bone loss in healthy women after menopause: results of a prospective study" which stressed that there is a periodical effect as it is possible to see from Fig.5.12-5.12. In this prospective study, the annual changes in lumbar bone mineral density (LBMD) and bone remodeling markers were measured in 238 healthy pre- and postmenopausal women, aged 45–74 years. The results obtained indicate that bone loss is not a constant process over time but rather exhibits cyclical damping oscillations. The harmonic regression model indicates the presence of a cyclical component of 7 years.

In their second work, Mazzuoli and coauthors (2006) studied a sample of 200 healthy women, aged 45–74 years, recruited by written invitation from a community-based listing of all residents, living locally, which made the trial quite homogeneous, 136 were enrolled in the follow-up study and 120 completed a year of the study. The experimental work was based on measurement of biochemical parameters and annual anterior vertebral body heights changes (AVHs). They were also have found to have periodical changes, Fig.5.14.

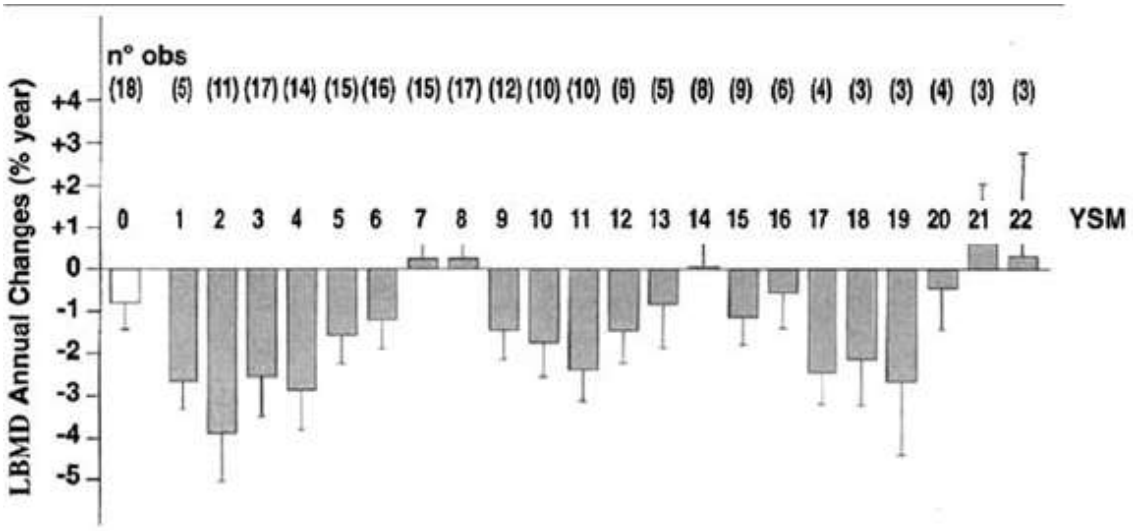

Fig.5.12 Mean annual percent changes in LBMD. YSM, years since menopause; YSM 0, premenopausal group. Number of observations given in parentheses. Adopted from Mazzuoli et al., 2002.

In the study of Tayyar and coauthors (Tayyar et al., 1999), a 3D simulation was employed for the modelling of trabecular bone remodelling. The modelling bone volume was about 50 mm^3 containing about 200 basic multicellular units. The authors proposed the periodical modes in basic multicellular units activation responses, see Fig.5.15.

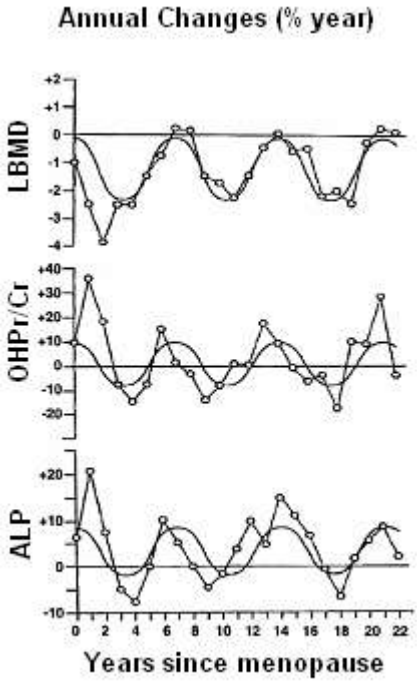

Fig.5.13 Mean annual percent changes in LBMD, in OHPr/Cr and ALP observed (dashed line/open circles) and predicted (solid lines). YSM, years since menopause; YSM 0, premenopausal group. Adopted from Mazzuoli et al., 2002.

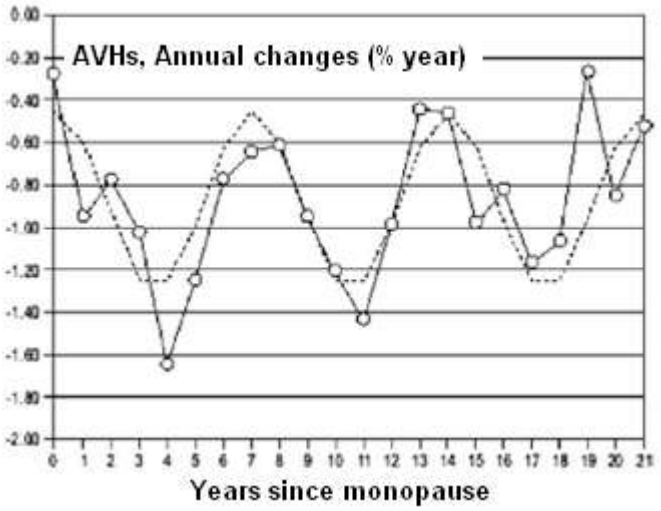

Fig.5.14 Mean annual percent changes in AVHs. Observed values (solid line/open circles) and predicted values (solid line). YSM, years since menopause; YSM 0, pre-menopausal group. Adopted from Mazzuoli et al., 2006.

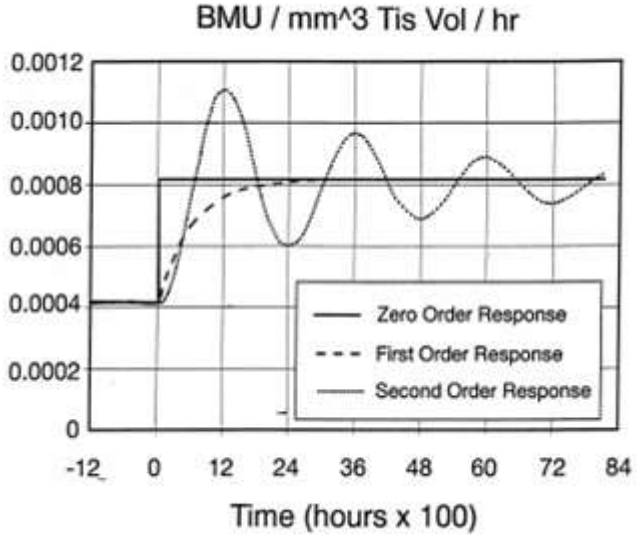

Fig. 5.15 The three BMU activation responses to the abrupt step change in estrogen at menopause. Adopted from Tayyar et al., 1999.

One of the mechanisms which can be employed to explain of periodic type modes was proposed by Martin, 2007, suggests the spatial character of microdamage removal /remodelling. This mechanism to some extent indirectly supports the results observed in this project, that BMU arranged for the repairing of one area of microdamage can be employed/used to remove nearby microdamaged area.

The results in the work of Martin 2007 considers the possibility that microdamage is not only able to activate new BMUs, but may also attract or "steer" existing BMUs as they continue to tunnel through the bone matrix, Fig.5.16. This suggestion is in line with the results of Vatsa et al, 2007. In their it study has been demonstrated that a single osteocyte can transfer information of a local mechanical signal to its surrounding cells at a distance ranging from 33 to 175 μm. This in fact supports the consideration of a cyclic mode in bone remodelling presented in this project.

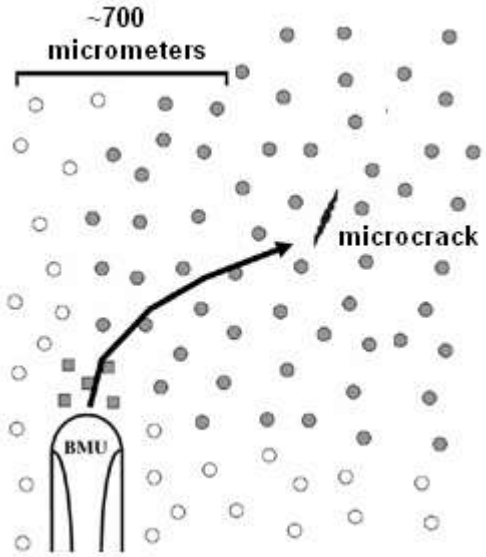

Fig.5.16 Schematic diagram of BMU being diverted to a microcrack (μck) surrounded by apoptotic osteocytes (filled circles). Filled squares are apoptotic osteocytes in the low stress area in front of BMU, and empty circles are healthy, intact osteocytes. Adopted from Martin, 2007.

In summary, verification of models is quite limited (perharps the most limited of the tissue types). The applicability of periodical modes of behaviour to the real situation *in vivo* in living hard tissue or to engineered prototypes is linked to the verification and is also limited. The relaxational mode could be applicable when taking into account the hierarchy of relaxation modes through the evaluation of the resorptional biological rates of hard tissue, implant resorption and natural bone tissue reformation/development. However, even the models having the problems with validation, they are important stage in developing an approach to understanding and controlling the remodelling process in tissue engineering.

6 On Optimal Control applications to BMU models

The models in the Sections 6.1-6.3 are to demonstrate the introduction of the optimal control via some parameters manipulation. In these sections (6.1-6.3) the optimal control problems are formulated following Moroz, 2011.One of the most known kinetic process is the binding a low molecular ligand to a macromolecule, generally having several binding sites.

6.1 Optimal control model of binding cooperativity

6.1.1 Importance of low molecular binding and its cooperativity

Cooperativity phenomenon (in its wide sense, auto-modulation) has been documented and studied for more than a century (Verhulst, 1838; Bohr et al., 1904; Hill, 1910; Pearl & Reed, 1920). It is believed to be one of the most intriguing properties of biological regulation, particularly in molecular binding.

Molecular binding is the simplest sort of chemical reactions/kinetics that demonstrate cooperativity, however it is very important in the overall regulation of cellular, tissue and body functioning. Cooperativity in the binding of low molecular weight ligands to a macromolecule (e.g. a transport molecule, like albumin, haemoglobin; numbers of receptors) is still of growing interest because of the non-linear cooperative molecular effects. It is very important for molecular gain and can trigger many effects at the level of cell and the body response. Different allosteric mechanisms (Perutz, 1990; Klotz 1997) are also involved in molecular binding and signal generations. Allosteric effects in binding, which can be defined as a coupling, synergism of conformational changes between spatially separated binding sites of a macromolecule.

The most advanced models of binding are developed for oxygen binding to heamoglobin (Hb), so we will concentrate on oxygen binding to this macromolecule. A classical example of cooperativity in binding, is in the binding of a low molecular weight ligand to a macromolecule, for example, O_2 binding to Hb, when cooperativity can be defined as a maximum slope, $n=2.8$. However, Hb has 4 subunits and therefore 4 binding sites. The binding

curve characterises as a “sigmoid” or “S”-shaped. Physiologically cooperativity allows control over the concentrations of a ligand, in this case oxygen in tissues.

There are three well-known models of cooperativity in binding oxygen to Hb. They are the Adair model (Adair, 1925), the Monod-Wyman-Changeux (MWC) model (Monod, Wyman & Changeux, 1965), sometimes referred as concerted model, and Koshland-Nemethy-Filmer (KNF) model (Koshland, Nemethy & Filmer, 1966), referred also as “induced-fit model. The MWC model is based on assumption that a binding macromolecul can be in two states: a low-affinity state T and a high-affinity state R. The KNF model assumes that ligand binding leads to the conformational change, which consequently changes the affinity to the next binding site. A lot experimental data through number of decades (e.g. extracellular Hb has coperativity n~6 and higher, Fushitani et al., 1986; 1992; Marques & Meirelles (Erythrocruorin), 1995; Mozarelli et al., 1996; Weber et al., 2003; Hellmann et al., 2003) and number of theotetical efforts (Acerenza and Mizraji, 1997; Eaton et al., 1999; Tsuneshige et al., 2002; Qian, 2003, 2008; Onufriev and Ullmann, 2004; Agnati et al., 2005; Olivier et al., 2006) indicate inexhaustible interest to the cooperativity and O2 binding as a good model to study cooperativity.

In summary, the cooperativity phenomena are represented at all levels of biologival regulation, molecular, cellular, tissue and body. It is no surprise that, if the transitional processes of species replacement, change in a trophic niche also have the cooperative character. Therefore, it is very inportant to understand the cooperativity, and cooperativity of molecular binding, in particular from the optimal control perspective. In this section, we illustrate the nonlinearity effects when macromolecular ligands bind to a large macromolecule in terms of optimal control.

6.1.2 Binding kinetics, cooperativity and its representation

The standard representation of binding of any low-molecular-weight ligands, molecular factors mentioned above, is widely interpreted in terms so-called Hill’s model (Hill, 1910; Weiss, 1997; Hofmeyr & Cornish-Bowden, 1997). This model is based on applying so-called

logit transformation to the experimental saturation data in order to linearise and produce a graphical representation (Hill plot), Fig.6.1.1. The coefficient of slope in the Hill plot establishes the so-called cooperativity. In a certain sense cooperativity characterizes the degree of rigidity of regulation for the local maintenance of concentration at some optimum in the case of binding. Let us therefore proceed to relate this parameter to a control parameter in the molecular concentration regulation. That means that one needs to investigate whether the problem of optimal control can be formulated for the molecular binding, where the Hill coefficient would play the role of a control parameter.

As was mentioned above, the allosteric model for the oxygen binding to haemoglobin is the most successfully studied from many perspectives. An obvious explanation for this comes from the exclusive role of oxygen in any biological process. As we mentioned, there is a various number of formal models for oxygen binding: Hill, 1962; Adair (Adair, 1925); Monod-Wyman-Changeux (Monod et al., 1965) and Koshland -Nemethy-Filmer (Koshland et al.,1966) and even recently global allostery of Hb has been reviewed (Yonetani at al, 2002; 2003).

If one considers a generalized scheme of the low molecular weight ligand L (NO, Oxygen, etc.) binding at N centers of macromolecule A (receptor, transport protein, enzyme, etc.),

$$A + L \overset{K_1}{\rightleftharpoons} AL$$
$$\cdots\cdots\cdots\cdots$$
$$AL_{i-1} + L \overset{K_i}{\rightleftharpoons} AL^i$$
$$\cdots\cdots\cdots\cdots$$
$$AL_{n-1} + L \overset{K_n}{\rightleftharpoons} AL^n$$

so, according, for example, to (Voet and Voet, 1995)

$$K_i = \frac{[AL^j]}{[AL^{j-1}][L]} \qquad (6.1.1)$$

is the value, referred to as the equilibrium constant of binding at the j-s stage, which for simplicity we can consider as equal for all binding centers, so K_j=K.

Then the relative binding (saturation) is described by the expression

$$\nu = \frac{K^n[L]^n}{1+K^n[L]^n}\ , \qquad (6.1.2)$$

where $\nu = \frac{\bar{A}_{bind}}{\bar{A}_{total}}$ is the relative binding, $[A]_{bind}$, $[A]_{total}$ are the bounded and total concentrations of a macromolecule, [L] - the ligand concentration, n is the number of binding centers, $K_j = K$ is the constant of binding to the j-s center. Fig.6.1.1 illustrates the dependences of relative binding on the concentration for some theoretical scheme expressed in (6.1.2) at *n =0.5, 1.0, 2.0, 4.0, 8.0*.

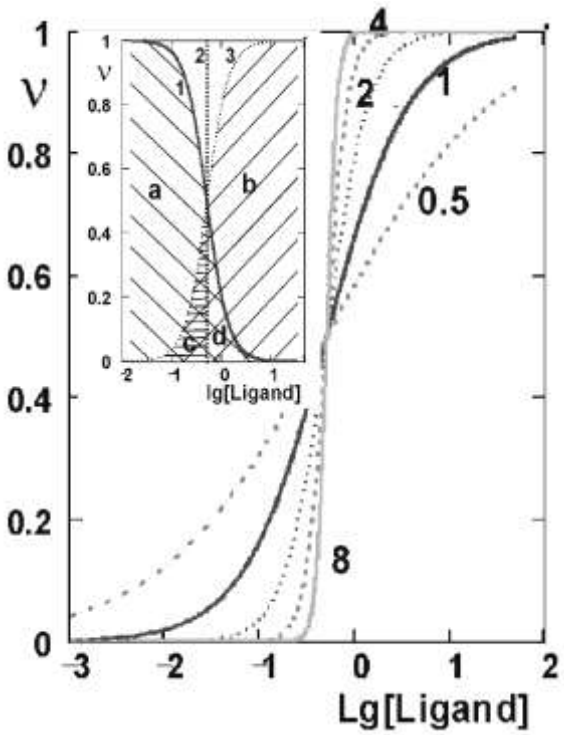

Fig.6.1.1 Graphical illustration of the relative binding; n=2.0-8.0 – positive cooperativity, n=1.0 – no cooperativity, and n=0.5 – negative cooperativity. ν - fraction of maximum value (saturation). Insert - the scheme of the optimal regulation at a ligand concentration shown by vertical line "2". Curve 3 – the saturation curve ν from figure A for n=2, curve "1" is 1-ν. Designations: "a" (under the curve "1")- the area of relative free ligand; "b" – area under the curve "2" relative binding of the ligand ν; "c" – the area indicating the relative binding of the ligand, when the ligand is bonded, however, does not needed relatively to ideal binding indicated by line "2". "d" the area where the ligand is still free, comparably to ideal binding indicated by line "2". Figure adopted from Moroz, 2011.

One can show that the expression for relative binding is related to the logistic curve, where the logarithm of ligand concentration is used as an independent coordinate. For

simplicity, let us apply the natural logarithm. By substitution of $[L]^n = e^{n\ln[X]}$ into (6.1.2) one can get

$$\nu = \frac{e^{n\ln[L]}}{k^{-n} + e^{n\ln[L]}}, \tag{6.1.3}$$

and, accordingly, this expression is the partial solution of the following differential equation

$$\frac{d\nu}{d\ln[L]} = n\nu - n\nu^2 \quad . \tag{6.1.4}$$

This can be easily checked up as follows. Assuming for simplification $z = \ln[\mathrm{L}]$, then

$$\nu = \frac{e^{nz}}{k^{-n} + e^{nz}} \tag{6.1.5}$$

and

$$\frac{d\nu}{dz} = \frac{ne^{nz}(e^{nz} + k^{-n}) - ne^{nz}e^{nz}}{(e^{nz} + k^{-n})^2} = \frac{ne^{nz}}{(e^{nz} + k^{-n})} - \frac{ne^{nz}e^{nz}}{(e^{nz} + k^{-n})^2},$$

and since (6.1.5), finally

$$\frac{d\nu}{dz} = n\nu - n\nu^2, \tag{6.1.6}$$

that, in fact, should be shown. Thus, from the formal structure of the last equation the *n* may be treated as an "autocatalytical" coefficient in the well-known differential equation of Verhulst-Pearl. The result acquired can be interpreted in the following way: in the presence of *n* binding sites, the increase in relative binding $d\nu/dz$ is proportional to the relative binding ν. This means that the process of binding complex formation is autocatalytical-like, one which is very important in binding regulation of low ligand concentrations. Thus, the Hill constant *n* can be interpreted as an autocatalytic parameter of the ligand binding to a macromolecule control, in respect to the relative binding ν.

6.1.3 Dynamical optimal control outline

As was discussed in (Moroz, 2009), similar equation as (6.1.6) can be obtained as a result of the following OC problem:

$$J = \int_0^z \left(G(\nu) + \frac{u^2}{2} \right) dz \to \min \tag{6.1.7}$$

subject to

$$\frac{d\nu}{dz} = u(1-\nu) \tag{6.1.8}$$

Applying the Pontryagin maximum principle [69,70], one can write the Hamiltonian:

$$H = -G(\nu) - \frac{u^2}{2} + pu(1-\nu) \tag{6.1.9}$$

Then the system will be

$$\begin{aligned} \frac{d\nu}{dz} &= u(1-\nu) \\ \frac{dp}{dz} &= G_\nu^{/} + pu \\ u &= p(1-\nu) \end{aligned} \tag{6.1.10}$$

together with the additional Pontryagin maximum principle demand $H(\nu^*,p^*,u^*)=0$ for the extreme trajectory (*). Substituting u from the last equation, we can get the system

$$\begin{aligned} \frac{d\nu}{dz} &= p(1-\nu)^2 \\ \frac{dp}{dz} &= G_\nu^{/} + p^2(1-\nu) \end{aligned} \tag{6.1.11}$$

and $H(\nu^*,p^*,u^*)=0$. Using the last equation from (6.1.10), the Hamiltonian can be written as

$$H(\nu, p) = -G(\nu) + \frac{p^2(1-\nu)^2}{2} \tag{6.1.12}$$

The surface plot and contour plot of the Lagrangian (6.1.7) and Hamiltonian (6.1.12) for quadratic approximation of the potential $G(\nu)$

$$G(\nu) = \frac{n^2\nu^2}{2} \tag{6.1.13}$$

is shown in Fig.6.1.2 for $n=2.0$. The Hamiltonian (6.1.12) can also be written as a dependent on $\nu, d\nu/dz$, which for optimal trajectory (*) is equal to zero, when the final state is not specified. In case of relaxational kinetics, the final state ($\nu=0$). However, in our model of binding we

haven't a time variable, instead we have the logarithm of ligand concentration, $z=ln[X]$. The open-end problem in this model is when the concentration reaches infinity, which has no real meaning. This consequently means that we need a different optimal control problem, rather than the open-end problem. However, assuming that the concentration is, in an ideal case, very high, we can follow our method to formulate the optimal control problem. This means that we can accept all states, not just the optimal and we can therefore choose from these states the real, optimal state, when $H^*=0$. Following this approach let us write the Hamiltonian which is dependent on relative binding ν, and its derivative $d\nu/dz$, then

$$H(\nu,\frac{d\nu}{dz}) = -G(\nu) + \frac{\left(\frac{d\nu}{dz}\right)^2}{2(1-\nu)^2} = Const = 0 \qquad (6.1.14)$$

which at the quadratic potential (6.1.13) for the optimal trajectory (*) this equation gives

$$\left(\frac{d\nu}{dz}\right)^2 = n^2\nu^2(1-\nu)^2 \qquad (6.1.15)$$

or

$$\frac{d\nu^*}{dz} = \pm n\nu^*(1-\nu^*) \ . \qquad (6.1.16)$$

This equation at certain values of constants coincides with the form given by (6.1.6). The analytical solution of this equation is

$$\pm nz + C = \ln\frac{\nu^*}{1-\nu^*} \qquad (6.1.17)$$

which is known as the Hill equation which is widely used for calculation the cooperativity n. It indicates a straightforward linear relation between variable z and the so-called logit:

$$\log it(\nu) = \ln\frac{\nu}{1-\nu} \ .$$

The numerical solutions of the system of equations (6.1.11) at quadratic potential are shown in Fig.6.1.3. Fig.6.1.3A shows the relative binding for different values of n. Fig.6.1.3B illustrates the trajectories of the control variable. Let us note that Fig.6.1.3C shows the positive

values of costate variable *p*, interpreted as the thermodynamic (kinetic) momentum of the binding process. This indicates that the solution (6.1.16) provides the maximum of the functional from the equation (6.1.7). The relative binding effectively strives to unity with the unlimited increase of the ligand concentration. However, one can take into account that the search for the maximum of a functional is equivalent to the search of its minimum with the negative sign. Additionally, the problem is symmetrical, which can be easily seen from Fig.6.1.2. It can also be illustrated by Fig.6.1.1 that the maximization of area "a" is the minimization of area "b". Minimization of area "c" is, in fact, the tightening the regulation around the regulatory point (vertical line "2", the concentration of the ligand at $v=0.5$), which leads to increase of cooperativity and consequently can be considered as the rigidity of regulation of the concentration of the ligand in the surrounding medium. Thus, the maximization the area under curve "3", Fig.6.1.1, is equivalent to the minimization of area "c". This can be interpreted from the optimal control perspective as characterizing the regulatory losses between logistic curve "3" and the vertical line of desired concentration, z_0, that should be minimized.

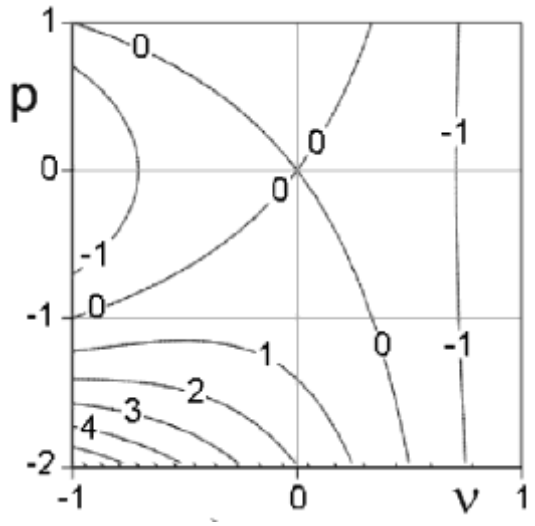

Fig.6.1.2 The contour plot of the Hamiltonian (6.1.12) for quadratic approximation of the potential G, (6.1.13). $\nu_0=1.0$, $n=2$. Figure adopted from Moroz, 2011.

One can see from Fig.6.1.2, that the Hamiltonian of the problem (6.1.12) is symmetrical relative to $p=0$. In our case, the physical sense has just area $0<\nu<1$. In this case

the kinetic (thermodynamic) momentum becomes infinite, approaching *v=1*. Then the optimal control problem looks rather incorrect as a problem of minimization, however, as one can see from Fig.6.1.2, the minimization and maximization problems are symmetrical.

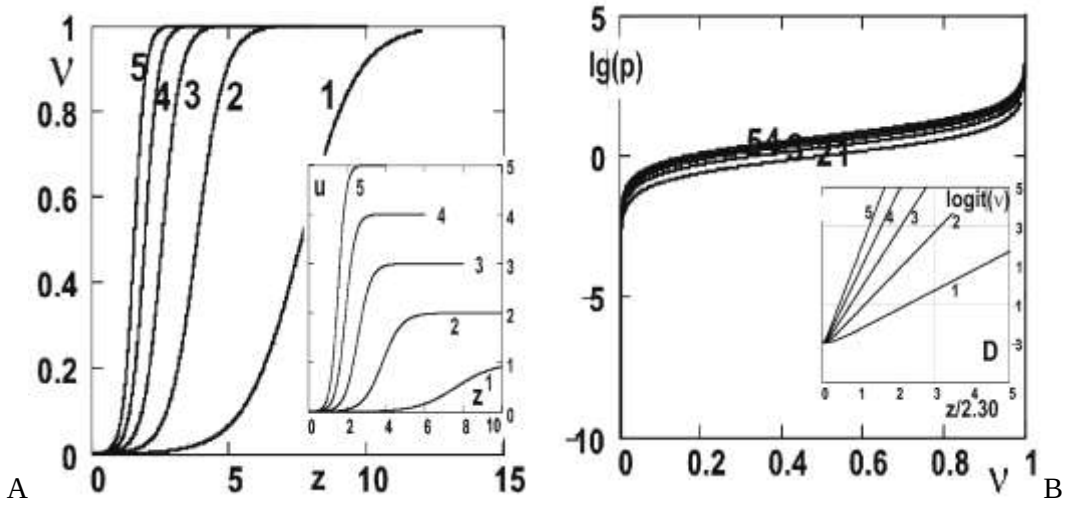

Fig. 6.1.3 Kinetics by solving system (6.1.11). A, plots of ν against z; insert - phase plane of costate variable p versus ν. B, phase plot of decimal logarithm of –p versus state variable ν; insert - plot of logit(ν) versus z/2.30, which, in fact, is transformed to a decimal logarithm in this way. Figure adopted from Moroz, 2011.

One can compare Fig.6.1.3A to Fig.6.1.1A and Fig.6.1.3D to Fig.6.1.1C. The form of the curves for n=1,2,4 from Fig.6.1.3d is identical to curves 1,2,4 in Fig.6.1.1C. In fact, this result validates the approach based on the optimal control methodology.

6.1.4 Optimal control Lagrange method

It is obvious that the same equations can be obtained by using the optimal control Lagrange method:

$$L_{OC} = G(\nu) + \frac{u^2}{2} + p\left(\frac{d\nu}{dz} - u(1-\nu)\right). \qquad (6.1.18)$$

then

$$\begin{aligned} \frac{dp}{dz} &= G_{\nu}^{/} + pu \\ \frac{d\nu}{dz} &= u(1-\nu) \\ u &= p(1-\nu) \end{aligned} \tag{6.1.19}$$

which is, in fact, the system (6.1.10) that gives (6.1.11). Since this is an open-end problem, the transversality condition is applied.

6.1.5 Conclusions

It has been illustrated above, how the equation (6.1.16) can be obtained by employing the optimal control/variational technique. It is coinciding in a form with the logistical differential equation (6.1.6). Initially, the variable *u* was the proportionality coefficient in the control equation (6.1.8). Finally, in the transformed equation (6.1.16), the control *u* linearly depends on *v* and the coefficient *n*, which characterizes cooperativity. So, in this way, the artificially introduced control *u* in the kinetic equation (6.1.8) later "materialises" into a function of state variable (saturation) ν with a characteristic constant *n* that can be considered as cooperativity.

One shall note that with an increase of cooperativity *n*, the rigidity of the regulation also increases, which results in an increase in the slope coefficient in the equation (6.1.16). Fig.6.1.1B and Fig.6.1.3A illustrate this graphically. It indicates that the binding and the binding control, expressed as its cooperativity, can be considered in terms of optimal control in an un-contradictory manner. It also means that the binding description can be formulated as an optimal control problem and also a variational problem. This consequently suggests the methodology of the least action principle. The coefficient of inclination which describes cooperativity is related to the control amplitude - this also being the specific cost of control.

However, one can note that the consideration presented here was based on assumptions of an ideal cooperativity. A disadvantage with this consideration is the phenomenological appearance of the energetic cost/penalty function, which is dependent on the state variable –

saturation. For other well known cooperativity models, like Adair (Adair, 1925); Monod-Wyman-Changeux (Monod et al., 1965) and Koshland -Nemethy-Filmer (Koshland et al., 1966) the optimal control formulations certainly will be much more sophisticated.

The methodology shown above demonstrates that the cooperative macroscopic binding behaviour can be explained from the OC perspective by considering the elementary binding as an optimal energetical process. In some sense, it extends the understanding of the control process, its evolution in adaptive systems, particularly. In mechanics, as we have seen, the formal introduction of the control by the rate allowed the OC formulation (Moroz, 2009), when the control appears as a dummy-like variable. Here, in biological and biochemical kinetics, when considering the OC formulation of binding, the control variable u does not look like an absolute dummy, see Fig.6.1.3B. The optimal control is involved in an optimal control regulation loop, when the Hill cooperativity constant can be interpreted from the OC perspective, as the rigidity of control and kinetic momentum (costate variable). It is an energetical-like partial penalty/price/cost of deviation from the optimal state.

6.2 Michaelis-Menten kinetics and optimal control

In this section the optimal control problem for Michaelis-Menten-like kinetics is formulated following Moroz, 2011.

6.2.1 The Michaelis-Menten model

Enzyme kinetics is one of the lowest regulatory levels in the complex hierarchy of metabolic regulation. The fundamental kinetic model of the enzyme kinetics, the Michaelis-Menten model, is based on the assumption of the intermediate complex (Michaelis and Menten, 1913). It is the basic approximations for many complex models in different fields of biochemistry, microbiology and biotechnology, for example, in metabolic (Acerenza, 2000;

Heinrich et al., 1991; Giersch, 1998; Schuster and Heinrich, 1987, 1991) or pharmacological models (Kakuji and Akapi, 1994). A number of research publications discuss the Michaelis-Menten control approach applied to the enzyme network (Heinrich and Holzhutter, 1985; Hofmeyr et al., 1993; Fell and Thomas, 1995; Fell, 1997; Elsner and Giersch, 1998; Ortega and Agenda, 1998; Yildirim at al., 2003). Recently, Michaelis-Menten kinetics has been used to describe the changing rates of cellular activity during bone resorption, Martin and Buckland-Wright (2004).

At the same time, there is the number of the Michaelis-Menten based models on optimization that are discussed with respect to modelling the feedback control - chemostat models or batch-kinetics models (Lenas and Pavlou, 1995; Rahman and Palanski, 1996; Sengupta and Modak, 2001; Keesman and Stigter, 2002; Srinivasan et al., 2003; Smets et al., 2002), with the perspective of overall output control in the biotechnological production. However, even from this perspective, it is very essential to investigate the optimal aspects of the regulation within the metabolic networks as an optimal control problem. Later it could be extended as a metabolic engineering approach to the optimization of the metabolic regulation *in vivo* from point of view of minimization of metabolic expenses for regulation and energetic optimisation in sense of processing at the minimum of thermodynamic potentials. In this sense the Michaelis-Menten kinetics is one of the basic model and studies are needed to revise and extend the understanding in the sense of optimal control and compare the results within others regulation approaches.

It is well known that enzymes are those structures indeed that affect the rate of chemical reactions without any shifting of the thermodynamic equilibrium (see, for example, Cannon, 2002). Therefore, it is even more reasonable to consider the enzyme kinetics in terms of optimal control technique, by the rates of chemical transformations. One of the simplest cases is the optimal control introduction into enzyme kinetics within the elementary Michaelis-Menten pattern when the possible results could be easy to interpret and expand on the number of applied biochemical and biotechnological cases.

The Michaelis-Menten model also is the basic model in this section. The goal of the present investigation is to revise the spectrum of dynamical behaviour after the introduction of optimal control into classic enzyme kinetic based on this equation. The optimal control interpretation in terms of metabolic costs/losses is another spotlight of our consideration. In this section we review the Michaelis-Menten kinetics regarding to the introduction of the optimal control methods in the way appropriate to this class of biochemical systems.

Standard Michaelis-Menten formal scheme of the reaction where the substance S transforms to substance P, is based on suggestion of so-called intermediate complex ES (Michaelis and Menten, 1913; see also Cornish-Bowden, 1995). If suppose that the first stage of this reaction is reversible, and the second one irreversible, then one can write classical design (see, for example, Cornish-Bowden, 2004)

$$E + S \underset{k_{-1}}{\overset{k_1}{\rightleftharpoons}} ES \xrightarrow{k_2} E + P \quad .$$

In the case, when the stoichiometric factor of the substrate S transformation to the product P is equal to unity, the kinetics of substrate S transformation described by the well known Michaelis-Menten equation, (Yildirim et al, 2003) be transformed to:

$$-\frac{dP}{dt} = \frac{dS}{dt} = -\frac{V_{\max} S}{K_M + S}, \tag{6.2.1}$$

where S is the concentration of the substrate, P is the concentration of the product, $K_M = \frac{k_{-1} + k_2}{k_1}$ is the Michaelis constant, $V_{\max} = k_2 E_0$ is the maximal reaction velocity.

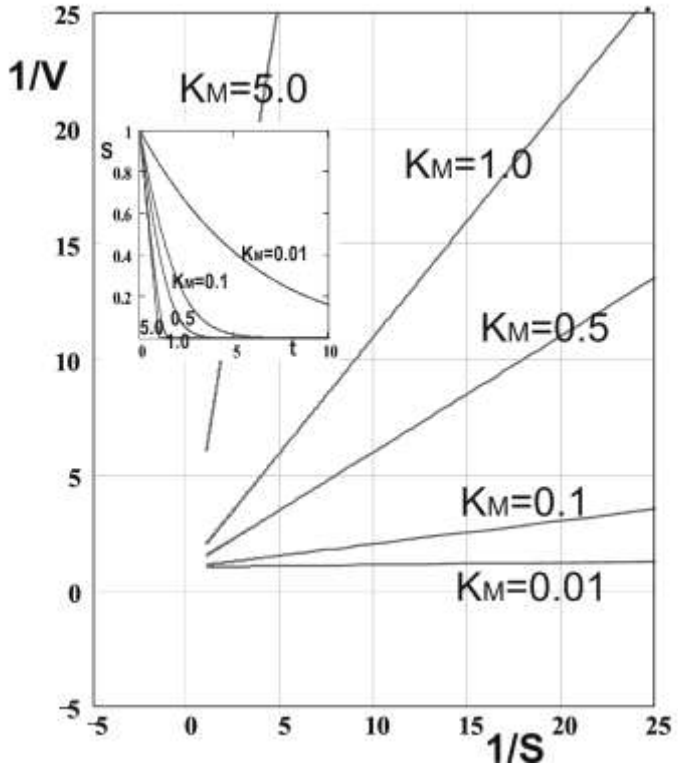

Fig.6.2.1 Double reciprocal plot of kinetics for Michaelis-Menten model (6.2.1), Lineweaver and Burk, 1934. $V = dS/dt$, s_0=*1.0*, V_{max}=1.0. Insert, the kinetic curves. Figure adopted from Moroz, 2011.

It can be seen from (6.2.1) that the velocity of enzymatic transformation can be formally controlled by means of the values for the K_M and V_{max} constants in the Michaelis-Menten equation (6.2.1). The kinetic properties of an enzyme reaction could be considered also in the so-called double reciprocal plot (Lineweaver and Burk, 1934). The latter representation has the convenience, which permits to determine directly the Michaelis constant K_M and the maximal reaction velocity V_{max} (Cornish-Bowden, 2004).

Let us formulate OC problem for enzyme kinetics represented by the above Michaelis-Menten equation. From the form of the kinetic equation (6.2.1) one can alter the Michaelis constant K_M or the maximal reaction velocity V_{max}. We are suggesting that such a control can take place *in vivo* in the cell, and that it is carried out in an optimal manner, and it follows, for example, Smets et al, 2004.

6.2.2 General optimal control approach to Michaelis-Menten kinetics

In a general one-dimensional case the optimal control problem accordingly to Pontryagin principle maximum principle, Pontryagin et al., 1962, can be written following (3.5-3.10) as

$$J = \int_{t_0}^{\tau} l(s,u)dt = \int_{t_0}^{\tau} G(s) + T(u)\,dt \to \min \tag{6.2.2a}$$

subject to dynamical constrains

$$\frac{ds}{dt} = f(s,u) \tag{6.2.2b}$$

and $s(t_0) = s_0$ and end-point condition $s(\tau)=s_{eq}$,

where s is state variable (substrate concentration), u is control variable (Michaelis constant K_M, maximal reaction velocity V_{max}), $f(s,u)$ is Michaelis-Menten function (as we mentioned, sometimes referred as Monod function) from equation (6.2.1), J is objective functional, $l(s,u)$ is the "running cost" of the optimal control that can have a metabolic sense and also sometimes is referred as instantaneous costs/losses for optimal control. Then accordingly to the Pontryagin maximum principle, the Hamiltonian function is

$$H = pf(s,u) - l(s,u) \tag{6.2.3}$$

and the canonical equations are

$$\frac{ds}{dt} = \frac{\partial H}{\partial p} = f(s,u) \quad \text{(state variable system)}$$

$$\frac{dp}{dt} = -\frac{\partial H}{\partial s} = -p\frac{\partial f}{\partial s} + \frac{\partial l}{\partial s} = -p\frac{\partial f}{\partial s} + \frac{\partial G}{\partial s} \quad \text{(adjoint/costate variable system)} \tag{6.2.4}$$

$$\frac{\partial H}{\partial u} = -\frac{\partial l}{\partial u} + p\frac{\partial f}{\partial u} = -\frac{\partial T}{\partial u} + p\frac{\partial f}{\partial u} = 0 \quad \text{(necessary conditions for optimality),}$$

and transversality condition: $H=0$ (since time τ is free, and terminal condition is specified $s(\tau)=s_{eq}$.

The alternative approach to this optimal control problem is directly based on variational calculus, see, for example, Gelfand and Fomin, 1963, because the control could be chosen as formally unlimited: the Michaelis constant K_M or the maximal reaction velocity V_{max} could formally vary from *0* to ∞. The objective functional could remain as (6.2.2a) subject to constrains (6.2.2b) and boundary conditions $s(\tau_0) = s_0$ and free end-point condition. Then the Lagrange method can be applied

$$L = l(s,u) + p\,\dot{s} - f(s,u) \tag{6.2.5}$$

and the Euler-Lagrange equations will be

$$\begin{aligned} &\frac{\partial L}{\partial s} = -p\frac{\partial f}{\partial s} + \frac{\partial l}{\partial s} = -p\frac{\partial f}{\partial s} + \frac{\partial G}{\partial s} = \frac{dp}{dt} \\ &\frac{\partial L}{\partial u} = \frac{\partial l}{\partial u} - p\frac{\partial f}{\partial u} = \frac{\partial T}{\partial u} - p\frac{\partial f}{\partial u} = 0 \\ &\frac{\partial L}{\partial p} = \dot{s} - f(s,u) = 0 \end{aligned} \quad . \tag{6.2.6}$$

The system (6.2.6) in fact coincides with (6.2.4). Once again one can note that the maximum principle is the non-classical method for solving the variational problem in the case of open-loop control. In the case the Lagrange function (6.2.5) is not explicitly depend on time so the first integral of the problem could be found in (Gelfand and Fomin, 1963]:

$$E(s, \frac{ds}{dt}) = \frac{\partial L}{\partial \frac{ds}{dt}} - L = Const \tag{6.2.7}$$

which could significantly simplify the process of finding analytical solution and play important role on the stage of interpretation. On the basis of this general approach two different enzyme control models were investigated.

In order to get some insight into the mechanisms driving the optimal control dynamics pattern of the Michaelis-Menten system, the effect of the optimal control introduction into Michaelis-Mention equation has been considered in this part, which is divided into the two contributions: control by Michaelis-Mention constant K_M and maximal reaction velocity constant V_{max}. Thus, the control sources have been split in two categories. On the one hand, the

terms denoted by K_M in system (6.2.1), which constitute the binding contribution, are considered and, on the other hand, the maximal reaction velocity term V_{max} was formally used as opposite way of activity regulation.

6.2.3 Control by means of maximal reaction velocity V_{max}

In this section the optimal control problem is formulated following Moroz, 2011 by means of the maximal reaction velocity in equation (6.2.1), where the study of the influence of control introduction is made by V_{max} on usual kinetic pattern of Michaelis-Menten system. Formally it is the simplest way of the OC introduction into the Michaelis-Menten kinetic equation. It can be formally carried out by alteration of the maximal reaction velocity V_{max}. Then the problem of optimal control will be

$$\frac{ds}{dt} = -\frac{us}{K_M + s}, \tag{6.2.8a}$$

where u is the control, K_M is the Michaelis constant; s is the concentration of substrate. The objective functional could be defined as

$$J = \int_{t_0}^{\tau} \left(G(s) + \frac{(u - V_{\max})^2}{2} \right) dt \to \min. \tag{6.2.8b}$$

The $G(s)$ is the cost function describing the instantaneous metabolic, free energy related losses, for the deviation of the substrate concentration s from the metabolic optimum. The second term describes the metabolic cost for the regulation by alteration of the maximal reaction velocity from an optimal $V_{\max}$. Applying the Pontryagin maximum principle (Pontryagin et al., 1962) to solve the OC problem (6.2.8) we can construct the Hamiltonian

$$H = -G(s) - \frac{(u - V_{\max})^2}{2} - p\left(\frac{us}{K_M + s}\right). \tag{6.2.9}$$

So optimal solution must satisfy following conditions:

$$\begin{aligned}
\frac{ds}{dt} &= -\frac{us}{K_M + s} \\
\frac{dp}{dt} &= \frac{K_M pu}{(K_M + s)^2} + \frac{\partial G}{\partial s} \\
\frac{\partial H}{\partial u} &= (u - V_{\max})(K_M + s) + ps = 0
\end{aligned} \quad . \qquad (6.2.10)$$

By excluding *u*, the above system can be reduced to the system of two equations

$$\begin{aligned}
\frac{ds}{dt} &= -\frac{V_{\max}(K_M + s) - ps}{K_M + s}\frac{s}{K_M + s}; s(t_0) = s_0 \\
\frac{dp}{dt} &= \frac{\partial G}{\partial s} + \frac{pK_m(V_{\max}(K_M + s) - ps)}{(K_M + s)^3}; p(\tau) = 0
\end{aligned} \quad , \qquad (6.2.11)$$

which allows us to write dynamical system for state variable *s* and co-variable *p* .

General application to Michaelis-Menten kinetics

Let us employ general approach to Michaelis-Menten kinetics. In the case, when the optimal control can be set by V_{max} in the Michaelis-Menten equation (6.2.1), we can rewrite it as

$$\frac{ds}{dt} = \frac{(u - V_{\max})s}{K_M + s} \qquad (6.2.12)$$

where *u* is a control additively to V_{max}. Then OC formulation can be written as

$$\int_{t_0}^{\tau} L_{OC}(s,u)dt = \int_{t_0}^{\tau} G(s) + T(u)\,dt \to \min \qquad (6.2.13)$$

subject to $$\frac{ds}{dt} = \frac{(u - V_{\max})s}{K_M + s}; s(t_0) = s_0$$

where L_{OC} is the optimal control Lagrangian, which we can choose in form more specific for the Michaelis-Menten kinetics:

$$L_{OC}(s,u) = G(s) + T(u) = G(s) + \frac{u^2}{2} \qquad (6.2.14)$$

Then we can find from (6.2.12) that

$$u = V_{\max} + \frac{(K_M + s)\dot{s}}{s} \tag{6.2.15}$$

and substitute it into the optimal control Lagrangian (6.2.14) and find the variational Lagrangian

$$L_{VA}(s,\dot{s}) = G(s) + \frac{1}{2}\left[V_{\max} + \frac{(K_M + s)\dot{s}}{s} \right]^2 \tag{6.2.16}$$

Finally, the Euler-Lagrange equation becomes

$$s(K_M + s)^2 \ddot{s} = \frac{\partial G}{\partial s} s^3 + K_M (K_M + s)\dot{s}^2 \tag{6.2.17}$$

The transversality condition gives

$$\dot{s}\frac{\partial \Lambda_{VA}(s,\dot{s})}{\partial \dot{s}} - L_{VA}(s,\dot{s}) = \left(-G(s) + \frac{\dot{s}^2 (K_M + s)^2 - V_{\max}^2 s^2}{2s^2} \right)_{\tau^*, s^*} = 0 \tag{6.2.18}$$

which gives for optimal (*) trajectory:

$$G(s^*) + \frac{\dot{s}^{*2} (K_M + s^*)^2 - V_{\max}^2 s^{*2}}{2s^{*2}} = 0 \tag{6.2.19}$$

or

$$\dot{s}^* = \pm \frac{s^* \sqrt{2G(s^*) + V_{\max}^2}}{K_M + s^*} \tag{6.2.20}$$

Integrating this equation we can get

$$\int \frac{K_M + s}{s\sqrt{2G(s) + V_{\max}^2}} ds = \pm \int dt + C_2 \tag{6.2.21}$$

where C_2 can be found from initial condition $s(\tau_0) = s_0$.

Using Legandre transform we can write variational Hamiltonian

$$H_{VA}(s,p) = -G(s) + \frac{p^2 s^2 - 2psV_{\max}(K_M + s)}{2(K_M + s)^2} \tag{6.2.22}$$

then the canonical equations are

$$\dot{s} = \frac{ps^2 - sV_{\max}(K_M + s)}{(K_M + s)^2}$$
$$\dot{p} = \frac{\partial G}{\partial s} - \frac{pK_M \ ps - V_{\max}(K_M + s)}{(K_M + s)^2} \quad . \tag{6.2.23}$$

This equation coincides with Eq.(6.2.11).

The variational Lagrangian for quadratic penalty can be written as

$$L_{VA}(s,\dot{s}) = \frac{l(s - s_{eq})^2}{2} + \frac{1}{2}\left[V_{\max} + \frac{(K_M + s)\dot{s}}{s}\right]^2 \tag{6.2.24}$$

The contour plot of the first integral of this example is shown in Fig.6.2.2. The contour plot of the Lagrangian is shown in Fig.6.2.2, upper insert and the Hamiltonian is shown in the lower insert of Fig.6.2.2. In this figure the first integral as the function of state coordinate and its derivative is illustrated.

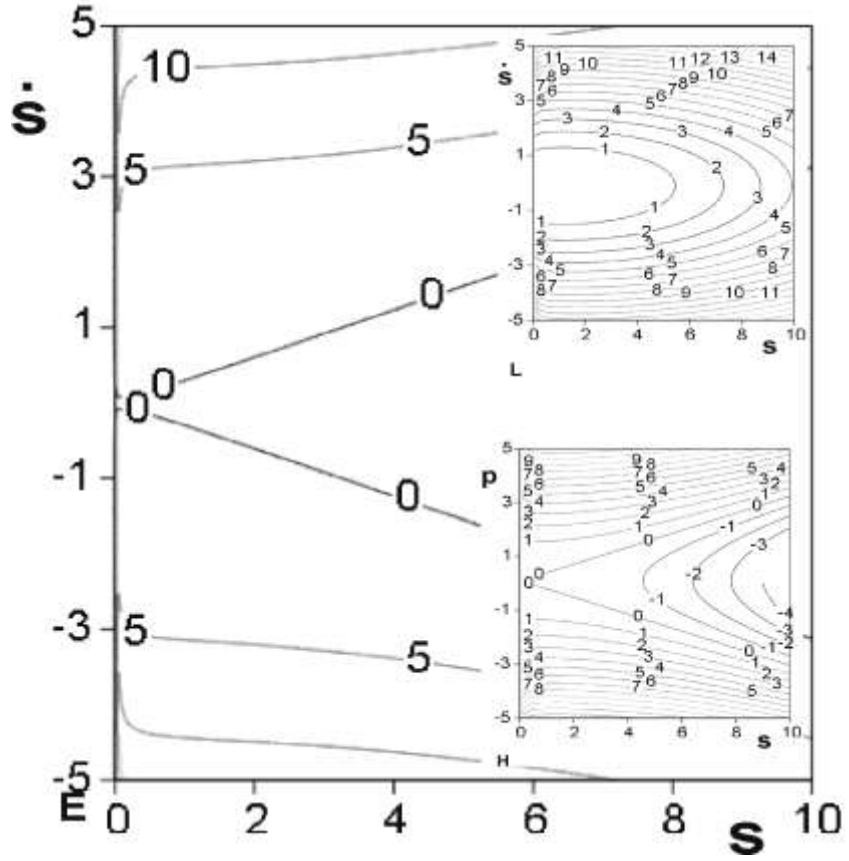

Fig.6.2.2. The first integral as the function of state coordinate and its derivative at quadratic approximation of the potential *G* and s_0*=0.1*, *l=0.1*, V_{max}*=0.1*, K_M*=0.01*. Upper insert - the contour plot of the Lagrangian L_{VA} (6.2.24). Lower insert - the Hamiltonian (6.2.22). Figure adopted from Moroz, 2011.

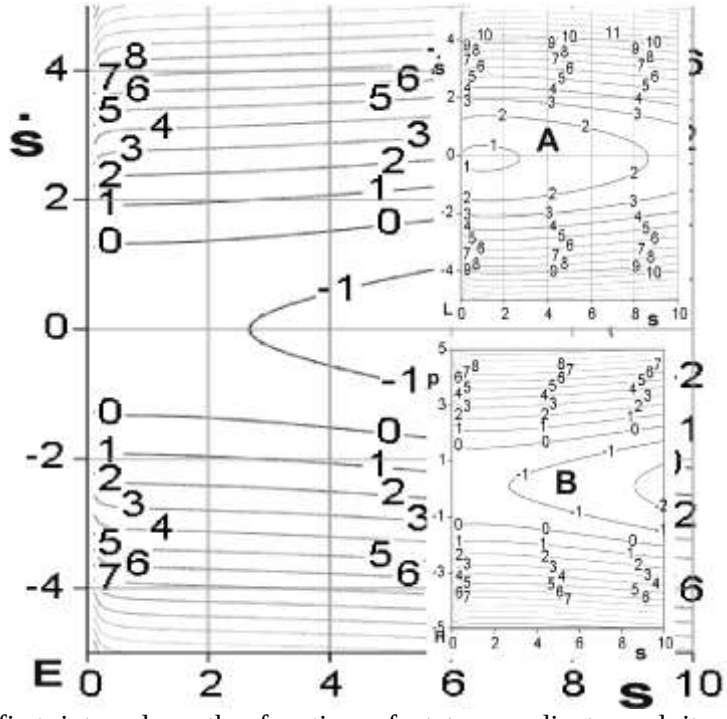

Fig.6.2.3. The first integral as the function of state coordinate and its derivative at the logarithmic approximation of the potential G (6.2.26) and $\underline{\boldsymbol{s_{eq}=0.1,}}$ $l=0.1$, V_{max}=0.1, K_M=0.01. Insert A – the contour plot of the Lagrangian L_{VA} (6.2.16). Insert B - the Hamiltonian for logarithmic approximation of the potential. Figure adopted from Moroz, 2011.

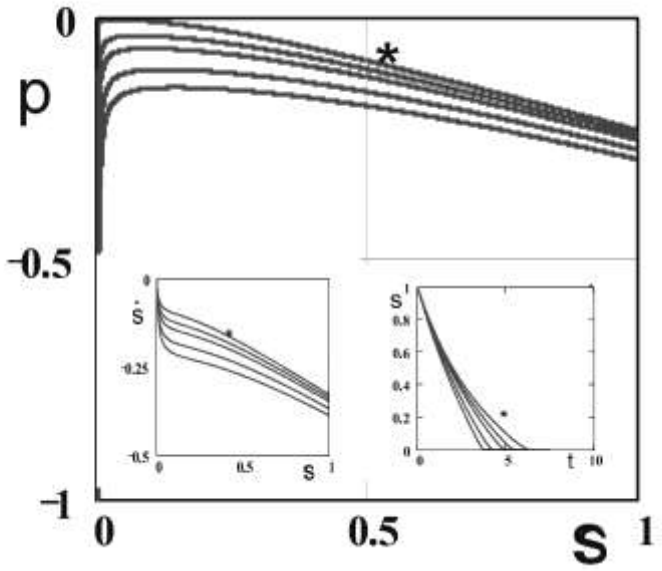

Fig.6.2.4. The phase plot (s,p) of the numerical solutions of Eq(6.2.23) for pure variational formulation is shown for $s_{eq}=0.1$, $l=0.1$, $V_{max}=0.1$, $K_M=0.01$ for different values of numerically calculated Hamiltonian, t – dimensionless time. Insert left - phase plot (s,ds/dt); Insert right, the trajectories of the state variable s (substrate concentration) scale versus time t. The curve designed as (*) is the closest approximation of real trajectory ($H^*=0$). Figure adopted from Moroz, 2011.

In the plots indicated in Fig.6.2.2 the squared-law penalty (potential) is employed. This is a simplest approximation widely accepted in the optimal control studies

$$G(s) = (s - s_{eq})^2 / 2 \quad . \tag{6.2.25}$$

However, as we mentioned previously, in natural case of kinetics when only positive concentrations only are accepted, and effectively the consideration of system is not limited by to be closed to steady state, it is reasonable to introduce the form of cost (here it is the instantaneous cost/penalty for the deviation of this concentration from the optimum) in the logarithmic approximation (which is related to a form sometime used for the Lyapunov function, or free energy approximation) see for example, Kondepudi and Prigogine, 1998:

$$G(s) = ks(\ln\frac{s}{s_{eq}} - 1) + G_0 = k\left(s(\ln\frac{s}{s_{eq}} - 1) + G_0 / k \right) \quad , \tag{6.2.26}$$

where $k = 1/G_0$, then the first integral (that could be interpretable as energy-like value of this process). Comparing (6.2.25) and (6.2.26) at different equilibrium state shows small differences near to the equilibrium. Using the logarithmic form of the cost we have calculated and shown the Lagrangian (6.2.16) and the Hamiltonian Eq (6.2.9), in Fig.6.2.3 as a contour plot of the first integral and Fig.6.2.3 (insert A and B) as a contour plot of the Lagrangian and Hamiltonian for the logarithmic form of the cost (6.2.26), where state variable is $s_{eq}=0.1$ and control variable is $V_{\max} = 1.0$.

For the comparison of the results based on the Lagragian/Hamiltonian calculations (6.2.13)/(6.2.22) shown in Fig.6.2.2 with the results of numerical calculation for dynamic system (6.2.23/6.2.11) the calculations were performed using Runge-Kutta method. The plots of the phase trajectories lines for some initial values for the system (6.2.23) when the square-low penalty approximation *G(x)* employed, are indicated in Fig.6.2.4 for the square-low form ($V_{max} = 1.0$, $s_{eq} = 0.0$).

In the Fig.6.2.4 the phase plot of co-state variable *p* against the state variable *s* is shown. In the figure Fig. 6.2.4(lest insert), the graphs show also the phase trajectories of the concentration derivative and state variable *s*. The Fig.6.2.4 (right insert) shows the relaxation trajectories substrate concentration in dimensionless time. The figures in Fig.6.2.4 indicate the

same character of extreme trajectory (designated as *) as in Fig.6.2.2 (lower insert, H=0), correspondingly. So, the results shown in Fig.6.2.4 are in good agreement with the results in Fig.6.2.2.

Thus, one can see that all these phase plots coincide with the contour plots for the Hamiltonians that obtained by the direct numerical calculations from the dynamic system (6.2.22), which indicates correctness of the approach.

6.2.4 Optimal control formulation in terms of state and control variables

However, let us not that the consideration of a problem in terms of state and co-state variables is somewhat difficult in the interpretation, in particular, in interpretation of the costate variable. From this perspective, the consideration of problem in terms of control variable is more convenient and interesting. Let us then reconsider the optimal control by V_{max} when the control variable is explicitly covered in the dynamic equations.

Employing the Lagrange method we can construct the Lagrangian of the optimization problem (6.2.8a-8b) is (regarding to control by maximal velocity):

$$L = G(s) + \frac{(u-u_{eq})^2}{2} + p\left(\frac{ds}{dt} + \frac{us}{K_M + s}\right), \tag{6.2.27}$$

then the Euler-Lagrange equations in fact repeat the system (6.2.10).

$$\frac{dp}{dt} - \frac{\partial L}{\partial s} = \frac{dp}{dt} - \frac{K_M pu}{(K_M + s)^2} - \frac{\partial G}{\partial s} = 0$$
$$\frac{\partial L}{\partial p} = \frac{ds}{dt} + \frac{us}{K_M + s} = 0$$
$$\frac{\partial L}{\partial u} = (u - u_{eq})(K_M + s) + ps = 0$$

By excluding p from this system one can get the system, describing the process in terms of state variable s and control variable u. As it was mentioned above by this method, because Lagrangian does not depend explicitly on time, it is possible to find so-called first integral (6.2.7) of the system that means that there is a conservative value, which duplicates in fact Hamiltonian. Generally speaking it is not obvious, because (as for example in classic

mechanics) energy (first integral) and Hamiltonian not always formally match. Excluding p from systems (6.2.10) one can obtain new system for the state variable s and control variable u:

$$\frac{ds}{dt} = -\frac{us}{K_M + s}, \frac{du}{dt} = -\frac{s(\partial G/\partial s)}{K_M + s} \quad . \tag{6.2.28}$$

Since $u > 0$, $K_M > 0$, $s + K_M > 0$, the denominator does not give any singularity, therefore it is possible to subdivide the right parts of equations. Then the system could be transformed to

$$\frac{du}{ds} = \frac{\partial G/\partial s}{u} \quad . \tag{6.2.29}$$

Having solved this differential equation it is possible to find clear relationships between the concentration s and the amplitude of control u and consider some interpretations. On the other hand from above equation it is possible to find the first integral:

$$H = -G(s) + \frac{u^2}{2} - \frac{V_{\max}^2}{2}. \tag{6.2.30}$$

Let us now come back to the special cases of penalty for deviation from equilibrium. So, if it were limited by the squared form of the form of cost (6.2.12) then the first integral (6.2.17) is:

$$H = -\frac{(s - s_{eq})^2}{2} + \frac{(u + V_{\max})(u - V_{\max})}{2}. \tag{6.2.31}$$

The surface plot and the contour plots of the lines of an identical level for the first integral are indicated in Fig.6.2.5 for $V_{max} = 1.0$, $s_{eq} = 1.0$ and $s_{eq} = 0.0$. The Fig. 6.2.6 shows the lines of identical level E in case of the logarithmic form of cost (6.2.26) when $k = s_{eq}$, $G_0 = 1$, $s_{eq} = 0.10$ and $V_{max} = 1.0$, when the first integral value E is

$$H = -s(\ln\frac{s}{s_{eq}} - 1) - 1 + \frac{u^2}{2} - \frac{V_{\max}^2}{2}. \tag{6.2.32}$$

Let us note that these quantities (6.2.31, 6.2.32) cannot be associated with the energy of the process. Finally after elimination of p , both systems are shown below for state variable s and control variable u ; under the square-law form of cost (6.2.25) and for $V_{max} = 1.0$ and $s_{eq} = 1.0$

$$\frac{ds}{dt} = -\frac{us}{1+s}, \frac{du}{dt} = -\frac{s(s-1)}{1+s} \quad , \tag{6.2.33}$$

and for the logarithmic form of cost (6.2.26) when $G_0=k=1$:

$$\frac{ds}{dt}=-\frac{us}{1+s},\frac{du}{dt}=-\frac{s\ln s}{1+s} \quad , \tag{6.2.34}$$

and at the Michaelis constant $K_M=1$, what indicates that the systems are scaled.

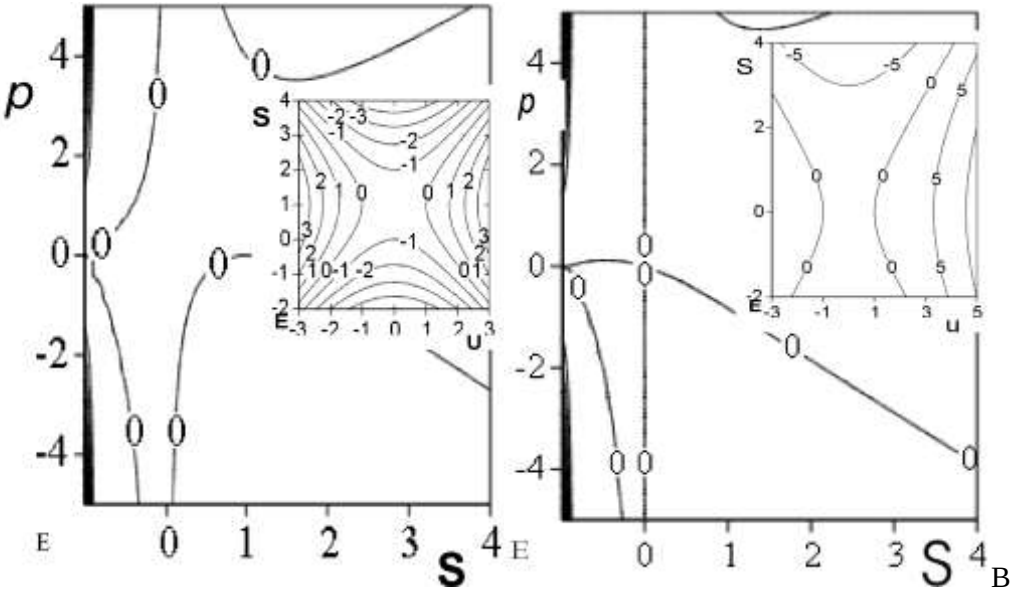

A B

Fig. 6.2.5 First integral H (6.2.31) contour plots corresponding to the systems (6.2.33). A, contour plot of the first integral described by the expression (6.2.31) at value $s_{eq}=1.0$ and $V_{max}=1.0$; B, the contour plot of the first integral described by the expression (6.2.31) when $s_{eq}=0$ and $V_{max}=1.0$. Figure adopted from Moroz, 2011.

The numerical solutions of these systems (6.2.33,34) repeat the solution of system (6.2.11) for state variable *s* and costate variable *p*, however in terms of state variable and control variable u. Performing the numerical calculations using these two representations (*s*,*p*) and (*s*,*u*) to obtain trajectories of these two-dimensional dynamical systems obviously shows no difference in the results. Interesting indication comes up when the kinetic data obtained is shown in so-called double-reciprocal Lineweaver-Burk (1934) plot (also see for example recent linearization development in [96]).

It is known that double-reciprocal plot is widely used in enzyme kinetics for estimation of V_{max} and K_M, where the slope is K_M/V_{max} and y-intercept is $1/V_{max}$, see the dotted line on every double-reciprocal plot. We used the system when $K_M = 1.0$ and $V_{max} = 1.0$ so the

intercept of this curve is equal to unity and slope in the case when V_{max} = *1.0* is equal to unity, too.

The figures Fig.6.2.7 and Fig.6.2.8 show the trajectories of (6.2.31) and (6.2.32) in double-reciprocal plot for square-law and logarithmic potential. The inserts A in figures Fig.6.2.7, Fig.6.2.8 indicate the phase plots in terms of *p* and *s* and inserts B –in terms of *s* and *u* in case of the square-law approximation of the potential and for the logarithmic form of cost.

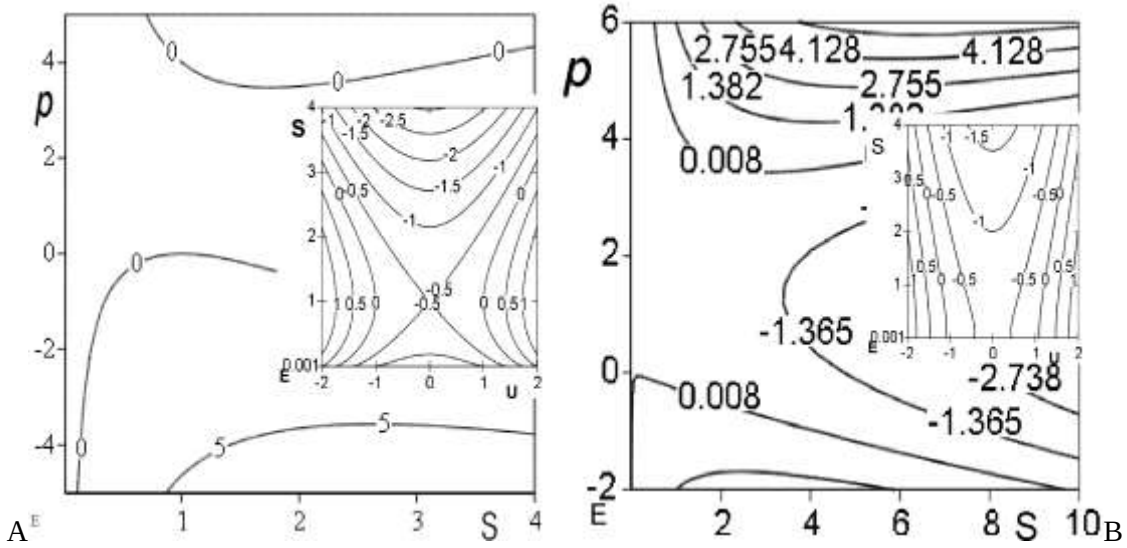

Fig. 6.2.6 The first integral contour plot corresponding to the Eq.(6.2.32) and the systems (6.2.34). A, contour plot of the first integral *E(S,p)* described by the expression (6.2.32) at value V_{max} *=1.0* and s_{eq}*=1.0* ; B, contour *E(s,u)* plot of (6.2.32) described employing expression (6.2.26) when G_0*=k=1* and values s_{eq}*=0.1,* V_{max} *=1.0*. Figure adopted from Moroz, 2011.

One can see from Fig.6.2.7 and Fig.6.2.8 that the trajectories "a" are the closest to the curves *H=0,* in Fig.6.2.5 and Fig.6.2.6 correspondingly. For both forms of cost when s_{eq}*= 1.0* the dotted curve is the tangent line to the *E=0* kinetic curve designed as "a" in all Fig.6.2.7 and Fig.6.2.8. The tangent curve not just touches the kinetic curve "a" corresponding to *H=0*, but coincides with this kinetic curve in long range of values.

That in fact indicates good reliability of consideration of Michaelis-Menten kinetics in the optimal control terms. Moreover, it illustrates that the Michaelis-Menten kinetics is an optimal kinetics in sense on energetical criteria, which are set in (6.2.2) and (6.2.13).

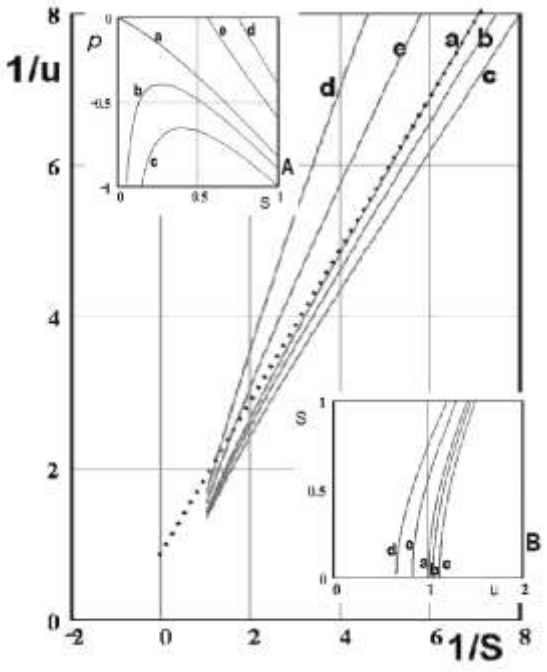

Fig.6.2.7 Solutions of the system (6.2.33) obtained numerically for the quadratic form of cost at values $s_{eq}=0.0$ and $V_{max}=1.0$: The trajectories in double reciprocate coordinates. Curves "a" in corresponds to $H^*=0$ level of Fig.6.2.5B, for the quadratic form of cost, dotted line corresponds to the Michaelis-Menten equation scaled to $V_{max}=1$ and $K_M = 1$. Insert A, shows the phase trajectories in (s,p) plane; Insert B, the phase trajectories in (u,s) plane. Figure adopted from Moroz, 2011.

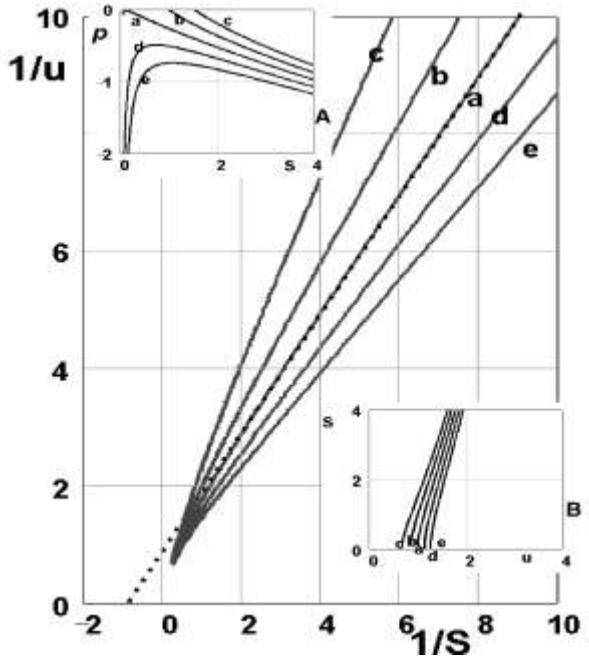

Fig.6.2.8 Solutions of the system (6.2.34) obtained by numerical method for the logarithmic form of the cost at values $s_{eq}=0.1$ and $u_{eq}=1.0$. The trajectories in double reciprocate coordinates. Curves "a" correspond to $H=0$ level of Fig.6.2.3 (insert B), for the logarithmic form of cost. The dotted line in figure A corresponds to Michaelis-Menten equation scaled to $V_{max}=1$ and $K_M = 1$. Insert A, shows the phase trajectories in (S,p) plan; insert B, the phase trajectories in (s,u) plan. Figure adopted from Moroz, 2011.

6.2.5 Control by the Michaelis constant K_M

Formally there is another, much more important way of the optimal control introduction into the Michaelis-Menten kinetic equation because of its link to allosteric regulation. Let us now amend the Michaelis-Menten equation, where the Michaelis constant K_M is replaced by some time-dependent amplitude of control *u(t)*:

$$\frac{ds}{dt} = -\frac{V_{\max} s}{u + s} \quad , \tag{6.2.35}$$

where *u(t)* is a control variable formally from unlimited area [0, ∞], V_{max} is the maximal reaction velocity, state variable *s* is the substrate concentration. We can define the objective functional as

$$\int_{t_0}^{\tau} \left(G(s) + \frac{(u - K_M)^2}{2} \right) dt \to \min , \tag{6.2.36}$$

where *G(s)* is cost function that formally describes the instantaneous metabolic cost for the excessive deviation of the substrate concentration *s* from the optimum. The second term is the cost function describing the metabolic expenses for the regulation.

When formulating the variational outline for control by the Michaelis-Menten constant the situation is more complicated. Let us follow our scheme/outline. From (6.2.35) we can find that

$$u = -\frac{V_{\max} s}{\dot{s}} - s \tag{6.2.37}$$

Then variational Lagrangian can be written as

$$L_{VA}(s, \dot{s}) = G(s) + \frac{(V_{\max} + \dot{s})s + K_M \dot{s}}{2\dot{s}^2} \tag{6.2.38}$$

Then we can find the Euler-Eagrange equation using Legandre transform

$$\frac{\partial L_{VA}(s, \dot{s})}{\partial \dot{s}} = -\frac{V_{\max} s \, V_{\max} s + \dot{s}(K_M + s)}{\dot{s}^3} \tag{6.2.39}$$

and

$$\frac{\partial L_{VA}(s,\dot{s})}{\partial s} = \frac{\partial G}{\partial s} + \frac{(V_{\max} + \dot{s})\, V_{\max} s + \dot{s}(K_M + s)}{\dot{s}^2} \tag{6.2.40}$$

Finally, the Euler-Lagrange equation is

$$\begin{aligned} & s\,2\dot{s}(K_M + s) + 3V_{\max} s\,\ddot{s} - V_{\max}\dot{s}^2\,2s(V_{\max} + \dot{s}) + K_M\dot{s} = \\ & \dot{s}^4 \frac{\partial G}{\partial s} + \dot{s}^2(V_{\max} + \dot{s})\, s(V_{\max} + \dot{s}) + K_M\dot{s} \end{aligned} \tag{6.2.41}$$

The solution of this equation is very unlikely to obtain in a general case. The transversality conditions are

$$\left[\dot{s}\frac{\partial L_{VA}}{\partial s} - L_{VA} \right]_\tau = \left[\frac{(V_{\max} s)^2 - \dot{s}^2(K_M + s)^2}{2\dot{s}^2} - G(s) \right]_\tau = 0\,, \tag{6.2.42}$$

then one can write for optimal trajectory

$$\dot{s}^* = \pm \frac{V_{\max} s^*}{\sqrt{2G(s^*) + (K_M + s^*)^2}} \tag{6.2.43}$$

Integrating this equation we can get

$$\int \frac{\sqrt{2G(s) + (K_M + s)^2}}{s}\, ds = \pm V_{\max} \int dt + C_2 \tag{6.2.44}$$

where C_2 can be found from initial condition $s(\tau_0) = s_0$. To find the Hamiltonian, using the Legandre transform it is not easy. From general expression for the Hamiltonian we can write that the variational Hamiltonian is

$$H(s,\dot{s}) = \left[\frac{(V_{\max} s)^2 - \dot{s}^2(K_M + s)^2}{2\dot{s}^2} - G(s) \right] \tag{6.2.45}$$

where derivatives have to be changed by expression in terms of momentum *p*. To find the numerical solution of Euler-Lagrange equation it is useful to go to the transformation $\dot{s} = q$. Then the system is

$$\begin{aligned} & \dot{s} = q \\ & \dot{q} = \frac{V_{\max}\dot{s}^2\,2s(V_{\max} + \dot{s}) + K_M\dot{s} + \dot{s}^4 \frac{\partial G}{\partial s} + \dot{s}^2(V_{\max} + \dot{s})\, s(V_{\max} + \dot{s}) + K_M\dot{s}}{s\,2\dot{s}(K_M + s) + 3V_{\max} s} \end{aligned} \tag{6.2.46}$$

In case of square law potential this system will be

$$\dot{s} = q$$

$$\dot{q} = \frac{V_{\max}\dot{s}^2\left[s(V_{\max}+\dot{s}) + K_M\dot{s}\right] + \dot{s}^4 l(s-s_{eq}) + \dot{s}^2(V_{\max}+\dot{s})\left[s(V_{\max}+\dot{s}) + K_M\dot{s}\right]}{s\left[\dot{s}(K_M+s) + 3V_{\max}s\right]} \quad (6.2.47)$$

In Fig.6.2.10 the numerical solutions of this system are shown.

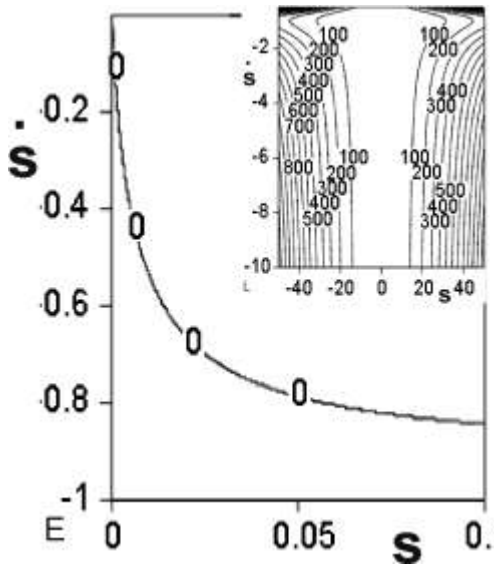

A B

Fig.6.2.9 The contour plots of Hamiltonian (6.2.45) for pure variational formulation corresponding to the optimal control by the Michaelis constant, $s_{eq}=0.0$, $l=0.2$, $V_{max}=1.0$, $K_M=0.01$. Insert - the contour plot for the Lagrangian L_{VA} (6.2.38) the at square law potential G. Figure adopted from Moroz, 2011.

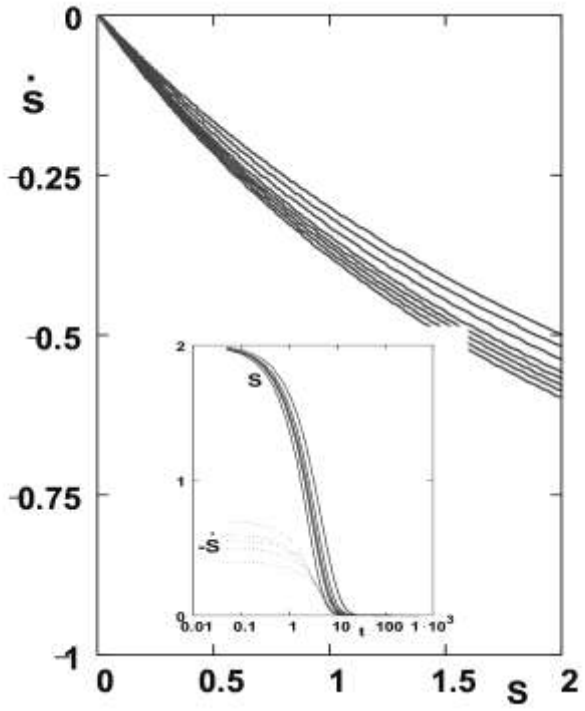

A **B**

Fig.6.2.10 The numerical data obtained as results of numerical calculation of equation (6.2.45) at $s_{eq}=0.0$, $l=0.1$, $V_{max}=0.1$, $K_M=0.01$ for different values of the first integral. Insert - the trajectories in time, t – dimensionless time. Figure adopted from Moroz, 2011.

Comparing Fig.6.2.9 and Fig.6.2.10 one can see clear topological similarities. Let us note that quantity *q* in the case of system (6.2.46-47) is not the Lagrange multiplier (momentum) because is not obtained using the Legandre transformation. One can also see, that the kinetic curves in Fig.6.2.10 (insert) clearly indicate the sigmoid character of relaxation; the derivative has the negative sign. Since it was difficult to apply directly the Legandre transform and formulate the Hamiltonian approach let us formulate problem in terms of state variable (the substrate concentration s and the control variable *u*). Let us build the Hamiltonian

$$H = -G(s) - \frac{(u - K_M)^2}{2} - p(\frac{V_{\max} s}{u + s}). \tag{6.2.48}$$

Then applying the Pontryagin maximum principle we can write the necessary conditions; the optimal solution must satisfy these necessary conditions:

$$\begin{aligned} \frac{ds}{dt} &= \frac{\partial H}{\partial p} = -\frac{V_{\max} s}{u + s} \\ \frac{dp}{dt} &= -\frac{\partial H}{\partial s} = \frac{V_{\max} pu}{(u + s)^2} + \frac{\partial G}{\partial s} \\ \frac{\partial H}{\partial u} &= -(u - K_M) + \frac{V_{\max} ps}{(u + s)^2} = 0 \end{aligned} \quad , \tag{6.2.49}$$

By reducing this system to the system of two equations for *s* and *u* we obtain the dynamic system

$$\begin{aligned} \frac{ds}{dt} &= -\frac{V_{\max} s}{u + s} \\ \frac{du}{dt} &= \frac{V_{\max} s(u - K_M + \frac{\partial G}{\partial s})}{(3u + s - 2K_M)(u + s)} \end{aligned} \quad . \tag{6.2.50}$$

Since *u> 0, s> 0, u + s> 0*, therefore it is possible to subdivide the right parts of the equations. Then the system could be transformed to

$$\frac{du}{ds} = -\frac{u - K_M + \frac{\partial G}{\partial s}}{3u + s - 2K_M} \quad . \tag{6.2.51}$$

Having solved this differential equation one can find clear relationships between the state variable (concentration) *s* and the amplitude of control *u* and give some interpretations.

Since the Hamiltonian function (6.2.48) is not dependent on time explicitly, the first integral of this problem is *H=Const*. On the other hand the first integral that could be calculated from direct variational approach [70] is:

$$H = -G(s) - \frac{(u - K_M)(3u + 2s - K_M)}{2} \quad . \tag{6.2.52}$$

Let us consider some special cases. One specific case arises when objective function describing the formal penalty for the deviation of the substrate from the optimal/steady state has squared approximation (6.2.25), then the first integral H (in fact, the Hamiltonian of process) could be written as

$$H = -\frac{(s - s_{eq})^2}{2} - \frac{(u - K_M)(3u + 2s - K_M)}{2} \quad . \tag{6.2.53}$$

The contour plot of the lines of an identical levels of H (6.2.53) are indicated in Fig.6.2.11A and B for values $s_{eq} = 0.1$, $K_M = 1.0$.

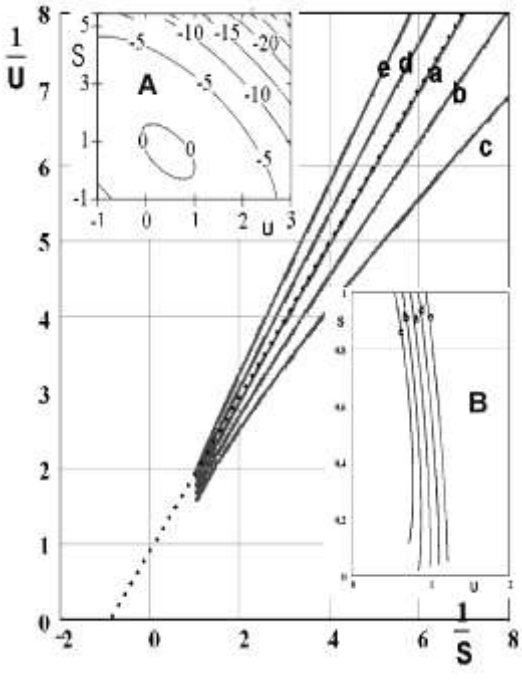

C

Fig.6.2.11 Double-reciprocal plot in the case of the square-law cost for the substrate deviation from equilibrium/steady-state at value $K_M = 1.0$ and $s_{eq} = 0.1$, calculated by Runge-Kutta method. phase trajectories in (s,u) plane from system (6.2.55). Insert A, the first integral H (6.2.53) contour plot. Insert B, the trajectories (6.2.55) in double reciprocate coordinates. Curves "a" correspond *to H*=0* level of insert A for the quadratic form of cost, dotted line corresponds to Michaelis-Menten equation with $V_{max} = 1$ and $K_M = 1$. Figure adopted from Moroz, 2011.

At the logarithmic approximation form (form that qualitatively coincide to form of thermodynamic potential in an ideal one-dimensional case, see Fig.2.1.6) then the first integral (that is interpretable as energy-like value of this process) is

$$H = -s(\ln(s/s_0)-1) - G_0 - \frac{(u-K_M)(3u+2s-K_M)}{2}. \qquad (6.2.54)$$

The surface plot and the contour plot of the lines of its identical level for logarithmic form of cost (6.2.54) are indicated in Fig.6.2.12 for when $G_0 = k = 1$ and $K_M = 1.0$.

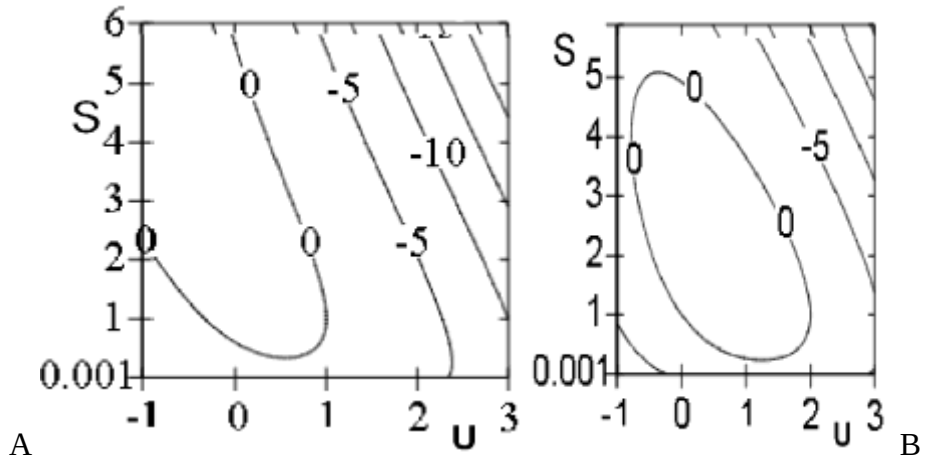

A B

Fig.6.2.12 The first integral *H* (6.2.54) contour plot corresponding to the systems (6.2.56) at the logarithmic cost for the deviation (6.2.26). A, contour *H(s,u)* plots of the first integral at values $K_M = 1.0$ and $s_{eq} = 1.0$; B, contour plot *H(s,u)* described by the expression (6.2.52) when values are $G_0 = k = 1$ and $s_{eq} = 0.1$, $K_M = 2.0$. Figure adopted from Moroz, 2011.

Let us have a more detailed look on the system (6.2.50) at the square-law form of cost (6.2.25). At $s_{eq} = 0.1$, $K_M = 1.0$ and $V_{max} = 1.0$, then the system of differential equations (6.2.50) transforms into

$$\begin{aligned} \frac{ds}{dt} &= -\frac{s}{u+s} \\ \frac{du}{dt} &= \frac{s(u+s-2)}{(3u+s-2)(u+s)} \end{aligned}. \qquad (6.2.55)$$

Fig.6.2.11 shows double-reciprocal plot of corresponding kinetic curves of system (6.2.55). Fig.6.2.11 (insert B) demonstrates some phase trajectories for this dynamical system obtained by the numerical method, when control $u>0$. One can see that topologically the picture poorly differs from Fig. 6.2.11 (insert A). It is clear from the comparison of Fig.6.2.11(insert B) and

the Fig. 6.2.11(insert A) that the curve "a" in Fig. 6.2.11 corresponds most closely to the zero value curve for which the first integral $H^* = 0$.

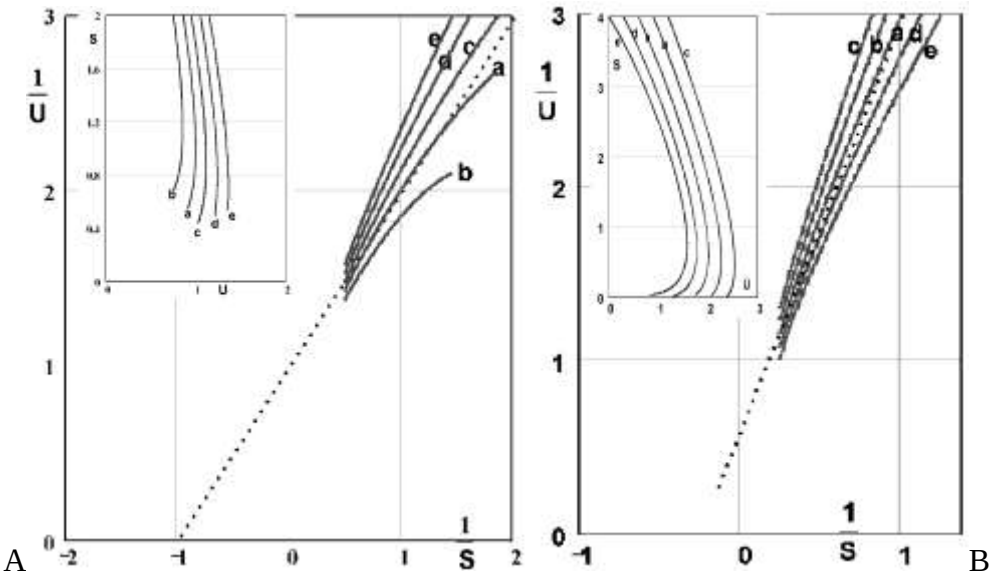

Fig.6.2.13 The double reciprocal plot of the numerical calculations of the systems (6.2.50) at the logarithmic cost for the deviation (6.2.26) that finally described by (6.2.56). A, double reciprocal plot of numerical solutions *(S,u)* described by the expression (6.2.56) when the values in $G_0 = k = 1$ and $K_M = 1.0$, $V_{max} = 1.0$; insert in A -phase trajectories of the system (6.2.56) with the logarithmic form of cost (6.2.26), $u > 0$ domain. B, double reciprocal plot of trajectories of system (6.2.55), when $K_M = 2.0$, $V_{max} = 1.0$; insert in B – corresponding phase trajectories of the system (6.2.56) with the logarithmic form of cost (6.2.26), $u > 0$ domain. Figure adopted from Moroz, 2011.

At the logarithmic approximation of the metabolic cost (6.2.26) for the substrate deviation from optimum state, the system (6.2.50) takes the form when $G_0 = k = 1$

$$\begin{aligned} \dot{s} &= -\frac{s}{u+s} \\ \dot{u} &= \frac{s(u+\ln s-1)}{(3u+s-2)(u+s)} \end{aligned} . \qquad (6.2.56)$$

The numerical solution of this system is represented in Fig.6.2.13. The curves designated as "a" in Fig. 6.2.13 correspond most closely to the zero value for energy (contour plot is shown in Fig.6.2.12A,B correspondingly). One can see, if to extend the curve s designated as "a" to the ordinate, it gives the V_{max} value equal to $K_M = 1.0$ (Fig. 6.2.13A) or to $K_M = 2.0$ (Fig. 6.2.13B) as it was initially set in the system (6.2.56), accordingly.

If to consider more general case, then the objective functional can be defined as

$$\int_{t_0}^{\tau} G(s) + T(u)\, dt \to \min \tag{6.2.57}$$

subject to the dynamical constrains Eq(6.2.35) and $s(0) = s_0$.

By reducing the Euler-Lagrange equations to the system of two equations we obtain

$$\frac{ds}{dt} = -\frac{V_{\max} s}{u+s}$$
$$\frac{du}{dt} = \frac{V_{\max} s\left(\frac{\partial T}{\partial u} + \frac{\partial G}{\partial s}\right)}{\left(\frac{\partial^2 T}{\partial u^2}(u+s) + 2\frac{\partial T}{\partial u}\right)(u+s)} \quad . \tag{6.2.58}$$

The first integral *H*, will be

$$H = -G(s) - T(u) - \frac{\partial T}{\partial u}(u+s) \tag{6.2.59}$$

In the case of logarithmic approximation for the cost for the metabolic control *T(u)*, as well as logarithmic approximation for *G(s)*, see Eq.(6.2.26), $T(u) = k_u(u(\ln u - 1) + 1)$ the first integral *H* will be

$$H(s,u) = -k_s s(\ln s - 1) + G_0 - k_u(u(\ln u - 1) + 1) - k_u(u+s)\ln u = const. \tag{6.2.60}$$

The double-reciprocal plot of (6.2.58) at (6.2.60) is shown in Fig. 6.2.14. The contour plot corresponding to this equation that contains the logarithmic cost approximation for the substrate deviation and for the control at the values k_u*=0.5* and k_s*=1.0* is shown in Fig. 6.2.14(insert A). The numerical solution of the system (6.2.56) is shown in Fig. 6.2.14 (phase plot, insert B). One can see that curve denoted as "a" in the double-reciprocal plot plane, Fig. 6.2.14 corresponds to *H=0* curve in Fig.6.2.14(insert B). The expansion of this curve "a" in double-reciprocal plot plane, Fig.6.2.14 from area near to equilibrium gives V_{max} *=1.0* and average K_M about the unity, also.

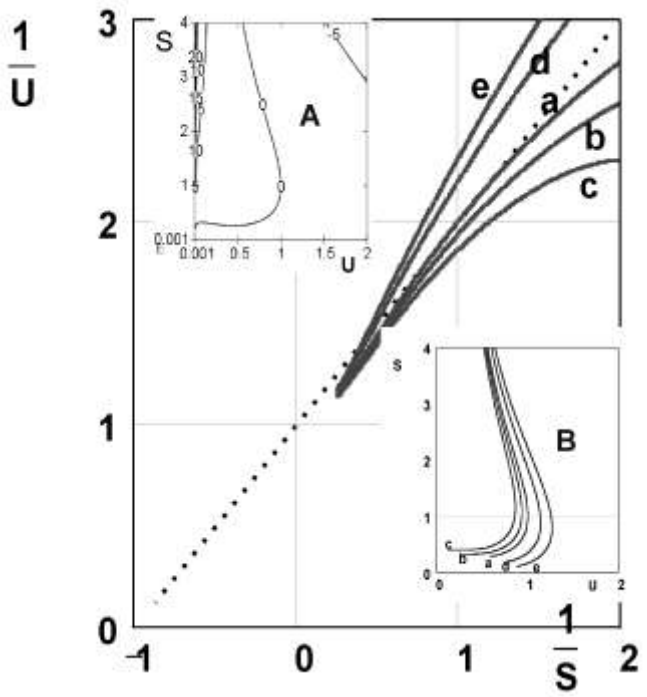

Fig. 6.2.14 The plot in double reciprocal coordinates of the system (6.2.58), dotted line corresponds to the Michaelis-Menten equation scaled to $V_{max}=1.0$ and $K_M = 1.0$. Insert A, the first integral H (6.2.60) contour plot corresponding to the system (6.2.58) with the logarithmic form of cost (6.2.26) for the substrate deviation s and for the control u, $k_u=1.0$; $k_s=1.0$. Insert B, phase trajectories of the system (6.2.58) with the logarithmic form of the cost, obtained by the numerical method. Curves "a" in main figure and insert B correspond to $H^*=0$ level of insert B. Figure adopted from Moroz, 2011.

Simultaneous optimal control by the V_{max} and the Michaelis constant K

In the general case the control could be implemented by the maximal velocity V_{max} and by the Michaelis constant K_M simultaneously. Then the objective functional could be defined as

$$J = \int_{t_0}^{\tau} G(s) + T(u,v)\, dt \to \min \tag{6.2.61}$$

subject to the dynamical constrains

$$\frac{ds}{dt} = -\frac{vs}{u+s} \tag{6.2.62}$$

and $s(0) = s_0$, where v is the control variable responsible for regulation by V_{max}, and u – is the control variable responsible for control by Michaelis constant K_M. Then employing the Lagrange method we construct

$$L = G(s) + T(u,v) + p\left(\dot{s} + \frac{vs}{u+s}\right) \tag{6.2.63}$$

canonical system similar to (6.2.4) or Euler-Lagrange system (6.2.6).

$$\begin{aligned}
\frac{\partial L}{\partial s} &= \frac{\partial G}{\partial s} + \frac{puv}{(u+s)^2} = \frac{dp}{dt} \\
\frac{\partial L}{\partial u} &= \frac{\partial T}{\partial u} - \frac{pvs}{(u+s)^2} = 0 \\
\frac{\partial L}{\partial v} &= \frac{\partial T}{\partial v} - \frac{ps}{u+s} = 0 \\
\frac{\partial L}{\partial p} &= \dot{s} - \frac{vs}{u+s} = 0
\end{aligned} \tag{6.2.64}$$

Employing squared form (6.2.25) for *G(s)* and squared form for the cost of control:

$$T(u,v) = \frac{(u-K_M)^2}{2} + \frac{(v-V_{\max})^2}{2} \tag{6.2.65}$$

we can simplify the Euler-Lagrange system. The results of the numerical calculations for simplified system are shown in Fig.6.2.15A as a Lineweaver-Burk plot for $s_{eq}=0.01$, $V_{max}=1.0$, $K_M=1.0$ at initial values of the state variable $s(t_0)=0.9$, costate variable $p(t_0)=-0.285$, and control variables $v(t_0)=1.1$, $u(t_0)=0.9$ for the optimal trajectories ($H^*=0$). One can see that curves remain linear but slope and intercept, characterised kinetics are to some extent changed from the standard Michaelis-Menten kinetics without control.

Fig.6.2.15B shows the plot of the control variables u and v in time when logarithmic form (6.2.26) of function G(s) is employed for $s_{eq}=0.01$, $V_{max}=1.0$, $K_M=1.0$ and different initial values of state and control variables for $H^*=0$. All curves have linear character, slope and intercept of them are different from the reciprocal curves for ideal systems when V_{max} and K_M are fixed, which obviously is caused by considering the V_{max} and K_M as the control variables.

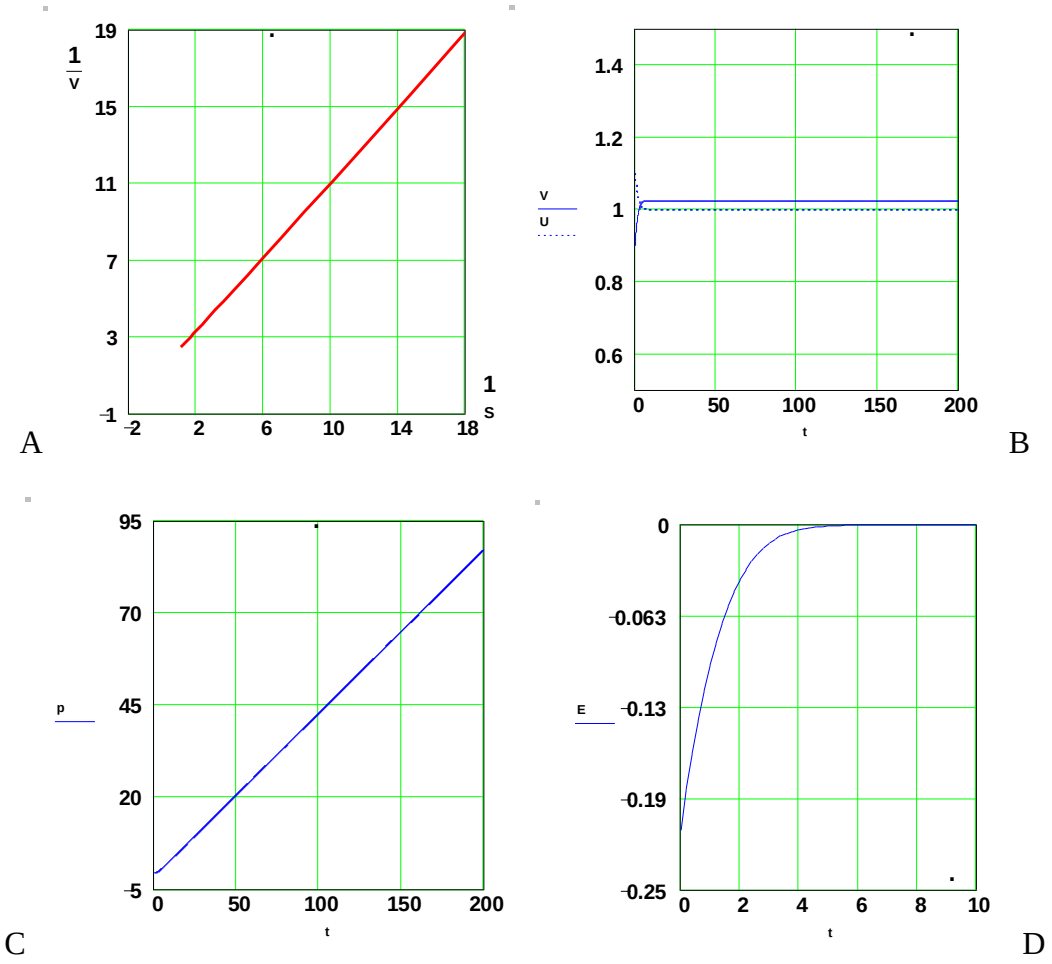

Fig.6.2.15 Phase trajectories of the problem (6.2.61-64) in double reciprocal coordinates with the square form of cost (6.2.25) in the case of logarithmic form of potential, obtained by the numerical method. A, curve corresponds to $H^*=0$. Curve corresponds to the equation (6.2.1) when $v(t_0)=1.1$, $u(t_0)=0.9$. B, kinetic curves u and v in time. C, decimal logarithm of –p in time. Relaxation of the calculated Hamiltonian in time. Figure adopted from Moroz, 2011.

6.2.6 The link to the biochemical mechanisms

The method of optimal control implementation we want to bring into focus is, that all types of the OC introduction that are suggested in this section can find their analogy *in vitro* in batch kinetics control or *in vivo* in the enzyme activity regulation in the cell. First important note should be indicated, as was already specified according to (6.2.1), the maximal reaction velocity is equal to $V_{\max} = k_2 E_0$, where E_0 is the enzyme concentration, k_2 is the rate constant of substrate-enzyme complex disintegration, then the control by means of changing V_{max} can be related both to the regulation by particular enzyme synthesis (the increase or the reduction of enzyme concentration) and to change of the rate constant k_2 of disintegration of the substrate-

enzyme complex into the enzyme and the final product. In terms of enzyme kinetics the control by maximal reaction velocity is associated to *non-competitive* inhibition formally introduced by the substitution in the equation (6.2.1) of maximal reaction velocity V_{max} by the so-called effective velocity $V_{\max}^{/}$, see, for example, [92, 97]:

$$V_{\max}^{/} = \frac{V_{\max}}{1+\frac{[\mathrm{i}]}{\mathrm{k_i}}} \quad , \tag{6.2.66}$$

where $[\mathrm{i}]$ are the concentrations of the i-s inhibitors, $\mathrm{k_i}$ are the binding constants.

Secondary, it should also be noted, that the regulation formally expressed through the control by means of the Michaelis constant K_M, has an enzymologic equivalence to the competitive inhibition. In the case of allosteric mechanisms of enzyme activity regulation, such inhibition by means of the alteration in the Michaelis constant K_M is expressed formally by the so-called effective constant $K_m^{/}$ (Cornish-Bowden, 2004; Hsu et al., 2000):

$$K_M^{/} = K_M\left(1+\frac{[\mathrm{I}]}{\mathrm{k_i}}\right) \quad , \tag{6.2.67}$$

where [I] is the concentration of free inhibitor; k_i is the inhibition constant

$$k_i = \frac{[E][I]}{[E+I]} \quad , \tag{6.2.68}$$

and [E] is the enzyme concentration. Thus, the optimal control by means of the Michaelis constant has a metabolic analogy in the molecular form of *competitive* inhibition, because effectively the inhibition (or activation) changes the affinity (i.e. K_M) of the substrate to the active site of an enzyme. The simultaneous control by the V_{max} and K_M could be explained by the above mechanisms of non-competative and competitive inhibition that take place at the same time in vivo.

Interesting are the physical aspects of this way of the optimal control implementation into Michaelis-Menten formal scheme. For example, from the comparison of Fig.6.2.5H and Fig.6.2.7B it is also seen that curve “a” in Fig.6.2.7B corresponds most closely to the zero value

curve of the first integral $H^*(s,u)=0$, $u>0$, in Fig. 6.2.5H. In double reciprocal coordinates, Fig.6.2.7C, the dotted line represents the Lineweaver-Berk plot for scaled ($V_{max}=1.0$ and $K_M=1.0$) Michaelis-Menten process. One can see that this line is a tangent to the curve "a" which corresponds to an optimal curve when the Hamiltonian equals to zero (so the first integral equals to zero as well). The similar comparison for logarithmic form of the cost, Fig. 6.2.6B,D and Fig.6.2.8A,B, accordingly, shows the similar result for curve "a", what means that energy-like first integral (because it concedes with Hamiltonian expression in the case of the Pontryagin maximum principle) is, in fact, the Hamiltonian function *H*. From the mechanical point of view, the Hamiltonian and energy cannot be negatively defined. On the other hand, from the Pontryagin maximum principle the Hamiltonian function for the optimal trajectory is maximal, and in our case it equals to zero.

In the case of optimal control by the Michaelis constant, from the comparison of Fig. 6.2.9E (Fig.6.2.11B in the case of logarithmic cost) and Fig.6.2.10A (Fig.6.2.11C in the logarithmic penalty case) correspondingly, it can also be seen that curve "a" in Fig.6.2.10A (Fig.6.2.11C in logarithmic case) corresponds to the zero value of the Hamiltonian H(s,u). In the double reciprocal plot, Fig.6.2.11D (Fig.6.2.13B,D in logarithmic case), the corresponding curve "a" is the closest to the ideal dotted line for pure Michaelis-Menten kinetics (without control) scaled by $K_M=1.0$ and $V_{max}=1.0$, also. As well as, the continuation of these curves from data points closed to the equilibrium point until crossing with the vertical axes $1/V$ gives the V_{max} values equal to 1.0 (Fig.6.2.11D), as was initially set in the system (6.2.55) or system (6.2.56) in the case of logarithmic form of the cost. It is topologically clear, that near the equilibrium the picture for logarithmic form of cost poorly differs from those for the square-law cost. The same picture is observed for the trajectories $H^*=0$ (corresponding to zero-value of the first integral) when logarithmic approximation is applied to both for the metabolic control cost $T(u)$, as well as for the metabolic/thermodynamic losses (costs for deviation from equilibrium s_{eq}) expressed by $G(s)$, Fig.6.2.14. It also gives the Michaelis constant close to the value K_M

=1.0, as well as maximal reaction velocity V_{max} , also close to unit, as is initially set in the system of equations (6.2.60) for numerical calculations.

All the plots discussed above show one, among the family of these curves, truly optimal curve matching to the first integral that corresponds to the Pontryagin maximum principle *H*=0*. It is also typical that such curves in the plot of double reciprocal coordinates are tangent to the line directly corresponding to standard Michaelis-Menten scaled system. Moreover, its continuation until crossing with the vertical axes *1/V*, as is known, gives two values: the Michaelis constant K_M and the maximal reaction velocity V_{max} . As it is clear from the figures, if to determine these values from the corresponding curve (*H*=0*) in reciprocal coordinates, the K_M and V_{max} are close to the values initially set in cost for control, which confirms the correctness of the approach in the case of the introduction of control.

Thus, the introduction of the optimal control does not also change the topology of kinetic variables on standard plots. Furthermore, in the optimal case when the Hamiltonian function (the first integral) is equal to zero *H*=0*, the results of optimal control introduction quantitatively agree with the well-known results as one can see from double reciprocal plots. The condition *H*=0* that follows from the Pontryagin maximum principle (Pontryagin et al., 1962), is needed for problem of the maximization of the Hamilton functions. In mechanics, and, generally in physics, the physical sense of the Hamiltonian is energy. Taking into account that the potential *G(s)* describing the metabolic losses, has direct energetical meaning related to thermodynamic form of penalty of being not in the equilibrium state (particularly in logarithmic approximation), it is possible to suggest that the first integral has the energetical sense, too, which does not contradict to physical logic. The way in what the optimal control can be applied to the Michaelis-Menten kinetics creates good background to use it for the study more complicated metabolic chains.

At the same time, the introduction of optimal control expands formally the conceptual opportunities of the consideration and the interpretation of the experimental data. It does not simply state that the control is possible by the Michaelis constant or the maximal reaction

velocity or both, but that this control is carried out in an optimal way toward minimal metabolic expenditures for the regulation. Thus, the introduction of control into enzyme kinetics extends (in a sense related to thermodynamic one) the standard kinetics views and the suggestion about the enzyme control of activity in the cell.

Regarding to the consideration of two optimal control methods (Pontryagin maximum principle and direct variational Lagrange multipliers method) used in this section we should note the following. The last method seems to be also interesting with respect that the Lagrange multipliers (momenta) can be singled out and it is possible to concentrate on the direct relation of the substrate concentrations to the control parameters u or v , when the control is introduced by the maximal reaction velocity or the Michaelis-Menten constant in equations (6.2.33, 6.2.34, 6.2.50).

Similar to the static optimal control problem widely explored in economical applications, the dynamic Lagrange multipliers (or costate variables) assign the marginal increase (or decrease) in terms of metabolic utility (or metabolic profits) if there is an alteration in the state variables. In this sense, the scheme of variational approach or the Pontryagin maximum principle is to build a set of costate variables that evaluate the influence on the state variables in the manner that maximizes the total value of the Hamiltonian.

Thus, the introduction of optimal control into the standard enzyme kinetics scheme (Michaelis-Menten) can be considered by employing direct Lagrange variational approach and the Pontryagin maximum principle to the optimal control problem formulated. As a conclusion, we can state that three considered ways (by maximal reaction velocity V_{max}, by the Michaelis constant K_M and simultaneously by V_{max} and K_M) of introduction of optimal control into the Michaelis-Menten scheme of the enzyme kinetics can be considered without any contradictions to the classic enzyme kinetics results. Described optimal control models are biochemically acceptable representations of simple enzyme kinetics, moreover, they broaden the interpretation of the pattern of regulation. Extended from the Michaelis-Menten equation, the dynamical systems can be obtained as a result of the Euler-Lagrange equations or canonical equations. The

real trajectories can be chosen under physical demand of non-negativity of first integral (energy) and the Pontryagin maximum principle, when Hamiltonian function is equal to zero for the optimal trajectory. The results on different ways of enzyme activity regulation can be also employed to get a snapshot of the different types of regulation contributions. A good agreement between optimal control results and classical enzyme kinetics in Lineweaver-Burk plots can be seen.

6.3 Optimal control and multi-enzymatic kinetics

6.3.1 Optimal control method in modelling of multi-enzymatic chains

Optimal control approach is widely applied to study the regulation of homeostasis (Pörtner and Schäfer, 1996; van Riel et al., 2000; Visser et al., 2004). There are a number of the optimal control models based on the Michaelis-Menten kinetics that in relation to modelling, discuss feedback control - chemostat models or batch-kinetics models (Lenas and Pavlou, 1995; Van Impe and Bastin, 1995; Rahman and Palanski, 1996; Cacik et al.,2001; Sengupta and Modak, 2001; Keesman and Stigter, 2002; Srinivasan et al., 2003; Valentinotti et al., 2003; Smets et al., 2004, Gadkar et al., 2006; Mohseni et al., 2009; Yüzgeç et al., 2009), with the perspective of overall output control in biotechnological production. Optimal control methods have shown to be useful in the control of different treatment optimisation (Liang et al., 2008; Itik et al., 2009; Chávez et al., 2009), and blood glucose level regulation (Eren-Oruklu et al., 2009; Acikgoz and Diwekar, 2010).

However, even from the perspective of regulation in the short chains/fragments of overall cellular metabolic network, it is essential to investigate the optimal aspects of regulation within these fragments as an optimal control problem. Following this, the developed experience could be extended to a description or to OC metabolic engineering to optimise metabolic regulation *in vivo;* from the perspective of minimising metabolic expenses for an optimal substrate/product output regulation, and thermodynamic optimisation by processing at the

minimum of thermodynamic potentials. In this sense glycolysis is one of the basic metabolic pathways and further studies are required to revise and extend the understanding of optimal controllability, comparing results with alternative regulation approaches where appropriate.

It is well known that enzymes are structures that affect the rate of chemical reactions without shifting the thermodynamic equilibrium, see for example, Cannon, 2002. The models in this section employ the glycolysis model as one of the basic models (good working examples) in metabolic network kinetics. The goal of the present consideration is to illustrate that the spectrum of dynamical behaviour after the introduction of optimal control into this kinetics does not change the topology of the main, metabolically sensible and steady state/equilibrium taking place within the system without explicit control. Optimal control interpretation of the extended model in terms of metabolic/catabolic costs/losses is another area of focus in this section.

6.3.2 Optimal control introduction into the Bier and coauthors–Volkenstain (BTKW-V) model of glycolysis

The results in previous sections encourage one to apply the proposed approach to study a more complicated system. It would be interesting to consider a well-investigated pathway of biochemical reactions, and when the behaviour in this pathway is imposing the requirement of optimal control on the pathway regulation. A good example could be the model of glycolysis, well-investigated from many aspects including biochemical, evolutionary and mathematical. It is also known, that glycolysis contains more than 20 intermediate stages (Neilsen et al., 1997; Heinrich et al., 1997) and some of them are shown on the diagram below:

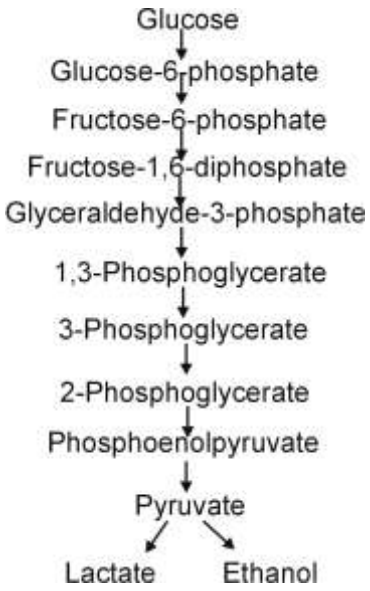

Fig.6.3.1 Metabolic glycolytic pathway: FBP – Fructose1,6bis-phosphoglycerate is inhibited by a reaction of phosphorfructokinase (PFK); combined with hexokinase (HK), which needs ATP, see Higgins, 1967, or Selkov, 1968; or Bier et al., (1996, 2000). This reaction is incorporated in x_1.

The system of kinetic equations, first proposed by Higgins, 1967, and Selkov, 1968, can be taken as a formal mathematical model of glycolysis. This model was modified by Bier and co-authors in Bier et al., (1996, 2000) for the glycolytic dynamics in a yeast cell to the following dynamical system. Different modification was also described by Volkenstain in (Volkenstain, 1989):

$$\begin{aligned} \dot{x} &= V_{in} - k_1 xy; \\ \dot{y} &= \nu k_1 xy - k_p \frac{y}{K_M + y} \end{aligned} \quad , \qquad (6.3.1)$$

where x is the concentration of glucose (fructose-6-phosphate), y is the ATP concentration, V_{in} represents the constant inflow of glucose, k_1 represents the phosphofructokinase activity, K_M is the Michaelis constant for pyruvate kinase (PK), ν is the stoichiometric ratio; ν=1 the system described by Volkenstain, (Volkenstain, 1989) and ν=2 for the model described by Bier and co-authors (1996), BTKW-model. In Fig.6.3.2 the numerical solutions are illustrated for the Volkenstain and the Bier systems (with parameters described in Bier et al., 2000); one can see topological identities of these two models, therefore we will designate as the BTKW-V model.

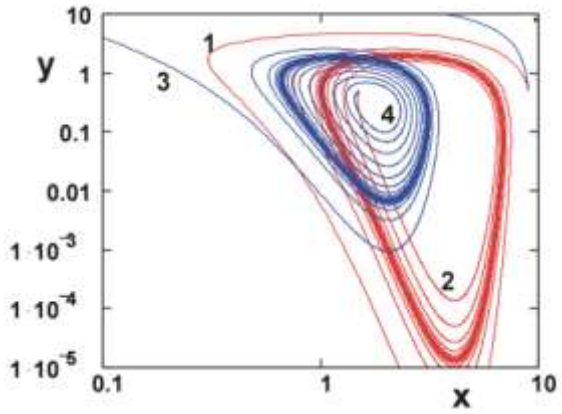

Fig.6.3.2 The numerical solutions of system (6.3.1) in double logarithmic coordinates. Red curves - the system described by Volkenstain, (1989) (stoichiometric ratio ν=1). Blue curves - model described by Bier and coauthors (Bier et al., 2000), (stoichiometric ratio ν=2). $K_M=2$, $k_1=0.5$, $k_p=3.5$, $V_{in}=0.250$. Curve "1", $x(t_0)=9.0$, $y(t_0)=0.5$. Figure adopted from Moroz, 2011.

As it was pointed out in Bier at al., 1996, model (6.3.1) has only limit cycle steady state in the range of constants employed by authors, which gives the oscillation trajectories, Fig.6.3.2. The spectrum of steady states and conditions of this system was also studied in detail by Volkenstain, 1989. Therefore the interest of our consideration was to study the robustness of this limit cycle at the OC by the rate constants.

6.3.3 Direct optimal control outline

To study the effect of the OC implementation with respect to the control of system behaviour, we used the Pontryagin maximum principle in the way as it was used within Michaelis-Menten system, Section 6.2. Let us formulate the problem of the introduction of optimal control into the BTKW-V model (6.3.1) by k_1 and k_p. Then the constrain system of equations will be

$$\begin{aligned} \dot{x} &= V_{in} - (k_1 - u)xy; x(t_0) = x_0 \\ \dot{y} &= 2(k_1 - u)xy - (k_p - v)\frac{y}{K_M + y}; y(t_0) = y_0 \end{aligned}. \qquad (6.3.2)$$

Let us consider the optimal control problem for this system, taking into account the metabolic losses for control $T(u,v)$ and the metabolic losses for not being in thermodynamic steady state/equilibrium as $G(x,y)$. The minimising functional will be similar to (6.2.57)

$$\int_{t_0}^{\tau} G(x,y) + T(u,v)\,dt \to \min, \tag{6.3.3}$$

and the Hamiltonian function

$$H = -G - T + p_x \cdot V_{in} - (k_1 - u)xy + p_y \cdot \left(2(k_1 - u)xy - (k_p - v)\frac{y}{K_m + y} \right). \tag{6.3.4}$$

Then the canonical system will be

$$\begin{aligned}
&\dot{x} = V_{in} - (k_1 - u)xy; x(t_0) = x_0 \\
&\dot{y} = 2(k_1 - u)xy - (k_p - v)\frac{y}{K_M + y}; y(t_0) = y_0 \\
&\dot{p}_x = \frac{\partial G}{\partial x} + p_x(k_1 - u)y - 2p_y(k_1 - u)y; p_x(\tau) = 0 \\
&\dot{p}_y = \frac{\partial G}{\partial y} + p_x(k_1 - u)x - 2p_y(k_1 - u)x + p_y(k_p - v)\frac{K_M}{(K_M + y)^2}; p_y(\tau) = 0 \\
&\frac{\partial H}{\partial u} = -\frac{\partial T}{\partial u} + p_x xy - 2p_y xy = 0 \\
&\frac{\partial H}{\partial v} = -\frac{\partial T}{\partial v} + p_y \frac{y}{(K_M + y)} = 0
\end{aligned} \tag{6.3.5}$$

By using the last two equations it is possible to reduce the canonical system to 4 equations – for 2 state and 2 costate variables. For the square-law cost for the deviations of the constants k_1 and k_p from optimal k_1 and k_p and square-law form of $G(x,y)$ and $T(u,v)$can be used:

$$G(x,y) = \frac{k(x - x_{eq})^2}{2} + \frac{k(y - y_{eq})^2}{2}, \quad T(u,v) = \frac{u^2}{2} + \frac{v^2}{2}. \tag{6.3.6}$$

Finally we can get the system

$$\begin{aligned}
&\dot{x} = V_{in} + (p_x - 2p_y)x^2y^2 - k_1xy; x(t_0) = x_0 \\
&\dot{y} = -2(p_x - 2p_y)x^2y^2 + 2k_1xy + \frac{p_y y^2}{(K_M + y)^2} - \frac{k_p y}{K_M + y}; y(t_0) = y_0 \\
&\dot{p}_x = \frac{\partial G}{\partial x} - xy^2(p_x - 2p_y)^2 + k_1 y(p_x - 2p_y); p_x(\tau) = 0; p_y(\tau) = 0 \\
&\dot{p}_y = \frac{\partial G}{\partial y} + x^2 y(p_x - 2p_y)^2 - \frac{p_y^2 K_M y}{(K_M + y)^3} + k_1(p_x - 2p_y)x + \frac{K_M k_p p_y}{(K_M + y)^2};
\end{aligned} \tag{6.3.7}$$

Numerical solutions of the system show the existence of the torus-like steady near former two-dimensional limit cycle. Fig.6.3.3 shows the trajectories for state variables *x,y*; momenta p_x, p_y (costate variables), and control *u*,*v* for system (6.3.5).

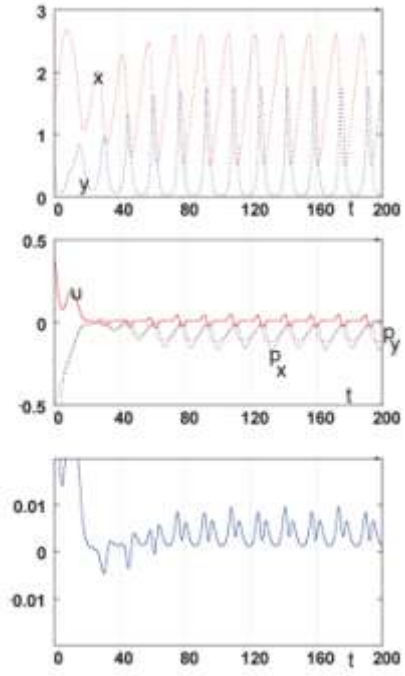

Fig.6.3.3 Trajectories for state variables *x,y*; momenta (costate variables, p_x, p_y and control *u*,*v* for system (6.3.7). $x(t_0)=1.5$, $y(t_0)=0.5$, $p_x(t_0)=p_y(t_0)=-0.01$, $V_{in}=0.250$, $K_M = 2$, $k_1=0.5$, $k_p=3.5$, $V_{in}=0.250$, potential ($k=0.01$). Figure adopted from Moroz, 2011.

The limit cycle phase plots, which characterise the *6*-dimensional phase space of *2* state variables, *2* co-state variables and *2* control variables, together *6* variables, is illustrated in Fig.6.3.4 for the system (6.3.7) at square-low potential and at the values of constants, specified directly in the figure. The plots are shown as a graphical matrix, where just a half of it, as it is shown in figure, can fully characterise the 6 dimensional limit cycle. The first row contains 2 dimensional graphs for the vertical *x* coordinate versus all other coordinates (e.g. *y*, p_x, p_y, *u*, *v*) spanned horizontally. The second row contains vertical (*y*) coordinate against p_x, p_y, *u* and *v*; *y* against *x* already is plotted in the first row. Effectively, the combination of any pair of coordinates can be found using the designations for correspondent row (at first left plot in the row) and for the correspondent column (at the bottom at any column). For example, the top row and right column illustrates the phase plot in *x**v* diagram.

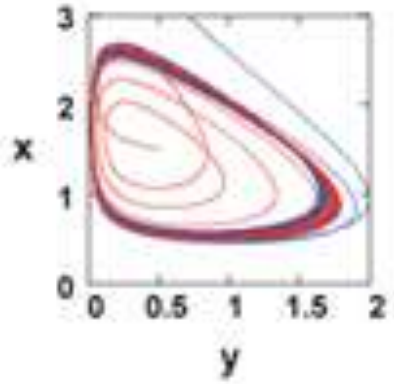

Fig.6.3.4 The behaviour of the limit cycle (6.3.7) in the phase space by projection of it into x,y 2-dimensional plane. The red trajectories are for starting values $x(t_0)=1.5$, $y(t_0)=0.5$. Blue curve, for $x(t_0)=4.0$, $y(t_0)=0.1$. Constants were chosen following BTKW-V model (Bier et al., 1996; 2000); $V_{in}=0.250$, $k_1=0.5$, $k_p=3.5$; $K_M=2.0$. Figure adopted from Moroz, 2011.

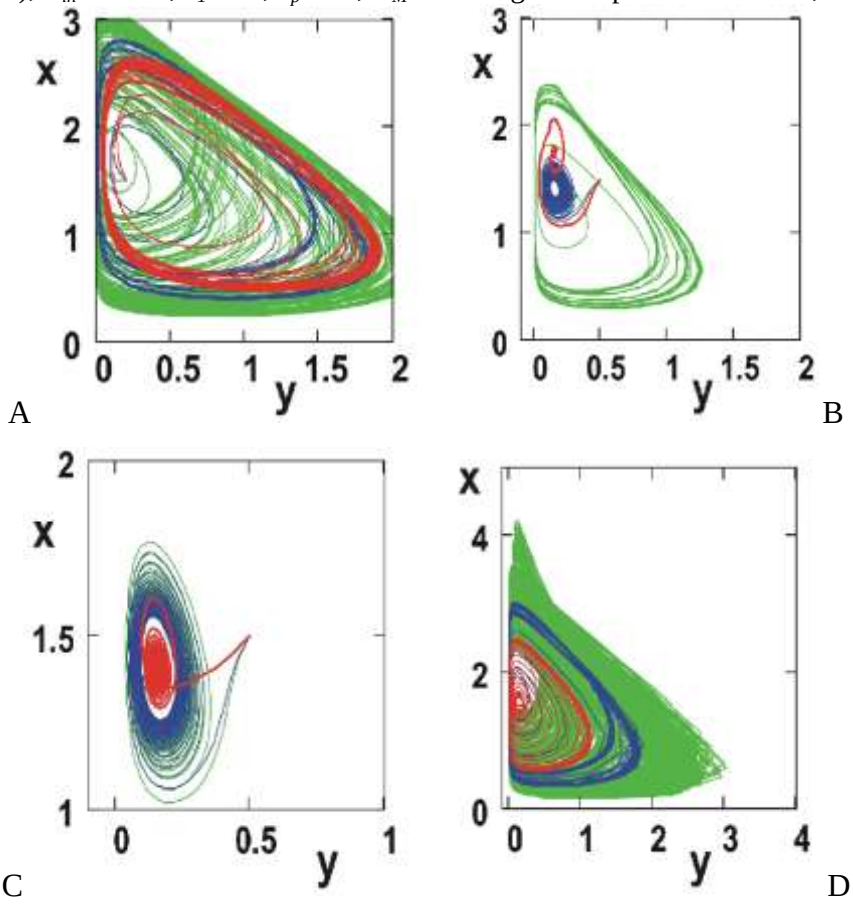

Fig.6.3.5 The phase-plot of the limit cycle illustrating the effect of different constants in the system (6.3.7) on the limit cycle. A, the effect of V_{in} (green colour $-V_{in}=0.1$; blue – $V_{in}=0.2$; red – $V_{in}=0.3$; other constants ($k=0.01$, $x_{eq}=1.3$, $y_{eq}=0.2$, $k_1=0.5$, $v_{eq}=3,5$, $K_M=2.0$). B, the effect of x_{eq} (green colour $-x_{eq}=1.2$; blue – $x_{eq}=1.5$; red – $x_{eq}=2.0$; other constants ($V_{in}=0.1$, $k=0.01$, $y_{eq}=0.2$, k_1=0.5, $v_{eq}=3,5$, $K_M=2.5$). C, the effect of y_{eq} (green colour $-y_{eq}=0.01$; blue – $y_{eq}=0.1$; red – $y_{eq}=1.0$; other constants ($V_{in}=0.1$, $k=0.1$, $x_{eq}=1.5$, $k_1=0.5$, $v_{eq}=3.5$, $K_M=2.5$). D, the effect of K_M (green colour $K_M=1.8$; blue – $K_M=2.0$; red – $K_M=2.5$; other constants ($V_{in}=0.1$, $k=0.01$, $x_{eq}=1.5$, $y_{eq}=0.2$, $k_1=0.5$, $v_{eq}=3.5$). Figure adopted from Moroz, 2011.

The effect of a number of constants is illustrated in Fig.6.3.5 for system (6.3.7); the phase plot for control variables is not included. The plots are shown as matrixes, similar to Fig.6.3.4.

As one can see from Fig.6.3.5A, an increase in V_{in} in the range which shown in figure reduces the limit cycle. A span in the value of x_{eq} through the equilibrium point of the system (6.3.7) leads to the collapse of the limit cycle, Fig.6.3.5B. Similarly, the span in y_{eq} through the equilibrium point of the system also leads to the collapse of the limit cycle, Fig.6.3.5C. Fig.6.3.5D indicates that the increase in K_M (inhibition) leads to a reduction in the size of the limit cycle. However, a simultaneous change of the parameters of the system (6.3.1/6.3.7) in the effect of the robustness (stability of the equilibrium points of the system) will be illustrated further in this section.

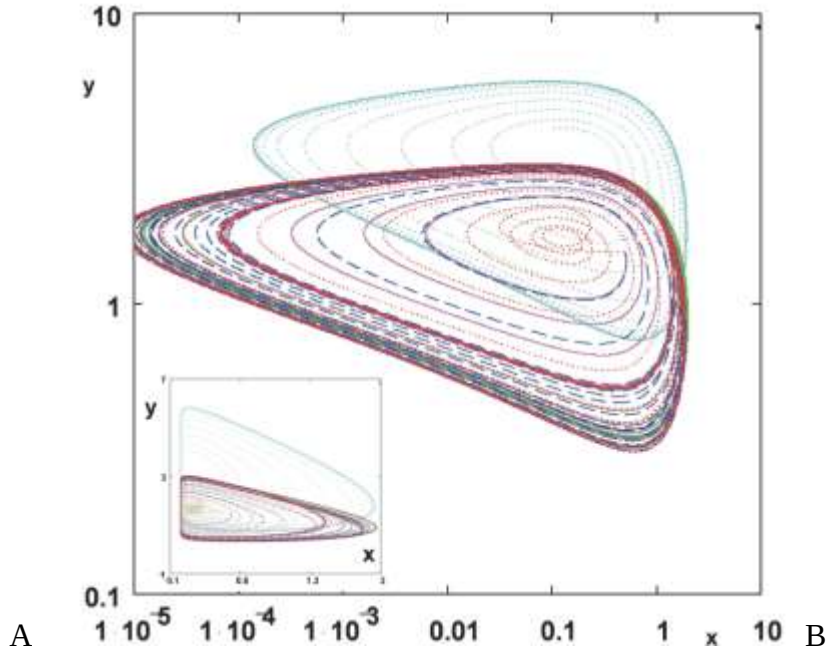

Fig.6.3.6 The comparison of the limit cycle in the phase plane of state variables for different systems. The limit cycles in the logarithmic coordinates, incert in normal coordinates for comparison. Cyan curve - original system (6.3.1) without OC; magnolia curve – system (6.3.7) with the OC introduction, no potential term ($k=0$), initial momenta ($p_x=p_y=0.0$); green curve - system (6.3.7) in the presence of OC, no potential term ($k=0$), startin momenta $p_x=p_y=-0.5$; blue curve – OC, potential ($k=0.01$), initial momenta ($p_x=p_y=0.0$); red dashed curve – OC, potential term ($k=0.01$) and initial momenta $p_x=p_y=-0.5$. Constants were chosen following Bier et al., 1996; $V_{in}=0.10$, $k_1=0.5$, $k_p=3.5$; $K_M=2.0$. The axes are as in Fig.6.3.2. Figure adopted from Moroz, 2011.

It can be useful to illustrate the comparison of the effects on the limit cycle in normal and logarithmic coordinates, Fig.6.3.6. While the normal coordinates clearly show what is happening at large values of the state variables (Fig.6.3.6A), the logarithmic coordinates (Fig.6.3.6B) efficiently illustrate what is happening at the very low values of the state variables. Particularly, for the systems (6.3.1) and (6.3.7), one can see that implementation of the optimal control and demonstrating that a quadratic form of the penalties does not significantly change the character and robustness of the limit cycle. However, by using the standard method we are limited in analysing the effects of the parameters on the character of stability in a wide range.

6.3.4 Monte-Carlo method to study the robustness

To study the character of the equilibrium points in a wider range of parameters, one can span these parameters in a range, keeping all others at certain values, as illustrated in Fig.6.3.7. One can also see the existence of a limit cycle (designated as "o") in quite a wide range of parameters. However, it does not show the complete picture of the parameter's role in the equilibrium.

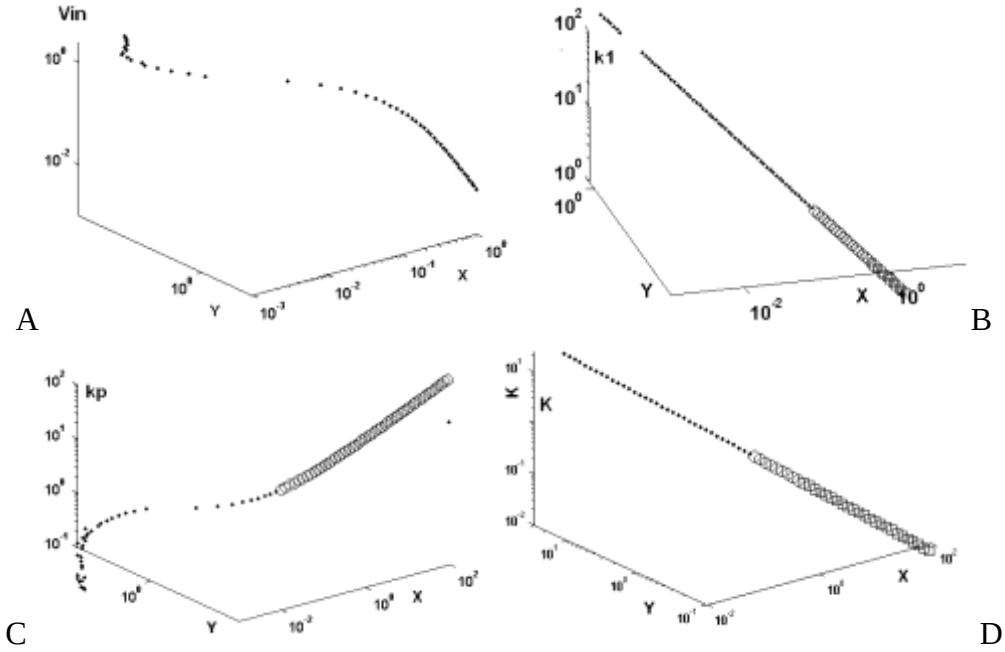

Fig.6.3.7 The illustration of parameter scanning in model (6.3.1) at V_{in}*=0.25*, k_1*= 0.5*, k_p*= 1.0*, K_M*= 1*. A, scanning V_{in}; B, scanning k_1; C, scanning k_p; D, scanning K_M. Designations: dots – stable steady state, circles – limit cycles. Figure adopted from Moroz, 2011.

On the other hand, the stability of the system can be studied in the following way: one can generate a set of random combinations of all the parameters (V_{in}, k_1, k_p and K_M) employing the Monte-Carlo method for statistical investigation of the equilibrium points of this system (6.3.1), with the purpose to compare to the extended by the OC system. The Monte-Carlo simulation results are shown in Fig.6.3.8 at range of parameters (V_{in}, k_1, k_p and K_M) are much more informative. From Fig.6.3.8 one can see main characteristic states (the designations are shown in Fig.6.3.8F). One can also clearly see borders between main areas, which indicating the transitional surfaces between areas of different types of equilibrium. Results, obtained by this method, can be considered as being in good agreement with analytical results from Bier and coauthors, 1996, 2000.

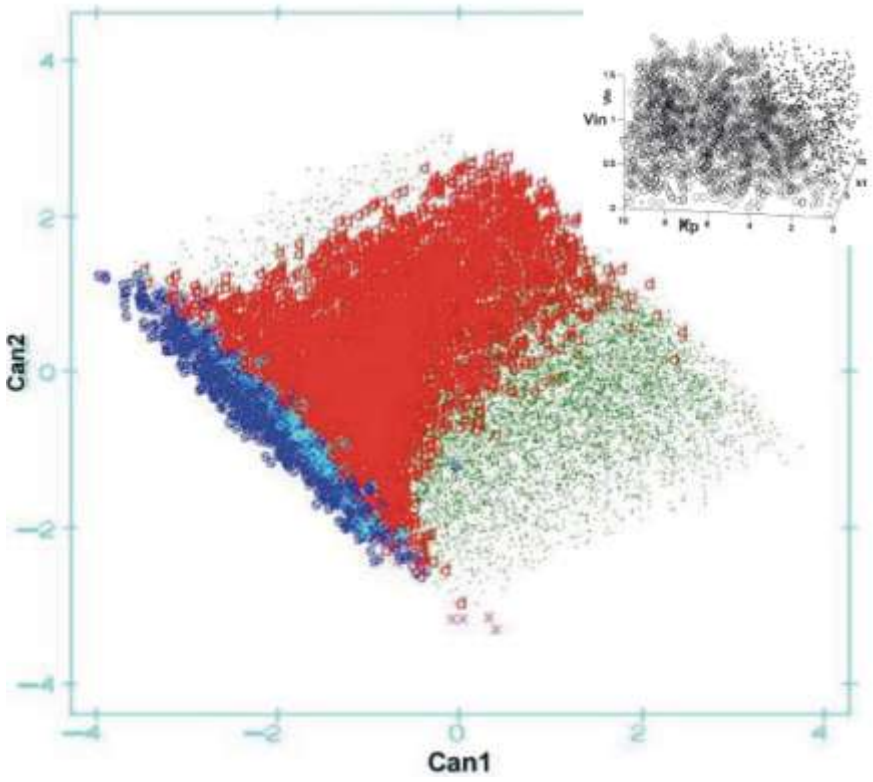

Fig.6.3.8 The results of equilibrium simulation study of the system (6.3.1), described by Bier and coauthors, [117, 118] for the range of parameters ($V_{in}=10^{-4}$-1.5; $k_1=0$-10; $k_p=0$-10; $K_M=0.001$-10.0). 2D scatter plot in the plane first two canonical variables, $K_M=1.0$. Insert - 3D scatter plot, $K_M=1.0$; C, $K_M=1.0$-10.0 (inhibition); The equilibrium point designation: "." – stable node, ◊- stable focus, "x" saddle, "o" unstable focus, □ - unstable node, ⌂ limit cycle. E, dataset in 2D plane of 2 first canonical variables, designations: "."(green) – stable node, "d"(red)- stable focus, "x" saddle, "o"(cyan) unstable focus, "s"(blue) - unstable node. Can1, Can2 –the first and second canonical variable. Figure adopted from Moroz, 2011.

Well known that different equilibrium scenarios follow from the spectrum of eigenvalues of the Jacobian matrix at an equilibrium state, see Fig. 6.3.8F for a 4-dimensional system. The transitions between qualitatively different states (bifurcations) are also of immense interest because they indicate qualitative changes in the system dynamics, suggesting that a closer look on the robustness and equilibrium of the system is needed.

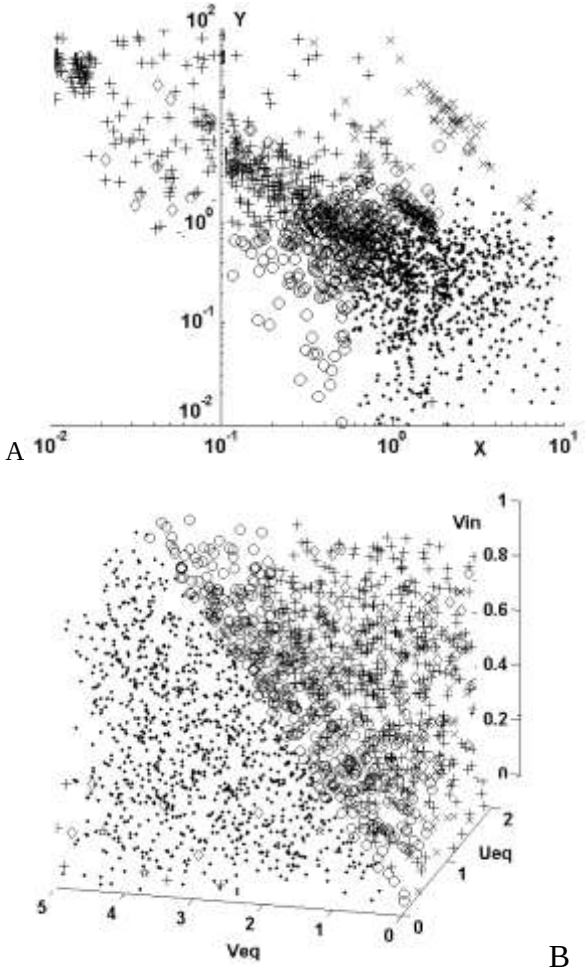

Fig 6.3.9 Results of numerical calculations of (6.3.7) when the OC in implemented by k_1 and k_p. A, the scatterplot in plane of state variables x and y ($k=0$) and B, 3D plot no potential ($k=0$). The parameter ranges in this simulation are $V_{in}= 10^{-7}\text{-}1$; $x_{eq}=0.0\text{-}0.2$; $y_{eq}=0\text{-}2$; $k=0\text{-}2$; $k_p=0\text{-}5$; $K_M=1$; $k= 0\text{-} 1.0$. Designation of equilibrium points is from Fig.6.3.8. Figure adopted from Moroz, 2011.

As it is possible to see, the scatter plots, shown in Fig.6.3.9, qualitatively reproduce plots for the reduced Bier model, Fig.6.3.8, however the difference is in the character of stability. This is not obvious because the model is significantly changed, as can be seen from

Eqs.(6.3.1) and (6.3.7). One can see that with different fixed levels of potential Fig.6.3.9 (B, *k=0*; C, *k=0.1* and D, *k=1.0*) the 3D scatter plot of the dataset becomes more not-transparent (Fig. 6.3.9B-D) in the sense of the different character of equilibrium areas. Fig. 6.3.10A shows that when the Monte-Carlo method is applied to randomly generate the values of the variable *k* (potential weight) and K_M, the scatter plot of dataset is not transparent. However, by applying the canonical correlation analysis (CCA) , Hotelling, 1936, method to the dataset it is possible to distinctly observe the regions of stability in the plane of two first canonical variables, Fig. 6.3.10B.

Parameter	Can1	Can2
V_{in}	1.2	-1.6
k_1	0.1	0.5
k_p	-0.3	-0.3
K_M	0.4	0.2

Table 6.3.1 The raw canonical coefficients for first two canonical variables (Can1, Can2) for system (6.3.1).

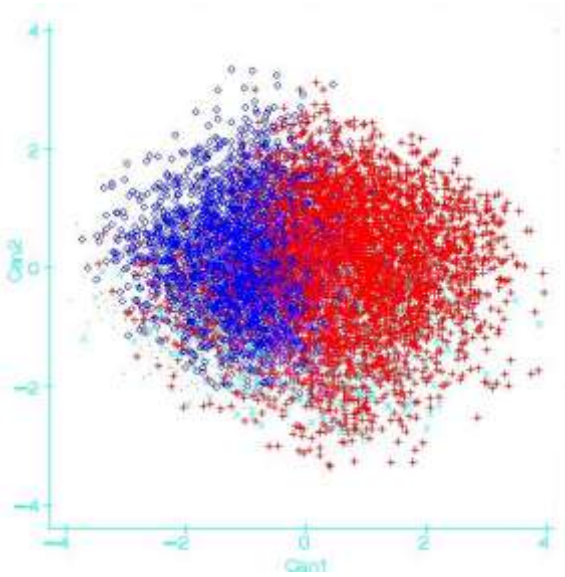

Fig.6.3.10 Results of numerical calculations of (6.3.7) when the OC in implemented by k_1(changed to *u*) and k_p(changed to *v*). B, scatterplot of dataset of 10K points in the plane of first two canonical variables, Can1, Can2, generated by Monte-Carlo method at the range of parameters: $V_{in}=10^{-6}$ *-1.0*; x_{eq}*= 0.01-10.0*; y_{eq} *=0.01 - 10.0*; k_1*=0.01-10.0*; k_p*=0.01- 10.0*; K_M*= 0.01-10*; *k=0.0-1.0*. The equilibrium point designation as in Fig.6.3.8. Figure adopted from Moroz, 2011.

In Table 6.3.1 the results of applying of the Monte Carlo method (Metropolis and Ulam, 1949) that we used to study the character of stability of the equilibrium points (*x*,*y*) for system (6.3.1) shows the impact of the system parameters on stability. About 10 thousands

combinations of parameters in the range (see, Fig.6.3.9) were generated, and the frequency ratio was calculated: (./d/o/s/x) – *0.58/0.33/0.03/0.06/0.0004*. The first three eigenvalues obtained, were *0.8345*, *0.0766* and *0.003* with F-statistics values *669*, *121* and *11* correspondingly, and the probabilities levels less than *0.0001* each. As it is shown in Table 6.3.1, the raw canonical coefficients for the first canonical variable, Can1, indicate that the classes differ most widely on the linear combination of the centered variables $1.20*V_{in}+0.10*k_1-0.26*k_p+0.38*K_M$. Thus the results indicate the crucial role of V_{in} on the character of stability.

Results in Fig.6.3.9 relating to the existence of different areas of stability, qualitatively agree with the numerical results for system (6.3.1), which is without the OC, Fig.6.3.8. The cooperative form indicates the goal of the optimal adaptive regulation that in the metabolic network could strengthen the rigidity of the regulation around macroscopically important state.

Parameter	Can1	Can2
V_{in}	2.2	-1.1
x_{eq}	0.05	0.01
y_{eq}	-0.005	-0.1
k_1	0.02	0.18
k_p	-0.3	0.15
K_M	0.2	0.2
k	0.5	-0.7

Table 6.3.2 Raw canonical coefficients for first two variables (Can1, Can2) when the OC by k_1 and k_p is implemented.

To study the stability character of the points of equilibrium (x, y, p_x, p_y) of the system (6.3.7), when the control variable u and v are eliminated, the Monte Carlo method was also employed. 5 thousand random combinations of parameters were generated, and the relative proportions (./+/o/x) were correspondently *0.045/0.564/0.334/0.045*. The 4 first eigenvalues were *0.86, 0.11, 0.04* and *0.005* with the Fisher statistics F values *242, 67, 35* and *8.9* with the corresponding probabilities less than *0.0001* each. As one can see from Table 6.3.2 for the raw canonical coefficients, the first canonical variable, Can1, shows that the linear combination of the centered variable $Can1=2.2*V_{in} - 0.05*x_{eq} - 0.005*y_{eq} + 0.02*k_1 -0.3*k_p + 0.3*K_M + 0.5*k$ separates the areas with different character of stability most effectively.

Finally, one can conclude that the first canonical variable Can1 explains more than 75% of total variability. It is mainly laded by V_{in} and k, which means that the rate inflow and the coefficient in the term of energetical penalty k for alteration from a steady state play the main role in determination of the robustness of the steady state. The Michaelis constant K_M and the rate constant k_p play the minority roles.

6.3.5 Optimal control by K_M in the BTKW-V model of glycolysis

The optimal control implementation into the Bier et al model (1996, 2000) of glycolysis by K_M can be done in a similar way, by replacing K_M with u in (6.3.1) and apply functional in the form

$$\int_{t_0}^{\tau} G(x, y) + T(u)\, dt \to \min \tag{6.3.8}$$

and the dynamical constrains in the form

$$\dot{x} = V_{in} - k_1 xy; \dot{y} = 2k_1 xy - k_p \frac{y}{u + y}. \tag{6.3.9}$$

Then employing the Pontryagin maximum principle we could write the canonical system.

$$\begin{aligned}
&\dot{x} = V_{in} - k_1 xy; x(t_0) = x_0 \\
&\dot{y} = 2k_1 xy - k_p \frac{y}{u + y}; y(t_0) = y_0 \\
&\dot{p}_x = \frac{\partial G}{\partial x} + (p_x - p_y) k_1 y; p_x(\tau) = 0 \\
&\dot{p}_y = \frac{\partial G}{\partial y} + (p_x - p_y) k_1 x + \frac{k_p p_y u}{(u + y)^2}; p_y(\tau) = 0 \\
&\frac{\partial H}{\partial u} = -\frac{\partial T}{\partial u} + \frac{k_p p_y y}{(u + y)^2} = 0
\end{aligned} \tag{6.3.10}$$

The results of numerical calculations are shown in Fig.6.3.11, when the random combinations of parameters V_{in}, k_1, k_p, x_{eq} and y_{eq} are generated by the Monte-Carlo method, Fig.6.3.11A-B.

We studied stability of the real roots (x, y, p_x, p_y, u) of the canonical system for the optimal control problem (6.3.10), using the Monte-Carlo method when square form of cost was

applied to *G(x,y)* and *T(u)*, similar to (6.3.6). 5K points were generated, and relative frequency ratio for the equilibrium points designated accordingly to Fig.6.3.8 as (./+/o/p) was – *162/1950/2958/17*. The first three eigenvalues were *0.7881, 0.0544* and *0.0075* with the Fisher statistics F values *173.83, 25.98* and *7.6* the probabilities less than *0.0001* each. As shown in Table 6.3.3, the raw canonical coefficients for the first canonical variable, Can1, show that the classes differ most widely on the linear combination of the centered variables $2.5*V_{in}$-$0.1*x_{eq}+0.1*y_{eq}+0.2*k_1-0.37*k_p+0.37*k_1+1.0*k$.

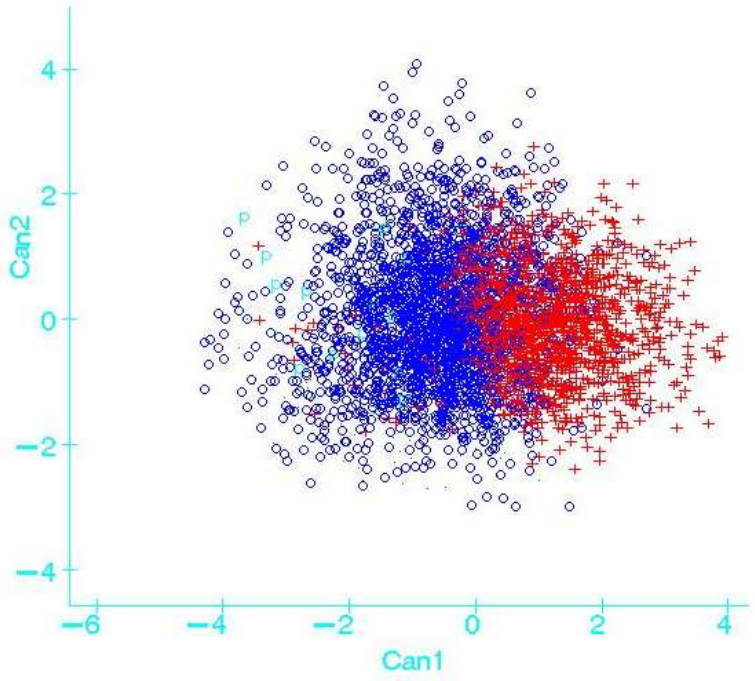

Fig.6.3.11 Optimal control by the Michaelis constant, K_M; Monte-Carlo numerical experiment. The scatterplot of dataset for the range of randomly distributed parameters: $V_{in}=10^{-6}$ – *1.0*, k_1= *0.01-10.0*; k_p=*0.01-10.0*, x_{eq}=*0.01-10.0*; y_{eq}= *0.01-10.0*; K_M= *0.001-10.0*; *k=0.00001 - 1.0* from equation (6.3.6). Canonical discriminant analysis of dataset (5K points) shown in the plane of first two canonical variables, Can1, Can2. The equilibrium point designation as in Fig.6.3.8. Figure adopted from Moroz, 2011.

Parameter	Can1	Can2
V_{in}	2.5	-0.25
x_{eq}	-0.1	0.2
y_{eq}	0.1	-0.2
k_1	0.2	0.1
k_p	-0.37	-0.03
K_M	0.37	0.2
k	1.0	-2.0

Table 6.3.3 Raw canonical coefficients for first two canonical variables (Can1, Can2) when the optimal control by the Michaelis constant K_M is implemented, adopted from Moroz, 2011.

The results in Fig.6.3.11 show that the combination of the Monte-Carlo method together with the statistical canonical analysis method can be useful in study of the character of equilibrium points of a dynamic system, also significantly reducing the dimensionality of the data analysed. However, other alternative methods could be useful to establish the relationship between the rate or control parameters and the indexes of equilibrium of characteristic points of a dynamic system.

6.3.6 Optimal control and multi-enzyme kinetics

The introduction of the optimal control into the basic kinetic BTKW-V (Bier et al., 1996; 2000; Volkenstain, 1989) model of glycolysis can been considered by employing the Pontryagin maximum principle to the formulated the OC problem. As a conclusion, one can state that the introduction of optimal control into the basic glycolysis model BTKW-V can be performed without contradicting to the classic glycolysis kinetics results. The 6-dimensional limit cycle in dimensions (x, y, p_x, p_y, u, v), obtained in the OC model, gives the projection to (x,y) plane the standard 2D cycle (see diagram for x,y from Fig.6.3.4), characteristic for modelling glycolitic oscillations. However, the OC consideration in terms of state, costate and control variables extends not only the dimensionality of the system, but also provide the OC interpretable regulatory pattern from the energetical perspective, linked to the maximum energy dissipation principle. Physically speaking, the control variables (related to the rate constants, see Eq.6.3.2) are some variable constants that can be changed by enzymes in a metabolic network. The Lagrange multipliers (or thermodynamic momenta from thermodynamic perspective, could be called the kinetic momenta) can be interpreted as partial energetical costs/penalties for deviation of metabolic mechanism from an optimal one. The extended equations for these variables can been obtained as a result of the Euler-Lagrange equations, or canonical equations in the case of Pontryagin maximum principle, Eqs.(6.3.5), (6.3.7). The real trajectories can be chosen under the demand of equality of the first integral to zero. This is

according to the additional demand of the Pontryagin maximum principle, when the Hamilton function is equal to zero for the optimal trajectory.

The implementation of the optimal control into the BTKW-V model of glycolysis, which is performed in the same methodological way as it was done for pure Michaelis-Menten system, extends the interpretation of the controlability of this system in a general sense. Statistical method canonical analysis has been employed in the study helps to range the influence of model parameters on the stability of near steady state. The introduction of the metabolic penalty G for being in a non-steady state identifies the character of stability (qualitatively illustrated by Fig.6.3.9B,C,D-6.3.10). As one can see from Table 6.3.2 the effect of x_{eq} and y_{eq} on the first canonical variable Can1 is the smallest. The parameter V_{in} influences in the highest way and k (characterising the impact of cost for not being in an optimal/steady state) is second. This effectively means that inflow into this metabolic chain is the most important factor and the metabolic penalty for being in not-steady/optimal state influences the system stability is second, from a physical perspective. Effectively, one can see the similarities to the OC model when the control is introduced by K_M, Table 6.3.3 (as well as from comparison of Fig.6.3.10B and Fig.6.3.11C). The load on the first canonical variable Can1 is highest for V_{in} and second highest for k, what actually there is in agreement with the control by the rate constants k_1 and k_p. The effect of x_{eq} and y_{eq} is smaller, the rate (k_1 and k_p) effect has the same order as for the control by the rate constants. One can note that the V_{in} has the highest load also for the system without control, Table 6.3.1. However, one should bear in mind that this was performed within a specific parameter range, and can change if the range is altered and an systemic analysis is needed. This consideration illustrates that the canonical analysis with the combination of the Monte-Carlo method can be useful when studying the equilibrium and can significantly reduce the dimensionality of the analysis.

Additionally, the method that has been applied to study the stability is of particular interest because of possible universality. The method is based on statistical canonical analysis and can significantly reduce the dimensionality of the parameters' space to analyse for a

complex nonlinear model when the number of parameters in the system is significantly large (>10-20). Such analysis could link the parameters characterising the equilibrium points (the linear combination of the eigenvalues) from one hand and the rate constants parameters incorporated into the model (their linear combinations), ranking these linear combinations with respect to the effect on the variance.

It is well known, that in the long path of substrates and products the metabolic regulation is carried out by so-called "key-points" (for example, Hsu et al., 2000). In the sense of the variability of data when such a path/network is studied it could be statistically interpreted as variables that maximally load the canonical variables. Perhaps this circumstance testifies for the benefit of optimal control and could simplify the formulation of the optimal control problem in case of the more complex chain or a network, for example, glycolysis. In this case the adaptive optimal control by number of mechanisms – competitive, non-competitive, allosteric ones, provides vast flexibility of adaptation of whole network from oscillations to other states with different stability character in optimal manner. One can see that such a selective control could solve a twin problem: making the network or chain flexible and rigid at same time.

Finally, the optimal control introduction into more complicated system like the yeast glycolysis model comparably to the Michaelis-Menten/Monod system, makes the resulting dynamical system more complicated, the stability character of the equilibrium points of the system changes. Then the multivariate statistical methods can also be useful to study the altered system when the optimal control is explicitly presented. The canonical analysis can be a particular useful method to study the character of robustness because of dimension reduction possibility that this analysis simplifies. Canonical spaces, manifolds, other linear and nonlinear combination of variables could be the key-subspaces, of the optimal regulation of the metabolic network or its part. This is when metabolic system needs to be controllably and optimally moved from one qualitative mode of behaviour to another, for example in cases of an optimal therapy. However, statistical studies need to be considered to complete the global vision of the robustness of the models when the optimal control is introduced explicitly.

6.4 Approaches to dynamic OC model of bone turnover

6.4.1 Introduction

Having undertaken the study of behaviour of the models in sections 4 and 5 in different range of rate constants and the optimal control applications to simple models in sections 6.1-6.3, it was decided to apply the method to formulate the OC approach to investigate the bone remodelling models. The interest was dictated by the possibility to alter the BMU behaviour, and to control it in accordance with some criteria. Initially, the model of bone remodelling described in Chapter 4 was considered as a good example for investigation.

To study the effect of the optimal control implementation, the OC method can be used based on the Pontryagin maximum principle. The problem of the introduction of optimal control into model (4.1) by parameter *s* can be formulated in the same way as it was done in (6.3.2-6.3.3). Then the constraint system of equations is

$$\begin{aligned}
\dot{x}_1 &= f^{+}_{OCl}(x_1, x_2, x_3) - f^{-}_{OCl}(x_1, x_2) \equiv F_1 \\
\dot{x}_2 &= f^{+}_{OBl}(x_1, x_2) - f^{-}_{OBl}(x_2, x_3, x_4) \equiv F_2 \\
\dot{x}_3 &= f^{+}_{OCt}(x_2, x_4) - f^{-}_{OCt}(s+u, x_3) \equiv F_3 \\
\dot{x}_4 &= f^{+}_{B}(x_2) - f^{-}_{B}(x_1) \equiv F_4
\end{aligned} \quad . \tag{6.4.1a}$$

The OC problem for this system can be formulated by taking into account the metabolic losses for control $T(u_j)$ and metabolic losses for not being in thermodynamic steady state/equilibrium as $G(x_i)$ in the same way as it was done for the glycolitic model. The minimising functional at the square-law cost form will be similar to (6.1.7a) or (6.2.2)

$$J \int_{t_0}^{\tau} G(x_i) + T(u) \, dt \to \min , \tag{6.4.1b}$$

The optimal control problem will be formulated as (6.4.1b) subject to (6.4.1a), and the Hamiltonian function will be

$$H = -G(x_i) - T(u) + \sum_{i}^{4} p_i \cdot F_i . \tag{6.4.2}$$

Then the canonical system will be

$$\dot{x}_i = \frac{\partial H}{\partial p_i}, \dot{p}_i = -\frac{\partial H}{\partial x_i}, \frac{\partial H}{\partial u} = -0. \tag{6.4.3}$$

Solving this system one could optimise the biological properties incorporated into functional 6.4.1b.

6.4.2 Optimal control in cellular model

Following developed in Section 4 cellular model, which for the notion simplification we can write

$$\begin{aligned} \dot{x}_1 &= a_1 x_1 - b_{12} x_1 x_3 - b_{01} x_1 x_2 \\ \dot{x}_2 &= a_{01} x_1 x_2 - b_2 x_2 x_4 - b_{23} x_2^2 \\ \dot{x}_3 &= a_3 x_4 - (s-u) x_3 \\ \dot{x}_4 &= -k_1 x_1 + k_2 x_2 \end{aligned} \tag{6.4.4}$$

The formulation of the optimisation criterion can be quadratic

$$J = \int_{t_0}^{\tau} \left(\frac{(x_4 - 1)^2}{2} + \frac{u^2}{2} \right) dt \to \min \tag{6.4.5a}$$

Subject to

$$\begin{aligned} \dot{x}_1 &= a_1 x_1 - b_{12} x_1 x_3 - b_{01} x_1 x_2 \\ \dot{x}_2 &= a_{01} x_1 x_2 - b_2 x_2 x_4 - b_{23} x_2^2 \\ \dot{x}_3 &= a_3 x_4 - (s-u) x_3 \\ \dot{x}_4 &= -k_1 x_1 + k_2 x_2 \end{aligned} \tag{6.4.5b}$$

Then the Hamiltonian will be

$$\begin{aligned} H = &-\frac{(x_4 - 1)^2}{2} - \frac{u^2}{2} + \\ &p_1 \left(a_1 x_1 - b_{12} x_1 x_3 - b_{01} x_1 x_2 \right) + \\ &p_2 \left(a_{01} x_1 x_2 - b_2 x_2 x_4 - b_{23} x_2^2 \right) + \\ &p_3 \left(a_3 x_4 - (s-u) x_3 \right) + \\ &p_4 \left(-k_1 x_1 + k_2 x_2 \right) \end{aligned} \tag{6.4.6}$$

Then on the basis of Pontryagin Maximum principle the conditions for minimum of the functional with constrained system (6.4.5b) are

$$
\begin{aligned}
\dot{x}_1 &= \frac{\partial H}{\partial p_1} = a_1 x_1 - b_{12} x_1 x_3 - b_{01} x_1 x_2 \\
\dot{x}_2 &= \frac{\partial H}{\partial p_2} = a_{01} x_1 x_2 - b_2 x_3 x_4 + a_{21} x_2 - b_{23} x_2^2 \\
\dot{x}_3 &= \frac{\partial H}{\partial p_2} = a_3 x_4 - (s-u) x_3 \\
\dot{x}_4 &= \frac{\partial H}{\partial p_2} = -k_1 x_1 + k_2 x_2 \\
\dot{p}_1 &= -\frac{\partial H}{\partial x_1} = p_1 (b_{12} x_3 - a_1 + b_{01} x_2) - p_2 a_{01} x_2 + p_4 k_1 \\
\dot{p}_2 &= -\frac{\partial H}{\partial x_2} = p_1 b_{01} x_1 - p_2 (a_{01} x_1 - b_2 x_4 - 2 b_{23} x_2) - p_4 k_2 \\
\dot{p}_3 &= -\frac{\partial H}{\partial x_3} = p_1 b_{12} x_1 + p_3 (s-u) \\
\dot{p}_4 &= -\frac{\partial H}{\partial x_4} = x_4 - 1 + p_2 b_2 x2 - p_3 a_3 \\
\frac{\partial H}{\partial u} &= -u + p_3 x_3 = 0
\end{aligned}
\tag{6.4.7}
$$

and H*(T)=0 and $\lambda_i \le 0$. The last system can be simplified to

$$
\begin{aligned}
\dot{x}_1 &= a_1 x_1 - b_{12} x_1 x_3 - b_{01} x_1 x_2 \\
\dot{x}_2 &= a_{01} x_1 x_2 - b_2 x_3 x_4 + a_{21} x_2 - b_{23} x_2^2 \\
\dot{x}_3 &= a_3 x_4 - (s - p_3 x_3) x_3 \\
\dot{x}_4 &= -k_1 x_1 + k_2 x_2 \\
\dot{p}_1 &= p_1 (b_{12} x_3 - a_1 + b_{01} x_2) - p_2 a_{01} x_2 + p_4 k_1 \\
\dot{p}_2 &= p_1 b_{01} x_1 - p_2 (a_{01} x_1 - b_2 x_4 - 2 b_{23} x_2) - p_4 k_2 \\
\dot{p}_3 &= p_1 b_{12} x_1 + p_3 (s - p_3 x_3) \\
\dot{p}_4 &= x_4 - 1 + p_2 b_2 x_2 - p_3 a_3
\end{aligned}
\tag{6.4.8}
$$

This system was studied in the same way as system (2.1.3) at the range of parameters: a_1, 1000-100000 day^{-1}; b_{12}, 0.002-0.05 $cell^{-1}day^{-1}$; b_{01}, 1.050-9.0 $cell^{-1}day^{-1}$; a_{01}, 1.50-300.0 $cell^{-1}day^{-1}$; b_2, 50.0-600.0 $cell^{-1}day^{-1}$; b_{23}, 0.001-0.09 $cell^{-1}day^{-1}$; a_3, 2300-66000 day^{-1}; s, 0.01-15.0 $cell^{-1}day^{-1}$; k_1, 0.01-0.50 day^{-1}; k_2, 0.0003-0.0030 day^{-1}.

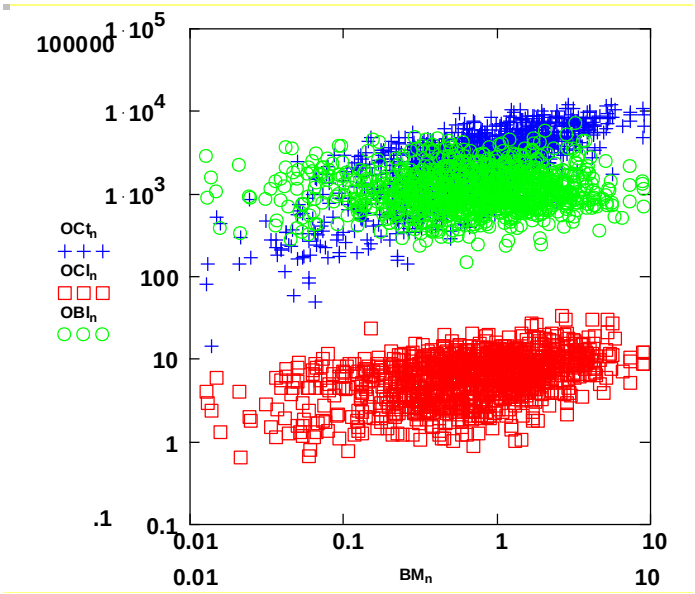

Fig. 6.4.1 The scatteplot of calculated points of equilibrium of osteocells (Ocl, osteoclasts; OB, osteoblasts; Oct, osteocytes) against the total bone mass (BM) for the system (6.4.8). Calculations were performed using the following set of parameters: a_1, 1000-100000 day^{-1}; b_{12}, 0.002-0.05 $cell^{-1}day^{-1}$; b_{01}, 1.050-9.0 $cell^{-1}day^{-1}$; a_{01}, 1.50-300.0 $cell^{-1}day^{-1}$; b_2, 50.0-600.0 $cell^{-1}day^{-1}$; b_{23}, 0.001-0.09 $cell^{-1}day^{-1}$; a_3, 2300-66000 day^{-1}; s, 0.01-15.0 $cell^{-1}day^{-1}$; k_1, 0.01-0.50 day^{-1}; k_2, 0.0003-0.0030 day^{-1}.

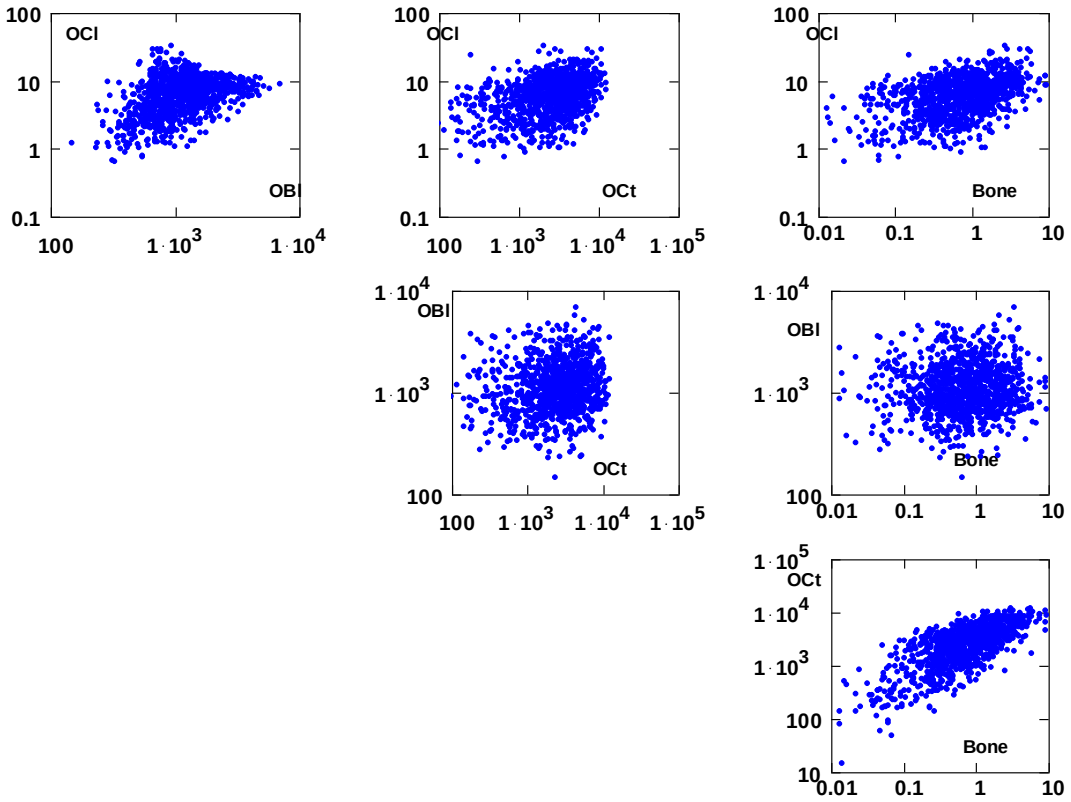

Fig. 6.4.2 The graphical matrix illustrates the scatterplot of populational densities of Ocl, Obl, Oct, BM (designated as "Bone") in 4D space of these quantities at the uniform distribution of the rate constant for the system (6.4.8). Calculations were performed using the set of parameters in Fig.6.4.1.

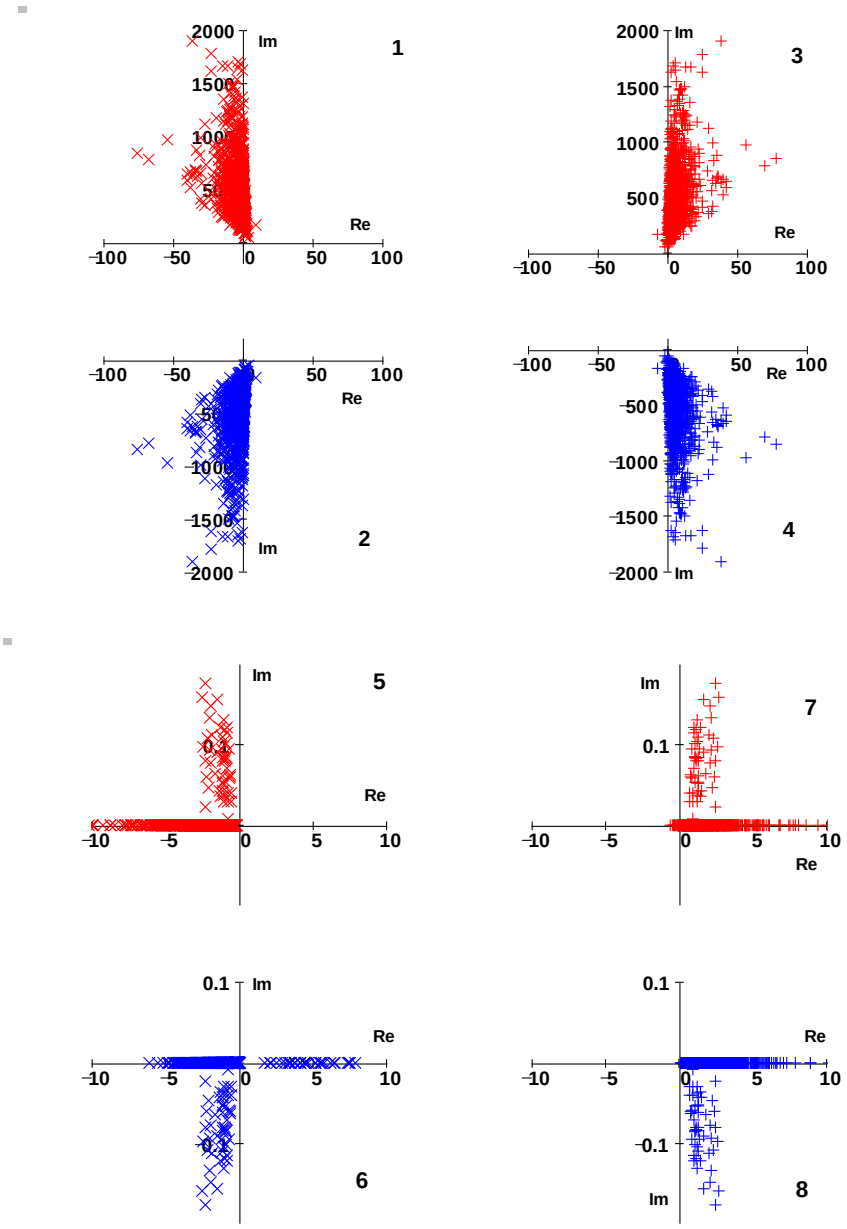

Fig. 6.4.3 Scattreplot of the eigenvalues of the Jacobian matrix for the linearised system (6.4.8). Calculations were performed using the set of parameters in Fig.6.4.1.

Fig.6.4.3 illustrates the character of the equilibrium point's stability. One can see that the first and second eigenvalues are complex-conjugate, as well as the third and fourth eigenvalues. The same symmetric picture characterises the 5th-8th eigenvalues. From the perspective of OC that means that the introduction of OC as it was done in (6.4.1-6.4.8) introduces instability into the system. However, it is still possible to link this to the method, proposed in Section 4 and 5, which is based on the Monte Carlo method. This demonstrates the

position of equilibrium and its character with the values of the rate constants. However, to obtain statistically significant results the range of the rate constant needs to be reduced as it was illustrated in Section 4 and 5.

6.4.3 Short range of the rate parameters: Monte Carlo method

The illustration of the method, applied in Sections 4 and 5, to the system (6.4.8) within the shorter range of the rate parameters (a_1, 7100-9850 day^{-1}; b_{12}, 0.0015-0.002 $cell^{-1}day^{-1}$; b_{01}, 2.0-3.6 $cell^{-1}day^{-1}$; a_{01}, 23.0-30. $cell^{-1}day^{-1}$; b, 270.0-290.0 $cell^{-1}day^{-1}$; b_{23}, 0.0049 -0.0055 $cell^{-1}day^{-1}$; a_3, 79000-90000 day^{-1}; s, 7.0-8.0 $cell^{-1}day^{-1}$; k_1, 0.3-0.4 day^{-1}; k_2, 0.0023- 0.0025 day^{-1}) is shown in Fig.6.4.4-6.4.6 and Table 6.4.1. Fig.6.4.4.indicates the scatterplot of the osteocell's population concentration against the total bone mass (BM), which shows a significant reduction in the scatter. This is seen comparably to Fig.6.4.1. That means that the regression of the equilibrium position and the relaxation characteristics can be calculated with some confidence.

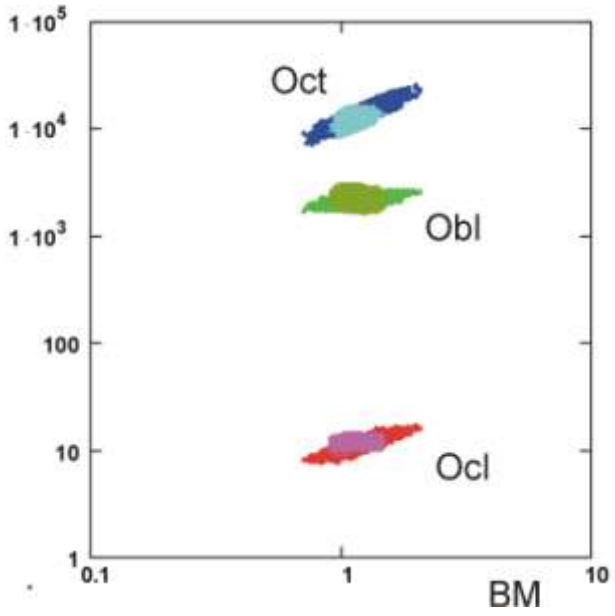

Fig. 6.4.4 Scatteplot of calculated points of equilibrium of osteocells (Ocl, red, osteoclasts; Obl, green, osteoblasts; Oct, blue, osteocytes) against the total bone mass (BM), for the system (6.4.8) and system (4.4) without optimal control (magnolia, brown and cyan colours, correspondingly). Calculations were performed using the same set of the rate parameters: a_1, 7100-9850 day^{-1}; b_{12}, 0.0015-0.002 $cell^{-1}day^{-1}$; b_{01}, 2.0-3.6 $cell^{-1}day^{-1}$; a_{01}, 23.0-30.0 $cell^{-1}day^{-1}$; b_2, 270.0-290.0 $cell^{-1}day^{-1}$; b_{23}, 0.0049 -0.0055 $cell^{-1}day^{-1}$; a_3, 79000-90000 day^{-1}; s, 7.0-8.0 $cell^{-1}day^{-1}$; k_1, 0.3-0.4 day^{-1}; k_2, 0.0023- 0.0025 day^{-1}.

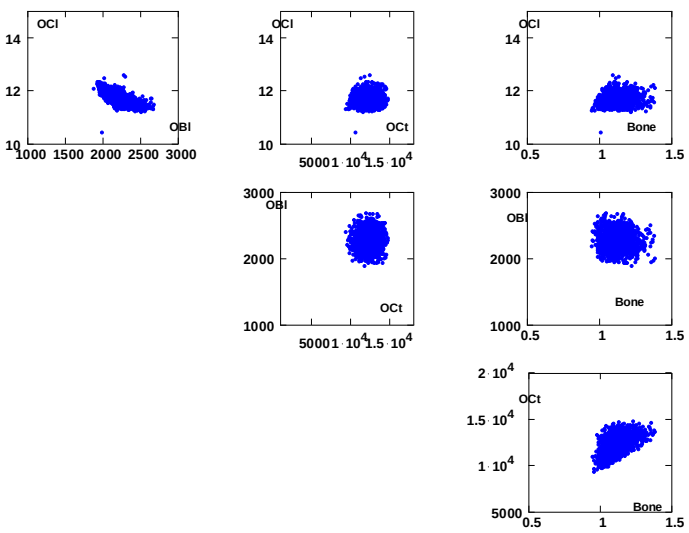

Fig. 6.4.5 The graphical matrix illustrates the scatterplot of populational densities of Ocl, Obl, Oct, BM(bone) in 4D space of these quantities at the uniform distribution of the rate constant for the system (6.4.8). Calculations were performed using the set parameters, Fig.6.4.4.

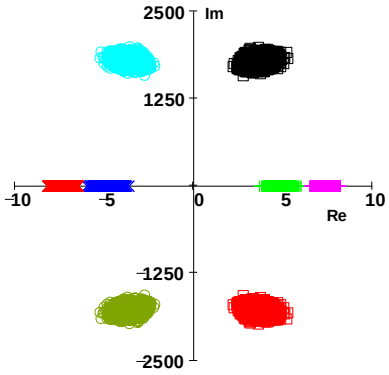

Fig.6.4.6. The scattreplot of the eigenvalues of the Jacobian matrix for the linearised system (6.4.8). Calculations were performed using the set parameters, Fig.6.4.4.

	Ocl	Obl	Oct	BM	Re1	Re5	Re6	Im1
R-square	0.990	0.997	0.995	0.996	0.996	0.997	0.999	0.998
A1	2.352	0.783	0.534	0.633	-0.562			1.302
B12						-0.008	0.006	-0.006
b01	-2.762	-0.910	-0.623	-0.745	0.653		-0.005	-0.725
a01	-0.015		0.648	0.789	-0.235	0.634	-0.008	0.751
b2	0.020	0.007	-0.608	-0.739	0.224	-0.612	0.008	0.008
b23			-0.027	-0.026	-0.707			
a3	-0.012		0.657				0.005	-0.005
s			-0.693			0.013	-0.999	
k1	-2.737		-0.638	-0.766	0.253	-0.681	0.010	-0.717
k2	2.999		0.704	0.840			0.005	0.791

Table 6.4.1 Summary table of the Monte-Carlo method application to the system (6.4.8) within the range of parameters indicated in Fig.6.4.4.

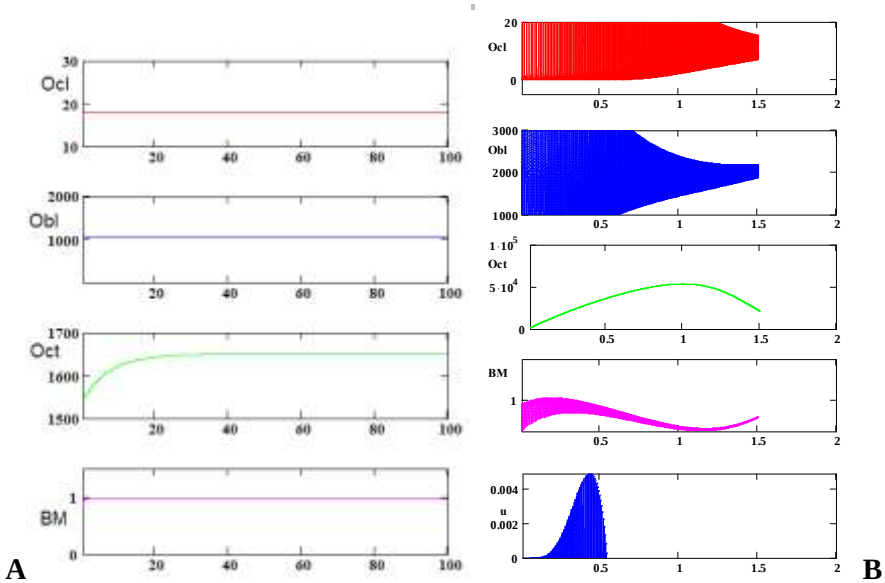

Fig. 6.4.7. Typical trajectories for state variables, time in days. A, short range, no OC; B, OC.

	Mean	Minimum	Maximum	Range	Std.Dev.	Error
OCL	11.646	10.409	12.560	2.151	0.228	0.006
OBL	2243.9	1879.4	2674.3	794.9	143.6	3.9
OCT	12222	9272	14706	5434	1029	28
BM	1.080	0.947	1.405	0.458	0.080	0.002

Table 6.4.2 The average population concentrations, maximum and minimum values and statistical deviations for the osteocells (cell/mm^3) and the relative bone mass, BM, for the model (6.4.8) for the short range of the rate parameters as in Fig.6.4.4.

Indeed, as it is seen from the Monte Carlo results, Table 6.4.1, the position of the equilibrium point and the relaxation characteristics can be calculated from the values of the rate constants with a good (R-square >0.99) confidence level. The regulatory pattern of the model, indicated in Table 6.4.1 by the values of coefficients and their signs matches the regulatory pattern of the system (4.3) without the OC, even though the system significantly changed after the OC implementation. The scatterplots (Fig.6.4.6) of the real and imaginary parts of the eigenvalues of the system (6.4.8) indicate that the equilibrium points in 8-dimensional space of 4 state variables and 4 costate variables is unstable. This means that solutions of the system are unstable and the optimal control problem in form (6.4.1-8) should be revised.

Thus, the introduction of the dynamic optimal control in such a way as it was done in (6.4.1-6.4.8) leads to a loss of stability of the main equilibrium point in new combined phase space of the state and costate variables.

6.4.4 Optimal control formulation for allosteric cellular-and-molecular model

Following the development in Section 5 of the allosteric cellular model (with some modifications) which includes the molecular regulation loop, which for notion simplification we can write as

$$\begin{aligned}
\dot{x}_1 &= -b_{12}x_1\frac{x_3}{K_{Oct}+u+x_3} + a_1x_1 - b_{01}x_1x_2 \\
\dot{x}_2 &= a_{01}x_1x_2 - b_2x_3x_4 - b_{23}x_2^2 \\
\dot{x}_3 &= a_3x_4 - sx_3 \\
\dot{x}_4 &= -k_1x_1 + k_2x_2
\end{aligned} \tag{6.4.9}$$

Let us constructed the optimisation criterion

$$J = \int_{t_0}^{\tau}\left(\frac{(x_4-1)^2}{2} + \frac{u^2}{2}\right)dt \to \min \tag{6.4.10a}$$

Subject to

$$\begin{aligned}
\dot{x}_1 &= -b_{12}x_1\frac{x_3}{K_{Oct}+u+x_3} + a_1x_1 - b_{01}x_1x_2 \\
\dot{x}_2 &= a_{01}x_1x_2 - b_2x_2x_4 - b_{23}x_2^2 \\
\dot{x}_3 &= a_3x_4 - sx_3 \\
\dot{x}_4 &= -k_1x_1 + k_2x_2
\end{aligned} \tag{6.4.10b}$$

Then the OC Hamiltonian will be

$$\begin{aligned}
H = {} & \frac{(x_4-1)^2}{2} + \frac{u^2}{2} + \\
& p_1\left(-b_{12}x_1\frac{x_3}{K_{Oct}+u+x_3} + a_1x_1 - b_{01}x_1x_2\right) + \\
& + p_2\left(a_{01}x_1x_2 - b_2x_2x_4 - b_{23}x_2^2\right) + \\
& + p_3\left(a_3x_2x_4 - sx_3\right) + \\
& + p_4\left(-k_1x_1 + k_2x_2\right)
\end{aligned} \tag{6.4.11}$$

Then on the basis of Pontryagin maximum principle the conditions for minimum of the functional with constrained system (6.4.10b) are

$$
\begin{aligned}
\dot{x}_1 &= \frac{\partial H}{\partial \lambda_1} = -b_{12}x_1\frac{x_3}{K_{Oct}+u+x_3} + a_{11}x_1 - b_{01}x_1x_2 \\
\dot{x}_2 &= \frac{\partial H}{\partial \lambda_2} = a_{01}x_1x_2 - b_2x_2x_4 - b_{23}x_2^2 \\
\dot{x}_3 &= \frac{\partial H}{\partial \lambda_2} = a_3x_4 - sx_3 \\
\dot{x}_4 &= \frac{\partial H}{\partial \lambda_2} = -k_1x_1 + k_2x_2 \\
\dot{p}_1 &= -\frac{\partial H}{\partial x_1} = p_1b_1\frac{x_3}{K_{Oct}+u+x_3} - a_1p_1 + b_{01}x_2p_1 - p_2a_{01}x_2 + p_4k_1 \\
\dot{p}_2 &= -\frac{\partial H}{\partial x_2} = p_1b_{01}x_1 - p_2a_{01}x_1 - p_2a_{21} + 2p_2b_{23}x_2 - p_3a_3x_4 - p_4k_2 \\
\dot{p}_3 &= -\frac{\partial H}{\partial x_3} = -p_1b_{12}x_1\frac{K_{Oct}+u}{(K_{Oct}+u+x_3)^2} + p_2b_2x_4 + p_3s \\
\dot{p}_4 &= -\frac{\partial H}{\partial x_4} = x_4 - 1 + p_2b_2x_3 - p_3a_3x_2 \\
\frac{\partial H}{\partial u} &= -u - \frac{p_1b_{12}x_1x_3}{(K_{Oct}+u+x_3)^2} = 0
\end{aligned}
\tag{6.4.12}
$$

and $H^*(\tau)=0$ and $p_i \le 0$. However, to study this system is quite difficult and it is planned for further work.

6.4.5 Summary

The first section reviews the molecular binding kinetics from the perspective of optimal control and variational description. Based on Pontryagin maximum principles an introduction of optimal control within the Hill kinetics model has been illustrated. The dynamical system has been obtained as a result of the Euler-Lagrange equations and canonical equations, in the case of the Pontryagin maximum principle approach. The numerical solutions have been obtained and discussed.

The Michaelis-Menten model of enzyme kinetics can be revised employing the optimal control and direct variational methods in combination, considering the introduction of control

into different ways within this model. The section discusses the problems where regulation is introduced by the reaction velocity, by the Michaelis constant and simultaneous optimal control by both of them. Corresponding dynamical systems can be found as a result of the Euler-Lagrange equations and canonical equations. The numerical solutions have a good agreement of the results without the optimal control. The biochemical allosteric regulatory aspects of optimal control models have been discussed.

Based on the Pontryagin maximum principles and the Lagrange method the possibility of the optimal control extension of the yeast model of glycolysis kinetics has been illustrated. Corresponding dynamical systems have been obtained as a result of canonical equations in the case of the Pontryagin maximum principle approach. The biochemical aspects of the optimal control explicit implementation have been discussed. Statistical canonical analysis is a particularly useful method to study the character stability dependences because of the dimension reduction possibility that simplifies analysis. The canonical spaces – the linear combinations of real variables (concentrations, rate constants, activities) could be the key-spaces of optimal regulation of the metabolic network or its part when system needs to be controllably moved from one qualitative mode of behaviour to another.

The OC problem can be formulated for the BMU functioning model. However, the instability of the main point can be observed. Further studies are needed to describe the OC formulation results for the allosteric model.

7 Conclusions and further work

7.1 Cellular model

The introduction of the osteocytes' regulation loop is necessary from biological perspective. Many authors (Landry et al., 1997; Martin, 2002; Noble, 2003) discussed possible mechanisms of this regulation, including some molecular mechanisms. However, the introduction of the osteocyte pathway into remodelling regulation loop in the mathematical model increases the dimensionality of the model and makes it more difficulty to validate. The number of terms that needed to be taken into account and the dimensionality of parameters to be measured both increase. This in turn demands precise measurement in-vivo, which can be difficult when conducting experiments with hard tissue.

The mathematical model of bone remodelling, that has been discussed in Chapters 4-6, formally introduces a level of octeocytes' regulation which certainly is more realistic from a cellular, biochemical and bio-cybernetic perspective (Frost, 2001), since the osteocytes are considered to participate actively in regulation of the BMU. This introduction was based on the assumption that the osteocytes' level of regulation is a primary part of bone remodelling, as it allows the completion of the loop of spatial control of BMU initiated from the bone marrow.

The introduction of the osteocytes' loop into cellular model increases the spectrum of behaviour described from relaxational and periodical to a chaotic mode. The cellular model has quite robust behaviour in the wide range of parameters implemented into model. The chaotical mode can be also interesting, however further studies need to establish the real relevance of this type of behaviour to the remodelling process in bone tissue.

Cellular models displays steady relaxational behaviour when employing the range of rate constants with certain biological sense. The existence of stable focus type of equilibrium in four-dimensional osteoclast–osteoblast–osteocyte-bone space indicates formally that there are time-constants for this dynamic system. Biologically, or rather physically, this time

constant characterises the recovering property of the bone tissue. This is related to the continuously operating, genetically predetermined BMU and provides a measure of the recovering potential of the BMU following mechanical and biochemical damage to bone.

One of the advantages of the cellular model is related to the model validation. Due to the simplicity of the model the low-dimensional kinetic constants are expected to be estimable. In this case simple measurements based on the population densities of cells can be employed.

7.2 Allosteric model

The model of the bone turnover cycle that has been developed in Chapter 5 introduces a non-linear, non-multiplicative cellular control loop, which is more rational from a biochemical and osteo-homeostatical perspective, since the osteocytes are considered to participate in regulation of BMU by producing the molecular messengers. As well as the effect of local factors on osteo-cells production and activity can have nonlinear sigmoid character. This development was based on the assumption that the nonlinear allosteric form of control is a vital part of bone remodelling, as it allows the modelling of the natural loop of control of BMU.

The allosteric molecular model also shows different modes of behaviour; relaxational and quasi-periodical with damping within a wide range of rate constants that can be interpreted biologically. In the sense of dynamic systems, the majority of equilibrium points, obtained in this range of parameters, using Monte Carlo method, can be characterised as the stable focus. At some constants the main equilibrium point attains the form topologically equivalent to a stable cycle.

However, in the framework of a very well known mechanism of nonlinear regulation (Michaelis-Menten) the stable focus, formerly described for pure cellular model (Chapter 4), prevails in a wide range of the rate constants. Moreover, it becomes a more physiological in the sense of the population densities of osteocells. This finding supports the idea of a non-

linear, not just multiplicative, feedback regulation from the osteocytes. That means also that the robustness of the system is maintained from the simple cellular level to the allosteric-like regulation, related to molecular and biochemical level of regulation. This implementation, based on the assumption that the allosteric form of control is a vital part of bone remodelling, provides the completion of the natural loop of control of BMU initiated from the osteocytes' networks. Simulations of the model demonstrate four-dimensional relaxation when employing the range of rate constants that can be interpreted biologically. Moreover, at the same time the existence of periodical modes of behaviour could provide the basis for the explanation of Paget's-disease-like physiological situation of overfeeding of the bone remodelling cycle. Cyclic modes might be play greater role in Paget's disease or maintaining plasma Ca^{2+} physiological concentration. Hence, the combined allosteric and cellular hybrid models represent some insights into the bone remodelling mechanisms of regulation. However, the validation of these kinds of models is a significant problem since, for example, the parameters of receptors should be estimated in vivo.

7.3 Optimisation problem formulation for the BMU

Molecular binding is the first stage of any biological regulation, including bone remodelling. Therefore it is important to understand its functioning from an optimal control perspective. The Section 6.1 reviews the molecular binding kinetics from the perspective of the optimal control and creates the basis to understand regulatory optimality. Based on Pontryagin minimum principles and the Lagrange method, an introduction of optimal control within the Michaelis-Menten kinetics model has been illustrated in the section 6.2. The dynamical systems have been obtained as a result of the Euler-Lagrange equations and canonical equations, in the case of the Pontryagin principle approach. The numerical solutions have been obtained and discussed. The results indicate that the cooperativity can be considered as the rigidity of the control. The cooperativity, implemented in many regulatory feedbacks in cell and physiological level, provides necessary robustness of the control over

the most vital parameters. In the bone remodelling regulation there are also indications of positive cooperativity, which one can see from Fig.5.2. That is why allosteric mechanisms were considered at the regulation of bone remodelling. Optimal control outline of cooperativity, undertaken in this project, allowed molecular binding and cooperativity of molecular binding to understand from energetical optimality perspective.

Enzyme kinetics is also an important part of regulation functioning, including the regulation of bone remodelling. Therefore, the basic enzyme kinetics model, the Michaelis-Menten kinetics, has been revised employing the optimal control, considering the introduction of control into different ways within this model. The Section 6.2 discusses the problems where regulation is introduced by the reaction velocity, by the Michaelis constant and simultaneous optimal control by both of them. The dynamical systems have been found as a result of the Euler-Lagrange equations and canonical equations. The numerical solutions have been obtained. The biochemical allosteric regulatory aspects of optimal control models have been discussed. Biochemical parallels to these two ways of OC introduction were also considered. In this context two main biochemically-sensible interpretations were discussed: the OC by maximal velocity is analogical to the non-competitive inhibition, OC by Michaelis constant is analogical to competitive inhibition with respect of enzyme kinetics. The Michaelis-Menten regulation was considered also in the variant of allosteric model of BMU.

As an intermediate OC model on the way to build the optimal control BMU model, the basic model of two-level metabolic system, the Bier and coauthors model of glycolysis was employed. Based on the Pontryagin maximum principles and the Lagrange method the possibility of the optimal control extension of the yeast model of glycolysis kinetics has been illustrated. Corresponding dynamical systems have been obtained as a result of canonical equations in the case of the Pontryagin maximum principle approach. The biochemical aspects of the optimal control explicit implementation have been discussed. Statistical analysis is a particularly useful method to study the character stability dependences because of the dimension reduction possibility that simplifies the analysis.

Finally, the OC formulation for cellular BMU model and hybrid molecular-and-cellular allosteric model of BMU was performed in Section 6.4. The control by the load rate constant and the Michaelis constants was considered. Due to the complexity of the model further work is required to study all of the implications of the models developed.

The results and their analysis also illustrate the complexity of the relationship between the system level of regulation and local factor regulation in hard tissue considering the steady tissue remodelling. Even after simplification and reduction in the number of the model variables, the behaviour of tissue shows multiple modes of behaviour that sometimes have limited relevance from a biological perspective.

In summary, the results from the OC (Section 6) are encouraging and the regulatory model of BMU is expected to be the subject of future work. Modelling of BMU, including hierarchical modelling that involves system and local regulatory loops, could be particularly useful for development optimised tissue engineered bone substitutes.

7.4 Conclusions

This study shows the complexity of formalisation of the metabolic processes, the relations between hierarchical subsystems in hard tissue where there are a relatively small number of active cells.

The different types/modes of behaviour have been compared in the study: relaxational, periodical and chaotic modes. All of these types of behaviour can be found even tissue such as bone. However, a periodic mode of behaviour is one the hardest to verify although a number of periodical phenomena have been observed for bone and skeletal development. Implementation of the molecular loops into the cellular model results in the loss of the chaotical behaviour/modes. In this way it improves the robustness and predictability and control of the system.

The following conclusions can be drawn from this study;

1. The cellular and combined allosteric-cellular regulation approaches to modelling of bone turnover (based on the osteocyte involvement/regulation by apoptosis) can be developed using dynamic systems.
2. Within both approaches, the different modes of behaviour can be found.
3. Different approaches to model validation can be considered as useful, including approaches based on the Monte-Carlo simulation of random combination of model parameters (rate constants) and further arrangement of regression analysis to establish the relation between parameters and character of equilibrium points.
4. From the model validation perspective, the cellular class of models is preferable, since it has less parameters (the rate constants) to analyse. The rate constants in particularly are difficult to estimate for the bone tissue in vivo.
5. In both types of models the mechanical stress parameter can be included.
6. On the basis of fundamental OC models (Hill model, Michaelis-Menten model, 2D glycolysis model), the optimal control framework for regulation of bone remodelling can be proposed. This framework can be essential for development with respect to application to hard scaffold adaptation.
7. Future works in the improvement of the models and their application to modelling resorption and formation of scaffold/bone tissue have been considered.

Developed models can be a first step in a hierarchical model of bone tissue (system effects versus local effects). Limited autonomy of any organ or a tissue implies the differentiation of regulatory level as well as physiological functions and metabolic differences. An implementation into the cellular phenomenological model of molecular loop of regulation has been performed. The results show that the robustness of regulation can be inherited form the phenomenological model however the regulatory degrees of freedom considerably increases.

An attempt to correlate the main bone disorders with different modes of behaviour has been undertaken using well known Paget's disorder of bone, osteoporosis and some more

general skeleton disorders leading to periodical changes in bone mineral density reported by some authors (Mazzuoli et al., 2002,2006). However additional studies are needed to make this hypothesis significant.

When studying a multidimensional phenomena as a bone tissue is, the visualisation and data reduction is important for analysis and interpretation of results. In the study two technical methods have been proposed. First one is the graphical matrix method of transforming/visualise/project the multidimensional phase space of variables into diagonal matrix of regular combination of two-dimensional graphs. That significantly simplifies the analysis and in principle makes possible to visualise the phase space higher than three-dimensions.

The second important technical development is the application of the Monte-Carlo method in combination with statistical methods (principal component and regression) to study the character of stability of the equilibrium points of a dynamical system. The advantage of the method is that it allows the large number of parameters/constants of the dynamical system the most influential parameters (or their linear combinations) that effect the character of stability of the equilibrium point and in wide range of constant values to be found. This makes the interpretation of parameters and conceptual verification of the model much easier.

Summarisingly, the novelty of this study was:

- *For first time the OCts feedback of regulation was considered in the BMU model.*
- *The 4D model was proposed, which includes allosteric-like control*
- *OC approach illustrated for simple kinetics, 2D model of glycolysis and BMU model*
- *The method, based on combination of Monte-Carlo generation of model parameters simulation and regression analysis, was proposed to study the relationship between the character of equilibrium of dynamic system and parameters of the model.*
- *Graphical matrix method was proposed for visualisation dynamic systems D>4*
- *The method of optimal control of performance of the model with respect to some optimisation criteria was proposed.*

7.5 Overall implications of this research

This research conducted in this PhD study clearly indicates that while building mathematical model of bone remodelling (BMU functioning) the role of osteocytes has to be taken into account. The osteocytes play vital role in the producing signal for osteoclasts arrangement: differentiation, maturation and bone resorption, (Landry et al., 1997; Martin, 2002; Noble, 2003), therefore their role should not be ignored. The cellular model, developed in this research offered the osteocytes' regulatory loop together with the extended spectrum of functional behaviour. In this research the combined cellular and allosteric regulation approaches to modelling of bone turnover (based on the osteocyte involvement/regulation by apoptosis) have been considered. Within both approaches different modes have been investigated.

Important conclusion is that osteoblastic activity has indirect negative feed back regulatory loop, which phenomenologically contains the osteocytes and its molecular explanation could be based on sclerostin production by osteocytes. So inclusion of osteocytes phenomenological loop of regulation can be relevant to sclerostin action. However detailed molecular mechanisms are unclear.

The research creates a platform for the development a general method to introduction of the optimal control into a small biochemical or cellular network, like the bone remodelling network. The optimal control approach to interpret molecular binding from energetical optimality perspective, to consider the Michaelis-Menten basic enzyme model, and application to the glycolytic network provides good technical basis to consider a metabolic network from energetical and functional optimality. The models developed and the underpinning approach to control bone remodelling has implications for bone graft substitute's development and optimisation.

This study also has some implications on some technical methods used in the dynamic systems research. That is first of all the statistical approach and reduction of parameters approach based on the Monte-Carlo simulation of random combination of model

parameters (rate constants) and further arrangement of regression/canonical correlation analysis to establish the relation between parameters and character of equilibrium points.

Another important development is the visualisation technique of graphical matrixes, proposed for analysis of dynamic systems behaviour when dimensionality is higher than 3. This visualisation method can be implemented as a graphical analysis instrument for dynamic systems software.

7.6 Further work

The limitations of the study and time factor and resources did not allow to build a full formal picture of the processes involved in bone remodelling.

Significant improvement that can lead to use the osteocyte's regulatory model/approach and can lead to develop criteria for scaffold design, it will be the spatial model of remodelling. It can be based, for example, on the cellular automata technique or the partial differential equation technique.

- Further structural robustness study on the models
- Incorporation of different allosteric feedbacks into osteocells' regulation
- Implementation of Hill-like feedback function with effective cooperativity 2.
- Development of approaches to build the spatial models, describing 3D properties of bone tissue remodelling
- Cellular automata.

On the basis of spatial models, further development of dynamic optimal control approach to bone grafts and bone substitutes design can be achieved.

Based on the results generated from this study, in future research the methodology for a common mathematical framework based on the optimal energy regulation needs to be considered. This principle leads to formulate the energetical effectiveness at different levels of biochemical/physiological organisation in the organism, tissue or ecological system. However, it is envisaged that a complex system of interlinking homeostatic sub-systems will

manifest adaptive and energetical effectiveness properties through synchronisation processes as a product of coupled nonlinear dynamic behaviour.

Due to the multivariable nature of the data that can be obtained from experiments in bone tissue, and the multileveled nature of studying tissue and processes, their descriptions and methods of data reduction and visualisation are an important technical issue that should be considered for further development.

Regeneration of damaged bone tissue remains an important problem, the field of tissue engineering looks to provide structural support for the regenerating material via bone tissue scaffolds. Optimisation of scaffold properties, known as scaffold variables, is closely related to the study of remodelling properties. Developing a mathematical model that can be used as a dynamical constraint for optimisation of remodelling, as well as the study of the usefulness of dynamic optimisation in developing resorbable implants/scaffolds can also be considered as a further research area.

The mathematical modelling of bone is an important part of mathematical physiology as bone remodelling is a highly organised physiological process that occurs in bone tissue and supports many physiological processes in the body. Researchers with a strong interdisciplinary and integrative interest in life support systems must have a clear vision of the role of bone tissue and its remodelling process as these processes are actively involved at the systemic regulation level of all metabolic processes. The modelling of "artificial bone" needs to take into account not only the mechanical properties of tissue but also consider that this "supporting system" might be important in other physiological functions at the systemic level.

References

Acerenza L., Mizraji E. 1997. Cooperativity: a unified view, *Biochimica et Biophysica Acta* 1339, 155–166.

Acerenza, L. 2000. Design of Large Metabolic Responces. Constrains and Sensityvity Analysis. *J. Theor. Biol*. 207, 265-282.

Acikgoz, S.U., Diwekar, U.M. 2010. Blood glucose regulation with stochastic optimal control for insulin-dependent diabetic patients. *Chem. Eng. Sci.* 65(3), 1227-1236.

Adair, G.S. 1925. The hemoglobin system. VI. The oxygen dissociation curve of haemoglobin. *J. Biol. Chem.* 63, 529-545.

Agnati, L. F., Tarakanov, A. O., Guidolin, D. 2005. A simple mathematical model of cooperativity in receptor mosaics based on the "symmetry rule". *Biosystems* 80(2), 165-173.

Albright F., Bloomberg E., Smith P.H. 1940. Post-menopausal osteoporosis. *Trans Assoc Am Physicians*. 55. 298-305.

Anderson P.A., May B.K., Morris H.A., 2003. Vitamin D Metabolism: New Concepts and Clinical Implications Clin Biochem Rev 24, 13-26.

Atkins, G.J., P.H. Anderson, D.M. Findlay, K.J. Welldon, C. Vincent, A.C.W. Zannettino, P. D. O'Loughlin, H. A. Morris 2007. Metabolism of vitamin D_3 in human osteoblasts: Evidence for autocrine and paracrine activities of 1α,25-dihydroxyvitamin D_3 . Bone, 40, 1517-1528.

Bailon-Plaza A. and van der Meulen M. C. H. 2001. A Mathematical Framework to Study the Effects of Growth Factor Influences on Fracture Healing. JTB, 212(2), 191- 209.

Bailon-Plaza A., van der Meulen M. C. H., 2003. Beneficial effects of moderate, early loading and adverse effects of delayed or excessive loading on bone healing. J Biomech 36(8) 1069-1077.

Bakker, A.D., Soejima1, K., Klein-Nulend, J., Burger, E.H., 2001. The production of nitric oxide and prostaglandin E2 by primary bone cells is shear stress dependent. J. Biomech. 34, 671–677.

Bakwin H., Eiger M., 1956. Fragile bones and macrocranium. *J. Pediatr*. 49. 558–564.

Bax B.E., Wozney J.M., Ashhurst D.E. 1999. Bone morphogenetic protein-2 increases the rate of callus formation after fracture of the rabbit tibia. *Calcif Tissue Int*. 65(1). 83-89.

Beaudreuil, J., Balasubramanian S., Chenais J., Tabeulet J., Frenkian M., Orcel P., Jullienne A., Horne W.C., de Vernejoul M.C., Cressent M., 2004. Molecular characterization of two novel isoforms of the human calcitonin receptor. *Gene* 343, 143–151.

Beaupre, G. S., Orr, T. E. and Carter, D. R. 1990. An approach for time-dependent bone modeling and remodelling - theoretical development. *J Orthop Res*. 8, 651-661.

Bender I.B. 2003. Paget's Disease. *J Endodontics*, 29 720-723.

Bier, M., Bakker, B.M. and Westerhoff, H.V. 2000. How Yeast Cells Synchronize their Glycolytic Oscillations: A Perturbation Analytic Treatment. *Biophys. J.* 78, 1087–1093.

Bier, M., Teusink, B., Kholodenko, B.N., Westerhoff, H.V. 1996. Control analysis of glycolytic oscillations. *Biophys. Chem.* 62, 15-24.

Bitsakos, C. Kerner J., Fisher I., Amis A. A., 2005. The effect of muscle loading on the simulation of bone remodelling in the proximal femur. *J Biomechanics*, 38(1), 133-139.

Blair H. C., Simonet S., Lacey D. L., Zaidi M., 2008. Osteoclast Biology, *Osteoporosis (Third Edition), 151-167.*

Blair, J.M., Zheng, Y., Dunstan, C.R. 2007. RANK ligand. *Int. J. Biochem. & Cell Biol.*, 39(6), 1077-1081.

Blobe, G.C, Schiemann WP, Lodish HF. 2000. Role of transforming growth factor beta in human disease. *N Engl J Med*. 342(18).1350-1358.

Body J.-J., 2002. Calcitonin for the long-term prevention and treatment of postmenopausal osteoporosis. *Bone*, 30, Suppl1, 75-79.

Bohr, C., Hasselbach, K.A., Krogh, A. 1904. Ubereinen in biologischen Beziehung wiechtigen Einfluss den die kohlensauresparnung de bluter auf dessen sauerstoff binduing Lift. *Skand. Arch. Physiol*. 16, 401-412.

Bonewald, L.F., 2004. Osteocyte biology: Its implications for osteoporousis, J. *Musculoskel. Neuron. Interact*. 4(1), 101-104.

Bosetti M., Boccafoschi F., Leigheb M., Cannas M. F. 2007. Effect of different growth factors on human osteoblasts activities: A possible application in bone regeneration for tissue engineering Biomolecular Engineering, 24, 613-618.

Boyden L.M., Mao J., Belsky J., Mitzner L., Farhi A., Mitnick M.A., Wu D., Insogna K., Lifton R.P. 2002. High bone density due to a mutation in LDL-receptor-related protein 5. *N. Engl. J. Med*. 346, 1513– 1521.

Braddock, M., Houston, P., Campbell, C., Ashcroft, P. 2001. Born again Bone, Tissue Engineering for Bone Repair. *News Physiol. Sci*. 16, 208-213.

Brosch S., Redlich K., Pietschmann P. 2003. Pathogenesis of osteoporosis in rheumatoid arthritis. *Acta Med. Austriaca*. 30(1), 1-5.

Bulstra S.K., Geesink R.G.T., Hoefnagels N.H.M. 1999. Osteogenic activity of OP-1, bone morphogenetic protein-7 (BMP-7), in a human fibular defect model. *Proc 45th Ann Mtg Orthop Res Soc*, 62.

Burger, E.H., Klein-Nulend, J. 1999. Mechanotransduction in bone- role of the lacuno-canalicular network. *FASEB J.* 13 (Suppl.), S101–S112.

Burgess T.L., Qian Y., Kaufman S., Ring B.D., Van G., Capparelli C., Kelley M., Hsu H., Boyle W. J., Dunstan C. R., Hu S., and Lacey D. L. 1999. The ligand for osteoprotegerin (OPGL) directly activates mature osteoclasts. *J Cell Biol*. 145, 527-538.

Burr, D.B., Martin, R.B., 1993. Calculating the probability that microcracks initiate resorbtion spaces. *J. Biomech*. 26, 613–616.

Cacik, F., Dondo, R. G., Marqués, D. (2001). Optimal control of a batch bioreactor for the production of xanthan gum, *Comp. & Chem. Eng.*, 25, s2-3, 409-418.

Canalis E., 1980. Effect of insulin-like growth factor I on DNA and protein synthesis in cultured rat calvaria. *J Clin Invest*, 66. 709-719.

Cannon, W.R., Singleton,S.F., Bencovic, S.J. (1996). A perspective on biological catalysis. *Nat. Struc. Biol.* 3, 821-833.

Cao X., Chen D., 2005. The BMP signaling and in vivo bone formation. *Gene*, 357,1-8.

Carpio L. C., H. Shiau, R. Dziak 2000. Changes in sphingolipid levels induced by epidermal growth factor in osteoblastic cells. Effects of these metabolites on cytosolic calcium levels Prostagl, *Leukotr Ess Fat Acids*, 62(4) 225-232.

Carter D.R., Orr T.E., Fyhrie D.P., Relationships between loading history and femoral cancellous bone architecture. *J Biomech*. 1989,22(3).231-44

Carter D.R., Van der Meulen M.C.H., Beaupre G.S., 1996. Mechanical factors in bone growth and development. *Bone*, 18(1), Supplt 1, S5-S10.

Carter, D. R. (1987) Mechanical loading history and skeletal biologv. *J. Biomechanics*, 20. 1095-1109.

Carter, D. R., Fyhrie, D. P. and Whalen, R. T. (1987) Trabecular bone density and loading history: regulation of connective tissue biology by mechanical energy. *J. Biomechanics* 20, 785-794.

Chambers, T.J., Magnus, C.J., 1982. Calcitonin alters behavior of isolated osteoclasts. *J. Pathol*. 136, 27– 39.

Chávez, I.Y.S., Morales-Menéndez, R., Chapa, S.O.M. (2009). Glucose optimal control system in diabetes treatment. *App.Math. and Comp.* 209(1), 19-30.

Chen D., Zhao M., and Mundy G. R., 2004. Bone Morphogenetic Proteins. *Growth Factors* 22 (4). 233–241.

Chen, H.-R., Ji, S.-Q.,Wang, H.-X., Yan, H.-M., Zhu, L., Liu, J., Xue, M., Xun, C.-Q. 2003. Humanized anti-CD25 monoclonal antibody for prophylaxis of graft-versus-host disease (GVHD) in haploidentical bone marrow transplantation without ex vivo T-cell depletion. *Exp. Hematol.* 31, 1019–1025.

Chien HH, Lin WL, Cho MI. 2000. Down-regulation of osteoblastic cell differentiation by epidermal growth factor receptor. *Calcif Tissue Int*. 67(2).141-50.

Cho T.-J., Gerstenfeld L.C., Einhorn T.A. 2002. Differential temporal expression of members of the transforming growth factor B superfamily during murine fracture healing. *J Bone Miner Res*,17.513–20.

Chow J.W., Wilson A.J., Chambers T.J., Fox S.W. 1998. Mechanical loading stimulates bone formation by reactivation of bone lining cells in 13-week-old rats. *J Bone Miner Res,* 13, 1760–1767.

Civitelli R., 2008. Cell–cell communication in the osteoblast/osteocyte lineage. *Arch Biochem Biophys*, 473(2), 188-192.

Colopy S. A., Benz-Dean J., Barrett J. G., Sample S. J., Lu Y., Danova N. A., Kalscheur V. L., Vanderby R. Jr., Markel M. D., Muir P. 2004. Response of the osteocyte syncytium adjacent to and distant from linear microcracks during adaptation to cyclic fatigue loading. *Bone, 35(4)*, 881-891.

Compston J.E., 2002. Bone Marrow and Bone. *J. Endocrin*. 173, 387-394.

Conover C. A., Rosen C., 2002. The Role of Insulin-like Growth Factors and Binding Proteins in Bone Cell Biology Principles of Bone Biology (Second Edition), 801-815.

Cornish-Bowden, A. 200). "Fundamentals of Enzyme Kinetics." 3rd ed. Portland Press, London.

Davidson B. P., Cheng L., Kinder S. J., Tam P. P. L., 2000. Exogenous FGF-4 Can Suppress Anterior Development in the Mouse Embryo during Neurulation and Early Organogenesis. *Dev.Biol*, 221(1), 41-52.

Davidson P. L., Milburn P. D. and Wilson B. D. 2004. Biological adaptive control model: a mechanical analogue of multi-factorial bone density adaptation. *J.Theor Biol*, 227(2) 187-195.

Davie M., Davies M., Francis R., Fraser W., Hosking D., Tansley R. Paget's disease of bone: a review of 889 patients. *Bone*, 24, (1999), 11S-12S

Delezoide A.-L., C. Benoist-Lasselin, L. Legeai-Mallet, M. Le Merrer, A. Munnich, M. Vekemans and J. Bonaventure 1998. Spatio-temporal expression of FGFR 1, 2 and 3 genes during human embryo-fetal ossification. *Mech. Devel*. 77(1), 19-30.

Delrieu I., 2000. The high molecular weight isoforms of basic fibroblast growth factor (FGF-2): an insight into an intracrine mechanism, *FEBS Letters*, 468, 6-10.

Demongeot, J., Kaufman, M., Thomas, R., 2000. Positive feedback circuits and memory. Life Sci. 323, 69–79.

Denhardt, D.T., Noda, M., 1998. Osteopontin expression and function: role in bone remodeling. *J. Cell. Biochem*. 30/31 (Suppl.), 92–102.

Denley A., Cosgrove L. J., Booker G. W., Wallace J. C., Forbes B. E., 2005. Molecular interactions of the IGF system. *Cytokin Growth Factor Rev*, 16(4-5) 421-439.

Dixon C.J., W.B. Bowler, C.A. Walsh and J.A. Gallaaher. 1995. Co-stimulation with ATP and PTH induces oscillations in intracellular free calcium concentration in single FURA-2 loaded primary human osteoblasts. *Bone* 17, 557-596.

Doblare M., Cueto E., Calvo B., Martínez M.A., Garcia J.M., Cegoñino J. 2005. On the employ of meshless methods in biomechanics. *Comp Meth Appl Mech Eng*, 194(6-8) 801-821.

Doblare M., Garcia J. M.. 2001. Application of an anisotropic bone-remodelling model based on a damage-repair theory to the analysis of the proximal femur before and after total hip replacement. *J Biomechanics*, 34(9)1157-1170.

Doblare, M., Garcıa, J.M. 2002. Anisotropic bone remodelling model based on a continuum damage-repair theory. *J Biomechanics*. 35, 1–17.

Dobnig, H., Turner R. T. 1996. Evidence that PTH induces modulation of bone lining cells to osteoblasts in vivo and that the therapeutic window for an anabolic PTH response is of short duration *Bone*, 19, Supplement 1, S 138.

Dreux A. C., Lamb D. J., Modjtahedi H., Ferns G. A.A. 2006. The epidermal growth factor receptors and their family of ligands: Their putative role in *atherogenesis Atherosclerosis*, 186(1), 38-53.

Duong L.T., Sanjay A., Horne W., Baron R., Rodan G.A. 2002. Integrin and Calcitonin Receptor Signaling in the Regulation of the Cytoskeleton and Function of Osteoclasts, Principles of Bone Biology (Second Edition), 141-150.

Duque, G., El Abdaimi, K., Henderson, J.E., Lomri, A., Kremer, R. 2004. Vitamin D inhibits Fas ligand-induced apoptosis in human osteoblasts by regulating components of both the mitochondrial and Fas-related pathways. *Bone* 35, 57–64.

Eaton, W.A., Henry, E.R., Hofrichter, J., Mozzarelli, A. 1999. Is cooperative oxygen binding by hemoglobin really understood? *Nat. Struct. Biol.* 6, 351–358.

Elefteriou F., 2008. Regulation of bone remodeling by the central and peripheral nervous system. *Archives of Biochemistry and Biophysics*, 473, 231-236.

Elsner, L., Giersch, C. (1998). Metabolic control analysis: Separable Matrixes and Interdependence of Control Coefficients. *J. Theor. Biol.* 193, 593-599.

Epstein S., 2006. Update of current therapeutic options for the treatment of postmenopausal osteoporosis *Clinical Therapeutics* 28, 151-173.

Eren-Oruklu M., Cinar, A., Quinn, L., Smith, D. 2009. Adaptive control strategy for regulation of blood glucose levels in patients with type 1 diabetes. *J. Proc. Contr.* 19(8), 1333-1346.

Fakhry A., Ratisoontorn C., Vedhachalam C., Salhab I., Koyama E., Leboy P., Pacifici M., Kirschner R. E., Nah H.-D. 2005. Effects of FGF-2/-9 in calvarial bone cell cultures: differentiation stage-dependent mitogenic effect, inverse regulation of BMP-2 and noggin, and enhancement of osteogenic potential. *Bone,* , 36(2).254-266.

Fan, X., Roy, E., Zhu, L., Murphy, T.C., Ackert-Bicknell, C., Hart, C.M., Rosen, C., Nanes, M.S., Rubin, J., 2004. Nitric oxide regulates RANKL and OPG expression in bone marrow stromal cells. Endocrinology 145, 751–759.

Farnworth, P.G., Harrison, C.A., Leembruggen, P., Chan, K.L., Stanton, P.G., Ooi, G.T., Rahman, N.A., Huhtaniemi, I.T., Findlay, J.K., Robertson, D.M., 2001. Inhibin binding sites and proteins in pituitary, gonadal, adrenal and bone cells. Mol. Cell. Endocrinol. 180, 63–71.

Feister H.A., Onyia J.E., Miles R.R., Yang X., Galvin R., Hock J.M., Bidwell J.P. 2000. The expression of the nuclear matrix proteins NuMA, topoisomerase II-α, and -β in bone and osseous cell culture: regulation by parathyroid hormone. Bone, 26(3) 227-234.

Fell, D.A. 1997. "Understunding the Control of Metabolism." Portland Press, London.

Fell, D.A., Thomas, S. 1995. Physiological control of metabolic flux: the requirement for multisite modulation. *Biochem. J.* 331, 35-39.

Feng X. 2005. Regulatory roles and molecular signaling of TNF family members in osteoclasts *Gene*, 350, 1-13.

Fernandes P. R., Folgado J., Jacobs C., Pellegrini V., 2002. A contact model with ingrowth control for bone remodelling around cementless stems. J Biomechanics, 35(2) 167-176

Fischer K. J., Jacobs C. R., Levenston M. E., Carter D. R. 1996. Different loads can produce similar bone density distributions. *Bone*, 19(2), 127-135.

Frost, H. M. 1964. Mathematical Elements of Lamellar Bone Remodelling. Charles C. Thomas Publisher.

Frost, H.M., 2001. Cybernetics aspects of Bone Modelling and Remodeling, With Special Reference to Osteoporosis and Whole-Bone Strength. Amer. J. Human. Biol. 13, 235-248.

Fuller K, Owens J.M. and Chambers T.J., 1995. Macrophage inflammatory protein-1 alpha and IL-8 stimulate the motility but suppress the resorption of isolated rat osteoclasts J Immun, 154, 6065-6072

Fuller K., Murphy Ch., Kirstein B., Fox S.W. and Chambers T.J. 2002. TNF-α potently activates osteoclasts, through a direct action independent of and strongly synergistic with RANKL, *Endocrinology*. 143, 1108–1118.

Fuller K., Wong B., Fox S., Choi Y., Chambers T.J. 1998. TRANCE is necessary and sufficient for osteoblast-mediated activation of bone resorption in osteoclasts. *J Exp Med*.188, 997-1001.

Fushitani, K., Imai, K., Riggs, A.F. 1986. Oxygenation Properties of Hemoglobin of the Earthworm, Lumbricus terrestris. *J. Biol. Chem.* 261(18), 8414-8423.

Fushitani, K., Riggs, A.F. 1992. The extracellular Hemoglobin of the Earthworm, Lumbricus terrestris. *J. Biol. Chem.* 266(16), 10275-10281.

Fyhrie D.P., Kimura J.H. 1999. Cancellous bone biomechanics. J Biomech 32 1139-1148

Gadkar, K.G., Mahadevan, R., Doyle, F.J. 2006. III Optimal genetic manipulations in batch bioreactor control. *Automatica.* 42(10), 1723-1733.

Gao, Y.H., Shinki, T., Yuasa, T., Kataoka-Enomoto, H., Komori, T., Suda, T., Yamaguchi, A., 1998. Potential role of cbfa1, an essential transcriptional factor for osteoblast differentiation, in osteoclastogenesis: regulation of mRNA expression of osteoclast differentiation factor (ODF). *Biochem. Biophys. Res. Commun*. 252, 697–702.

Garcia J. M., Doblare M. and Cegonino J. 2002. Bone remodelling simulation: a tool for implant design. Comp Materials Sci, 25(1-2), 100-114

Garcia-Aznar J.M., Kuiper J.H., Gómez-Benito M.J., Doblaré M. and Richardson J.B. 2007. Computational simulation of fracture healing: Influence of interfragmentary movement on the callus growth. *J Biomechanics*, 40(7) 1467-1476.

Gelfand, I.M., and Fomin, S.V. 1963. "Calculus of Variation." Prentice-Hall, Englewood Cliffs, NJ.

Geris L., Gerisch A., Sloten J. V., Weiner R. and Oosterwyck H. Van, 2008. Angiogenesis in bone fracture healing: A bioregulatory model. *J Theor Biol*, 251(1) 137-158.

Gerwins P., Sköldenberg E., Claesson-Welsh L., 2000. Function of fibroblast growth factors and vascular endothelial growth factors and their receptors in angiogenesis. *Crit Rev Oncol/Hemat*, 34(3) 185-194.

Giachelli C.M., Steitz S., 2000. Osteopontin: a versatile regulator of inflammation and biomineralization. *Matrix Biology*, 19(7), 615–622.

Giersch, C. 1998. Control analysis of metabolic networks 1. Homogeneous functions and the summution theorems for control coefficients. *Eur. J. Biochem.* 174, 509-513.

Giuseppin, M.L.F., van Riel, N.A.W. 2000. Metabolic Modeling of *Saccharomyces cerevisiae* Using the Optimal Control of Homeostasis: A Cybernetic Model Definition. *Metab. Eng*. 2(1), 14-33.

Goldring S.R., Gorn A.H., Yamin, M., Krane, S.M., and Wang J.T. 1993. Characterization of the structural and functional properties of cloned calcitonin receptor cDNAs. Horm Metab Res 25.477–480.

Goltzman, D., 1999. Interactions of PTH and PTHrP with the PTH/PTHrP receptor and with downstream signaling pathways: exceptions that provide the rules. J. Bone Miner. Res. 14, 173–177.

Govinden R., Bhoola K. D. 2003. Genealogy, expression, and cellular function of transforming growth factor-β. *Pharmacology & Therapeutics*, 98(2), 257-265

Gronthos S., Simmons P. J., Graves S. E., Robey P. G. 2001. Integrin-mediated interactions between human bone marrow stromal precursor cells and the extracellular matrix, *Bone* 28, 174-181.

Grover D. M., Chen A.A, Hazelwood S. J., 2007. Biomechanics of the rabbit knee and ankle: Muscle, ligament, and joint contact force predictions, *J. Biomech* 40, 2816–2821

Harrigan T. P., Hamilton J. J., Reuben J. D., Toni A., Viceconti M., 1996. Bone remodelling adjacent to intramedullary stems: an optimal structures approach. *Biomater* 17(2) 223-232

Harrison C. A., Wiater E., Gray P. C., Greenwald J., Choe S., Vale W., 2004. Modulation of activin and BMP signaling *Mol and Cell Endocriny*, 225(1-2), 19-24.

Hart, R. T. and Davy. D. T. 1989. Theories of bone modelling and remodeling. Bone Mechanics (Edited Edited by S. C. Cowin), pp. 253-277. CRC Press, Boca Raton.

Hashimoto M., Koda M., Ino H., Murakami M., Yamazaki M., Moriya H. 2003. Upregulation of Osteopontin Expression in Rat Spinal Cord Microglia after Traumatic Injury J Neurotrauma. 20(3) 287-296.

Hayman A. R., Cox T. M. 2004. Tartrate-resistant acid phosphatase: a potential target for therapeutic gold. *Cell Biochemistry and Function* 22 (5), 275 - 280.

He G., Xinghua Z., 2006. The numerical simulation of osteophyte formation on the edge of the vertebral body using quantitative bone remodeling theory. *Joint Bone Spine*, 73(1) 95-101.

Heckman JD, Ehler W, Brooks BP, et al. 1999. Bone morphogenetic protein but not transforming growth factor-beta enhances bone formation in canine diaphyseal nonunions implanted with a biodegradable composite polymer. *J Bone Joint Surg*, 81A. 1717–29.

Heino, T.J., Hentunen, T.A., Vaananen, H.K., 2004. Conditioned medium from osteocytes stimulates the proliferation of bone marrow mesenchymal stem cells and their differentiation into osteoblasts. *Exp. Cell Res*. 294, 458–468.

Heinrich, R., Holzhutter, H.-G., 1985. Efficiency and design of simple metabolic systems. Biomed. Biochim. *Acta 44*, 959–969.

Heinrich, R., Montero, F., Klipp, E., Waddell, T.G., Melendez-Hevia, E. 1997. Theoretical approaches to the evolutionary optimisation of glycolysis. Thermodynamics and kinetics constrains, *Eur. J. Biochem.* 243, 191-201.

Heinrich, R., Schuster, S., Holzhutter, H-G. 1991. Mathematical analysis of enzymic reaction systems using optimisation principle. *Eur. J. Biochem.* 201, 1-21.

Helgason B., Perilli E., Schileo E., Taddei F., Brynjólfsson S. and Viceconti M., 2008. Mathematical relationships between bone density and mechanical properties: A literature review. Clin Biomech, 23(2) 135-146.

Hellmann, N., Weber, R. E. and Decker, H. 2003. Nested Allosteric Interactions in Extracellular Hemoglobin of the Leech *Macrobdella decora*. *J. Biol. Chem.* 278(45), 44355–44360.

Herbst R.S. 2004. "Review of epidermal growth factor receptor biology". *Int. J. Radiat. Oncol. Biol. Phys.* 59 (2 Suppl). 21-26.

Hernandez C.J., Beaupre G.S. and Carter D.R., 2003. A theoretical analysis of the changes in basic multicellular unit activity at menopause. Bone 32 357–363.

Hershey C.L., Fisher D.E. 2004. Mitf and Tfe3: members of a b-HLH-ZIP transcription factor family essential for osteoclast development and function. Bone, 34, 689-696.

Heymann D., Guicheux J., Gouin F., Passuti N., Daculsi G. 1998. Cytokines, frowth factors and osteoclasts. *Cytokine*, 10(3) 155-168.

Heymann D., Rousselle A.-V. 2000. gp130 Cytokine family and bone cells. *Cytokine*, 12, 1455-1468.

Higgens, J. 1967. The theory of oscillating reactions, *Indust. and Eng. Chem.* 59(5), 19–62.

Hill P.A., Orth M. Bone Remodelling. Brit J Orthodont 1998 25 101-107.

Hill, A.V. 1910. The possible effects of the aggregation of the molecules of haemoglobin on its dissociation curves. *J. Physiol*. 40, iv-vii.

Hoare, S.R.J., De Vries, G., Usdin, T.B. 1999. Measurement of agonist and antagonist ligand-binding parameters at the human parathyroid hormone type 1 receptor: evaluation of receptor states and modulation by guanine nucleotide 1, *JPET*, 289, 1323–1333.

Hodsman A.B., Fraher L.J., Watson P.H., 1999. Parathyroid Hormone. *The Aging Skeleton, 1999, 563-578.*

Hofbauer, L.C., Dunstan, C.R., Spelsberg, T.C., Riggs, B.L., Khosla, S., 1998. Osteoprotegerin production by human osteoblast lineage cells is stimulated by vitamin D, bone morphogenetic protein- 2, and cytokines. Biochem. Biophys. Res. Commun. 250 (3), 776–781.

Hofbauer, L.C., Khosla, S., Dunstan, C.R., Lacey, D.L., Boyle, W.J., Riggs, B.L., 2000. The roles of osteoprotegerin and osteoprotegerin ligand in the paracrine regulation of bone resorption. J. Bone Miner. Res. 5, 2–12.

Hofbauer, L.C., Lacey, D.L., Dunstan, C.R., Spelsberg, T.C., Riggs, B.L., Khosla, S., 1999. Interleukin-1 and tumor necrosis factor, but not interleukin-6, stimulate osteoprotegerin ligand gene expression in human osteoblastic cells. Bone 25, 255–259.

Hofmeyr, J.H., Cornish-Bowden, A. 1997. The reversible Hill equation: how to incorporate cooperative enzymes into metabolic models. *Comput. Appl. Biosci.* 13(4), 377-85.

Hofmeyr, J-G.S., Cornish-Bowden, A., Rochwer, J.M., 1993. Taking enzyme kinetics out of control; putting control into regulation. Eur. J. Biochem. 212, 833–837.

Hogan BLM. Bone morphogenetic proteins: multifunctional regulators of vertebrate development. Genes Dev 1996,10.1580–94.

Horowitz, M.C., Xi, Yo., Wilson, K., Kacena, M., 2001. Control of osteoclastogenesis and bone resorption by members of the TNF family of receptors and ligands. Cytokine Growth Fact. Rev. 12, 9–18.

Horwood N. J., Udagawa N., Elliott J., Grail D., Okamura H., Kurimoto M., Dunn A.R., Martin T. J., and Gillespie M. T., 1998. Interleukin 18 Inhibits Osteoclast Formation via T Cell Production of Granulocyte Macrophage Colony-stimulating Factor. *J. Clin. Invest.* 101.595–603.

Hotelling, H., 1936. Relations between two sets of variates. *Biometrica* 28, 321-377.

Hsu, S. B., Yen-Sheng, L., Waltman, P. 2000. Competition in the presence of a lethal external inhibitor. *Math. Biosci.* 167, 171-199.

Hu D.E., Hori Y., Fan T.-P.D. 1993. Interleukin-8 stimulates angiogenesis in rats. Inflammation 17(2), 135-143.

Huber D.M., A. C. Bendixen, P. Pathrose, S. Srivastava, K. M. Dienger, N.K. Shevde and J. W. Pike, 2001. Androgens Suppress Osteoclast Formation Induced by RANKL and Macrophage-Colony Stimulating Factor. *Endocrinology*, 142(9) 3800-3808.

Huiskes R., Boeklagen R.. 1989. Mathematical shape optimization of hip prosthesis design. J Biomech, 22, Issues 8-9, 793-799.

Huiskes R., Favenesi J., Gardeniers J., Pöttgens M., Slooff T. J. 1985. Mechanical properties of trabecular bone, an experimental and finite element study *J Biomechanics*, 18(7) 522

Huiskes R., Weinans H., Grootenboer H.J., Dalstra M., Fudala B., Sloof T.J. 1987. Adaptive bone remodeling theory applied to prosthetic design analysis. *J Biomech* 20. 1135-1150.

Hurley M. M., Marie P. J., Florkiewicz R. Z. 2002. Fibroblast Growth Factor (FGF) and FGF Receptor Families in Bone *Principles of Bone Biology (Second Edition)*, 825-851.

Hynes, R.O., 2002. Integrins: bidirectional, allosteric signalling machines. Cell 110, 673–687.

Ibbotson K. J., Harrod J., Gowen M., D'Souza S., Smith D. D., Winkler M. E., Derynck R. and Mundy G. R., 1986. Human Recombinant Transforming Growth Factor α Stimulates Bone Resorption and Inhibits Formation in vitro. *Proceed Nat Acad Sci USA*, 83(7) 2228-2232

Ikegame M., Ejiri S., Ozawa H. 2004. Calcitonin-induced change in serum calcium levels and its relationship to osteoclast morphology and number of calcitonin receptors Bone, 35, 27-33.

Ishida Yo., Kawai Sh., 2004. Comparative efficacy of hormone replacement therapy, etidronate, calcitonin, alfacalcidol, and vitamin K in postmenopausal women with osteoporosis: The Yamaguchi Osteoporosis Prevention Study. *Amer J Med*, 117, 549-555.

Itik, M., Salamci, M.U., Banks, S.P. 2009. Optimal control of drug therapy in cancer treatment. *Nonlin. Anals: Theory, Meth. Appl.* 71(12), e1473-e1486.

Jacobs C.R., Levenston M. E., Beaupre G. S., Simo J. C. and Carter D. R., 1995. Numerical instabilities in bone remodeling simulations: The advantages of a node-based finite element approach. *J Biomechanics* 28(4) 449-459.

Janssens K., M. de Vernejoul , F. de Freitas , F. Vanhoenacker , W. Van Hul, An intermediate form of juvenile Paget's disease caused by a truncating mutation. Bone 36 , 2005, 542 - 548.

Jaunberzins A., Stomat D., Gutmann J. L., Witherspoon D. E., Harper R. P. 2000, Effects of Calcium Hydroxide and Tumor Growth Factor-β on Collagen Synthesis in Subcultures I and V of Osteoblasts *J Endodontics*, 26(9) 494-499.

Ji X., Chen D., Xu C., Harris S. E., Mundy G. R. and Yoneda T. 2000. Patterns of gene expression associated with BMP-2-induced osteoblast and adipocyte differentiation of mesenchymal progenitor cell 3T3-F442A J Bone Mineral Metab, 18, 132-139.

Jilka R. L. 2003. Biology of the basic multicellular unit and the pathphisiology of osteoporosis. *Med Pediatr Oncol Sep,* 41(3) 182-185

Jilka R.L., Weinstein R.S., Bellido T., Parfitt A.M., Manolagas S.C. 1998. Osteoblast programmed cell death (apoptosis): modulation by growth factors and cytokines. J Bone Miner Res 13 793–802.

Jilka R.L., Weinstein R.S., Bellido T., Roberson P., Parfitt A.M., Manolagas S.C. 1999. Increased bone formation by prevention of osteoblast apoptosis with parathyroid hormone. *J Clin Invest*. 104, 439–446.

Johnson C.S, Jerome C.P, Brommage R. *2000,* Unbiased determination of cytokine localization in bone: colocalization of interleukin-6 with osteoblasts in serial sections from monkey vertebrae *Bone,* 26,(5) 461-467.

Johnson E.E, Urist M.R. 1998. One-stage lengthening of femoral nonunion augmented with human bone morphogenetic protein. *Clin Orthop Rel Res* 347, 105–16.

Jones D.C., Wein M.N., Oukka M, Hofstaetter J.G., Glimcher M.J., and Glimcher L.H., 2006. Regulation of adult bone mass by the zinc finger adapter protein Schnurri-3. Science. 312(5777).1223-1227.

Jones G., 2002. Vitamin D and Analogs. Principles of Bone Biology (Second Edition), 1407-1422.

Jono S., Nishizawa Yo., Shioi A., Morii H. 1998. 1,25-Dihydroxyvitamin D_3 Increases In Vitro Vascular Calcification by Modulating Secretion of Endogenous Parathyroid Hormone–Related Peptide. *Clin Invest Rep*, 98, 1302-1306.

Kakuji, J.T., Akapi, O. 1994. Pharmacokinetic model of intravitreal drug injection. *Math. Biosci.* 123, 59–75.

Kameda H., Takeuchi T. 2003. Osteoporosis associated with rheumatoid arthritis Nippon Rinsho. 61(2), 292-298.

Kanis J.A., Melton III L.J., Christiansen C., Johnston C.C., Khaltaev N. 1994. The diagnosis of osteoporosis. *J Bone Miner Res,* 9, 1137–41.

Kapadia R. M., Guntur A. R., Reinhold M. I., Naski M. C.. Glycogen synthase kinase 3 controls endochondral bone development: Contribution of fibroblast growth factor 18. Develop Biol, 285, 2005, 496-507

Kaskani E., Lyritis G.P., Kosmidis C., Galanos A., Andypas G., Chorianopoulos K., Giagiosis A., Iliadou K., Karagianis A., Katsimichas K., Koskinas A., Matsouka K. 2005. Effect of intermittent administration of 200 IU intranasal salmon calcitonin and low

doses of 1alpha(OH) vitamin D3 on bone mineral density of the lumbar spine and hip region and biochemical bone markers in women with postmenopausal osteoporosis: a pilot study. *Clin Rheumatol*, 24(3), 232-238.

Kassem, M., Harris, S. A., Spelsberg, T. C., and Riggs, B. L. Estrogen inhibits interleukin-6 production and gene expression in a human osteoblastic cell line with high levels of estrogen receptors. *J Bone Miner Res*, 11, 193–199, 1996.

Kato, Y., Boskey, A., Spevak, L., Dallas, M., Hori, M., Bonewald, L.F. 2001. Establishment of an osteoid preosteocyte-like cell MLO-A5 that spontaneously mineralises in the culture. J. Bone Miner. Res. 16(9), 1622-1633.

Kawaguchi, H., Kurokawa, T., Hanada, K., Hiyama, Y., Tamura, M., Ogata, E., Matsumoto, T. 1994. Stimulation of fracture repair by recombinant human basic fibroblast growth factor in normal and streptozotocin diabetic rats. *Endocrinology,* 135, 774–781.

Keesman, K.J., Stigter, J.D. 2002. Optimal parametric sensitivity control for the estimation of kinetic parameters in bioreactors. *Math. Biosci.* 179, 95-111.

Kelman A., Lane N. E. 2005. The management of secondary osteoporosis. *Best Practice & Research Clinical Rheumatology*, 19, 1021-1037.

Kerner J., Huiskes R., van Lenthe G. H., Weinans H., van Rietbergen B., Engh C. A., Amis A. A., 1999. Correlation between pre-operative periprosthetic bone density and post-operative bone loss in THA can be explained by strain-adaptive remodelling. *J Biomech*, 32(7), 695-703.

King G. J., Holtrop M. E., Raisz L. G., 1978. The relation of ultra structural changes in osteoclasts to resorption in bone cultures stimulated with parathyroïd hormone. *Metab Bone Dis Rel Res, 1, 67-74.*

Kloen P., Di Paola M., Borens O., Richmond J., Perino G., Helfet D. L., Goumans M. J., 2003. BMP signaling components are expressed in human fracture callus. *Bone*, 33(3), 362-371.

Klotz, I. M. 1997. "Ligand-Receptor Energetics." John Wiley and Sons Inc., New York.

Kneissel, M. The conundrum of Wnt/beta-catenin signaling in bone Bone, 48, Suppl2, 2011, S60.

Kobayashi Ya., Take I., Yamashita T., Mizoguchi T., Ninomiya T., Hattori T., Kurihara S., Ozawa H., Udagawa N., and Takahashi N. 2005. Prostaglandin E2 Receptors EP2 and EP4 Are Down-regulated during Differentiation of Mouse Osteoclasts from Their Precursors. *J Biol Chem.* 280(25), 24035–24042.

Koch A.E., Polverini P.J., Kunkel S.L., Harlow L.A., DiPietro L.A., Elner V.M., Elner SG, Strieter RM. 1992. Interleukin-8 as a macrophage derived mediator of angiogenesis. Science 258(5089), 1798-1801.

Kochupillai N., 2008. The physiology of vitamin D : Current concepts. *Indian J Med Res*, 127, 256-262.

Koegler, W.S., Griffith, L.G., 2004. Osteoblast response to PLGA tissue engineering scaffolds with PEO modified chemistries and demonstration of patterned cell response. *Biomaterials* 25, 2819-2830.

Koka, S., Petro, T. M., and Reinhardt, R. A. Estrogen inhibits interleukin-1beta-induced interleukin-6 production by human osteoblast-like cells. J Interferon Cytokine Res. 18.479–483, 1998.

Komarova S.V. 2005. Mathematical model of paracrine interactions between osteoclasts and osteoblasts predicts anabolic effects of parathyroid hormone on bone. *Endocrinology* 146 (8). 3589-95.

Komarova, S.V., Shum, J.B., Paige, L.A., Sims, S.M., Dixon, S.J., 2003b. Regulation of osteoclasts by calcitonin and amphiphilic calcitonin conjugates: role of cytosolic calcium. *Calcif. Tissue Int*. 73, 265–273.

Komarova, S.V., Smith, R.J., Dixon, S.J., Sims S.M., Wahl L.M., 2003a. Mathematical model predicts a critical role for osteoclast autocrine regulation in the control of bone modelling. *Bone* 33, 206-215.

Kondepudi, D., and Prigogine, I. 1998. "Modern Thermodynamics: From Heat Engines to Dissipative Structures." John Wiley & Sons, Chichester.

Kong, Y.-Y., Penninger, J.M. 2000. Molecular control of bone remodelling and osteoporosis. Exp. Gerontol. 35, 947–956.

Koshland, D.E., Nemethy, G. & Filmer, D. 1966. Comparison of experimental binding data and theoretical models in protein containing subunits. *Biochemistry* 5, 365-385.

Kostenuik P. J., 2005. Osteoprotegerin and RANKL regulate bone resorption, density, geometry and strength *Cur Opin Pharmacol*, 5, 618-625.

Kramer, I., Halleux, C., Keller, H., Pegurri, M., Gooi, J.H., Weber, P. B., Feng, J.Q., Bonewald, L. F., and Kneissel M., Osteocyte Wnt/β-Catenin Signaling Is Required for Normal Bone Homeostasis. Molecular and Cellular Biology, 2010, 30(12) 3071-3085.

Kruithof B.P.T., van Wijk B., Somi S., K.-de Julio M., Pomares J. M. P., Weesie F., Wessels A., Moorman A.F.M., van den Hoff M.J.B. 2006. BMP and FGF regulate the differentiation of multipotential pericardial mesoderm into the myocardial or epicardial lineage. Dev Biol, 295(2) 507-522.

Kumar R., Panoskaltsis N., Stepanek F. and Mantalaris A. 2008. Coupled oxygen–carbon dioxide transport model for the human bone marrow Food Bioprod Process, 86(3) 211-219.

Kumar R., Stepanek F. and Mantalaris A. 2004. An Oxygen Transport Model for Human Bone Marrow Microcirculation Food Bioprod Proc, 82(2) 105-116.

Kumei Y., Shimokawa H., Katano H., Hara E., Akiyama H., Hirano M., Mukai C., Nagaoka S.,. Whitson P. A, Sams C. F., 1996. Microgravity induces prostaglandin E_2 and interleukin-6 production in normal rat osteoblasts: role in bone demineralization. J Biotech., 47(2-3), 313-324.

Kummer, B.K.F. 1972. Biomechanics of bone: Mechanical properties, functional structure, functional adaptation. In Y.C.Fung (Ed) Biomechanics: Ins Foundation and Objectives, 237 -271. Englewood Cleffs: Prentice-Hall.

Lacey, E. Timms H., Tan-L., Kelley M. J., Dunstan C. R., Burgess T., Elliott R., A. Colombero D. L., Elliott G., Scully S., Hsu H., Sullivan J., Hawkins N., Davy E., Capparelli C., Eli A., Qian Y.-X., Kaufman S., Sarosi I., Shalhoub V., Senaldi G., Guo, J. J. and Boyle W. J. 1998. Osteoprotegerin ligand is a cytokine that regulates osteoclast differentiation and activation. *Cell*. 93, 165-176.

Laitala-Leinonen, T., Rinne, R., Saukko, P.,Vaananen, H.K., Rinne, A., 2006. Cystatin B as an intracellular modulator of bone resorption. *Matrix Biol*. 25, 149–157.

Langton C.M., Haire T.J., Ganney P.S., Dobson C.A., Fagan M. J., 1998. Dynamic Stochastic Simulation of Cancellous Bone Resorption. Bone, 22(4), 375-380

Langton C.M., Haire T.J., Ganney P.S., Dobson C.A., Fagan M.J., Sisias G., Phillips R., 2000. Stochastically simulated assessment of anabolic treatment following varying degrees of cancellous bone resorption. *Bone*, 27(1), 111-118.

Lanyon, L.E., 1996. Using functional loading to influence bone mass and architecture. *Bone* 18 (Suppl. 1), 37s–43s.

Lari R., Fleetwood A. J., Kitchener P. D., Cook A. D., Pavasovic D., Hertzog P. J., Hamilton J. A. 2007. Macrophage lineage phenotypes and osteoclastogenesis - Complexity in the control by GM-CSF and TGF-β, *Bone*, 40 (2) 323-336.

Lazarus J. E., Hegde A., Andrade A. C., Nilsson O., Baron J., 2007. Fibroblast growth factor expression in the postnatal growth plate, *Bone*, 40(3), 577-586.

Lebman D., Edmiston J. 1999. The role of TGF-beta in growth, differentiation, and maturation of B lymphocytes". *Microbes Infect* 1 (15). 1297–304.

Ledzewicz U. and Schättler H., 2007. Optimal controls for a model with pharmacokinetics maximizing bone marrow in cancer chemotherapy. *Math Biosci*, 206(2), 320-342.

Lemaire V., Tobin F.L., Greller L.D., Cho C.R. and Suva L.J. 2004. Modeling the interactions between osteoblast and osteoclast activities in bone remodelling. *J Theor Biol*, 229(3) 293-309.

Lenas, P., Pavlou, S. 1995. Coexistence of three Competing Microbial populations in a chemostat with periodically varying dilution rate. *Math. Biosci.* 129, 111-142.

Lennon A. B. and Prendergast P. J. 2002. Residual stress due to curing can initiate damage in porous bone cement: experimental and theoretical evidence. *J Biomechanics* 35 (3), 311-321.

Lerner U., 1982. Indomethacin inhibits bone resorption *in vitro* without affecting bone collagen synthesis, *Inflammation Research*, 12, 466-470.

Li J., Li H., Shi L., Fok A.S.L., Ucer C., Devlin H., Horner K. and Silikas N., 2007. A mathematical model for simulating the bone remodeling process under mechanical stimulus. Dent Materials, 23(9) 1073-1078.

Li J., Sarosi I., Cattley R. C., Pretorius J., Asuncion F., Grisanti M., Morony S., Adamu S., Geng Z., Qiu W., Kostenuik P., Lacey D. L., Simonet W. S., Bolon B., Qian X., Shalhoub V., Ominsky M. S., Ke H. Z., Li X., Richards W. G. Dkk1-mediated inhibition of Wnt signaling in bone results in osteopenia. Bone 39 (2006) 754–766

Li L., Pettit A. R., Gregory L. S., Forwood M. R. 2006. Regulation of bone biology by prostaglandin endoperoxide H synthases (PGHS): A rose by any other name… Cyt Growth Fact Rev, 17(3) 203-216.

Liang, Y., Leung, K.-S., Mok, T.S.K. (2008). Evolutionary drug scheduling models with different toxicity metabolism in cancer chemotherapy. *Appl. Soft. Comput*. 8(1), 140-149.

Lineweaver, H., Burk, D. 1934. The determination of enzyme dissociation constants. *J. Am. Chem. Soc*. 56, 658-666.

Linkhart, T.A., Mohan, S., Baylink, D.J. 1996. Growth factors for bone growth and repair: IGF, TGF beta and BMP. *Bone*, 19, 1S–12S.

Little, R.D., Carulli, J.P., Del Mastro, R.G., Dupuis, J., Osborne, M., Folz, C., Manning, S.P., Swain, P.M., Zhao, S.C., Eustace, B., Lappe, M.M., Spitzer, L., Zweier, S., Braunschweiger, K., Benchekroun, Y., Hu, X., Adair, R., Chee, L., FitzGerald, M.G., Tulig, C., Caruso, A., Tzellas, N., Bawa, A., Franklin, B., McGuire, S., Nogues, X., Gong, G., Allen, K.M., Anisowicz, A., Morales, A.J., Lomedico, P.T., Recker, S.M., Van Eerdewegh, P., Recker, R.R., Johnson, M.L. 2002. A mutation in the LDL receptor-related protein 5 gene results in the autosomal dominant high-bone-mass trait. *Am. J. Hum. Genet*. 70, 11–19.

Liu F., Aubin J.E., and Malaval L. 2002. Expression of leukemia inhibitory factor (LIF)/interleukin-6 family cytokines and receptors during in vitro osteogenesis: differential regulation by dexamethasone and LIF. *Bone* 31, 212-219.

Liu X., Kirschenbaum A., Yao S. and Levine A.C. 2006. Interactive Effect of Interleukin-6 and Prostaglandin E_2 on Osteoclastogenesis via the OPG/RANKL/RANK System, in Anals of the New York Academy of Sciences, 1068 Skeletal Development and Remodeling in Health, Disease, and Aging, 225-233.

Loveringe N. 1999. Bone: More than a Stick, *J. Anim. Sci*. 77, suppl.2/J

Lowik C W, van der Pluijm G, Bloys H, Hoekman K, Bijvoet O L, Aarden L A, Papapoulos S E. 1989. Parathyroid hormone (PTH) and PTH-like protein (PLP) stimulate interleukin-6 production by osteogenic cells: a possible role of interleukin-6 in osteoclastogenesis. Biochem Biophys Res Commun.162, 1546–1552.

Luginbuehl V., Meinel L., Merkle H.P., Gander B. 2004. Localised delivery of growth factors for bone repair. *Eur. J. Pharm. Biopharm*, 58, 197-208.

Luo, B.H., Carman, C.V., Springer, T.A. 2007. Structural basis of integrin regulation and signaling. *Annu. Rev. Immunol*. 25, 619–647.

Maalmi, M., Strieder, W., Varma, A. 2001. Ligand diffusion and receptor mediated internalization: Michaelis–Menten kinetics. *Chem. Eng. Sci*. 56, 5609–5616.

Machwate M., Harada S., Leu C. T., Seedor G., Labelle M., Gallant M., Hutchins S., Lachance N., Sawyer N., Slipetz D., Metters K. M., Rodan S. B., Young R., and Rodan G. A. 2001. Prostaglandin Receptor EP_4 Mediates the Bone Anabolic Effects of PGE_2. *Mol Pharmacol*, 60, 36-41.

Maldonado S.Y., Findeisen R. and Allgöwer F. 2008. Understanding the process of force-induced bone growth and adaptation through a mathematical model. *Bone*, 42, Suppl1, S61.

Malthus T.R. 1798. An essay on the principle of population. Oxford World Classic reprint.

Maniscalco P., Urgelli S., Gatti S. and Bocchi L. 2004. Trombocyte growth factors from platelets concentrate and intramedularry nailing in diaphyseal lower limb pseudoarthroses: preliminary report. *J Bone Joint Surg*, 87-B, 66.

Mannstadt M., Juppner H., Gardella T.J. 1999. Receptors for PTH and PTHrP: their biological importance and functional properties. *Am J Physiol*, 277(5 Pt 2) F665–675.

Manolagas S. C. 1995. Role of cytokines in bone resorption. *Bone, 17(2)*, Suppl.1, S63-S67.

Mao Yo., Schwarzbauer J. E., 2005. Fibronectin fibrillogenesis, a cell-mediated matrix assembly process, Matrix Biology, 24 (6), 389-399

Margetic S., Gazzola C., Pegg G.G., Hill RA 2002. "Leptin: a review of its peripheral actions and interactions". *Int. J. Obes. Relat. Metab. Disord.* 26(11), 1407-1433.

Marie P.J. 2006. Strontium ranelate: A physiological approach for optimizing bone formation and resorption. *Bone*, 38, Suppl 1, 10-14.

Marie, P.J. 1999. Cellular and molecular alterations of osteoblasts in human disorders of bone formation. Histol. Histopathol. 14, 525–538.

Mariette X. 2004. Emerging biological therapies in rheumatoid arthritis. *Joint Bone Spine*, 71(6) 470-474.

Marques, M. B. and Meirelles, N.C. 1995. Erythrocruorin of *Glossoscolex paulistus* (Righi) (Oligochaeta, Glossoscolecidae): effects of divalent ions, acid-alkaline transition and alkali and urea denaturation. *Comp. Biochem. Physiol.* IIIB(2), 311-318.

Martel-Pelletier J., Di Battista J.A., Lajeunesse D., Pelletier J.P. 1998. IGF/IGFBP axis in cartilage and bone in osteoarthritis pathogenesis. *Inflamm Res*, 47, 90–100.

Martin R.B. 2000. Does osteocyte formation cause the nonlinear refilling of osteons? *Bone*, 26, 71–78.

Martin R.B., 2002. Is all cortical bone remodeling initiated by microdamage? *Bone* 30(1) 8-13.

Martin T. J. and Sims N.A. 2005 Osteoclast-derived activity in the coupling of bone formation to resorption. Trends Mol Med 11 76-80.

Martin T.J. 2004. "Does bone resorption inhibition affect the anabolic response to parathyroid hormone?". *Trends Endocrinol. Metab.* 15(2) 49-50.

Martin, M.J. and Buckland-Wright J.C. 2004. Sensitivity analysis of a novel mathematical model identifies factors determining bone resorption rates. *Bone*, 35(4), 918-928.

Martin, R.B. 2000. Towards unifying theory of bone remodeling. *Bone*. 26, 1-6.

Martin, R.B. 2007. Targeted bone remodeling involves BMU steering as well as activation, *Bone*. 40, 1574–1580.

Martinez P., Moreno I., Miguel F. De, Vila V., Esbrit P. and Martinez M. E. 2001. Changes in osteocalcin response to 1,25-dihydroxyvitamin D_3 stimulation and basal vitamin D receptor expression in human osteoblastic cells according to donor age and skeletal origin. *Bone*. 29, 35-41.

Massague J. 1998. TGF-b signal transduction. *Annu Rev Biochem*. 67, 753-91.

Massague J., Wotton D. 2000. Transcriptional control by the TGFb/SMAD signaling system. *EMBO J* ,19, 1745-54.

Massicotte F., Fernandes J. C., Martel-Pelletier J., Pelletier J.-P., Lajeunesse D.l. 2006. Modulation of insulin-like growth factor 1 levels in human osteoarthritic subchondral bone osteoblasts. *Bone*, 38(3) 333-341.

MathCad 2000 Professional, MathSoft Inc., (1999). Users manual.

Matsuura Y., Oharu S., Takata T. and Tamura A. 2003. Mathematical approaches to bone reformation phenomena and numerical simulations. *J Comp Appl Maths*, 158(1), 107-119.

Mayahara H, Ito T, Nagai H, Miyajima H, Tsukuda R, Taketomi S, Mizoguchi, J., and Kato, K. 1993. In vivo stimulation of endosteal bone formation by basic fibroblast growth factor in rats. *Growth Factors*, 9, 73–80.

Mazzuoli G., Diacinti D., D'Erasmo E., Alfò M. 2006. Cyclical changes of vertebral body heights and bone loss in healthy women after menopause. *Bone*, 38(6), 905-910.

Mazzuoli G., Marinucci D., D'erasmo E., Acca M., Pisani D., Rinaldi M. G., Bianchi G., Diacinti D., Minisola S. 2002. Cyclical behavior of bone remodeling and bone loss in healthy women after menopause: results of a prospective study. *Bone*, 31(6), 718-724.

McCarthy T.L., Centrella M., Raisz L.G. and Canalis E. 1991. Prostaglandin E2 stimulates insulin-like growth factor I synthesis in osteoblast-enriched cultures from fetal rat bone, Endocrinology, 128, 2895-2900.

McCarthy T.L., Centrella, M. 2001. Local IGF-I expression and bone formation. *Growth Hormone IGF Res*. 11, 213–219.

McCarty M. F. 2003. Estrogen agonists/antagonists may down-regulate growth hormone signaling in hepatocytes–An explanation for their impact on IGF-I, IGFBP-1, and lipoprotein(a). Med Hyp, 61(3), 335-339.

McKeehan W. L., Wang F., Kan M. 1997. The Heparan Sulfate-Fibroblast Growth Factor Family: Diversity of Structure and Function. *Prog Nucl Acid Res Mol Biol* 59, 135-176.

McQueeney K, Dealy C. 2001. Roles of insulin-like growth factor-I (IGF-I) and IGF-I binding protein-2 (IGFBP2) and -5 (IGFBP5) in developing chick limbs. Growth Horm IGF Res. 11. 346–63.

Meinel L, Zoidis E, Zapf J, Hassa P, Hottiger MO, Auer JA, R. Schneider, B. Gander, V. Luginbuehl, R. Bettschart-Wolfisberger, O. E. Illi, H. P. Merkle, B. von Rechenberg. 2003. Localized insulin-like growth factor delivery to enhance new bone formation. *Bone*, 33. 660-672.

Metropolis, N., Ulam, S. 1949. The Monte-Carlo method. *J. Amer. Stat. Ass.* 44(247), 335-341.

Michaelis, L., Menten, M. L. 1913. Die kinetik der Invertinwirkung. *Biochem. Z.* 49, 333-369.

Miki Y., Suzuki T., Sasano H. 2007. Aromatase inhibitor and bone *Biomedicine & Pharmacotherapy*, 61, 540-542.

Miyazono K. 1999. Signal transduction by bone morphogenetic protein receptors: functional roles of Smad proteins. *Bone*, 25, 91–93.

Mizuno Y., Hosoi T., Inoue S., Ikegami A., Kaneki M., Akedo Y., Nakamura T., Ouchi Y., Chang C., Orimo H.1994. Immunocytochemical identification of androgen receptor in mouse osteoclast-like multinucleated cells. *Calcif Tissue Int,* 54, 325–326.

Mohseni, S.S., Babaeipour, V., Reza Vali A. 2009. Design of sliding mode controller for the optimal control of fed-batch cultivation of recombinant *E. coli*. *Chem. Eng. Sci*. 64(21), 4433-4441.

Monod, J., Wyman, J., Changeux, J., 1965. On the nature of allosteric transitions: a plausible model. *J. Mol. Biol*. 12, 88–118.

Montero A., Okada Y., Tomita M., Ito M., Tsurukami H., Nakamura T., Doetschman, T., Coffin, J.D., Hurley, M.M. 2000. Disruption of the fibroblast growth factor-2 gene results in decreased bone mass and bone formation. *J Clin Invest*, 105, 1085-1093.

Moroz A, Wimpenny D I. 2007. Bone Turnover Cycle Model with a Torus-like Steady State". In "Matematical Modelling of Biological Systems. Vol 1. A Deutsch, L. Brusch, H. Byrne, G de Vries and H-P Hercel (eds). Birchauser, Boston, 261-270.

Moroz, A. 2009. A variational framework for nonlinear chemical thermodynamics employing the maximum energy dissipation principle. *J. Phys. Chem. B.* 113, 8086-8090.

Moroz, A. 2010. Cooperative and collective effects in light of the maximum energy dissipation principle. *Phys. Lett. A.* 374, 2005-2010.

Moroz, A. 2011. The Common Extremalities in Biology and Physics. Elsevier Insights, in press.

Moroz, A., Crane, C.M., Smith, G., Wimpenny, D.I. 2006. Phenomenological model of bone remodeling cycle containing osteocyte regulation loop. *BioSystems* 84, 183–190.

Moroz, A., Wimpenny, D.I. 2007. Allosteric Control Model of Bone Remodelling Containing Periodical Modes, *Biophys. Chem.* 127(3), 194-212.

Moseley, T.A., Haudenschild, D.R., Rose, L., Reddi, A.H. 2003. Interleukin-17 family and IL-17 receptors. Cytokine Growth Fact. Rev. 14, 155–174.

Mozarelli, A., Bettati, S., Rivetti, C., Rossi, G.L., Colotti, G., and Chiancone, E. (1996). Cooperative Oxygen Binding to Scapharca inaequivalvis Hemoglobin in the Cristal. *J. Biol. Chem.* 271(7), 3627-3632.

Mullender M. G., Huiskes R. 1997. Osteocytes and bone lining cells: Which are the best candidates for mechano-sensors in cancellous bone? *Bone* 20(6) 527-532.

Mundy G.R., 1993. Cytokines and growth factors in the regulation of bone remodeling, *J. Bone Miner. Res*. 8, Suppl. S505–S510.

Mundy G.R., Boyce B., Hughes D., Wright K., Bonewald L., Dallas S., Harris S., Ghosh-Choudhury N., Chen D., Dunstan C., Izbicka E., Yoneda T., 1995. The effects of cytokines and growth factors on osteoblastic cells. *Bone* 17(2), Supp 1, S71-S75.

Nakamura I., Jimi E. 2006. Regulation of Osteoclast Differentiation and Function by Interleukin-1. *Vitamins & Hormones*. 74, 357-370.

Nakamura T., Hanada K., Tamura M., Shibanushi T., Nigi H., Tagawa M., Fukumoto S., Matsumoto T. 1995. Stimulation of endosteal bone formation by systemic injections of recombinant basic fibroblast growth factor in rats. *Endocrinology*, 136. 1276-1284.

Nakamura, H., Kumei, Ya., Shimokawa, S., Ohya,K., Shinomiya, K. 2003. Suppression of osteoblastic phenotypes and modulation of pro- and anti-apoptic features in normal human osteoblastic cells under a vector-averaged gravity condition. *J. Med. Dent. Sci*. 50, 167-176.

Nakamura, I., Pilkington, M.F., Lakkakorpi, P.T., Lipfert, L., Sims, S.M., Dixon, S.J., Rodan, G.A., Duong, L.T., 1999. Role of alpha(v)beta(3) integrin in osteoclast migration and formation of the sealing zone. *J. Cell Sci.* 112, 3985–3993.

Nakase T, Nomura S, Yoshikawa H, Hashimoto J, Hirota S, KitamuraY, Oikawa S, Ono K, Takaoka K. 1994. Transient and localized expression of bone morphogenetic protein 4 messenger RNA during fracture healing. *J Bone Miner Res*, 9. 651–659.

Nanes, M.S., 2003. Tumor necrosis factor: molecular and cellular mechanisms in skeletal pathology. *Gene* 321, 1–15.

Neer R. M., Arnaud C.D., Zanchetta J. R., Prince R., Gaich G. A., Reginster J.-Y.s, Hodsman A. B., Eriksen E. F., Ish-Shalom S., Genant H. K., Wang O., Mitlak B. H., Mellstrom D., Oefjord E. S., Marcinowska-Suchowierska E., Salmi J., Mulder H., Halse J., and Sawicki Z.A.j, 2001. Effect of Parathyroid Hormone (1-34) on Fractures and Bone Mineral Density in Postmenopausal Women with Osteoporosis. *New England J Med* 344.1434-1441.

Neilsen, P., Srensen. G., Hynne, F. 1997. Chaos in Glycolysis. *J. Theor. Biol.* 186, 303-306.

Nemoto E., Koshikawa Yo., Kanaya S., Tsuchiya M., Tamura M., Somerman M. J., Shimauchi H., Wnt signaling inhibits cementoblast differention and promotes proliferation. Bone, 44, 2009, Pages 805-812

Nichols, J., Evans, E.P., Smith, A.G. 1990. Establishment of germ-linecompetent embryonic stem (ES) cells using differentiation inhibiting activity. *Development*, 110, 1341–1348.

Nicholson G.C., Moseley J.M., Sexton P.M., Mendelsohn F.A., and Martin T.J. 1986. Abundant calcitonin receptors in isolated rat osteoclasts. Biochemical and autoradiographic characterization. *J Clin Invest.* 78(2) 355–360.

Noble, B. 2003. Bome microdamage and cell apoptosis. *Europ. Cells Materials*. 6, 46-56.

Noble, B.S., Stevens, H., Loveridge, N., Reeve, J., 1997a. Identification of apoptotic changes in osteocytes in normal and pathological human bone. *Bone* 20, 273–282.

Noble, B.S., Stevens, H., Mosley, J.R., Pitsillides, A.A., Reeve, J., Lanyon, L.E. 1997b. Bone loading changes the number and distribution of apoptotic osteocytes in cortical bone. *J. Bone Miner. Res*. 12 (Suppl. 1), s111.

Notelovitz M., 2002. Androgen effects on bone and muscle. *Fertil Steril*, 77, S34-S41

Nowlan N. C., Prendergast P. J. 2005. Evolution of mechanoregulation of bone growth will lead to non-optimal bone phenotypes. *J Theol Bio*. 235(3) 408-418.

Nugent M.A., Iozzo R. V. 2000. Fibroblast growth factor-2. *Int J Biochem Cell Biol*, 32, 115-120.

Nyman J. S., Yeh O. C., Hazelwood S. J., and Martin R. B., 2004. A theoretical analysis of long-term bisphosphonate effects on trabecular bone volume and microdamage. *Bone*. 35, 296–305.

Oh C.D., Chun J.S. 2003. Signaling mechanisms leading to the regulation of differentiation and apoptosis of articular chondrocytes by insulin-like growth factor-1. *J Biol Chem* 278, 36563–36571.

Okada Yo., Montero A., Zhang X., Sobue T., Lorenzo J., Doetschman T., Coffin J. D. and Hurley M.M. 2003. Impaired Osteoclast Formation in Bone Marrow Cultures of Fgf2 Null Mice in Response to Parathyroid Hormone. *J. Biol. Chem*., 278, 21258-21266.

Okazaki H, Kurokawa T, Nakamura K, Matsushita T, Mamada K, Kawaguchi H. 1999. Stimulation of bone formation by recombinant fibroblast growth factor-2 in callotasis bone lengthening of rabbits. *Calcif Tissue Int*, 64, 542–546.

Olivier, B.G., Rohwer, J.M., Snoep, J.L. and Hofmeyr, J.-H.S. 2006. Comparing the regulatory behaviour of two cooperative, reversible enzyme mechanisms. *IEE Proc.-Syst. Biol.* 153, 335-337.

Omdahl J.L., Morris H.A., May B.K. 2002. Hydroxylase enzymes of the vitamin D pathway: expression, function, and regulation. *Ann Rev Nutr*, 22, 139–66.

Onufriev, A. and Ullmann, G. M. 2004. Decomposing Complex Cooperative Ligand Binding into Simple Components: Connections between Microscopic and Macroscopic Models *J. Phys. Chem. B*. 108, 11157-11169.

Ornitz D.M. 2000. FGFs, heparan sulfate and FGFRs: complex interactions essential for development. *Bioessays*, 22, 108– 12.

Ortega, F., Agenda, L. 1998. Optimal metabolic control design. *J. Theor. Biol*. 191, 439–449.

Paget J. 1877. On a form of cronick inflammation of bones (osteitis deformans). *Trans med-Chir Soc*, 60, 37-63.

Palmqvist P., Persson E., Conaway H. H. and Lerner U. H. 2002. IL-6, Leukemia Inhibitory Factor, and Oncostatin M Stimulate Bone Resorption and Regulate the Expression of Receptor Activator of NF-KB Ligand, Osteoprotegerin, and Receptor Activator of NF-KB in Mouse Calvariae. *J Immunol.* 169, 3353-3362.

Parfitt A.M., 2003. Parathyroid hormone and periosteal bone expansion. *J. Bone Miner. Res.* 17 (10) 1741-1743.

Parfitt, A.M., 1994. Osteonal and hemi-osteonal remodeling: the spatial and temporal framework for signal traffic in adult human bone. *J. Cell. Biochem.* 55, 273-286.

Parfitt, A.M., 2001. Targeted and non-targeted bone remodelling: relationship to basic multicellular unit organisation and progression. *Bone*, 30, 2–7.

Pauwels, F., 1965. Gesammelte Abhandlungen zur Funktionellen Anatomic des Bewegungs-apparates. Berlin. Springer-Verlag.

Pearl, R . and Reed, L. J. 1920. On the rate of growth of the population of the United States since 1790 and its mathematical representation. *Proc. Natl. Acad. of Sci. S.A.* 6, 275-288.

Pearson, K. 1901. On Lines and Planes of Closest Fit to Systems of Points in Space. *Philosophical Magazine* 2(6), 559–572.

Pena E., Calvo B., Martinez M.A., Palanca D., Doblare M., 2005. Finite element analysis of the effect of meniscal tears and meniscectomies on human knee biomechanics. *Clinic Biomechanics*, 20(5), 498-507.

Perutz, M.F. 1990. "Mechanisms of Cooperative and Allosteric Regulation in Proteins." Cambridge University Press, Cambridge.

Pontryagin, L.S., Boltyanskii, V.G., Gamkrelidze, R.V., Mischenko, E.F. 1962. "The mathematical Theory of Optimal Processes." *Interscience*, New York.

Poole K, Reeve J., 2005. "Parathyroid hormone - a bone anabolic and catabolic agent." *Curr Opin Pharmacol* , 5(6), 612-617.

Pörtner, R., Schäfer, T. 1996. Modelling hybridoma cell growth and metabolism - a comparison of selected models and data. *J. Biotechnology*, 49, s1-3, 119-135.

Pothuaud L., Fricain J.-C., Pallu S., Bareille R., Renard M., Durrieu M.-C., Dard M., Vernizeau M. and Amédée J., 2005. Mathematical modelling of the distribution of newly formed bone in bone tissue engineering. *Biomaterials*, 26(33), 6788-6797.

Potts, J.T., Jr., and Jüppner, H. 1997. Parathyroid hormone and parathyroid hormone-related peptide in calcium homeostasis, bone metabolism, and bone development: the proteins, their genes, and receptors. In *Metabolic bone disease and clinically related disorders*. L.V. Avioli and S.M. Krane, editors. Academic Press. San Diego, CA. 51–94.

Priestwood, K., Duque, G. 2003. Chapter 75: Osteoporosis. In: Hazzard et al. (Eds.), Hazzard's Textbook in Geriatric Medicine, fifth ed. McGraw Hill, New York.

Putra, D., Bingbing, J., Patton, R., Genever, P., Fagan, M. 2010. Simulation of the BMU remodelling cycle using a new predator-prey algorithm. *Bone*, 47. Supplement 1, S95.

Qian, H. 2003. Thermodynamic and kinetic analysis of sensitivity amplification in biological signal transduction. *Biophysical Chemistry*, 105, 585–593.

Qian, H. 2008. Cooperativity and Specificity in Enzyme Kinetics: A Single-Molecule Time-Based Perspective. *Bioph. J*., 95, 10-17.

Qin L., Raggatt L. J., Partridge N. C., 2004. Parathyroid hormone: a double-edged sword for bone metabolism. *Trends in Endocr Metab*, 15(2) 60-65.

Quinn J.M.W., Morfis M., Lam M.H.C., Elliott J., Kartsogiannis V., Williams E.D., Gillespie M.T., Martin T.J., Sexton P.M., 1999. Calcitonin receptor antibodies in the identification of osteoclasts. *Bone*, 25, 1-8.

Rahman, A.K.M.S., Palanski, S. 1996. On-line optimisation of batch processes with nonlinear manipulated input. *Chem. Eng. Sci.* 51, 449-459.

Rattanakul C., Lenbury Y., Krishnamara N. and Wollkind D. J. 2003. Modeling of bone formation and resorption mediated by parathyroid hormone: response to estrogen/PTH therapy. *Biosystems*, 70(1), 55-72

Rawadi, G., Vayssiere, B., Dunn, F., Baron, R., Roman-Roman, S. 2003. BMP-2 controls alkaline phosphatase expression and osteoblast mineralization by a Wnt autocrine loop. *J. Bone Miner. Res*. 18, 1842-1853.

Reddi, A.H. 2001. Bone morphogenetic proteins: From basic science to clinical applications. *J Bone Joint Surg*, 83-A(Suppl).S1–S6.

Regmi A., Fuson T., Yang X., Kays J., Moxham C., Zartler E., Chandrashekhar S., Galvin R.J.S. 2005. Suramin interacts with RANK and inhibits RANKL-induced osteoclast differentiation, *Bone* 36, 284–291.

Reina J.M., García-Aznar J.M., Domínguez J. and Doblaré M. 2007. Numerical estimation of bone density and elastic constants distribution in a human mandible. *J Biomechanics*, 40(4) 828-836.

Rennel E., Cross M. J., Klint P., Bai X., Arbiser J.L., Gerwins P.. 2003. Regulation of endothelial cell differentiation and transformation by H-Ras. *Exp Cell Res*, 291(1), 189-200.

Rico-Ramirez V., Diwekar, U. M., Morel B. 2003. Real option theory from finance to batch distillation. *Comp & Chem Eng*, 27(12) 1867-1882.

Rietbergen, Van, B., Huiskes R., Weinans H., Sumner D. R., Turner T. M., Galante J. O., 1993. The mechanism of bone remodeling and resorption around press-fitted THA stems. *J Biomech*, 26(4-5), 369-382

Rodan G.A., Martin T.J. 2006. Role of osteoblasts in hormonal control of bone resorption - a hypothesis. *Calcif Tissue Int*, 33, 349-351.

Romas E., Gillespie M. T., Martin T. J. 2002. Involvement of receptor activator of NFκB ligand and tumor necrosis factor-α in bone destruction in rheumatoid arthritis. *Bone, 30(2), 340-346.*

Rosen C.J. 2000. IGF-I and osteoporosis. Clin Lab Med, 20 591–602.

Rosen C.J. 2002. Growth Hormone and Insulin-like Growth Factor-I Treatment for Metabolic Bone Diseases. *Principles of Bone Biology* (Second Edition), 1441-1453.

Rosen, C.J. 2003. The cellular and clinical parameters of anabolic therapy for osteoporosis. *Crit. Rev. Eukaryot. Gene Expr*. 13, 25–38.

Rougier F., Cornu E., Praloran V. and Denizot Y., 1998. IL-6 and IL-8 production by human bone marrow stromal cells, *Cytokine*, 10(2) 93-97.

Roux W., 1895. Gessamelte Abhandlungen uber Entwicklungsmechanick der Organismen, vol. I and II. Leipzig: Wilhelm Engelman.

Ruffoni D., Fratzl P., Roschger P., Klaushofer K. and Weinkamer R., 2007, The bone mineralization density distribution as a fingerprint of the mineralization process. *Bone*, 40(5) 1308-1319.

Ruimerman R., P. Hilbers, B. van Rietbergen and R. Huiskes, 2005, A theoretical framework for strain-related trabecular bone maintenance and adaptation. *J Biomechanics*, 38(4) 931-941.

Sakou T, Onishi T, Yamamoto T, Nagamine T, Sampath T, ten Dijke P. Localization of Smads, the TGF-_ family intracellular signalling components during endochondral ossification. *J Bone Miner Res* 1999,14, 1145–52.

Sanjay, A., Houghton, A., Neff, L., DiDomenico, E., Bardelay, C., Antoine, E., Levy, J., Gailit, J., Bowtell, D., Horne, W.C., Baron, R., 2001. Cbl associates with Pyk2 and Src to regulate Src kinase activity, avb3 integrin-mediated signaling, cell adhesion, and osteoclast motility. J. Cell Biol. 152, 181–195.

SAS/STAT® 9.2 Users Guide, Second edition. 2009.

Schendel P.F., Turner K. J. 1998. Interleukin-11 *Cytokines*, 169-182.

Schmitt J.M., Hwang K., Winn S.R., Hollinger J.O. 1999. Bone morphogenetic proteins: an update on basic biology and clinical relevance. *J Orthop Res*,17, 269–278.

Schuster, S., Heinrich, R. 1987. Time hierarchy in enzymatic reactions chains resulting from optimality principles. *J. Theor. Biol.* 129, 189-209.

Schuster, S., Heinrich, R. 1991. Minimization of intermediate concentrations as a suggested optimality principle for biochemical networks. I. Theoretical analysis. *J. Math. Biol.* 29, 425-442.

Sel'kov E.E. 1968. Self-Oscillations in Glycolysis. 1. A Simple Kinetic Model. *Europ. J. Biochem.* 4, 79-86.

Sengupta, S., Modak, J.M. 2001. Optimization of fed-batch bioreactor for immobilized enzyme processes. *Chem. Eng. Sci.* 56, 3315-3325.

Seto H., Aoki K., Kasugai S., Ohya K. 1999. Trabecular bone turnover, bone marrow cell development, and gene expression of bone matrix proteins after low calcium feeding in rats. *Bone*, 25, 687-695.

Shao, Y.Y., Wang, L., & Ballock, R.T. 2006. Thyroid hormone and the growth plate. *Rev. Endocr. Metab. Disord.*, 7(4), 265–271.

Sharma P.K., Thakur M.K. 2006. Expression of estrogen receptor (ER) α and β in mouse cerebral cortex: Effect of age, sex and gonadal steroids. *Neurobiol Aging*, 27(6) 880 - 887

Shefelbine S. J., Augat, P. Claes L., Simon U. 2005. Trabecular bone fracture healing simulation with finite element analysis and fuzzy logic. *J Biomech*, 38(12) 2440-2450.

Sheppard, D., 2000. In vivo functions of integrins: lessons from null mutations in mice. *Matrix Biol*. 19, 203–209.

Shi Ya.-Ch, Worton L., Esteban L., Baldock P., Fong C., Eisman J. A., Gardiner E. M., *2007.* Effects of continuous activation of vitamin D and Wnt response pathways on osteoblastic proliferation and differentiation. *Bone*, 41, 87-96.

Sibonga J.D., Evans H.J., Sung H.G., Spector E.R., Lang T.F., Oganov V.S., Bakulin A.V., Shackelford L.C. and LeBlanc A.D., 2007. Recovery of spaceflight-induced bone loss: Bone mineral density after long-duration missions as fitted with an exponential function. *Bone*, 41(6) 973-978.

Silver J., Epstein E. and Naveh-Many T. 1996. Oestrogen deficiency—does it have a role in the genesis of skeletal problems in dialysed women? *Nephrol Dial Transplant*, 11, 565-574.

Simeoni I., Gurdon J.B. 2007. Interpretation of BMP signaling in early Xenopus development. *Dev Biol*, 308(1), 82-92.

Simon A. M., Goodenough D. A., 1998. Diverse functions of vertebrate gap junctions. *Trends in Cell Biology*, 8(12) 477-483.

Simonet W. S., Lacey D. L., Dunstan C. R., Kelley M., Chang M. -S., Lüthy R., Nguyen H. Q., Wooden S., Bennett L., Boone T., Shimamoto G., DeRose M., Elliott R., Colombero

A., Tan H. -L., Trail G., Sullivan J., Davy E., Bucay N., Renshaw-Gegg L., Hughes T. M., Hill D., Pattison W., Campbell P., Sander S., Van G., Tarpley J., Derby P., Lee R., Amgen EST Program, and Boyle W. J. 1997. Osteoprotegerin: A Novel Secreted Protein Involved in the Regulation of Bone Density. *Cell*, 89(2) 309-319.

Singh B., Berry J. A., Vincent L. E., Lucci A., 2006. Involvement of IL-8 in COX-2-mediated bone metastases from breast cancer. *J Surg Res*, 134, 44-51.

Skerry, T.M., Bitensky, L., Chayen, J., Lanyon, L.E. 1989. Early strainrelated changes in enzyme activity in osteocytes following bone loading in vivo. *J. Bone Miner. Res.* 4, 783–788.

Smets, I.Y., Claes, J.E., November, E.J., Bastin, G.P., Van Impe, J.F. 2004. Optimal adaptive control of (bio)chemical reactors: past, present and future. *J. Process Control* 14, 795-805.

Smets, I.Y.M., Versyck, K.J.E. Van Impe, J.F.M. 2002. Optimal control theory: a generic tool for identification and control of (bio)-chemical reactors. *Ann. Rev. Contr.* 26, 57-73.

Smink J.J., Koster J.G., Gresnigt M.G., Rooman R., Koedam J.A., Van Buul-Offers S.C., 2002. IGF and IGF-binding protein expression in the growth plate of normal, dexamethasone-treated and human IGF-II transgenic mice. *J Endocrinol*, 175, 143–53.

Southwood L.L., Frisbie D.D., Kawcak C.E., Ghivizzani S.C., Evans C.H., McIlwraith C.W. 2004. Evaluation of Ad-BMP-2 for enhancing fracture healing in an infected defect fracture rabbit model. *J Orthop Res*, 22(1), 66-72.

Srinivasan, B., Palanki, S., Bonvin, D. (2003). Dynamic optimisation of batch processes I. Characterisation of the nominal solution. *Comp. Chem. Eng.* 27, 1-26.

Stein G. S., Lian J. B., Stein J. L., Van Wijnen A. J. and Montecino M., 1996. Transcriptional control of osteoblast growth and differentiation. *Physiol. Rev.* 76. 593-629.

Suda, T., Takahashi, N., Udagawa, N., Jimi, E., Gillespie, M.T., Martin, T.J., 1999. Modulation of osteoclast differentiation and function by the new members of the tumor necrosis factor receptor and ligand families. *Endocr. Rev.* 20, 345–357.

Suzuki H, Nakamura I., Takahashi N., Ikuhara T., Matsuzaki K., Isogai Y., Hori M. and Suda T., 1996. Calcitonin-induced changes in the cytoskeleton are mediated by a signal pathway associated with protein kinase A in osteoclasts. *Endocrinology,* 137, 4685-4690.

Swarthout J.T., D'Alonzo R.C., Selvamurugan N., Partridge N.C. 2002. Parathyroid hormone-dependent signaling pathways regulating genes in bone cells. *Gene*, 282, 1-17.

Taboas, J.M., Maddox, R.D., Krebsbach, P.H., Hollister, S.J. 2003. Indirect solid free form fabrication of local and global porous, biomimetric and composite 3D polymerceramic scaffolds. *Biomaterials* 24, 181-194.

Takahashi, N., Yamana, H., Yoshiki, S., Roodman, G.D., Mundy, G.R., Jones, J.S., Boyde, A., Suda, T., 1988. Osteoclast-like cell formation and its regulation by osteotropic hormones in mouse bone marrow cultures. *Endocrinology* 122, 1373– 1382.

Taylor D, Kuiper J.H. 2001. The prediction of stress fractures using a "stressed volume" concept. *J Orthop Res*, 19(5), 919–26.

Taylor D., Casolari E. and Bignardi C. 2004. Predicting stress fractures using a probabilistic model of damage, repair and adaptation J Orthopaedic Res, 22(3), 487-494.

Taylor, D., Hasenberg, J.G., Lee, T.C. 2003. The cell transducer in damage-stimulated bone remodeling: a theoretical investigation using fracture mechanics. *J. Theor. Biol*. 224, 65-75.

Tayyar S., Weinhold P. S., Butler R. A., Woodard J. C., Zardiackas L. D., St. John K. R., Bledsoe J. M., Gilbert J. A., 1999. Computer simulation of trabecular remodeling using a simplified structural model. *Bone*, 25(6) 733-739.

Teitelbaum S. L., 2004. Postmenopausal osteoporosis, T cells, and immune dysfunction. *Proc Natl Acad Sci U S A*. 101(48). 16711–16712.

Theoleyre, S.,Wittrant, Y., Couillaud, S., Vusio, P., Berreur, M., Dunstan, C., Blanchard, F., Redini, F., Heymann, D. 2004. Cellular activity and signaling induced by osteoprotegerin in osteoclasts: involvement of receptor activator of nuclear factor nB ligand and MAPK. *Biochem. Biophys. Acta*, 1644, 1–7.

Thomadakis, G., Ramoshebi, L.N., Crooks, J., Rueger, D.C., Ripamonti, U. 1999. Immunolocalization of bone morphogenetic protein-2 and -3 and osteogenic protein-1 during murine tooth root morphogenesis and in other craniofacial structures. *Eur. J. Oral Sci*. 107, 368–377.

Thomas D. M., Udagawa N., Hards D. K., Quinn J. M. W., Moseley J. M., Findlay D. M., Best J. D. 1998. Insulin receptor expression in primary and cultured osteoclast-like cells *Bone*, 23 181-186.

Thompson, T.B., Cook, R.W., Chapman, S.C., Jardetzky, T.S., Woodruff, T.K. 2004. Beta A versus beta B: is it merely a matter of expression? *Mol. Cell. Endocrinol*. 225, 9–17.

Tiegs, R. D., 1997. Paget's disease of bone: indications for treatment and goals of therapy *Clinical Therapeutics*, 19, 1309-1329.

Tirapegui J. 1999. Effect of insulin-like growth factor-1 (IGF-1) on muscle and bone growth in experimental models. *Int J Food Sci Nutr*, 50, 231–236.

Tohyama, M., Patarinska, T., Qiang, Z., Shimizu, K. 2002. Modelling of the mixed culture and periodic control for PHB production. *Biochem. Eng. J*. 10, 157–173.

Tomkinson, A., Reeve, J., Shaw, R.W., Noble, B.S. 1997. The death of osteocytes by apoptosis in human bone is observed following estrogen withdrawal in human bone. *J. Clin. Endocrinol. Metab*. 82, 3128–3135.

Troen B. R., 2003. Molecular mechanisms underlying osteoclast formation and activation. *Exp Gerontology*, 38(6), 605-614.

Tsubota K., Adachi T. 2005, Spatial and temporal regulation of cancellous bone structure: characterization of a rate equation of trabecular surface remodelling. *Med Eng & Phys*, 27(4), 305-311.

Tsubota K., T. Adachi and Yo. Tomita, 2001. Cancellous bone adaptation in proximal femur predicted by trabecular surface remodeling simulation. *BED-Vol. 50, Bioengineering Conference ASME 2001*, 299-300.

Turner A.W.L., Gillies R.M., Sekel R., Morris P., Bruce W., Walsh W.R. 2005. Computational bone remodelling simulations and comparisons with DEXA results. *J Orthopaed Res,* 23 705–712.

Ueno K., Katayama T., Miyamoto T., Koshihara Y. 1992. Interleukin-4 enhances *in vitro* mineralization in human osteoblast-like cells. *Biochem Biophys Res Comm*, 189(3), 1521-1526.

Vaibhav B., Nilesh P., Vikram S., Anshul, C. 2007. Bone morphogenic protein and its application in trauma cases: A current concept update. *Injury*, 38(11), 1227-1235.

Valentinotti, S., Srinivasan, B., Holmberg, U., Bonvin, D., Cannizzaro, C., Rhiel, M. and von Stockar, U. 2003. Optimal operation of fed-batch fermentations via adaptive control of overflow metabolite. *Contl. Eng. Prac.* 11, 665-674.

Van Impe, J.F., Bastin, G. 1995. Optimal adaptive control of fed-batch fermentation processes. *Control Eng. Pract.* 3(7), 939-954.

Van Riel, N.A.W., Giuseppin, M.L.F., Verrips, C.T. 2000. Dynamic Optimal Control of Homeostasis: An Integrative System Approach for Modeling of the Central Nitrogen Metabolism in *Saccharomyces cerevisiae. Metabol. Eng.* 2(1), 49-68.

Vanderschueren D, Bouillon R. 1995. Androgens and bone. *Calcif Tissue Int*, 56, 341–6.

Vashishth, D., Gibson, G., Kimura, J., Schaffler, M.B., Fyhrie, D.P. 2002. Determination of bone volume by osteocyte population. *T. Anat. Rec*, 276, 292–295.

Vatsa A., Smit T. H., Klein-Nulend J. 2007. Extracellular NO signalling from a mechanically stimulated osteocyte. *J.Biomechanics*, 40, Suppl1, S89-S95.

Verhulst P.F. 1838. Notice sur la loi que la population suit dans son ccroisement. *Corr. Math. Phys*. X, 113-121.

Vestergaard P., Hermann A. P., Gram J., Jensen L. B., Eiken P., Abrahamsen B., Brot C., Kolthoff N., Sørensen O. H., Nielsen H. B., Nielsen S. P., Charles P. and Mosekilde L. 2001. Evaluation of methods for prediction of bone mineral density by clinical and biochemical variables in perimenopausal women. *Maturitas*, 40(3), 211-220.

Vignery A, McCarthy T.L., 1996. The neuropeptide calcitonin gene-related peptide stimulates insulin-like growth factor I production by primary fetal rat osteoblasts *Bone*, 18, 331-335.

Visser, D., Schmid, J. W., Mauch, K., Reuss, M., Heijnen J. J. 2004. Optimal re-design of primary metabolism in *Escherichia coli* using linlog kinetics. *Metabol. Eng.* 6(4), 378-390.

Voet, D., Voet, J. G. 1995. "Biochemistry.", 2nd ed. J. Wiley and Sons, New York.

Volkenstein, M.V. 1989. "Biofizika" Nauka, Moscow (in Russian).

Vozzi, G., Flaim C.J, Bianchi, F., Ahluwalia, A., Bhatia, S. 2002. Microfabricated PLGA scaffolds: a comparative study for application to tissue engineering, *Mat. Sci. and Eng. C*, 20, 43-47.

Vozzi, G., Flaim C.J, Bianchi, F., Ahluwalia, A., Bhatia, S., 2003. Fabrication of PLGA scaffolds using soft lithography and microsyringe deposition. *Biomaterials* 24, 2522-2540.

Wada S, Martin T.J. and Findlay D.M., 1995. Homologous regulation of the calcitonin receptor in mouse osteoclast- like cells and human breast cancer T47D cells. Endocrinology, 136, 2611-2621.

Wada S, Udagawa N., Nagata N., Martin T.J. and Findlay D.M., 1996. Calcitonin receptor down-regulation relates to calcitonin resistance in mature mouse osteoclasts. Endocrinology, 137, 1042-1048.

Wang F.-S., Ko J.-Y., Lin C.-L., Wu H.-L., Ke H.-J., Tai P.-J.. Knocking down dickkopf-1 alleviates estrogen deficiency induction of bone loss. A histomorphological study in ovariectomized rats. Bone 40 (2007) 485–492.

Wang F.-S., Ko J.-Y., Weng L.-H., Yeh D.-W., Ke H.-J., Wu S.-L. Inhibition of Glycogen synthase kinase -3β attenuates glucocorticoid-induced bone loss. Life Sci., 85, 2009, 685-692

Wang L., Liu S., Quarles L. D., and Spurney R. F. 2005. Targeted overexpression of G protein-coupled receptor kinase-2 in osteoblasts promotes bone loss. *Am J Physiol Endocrinol Metab*, 288. E826–E834.

Wang, D.S., Miura, M., Demura, H., Sato, K., 1997. Anabolic effects of 1,25-dihydroxyvitamin D3 on osteoblasts are enhanced by vascular endothelial growth factor produced by

osteoblasts and by growth factors produced by endothelial cells. Endocrinology 138, 2953–2962.

Wang, D.S., Yamazaki, K., Nohtomi, K., Shizume, K., Ohsumi, K., Shibuya, M., Demura, H., Sato, K., 1996. Increase of vascular endothelial growth factor mRNA expression by 1,25-dihydroxyvitamin D3 in human osteoblast-like cells. *J. Bone Miner. Res.* 11, 472–479.

Wang, F., McKeehan W. L. 2003. The Fibroblast Growth Factor (FGF) Signaling Complex, Handbook of Cell Signaling, 265-270.

Wang, F.S., Ko, J.Y., Lin, C.L., Wu, H.L., Ke, H.J., Tai, P.J. (2007) Knocking down dickkopf-1 alleviates estrogen deficiency induction of bone loss. A histomorphological study in ovariectomized rats. Bone, 40, 485-492.

Watkins, B.A., Seifert, M.F. 2000. Conjugated LLinoleic Acid and Bone Biology. *J Amer Col Nutr.* 19(4) 478S-486S.

Weber, R. E., Hourdez, S., Knowles, F. and Lallier, F. 2003. Hemoglobin function in deep-sea and hydrothermal-vent endemic fish: *Symenchelis parasitica* (Anguillidae) and *Thermarces cerberus* (Zoarcidae). *J. Exp. Biol.* 206, 2693-2702.

Weinans, H., Huiskes, R. and Grootenboer, H.J. 1992. The behaviour of adaptive bone-remodeling simulation models. *J Biomechanics,* 25(12), 1425–1441.

Weinans, H., Huiskes, R. and Grootenboer, H.J., 1994. Effects of Fit and Bonding Characteristics of Femoral Stems on Adaptive Bone Remodeling. *J Biomech Eng,* 116, 393-400.

Weiss, J. N. 1997. The Hill equation revisited: uses and misuses. *FASEBJ.* 11, 835-841.

Westendorf, J.J., Kahler, R.A., Schroeder, T.M., 2004. WNT signalling in osteoblasts and bone diseases. *Gene*, 341, 19–39.

Whitfield J.F., Morley P., Willick G.E. 2002.Bone growth stimulators. New tools for treating bone loss and mending fractures. *Vitam. Horm.* 65. 1-80.

Whyte M.P., Singhellakis P.N., Petersen M.B., Davies M., Totty W.G., Mumm S. 2007. Juvenile Paget's disease: the second reported, oldest patient is homozygous for the TNFRSF11B "Balkan" mutation (966_969delTGACinsCTT), which elevates circulating immunoreactive osteoprotegerin levels. *J. Bone Miner. Res.* 22, 938–946.

Wingfield, P., Pain, R.H., Craig, S. 1987. Tumour necrosis factor is a compact trimer. *FEBS Lett.* 211, 179–184.

Wipff P.-J., Hinz B. 2008. Integrins and the activation of latent transforming growth factor β1 – An intimate relationship. *Eur J Cell Biol,* 87(8-9) 601-615.

Wluka A.E., Davis S.R., Bailey M., Stuckey S.L., Cicuttini F.M. 2001. Users of oestrogen replacement therapy have more knee cartilage than non-users. *Ann. Rheum Diseas*. 60, 332-336.

Wolff J. 1986. The law of bone remodelling (1892, Das Gesetz der Transformation der Knochen, Hirschwald,) (Maquet P, Furlong R, Trans.). Springer, Berlin.

Wozney J.M. 2002. Overview of bone morphogenetic proteins. *Spine*. 15(16), Suppl. 1. 2-8. 109.

Wozney J.M., Rosen V. 1998. Bone morphogenetic protein and bone morphogenetic protein gene family in bone formation and repair. *Clin Orthop*, 346.26–37.

Wu, Y. and Kumar, R. 2000. Parathyroid hormone regulates transforming growth factor b1 and b2 synthesis in osteoblasts via divergent signaling pathways. *J. Bone Miner. Res*. 15, 879–884.

Xiao Y-T., Xiang L.-X., Shao J.-Z. 2007. Bone morphogenetic protein, *Biochem Biophys Res Comm.* 362, 550-553.

Xinghua Z., He G., Bingzhao G. 2005. The application of topology optimization on the quantitative description of the external shape of bone structure. *J Biomechanics*, 38(8) 1612-1620.

Xinghua Z., He G., Dong Z., Bingzhao G. 2002. A study of the effect of non-linearities in the equation of bone remodelling. *J Biomechanics*, 35(7) 951-960.

Yakar, S., Rosen, C. J., Beamer,W. G., Ackert-Bicknell, C. L.,Wu, Y., Liu, J.-L., Guck T Ooi, Jennifer Setser, Jan Frystyk, Yves R Boisclair, Derek LeRoith et al. 2002. Circulating levels of IGF-1 directly regulate bone growth and density. *J. Clin. Invest.*, *110*(6), 771–781.

Yamaguchi A., Komori T., Suda T. 2000. Regulation of osteoblast differentiation mediated by bone morphogenetic proteins, hedgehogs, and Cbfa1. *Endocr. Rev*. 221, 393–411.

Yamashita H, ten Dijke P, Heldin C-H, Miyazono K. 1996, Bone morphogenetic protein receptors. *Bone* 19, 569–74.

Yamauchi N., Ohishi K., Nishikawa S., Nagata T., Kataoka M., Shinohara H. and Ishida H. 2006. Expression and characterization of parathyroid hormone receptors on fetal rat calvaria cells in culture. *J Bone Miner Metabol*, 12, S33-S37.

Yan, Y., Xiong, Z., Hu, Yu., Wang, S., Zhang, R., Zhang, C. 2003. Layered manufacturing of tissue engineering scaffolds via multi-nozzle deposition. *Mat. Let*. 57, 2623-2628.

Yildirim, N., Akcay, F., Okur, H., Yildirim, D. 2003. Parameter estimation of nonlinear models in biochemistry: a comparative study on optimization methods. *Appl. Math.Comp.* 140, 29-36.

Yonetani, T., Park, S., Tsuneshige, A., Imai, K. and Kanaori, K. 2002. Global Allostery Model of Hemoglobine. *J. Biol. Chem.* 277, 34508-34540.

Yonetani, T., Tsuneshige, A. 2003. The global allostery model of hemoglobin: an allosteric mechanism involving homotropic and heterotropic interactions. *C. R. Biol.* 326, 523–532.

Yoshida K., Oida H., Kobayashi T., Maruyama T., Tanaka M., Katayama T., Yamaguchi K., Segi E., Tsuboyama T., Matsushita M., Ito K., Ito Yo., Sugimoto, Yu. Ushikubi F., Ohuchida S., Kondo K., Nakamura T., and Narumiya S. 2002. Stimulation of bone formation and prevention of bone loss by prostaglandin E EP4 receptor activation. *PNAS*, 99, 4580–4585.

You, L-D., Weinbaum, S., Cowin, S.C., Schaffler, M.B. 2004. Ultrastructure of the Osteocyte Process and its Pericellular Matrix. *T. Anat. Rec.* 278A, 505-513.

Yucel-Lindberg T. and Brunius G. 2006. Epidermal growth factor synergistically enhances interleukin-8 production in human gingival fibroblasts stimulated with interleukin-1β, *Archives of Oral Biology*, 51, 892-898.

Yue J., Mulder K. M. 2001. Transforming growth factor-β signal transduction in epithelial cells *Pharmacol Therap*, 91(1), 1-34.

Yüzgeç, U., Türker, M., Hocalar, A. 2009. On-line evolutionary optimization of an industrial fed-batch yeast fermentation process. *ISA Trans*. 48(1) 79-92.

Zaidi M., Inzerillo A. M., Moonga B. S., Bevis P. J. R., Huang C. L.-H. 2002. Forty years of calcitonin - where are we now? A tribute to the work of Iain Macintyre, FRS. *Bone* 30, 655-663.

Zhang J., Dai J., Lu Y., Yao Z., O'Brien C. A., Murtha J. M., Qi W., Hall D. E., Manolagas S. C., Ershler W. B., Keller E. T., 2004. In vivo visualization of aging-associated gene transcription: evidence for free radical theory of aging. *Exp. Geron* 39(2), 239-247.

Zhang, J., Fua, M., Mylesa, D., Zhua, X., Dub, J., Caoc, X., Chen, Y.E. 2002. PDGF induces osteoprotegerin expression in vascular smooth muscle cells by multiple signal pathways. *FEBS Lett* 521, 180–184.

Zofkova I. 2003. Pathophysiological and clinical importance of insulin-likegrowth factor-I with respect to bone metabolism. *Physiol Res* 52, 657–79.